

**CONTINENTAL RIFTING AND BREAK-UP AT THE WEST  
IBERIA MARGIN:  
AN INTEGRATED GEOPHYSICAL STUDY**

**Dissertation**

Zur Erlangung des Doktorgrades  
Der Mathematisch-Naturwissenschaftlichen Fakultät  
Der Christian-Albrechts Universität zu Kiel

Vorgelegt von  
**Marta Pérez Gussinyé**  
Kiel, 2000

Referent:  
Koreferent:  
Tag der mündlichen Prüfung:  
Zum Druck genehmigt:

Prof. Dr. Timothy Reston  
Prof. Dr. Jason Phipps Morgan  
17.07.2000  
Kiel, den

Der Dekan



## ABSTRACT

The purpose of this work has been to study the processes of continental extension and break-up at non-volcanic margins. In particular, we studied how extension halts leading to failed rifts. For this purpose, I have processed multichannel seismic reflection and modelled wide angle data from the Galicia Interior Basin, a failed rift located offshore west Iberia. Part of the data were provided by the oil company R.E.P.S.O.L (Chapter 1 and 3) and the rest were acquired during the Iberia Seismic Experiment (July 1997), (Chapter 2), which was a marine geophysical survey financed by the NSF (National Science Foundation) of the USA and the DFG (German Association of Science).

Our studies reveal the structure, amount of thinning and timing of extension at the Galicia Interior Basin, which was poorly known before (Chapter 2 and 3). We have integrated the new results on the GIB with those already existent at the rest of the segments of the margin and suggested possible causes for rift failure at the basin in connection with propagation of seafloor spreading at the final break-up margin (Chapter 3 and Outlook).

Additionally, we studied how extension leads to continental break-up and the birth of new oceans at non-volcanic margins of the west Iberia type. We developed a numerical model based on the seismic, petrological and chronological observations made at the segments of the west Iberia margin where continental break-up occurred (Chapter 4). We have applied this model successfully to other non-volcanic margins such as the south-west Greenland margin, the Rockall Trough and the Porcupine Basin (both located offshore west Ireland) (Chapter 5). We have also found that the differences in the initial thermal structure (and hence tectonic setting of the margins) may lead to the differences in the structural style of continental break-up between non-volcanic margins of the west Iberia type and those showing more magmatic activity during extension (e.g. the Woodlark basin, located at the eastern tip of Papua new Guinea), (Chapter 5). Our modelling stresses the importance of the rheological consequences of the process of serpentinisation (interaction of sea water with mantle rocks) at non-volcanic margins of the west Iberia type in contrast to those of a more robust magmatic production.



<b>CHAPTER 3. STRUCTURE OF THE GALICIA INTERIOR BASIN FROM MCS INDUSTRY LINES AND EVOLUTION OF THE WESTIBERIA MARGIN.....</b>	<b>79</b>
3.1 INTRODUCTION.....	79
3.2 INTERPRETATION OF TIME MIGRATED SECTIONS.....	80
3.2.1 Sedimentary Cover.....	80
3.2.2 Basement.....	83
3.3 DISCUSSION.....	89
3.3.1 Variation of crustal thickness and timing of the extensional phases along the West Iberia margin.....	89
3.3.2 Mechanisms for rift abandonment in the Galicia Interior Basin.....	93
3.4 CONCLUSIONS.....	95
<b>CHAPTER 4. RHEOLOGICAL EVOLUTION DURING EXTENSION AT NON-VOLCANIC MARGINS: ONSET OF SERPENTINISATION AND DEVELOPMENT OF DECOLLEMENTS LEADING TO CONTINENTAL BREAKUP.....</b>	<b>97</b>
4.1 ABSTRACT.....	97
4.1 INTRODUCTION.....	97
4.1.1 Lithospheric rheology during progressive extension - principles.....	101
4.2 MODEL DESCRIPTION.....	102
4.2.1 Thermal Calculation.....	103
4.2.2 Rheology.....	104
4.3 MODELLING RESULTS.....	108
4.3.1 Onset of rifting.....	108
4.3.2 Evolution of the brittle plastic transition during progressive extension.....	108
4.3.2.1 <i>Effect of the rheology of the lower crust.....</i>	111
4.3.2.2 <i>Effect of the strain rate.....</i>	111
4.3.2.3 <i>Dependence of the results on the initial thermal state of the lithosphere.....</i>	112
4.3.3 Stability field of serpentinites.....	115
4.3.4 Serpentine thickness.....	115
4.4 DISCUSSION.....	119
4.4.1 Effects on lithospheric rheology, strain localisation, and the development of detachment levels.....	119
4.4.2 Comparison with west Iberia.....	123
4.4.2.1 <i>Onset of serpentinitisation.....</i>	123
4.4.2.2 <i>Comparison of serpentinite thickness.....</i>	124
4.4.2.3 <i>Serpentine vs. melt thickness.....</i>	125
4.4.3 Development of passive non-volcanic margins, a case example: the western Iberia margin.....	126
4.5 CONCLUSIONS.....	127
<b>CHAPTER 5. RHEOLOGICAL AND MAGMATIC EVOLUTION AT NON-VOLCANIC MARGINS DURING EXTENSION: THE EFFECT OF THE INITIAL THERMAL STRUCTURE.....</b>	<b>129</b>
5.1 ABSTRACT.....	129
5.2 INTRODUCTION.....	129
5.2.1 Effect of progressive extension.....	130
5.3 MODEL DESCRIPTION.....	133
5.3.1 Initial Lithospheric models.....	136
5.3.2 Initial strength curves.....	140
5.4 RHEOLOGICAL EVOLUTION DURING PROGRESSIVE EXTENSION.....	141
5.5 COMPARISON WITH OBSERVATIONS.....	147
5.5.1 Woodlark Basin.....	147
5.5.2 West Iberia.....	148

5.5.3 West Greenland.....	149
5.5.4 Rockall Trough.....	150
5.6 DETACHMENTS AND DETACHMENTS.....	153
5.7 TEMPORAL EVOLUTION AT NON-VOLCANIC MARGINS.....	154
5.8 CONCLUSIONS.....	157
<b>CHAPTER 6. OUTLOOK.....</b>	<b>159</b>
6.1 Differential versus uniform stretching in the crust - or how to reconcile extension factors on faults with overall extension factors in the crust.....	159
6.2 Development of decollements and extension at the continent ocean transition zone of the West Iberia margin.....	161
6.3 Interplay between continental rifting and seafloor spreading propagation: the chicken or the egg?.....	162
<b>REFERENCES.....</b>	<b>167</b>
<b>ACKNOWLEDGEMENTS.....</b>	<b>177</b>
<b>CURRICULUM VITAE.....</b>	<b>179</b>
<b>APPENDIX 1.....</b>	<b>181</b>

## INTRODUCTION

Continental extension is a first order tectonic process that leads to the formation of rift basins and eventually to the growth of new oceans. A postulate of quantitative plate tectonics states that deformation occurs at plate boundaries, while their interiors remain undisturbed. This agrees with deformation patterns observed in oceanic plates. Here deformation is concentrated along the narrow plate boundaries that constitute the spreading centres and transform faults. However deformation in continental plates is often distributed in broad interior regions, forming wide mountain ranges (e.g. the Himalayas), broad extensional basins (e.g., the North Sea) and wide zones of faulting accommodating movements between the plates (e.g. the Anatolian fault which accommodates movement between Europe and Asia). The geologic and dynamic processes by which extension is progressively localised during rifting of the continental lithosphere leading to the development of seafloor spreading centres are not yet understood. Is seafloor spreading a consequence of rifting at continental margins, or do continental margins rift as a response to incipient propagation of an oceanic spreading centre into a rifted zone? How does the nature of a plate boundary change as it passes from a continental to an oceanic regime? Why do spreading centres propagate through certain continental rifted basins while leaving neighbouring areas, which are extremely thinned, abandoned (e.g. the Rockall Trough or the Galicia Interior Basin)?

Continental rifting and initiation of seafloor spreading involves a combination of tectonic and magmatic processes. Depending on the degree of rift associated, synrift, magmatism continental margins have been classified into one of two types. Margins where large amounts of intruded and extruded igneous rocks have been observed are classified as volcanic margins (Hinz et al., 1981). Those where no clear geophysical signature for synrift magmatic activity has been found are termed non-volcanic. In the past few years seismic reflection and wide angle profiles at an increasing number of margins have shown that classical volcanic margins, e.g.: east Greenland (Coffin and Bedlhom, 1994, Hinz, 1981) and non-volcanic margins, e.g. west Iberia (Boillot and Winterer, 1988, Whitmarsh and Sawyer, 1996, ODP Leg 173 Shipboard Scientific Party, 1998) are end members of a wide spectrum of margins that differ in their width, in the duration of the rifting episode, and amount of melt produced during the rifting (Mutter, 1993).

At the end of the non-volcanic spectrum are margins such as the west Iberia margin (Boillot and Winterer, 1988, Whitmarsh et al., 1996), the Newfoundland margin (Reid, 1994), most of the Labrador Sea conjugate margins (Chian and Loudon, 1994, Chian et al., 1995) and the south-east Australian margin (Finlayson, 1999). All of these formed away from the influence of a hotspot, by the rifting of relatively thin and cool continental crust that was part of an ancient paleo-orogen or a craton (see review in chapter 5). These



margins not only show a lack of significant synrift magmatism during rifting but also structural similarities in their style of continental break-up. Of them, the west Iberia margin has become the type example as in the last two decades a complete data set of geochronological, compositional, petrological and structural information about the crust and mantle have been recovered. These data have been available from 3 Ocean Drilling Program Legs (ODPs 103, 149 and 173) and several reflection and refraction seismic studies.

#### Rifting and spreading history at the west Iberia margin.

The growth of the west Iberia continental margin involved several phases of continental rifting from the Triassic to early Cretaceous (Pinheiro et al., 1996). These were followed by final separation from the conjugate Newfoundland margin as seafloor spreading propagated from south to north during the early Cretaceous (Srivastava, 1988, Figure 1). The first episodes of rifting at the margin are documented in the Lusitanian Basin located onshore in southwest Portugal (Wilson, 1989, Figure 2). This basin is thought to be part of a Triassic basin system formed between Europe, Africa and North America which preceded the opening of the central Atlantic in the Middle Jurassic (Klitgord and Schouten, 1986). The basin is delimited to the west by the Porto-Badajoz-Cordoba suture that separates different terranes of the Variscan Massif (Capdevila and Mougénot, 1988, Figure 2). To the north the Lusitanian basin has been interpreted to continue offshore along the Galicia Interior Basin (Wilson, 1989, Figure 2). This basin constitutes an aborted rift separated from the final break-up margin by the shallow Galicia Bank (Figure 2). The Galicia Interior Basin had been poorly studied and the amounts of extension and mechanisms of deformation remained unknown until now. Previously, only a seismic stratigraphy study based on stacked multichannel seismic (MCS) reflection lines has been carried out in the basin (Murillas et al., 1990). That study suggested that the main extensional phase in the basin is Valanginian (Murillas et al., 1990, 137-132 m.y., *note that throughout this thesis the Mesozoic time scale of Gradstein et al., 1994 will be used*).

The final break-up margin is structurally divided in three segments. From south to north these are: the Tagus Abyssal Plain, the Iberia Abyssal Plain and the Deep Galicia Margin (Figure 2). Offshore west Iberia and Newfoundland anomaly J is the first prominent magnetic anomaly that is observed. This, although not a seafloor spreading isochron, is thought to lie between anomalies M0 to M2 at the Central Atlantic (Rabinowitz et al., 1978, Tucholke and Ludwig, 1982). The J anomaly only exists at the southern part of the Grand Banks and the west Iberia margin, thus implies seafloor propagation from south to north. Although still under debate, seafloor spreading is thought to began at anomaly M11 (~132 m.y.) at the Tagus Abyssal Plain (Pinheiro et al., 1992), during anomaly M3 (~125

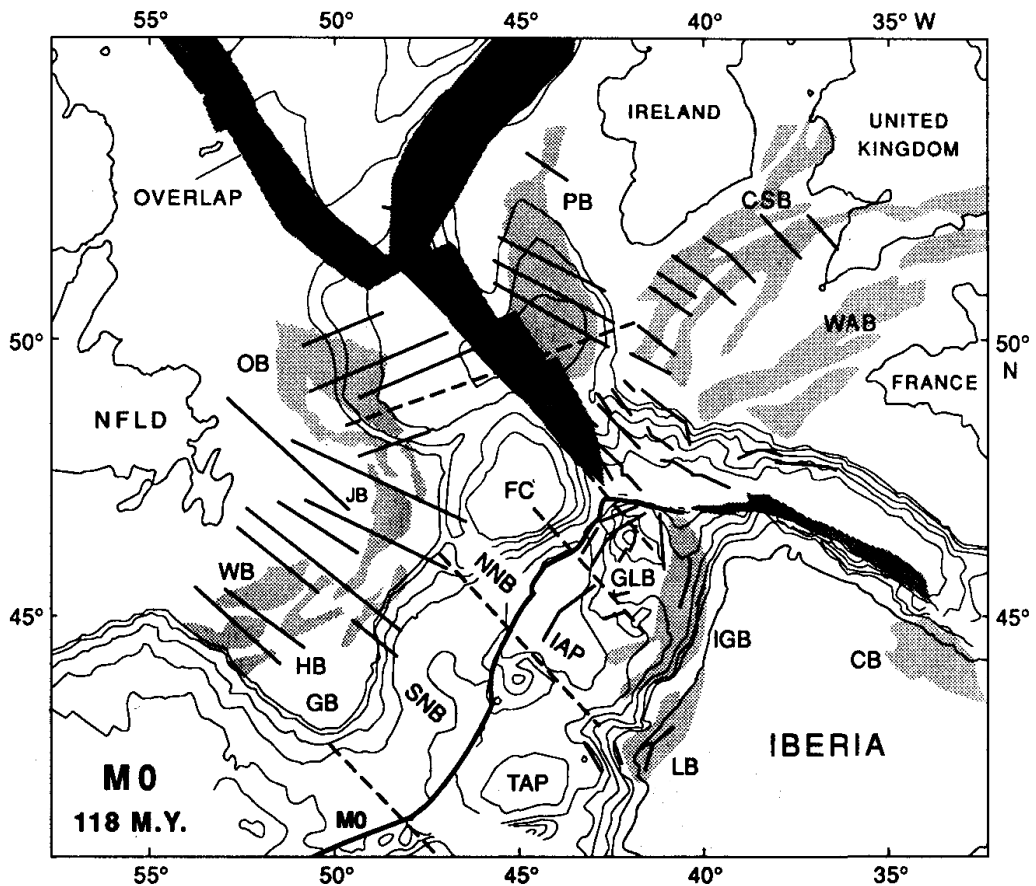


Figure 1. Reconstruction of the North Central Atlantic at chron M0 showing a simplified bathymetry on each plate, outlines of the sedimentary basins (shaded regions), and their plate tectonic features (continuous lines) (fig. 2 of Srivastava and Verhoef, 1992). Also shown are the direction of plate motion (dashed lines) and the resulting overlap between plate boundaries (dark stippled regions). JB = Jeanne d'Arc Basin, WB = Whale Basin, HB = Horseshoe Basin, OB = Orphan Basin, FC = Flemish Cap, CSB = Celtic Sea Basin, WAB = Western Approaches Basin, PB = Porcupine Basin, GLB = Galicia Bank, IGB = Inner Galicia Basin, LB = Lusitanian Basin, CB = Cantabrian Basin, NNB = North Newfoundland Basin, SNB = South Newfoundland Basin, IAP = Iberia Abyssal Plain, TAP = Tagus Abyssal Plain.

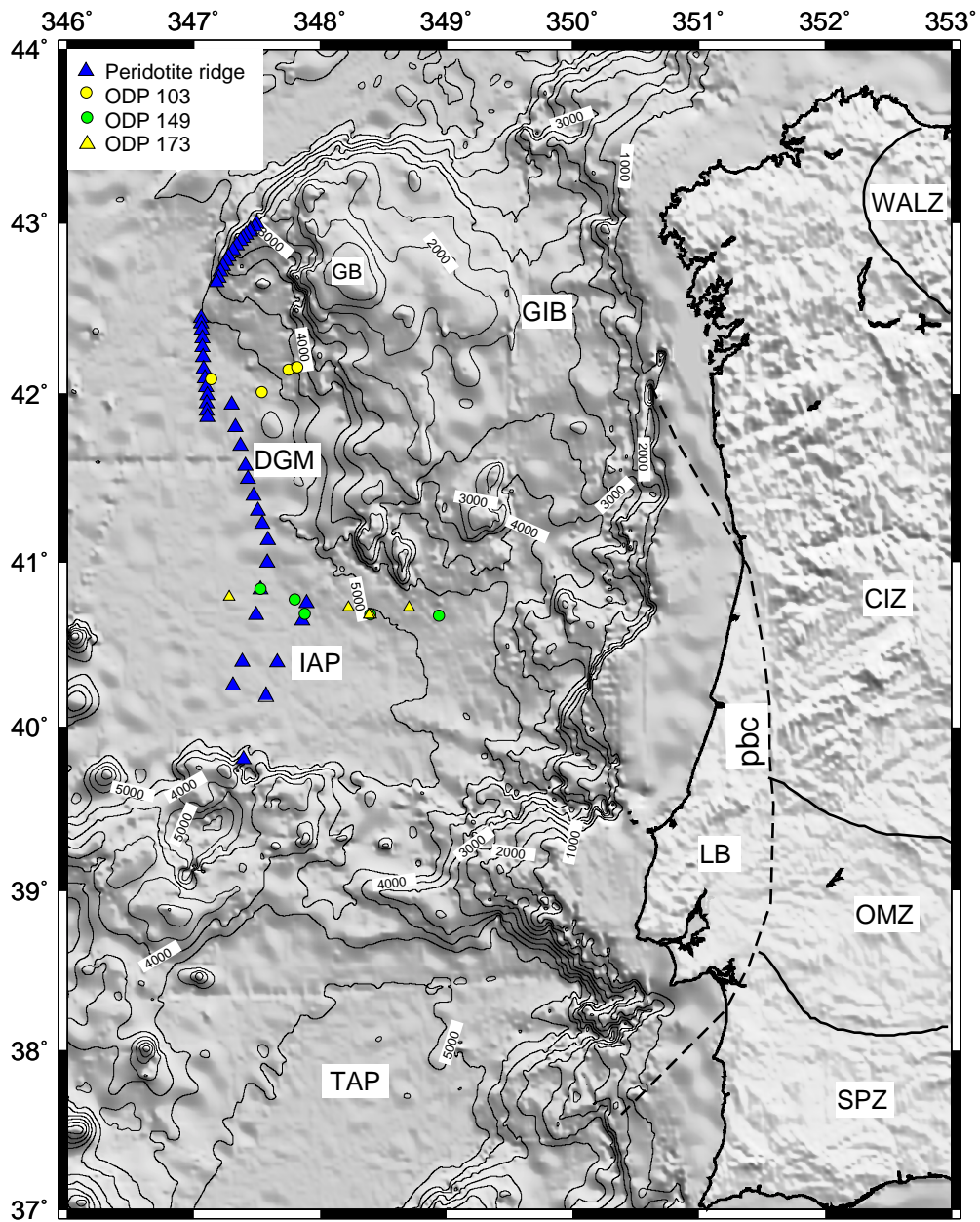


Figure 2. Bathymetric map of west Iberia. The margin is divided in three segments: the Tagus Abyssal Plain (TAP), the Iberia Abyssal Plain (IAP) and the Deep Galicia Margin (DGM). The Galicia Interior Basin (GIB) is located between the continental platform and the Galicia Bank (GB). The position of ODP drillings 103, 149 and 173 are shown. The location of the peridotite ridge is also shown (Beslier et al., 1993). Onshore the terranes of the Variscan massif are indicated (modified from Quesada et al., 1994): CIZ = Central Iberian Zone; OMZ = Ossa Morena Zone; SPZ = South Portuguese Zone; WALZ = West Asturian Zone; LB = Lusitanian Basin. The Porto-Badajoz-Cordoba suture (pbc) runs from south to north separating different terranes of the variscan massif. Its northwards continuation is believed to run offshore along the GIB (Capdevila and Mougénot, 1988).

m.y.) at the Iberia Abyssal Plain (Whitmarsh and Miles, 1995), and at the late Aptian (~112 m.y.) at the Deep Galicia Margin (Boillot and Winterer, 1988).

The Iberia Abyssal Plain and the Deep Galicia Margin constitute the best studied segments of the margin as ODP Legs 103, 149, 173 and most of the seismic surveys have been carried out here. These segments and also other non-volcanic margins of the Iberia type (cited above), are characterised by the lack of a sharp boundary between thinned continental crust and normal oceanic crust. Instead there exists a continent-ocean transition zone (COT) in which the basement appears geophysically to be typical of neither continental nor oceanic crust. It also does not exhibit the clear fault blocks observed further landward in what is clearly continental crust (e.g., west Iberia, Pickup et al., 1996, Krawczyk et al., 1996, Reston et al., 1996, Labrador Sea margins : Keen et al., 1993, Chalmers et al., 1995). It does not exhibit strong linear magnetic anomalies typical of oceanic crust (e.g. west Iberia: Whitmarsh and Miles, 1995, Labrador sea margins: Chalmers and Laursen, 1995, Srivastava and Roest, 1995). Furthermore, it has a velocity structure that differs from both thinned continental and normal oceanic crust (e.g., west Iberia margin; Chian et al., 1999; Dean et al., 1999; Discovery Group, 1998, Pinheiro et al., 1995, Whitmarsh et al., 1996 Labrador sea margins: Chian et al., 1995, Chian and Loudon, 1994, Newfoundland: Reid, 1994, southeast Australia: Finlayson, 1998). Where sampled by drilling or diving, the basement directly beneath the postrift sedimentary cover within the COT has been found to consist of partially serpentinised peridotites (e.g., west Iberia: Boillot et al., 1989, Whitmarsh and Sawyer, 1996, ODP Leg 173 Shipboard Scientific Party, 1998). Continental blocks, when present, appear to float in a sea of peridotites (e.g. west Iberia: ODP Leg 173 Shipboard Scientific Party, 1998; Krawczyk et al., 1996, southwest Greenland: Chalmers, 1997), whereas mafic igneous rocks that are thought to characterise oceanic crust are very scarce.

At the Iberia Abyssal Plain and the Deep Galicia margin, the last stages of continental extension seem to have involved a detachment fault or decollement (Boillot et al., 1989; Reston et al., 1996, Krawczyk et al., 1996; Chian et al., 1999). These detachments separate overlying very thin continental crust (c. 3 km thick, implying a crustal stretching factor of 10) from underlying serpentinised mantle. Landward of these detachments the basement is continental in origin, but oceanward basement consists of exhumed and serpentinised mantle (Boillot and Winterer, 1988, ODP Leg 173 Shipboard Scientific party, 1998, Discovery Group, 1998, Dean et al., 1999, Chian et al., 1999). Thus it appears that these detachments somehow mark a structural boundary between continental crust and serpentinised mantle, and thus may have played an important role in the unroofing of mantle rocks (e.g., Reston et al., 1996). They appear to have controlled final crustal separation (and consequent mantle exhumation), which occurred well before final lithospheric separation and the onset of well established seafloor spreading.

The origin of the continent-ocean transition zone is a matter of much debate. Two hypotheses seem to prevail, i) the continent-ocean transition zone is the product of the first phases of ultraslow oceanic accretion (Whitmarsh and Sawyer, 1996, Srivastava et al., 1998), and ii) the continent-ocean transition zone consists of tectonically exhumed continental mantle with very low synrift magmatic activity (Discovery Group, 1988, Chian et al., 1999, Dean et al., 2000). However, if the start of oceanic accretion is regarded as a transitional process between continental rifting and seafloor spreading, the differences between these two hypotheses may actually be very subtle. The critical element underlying this controversy is understanding how continental rifting evolves into oceanic spreading and which geophysical observations can help characterise this process.

#### Aims of the work and description of chapters

This work is devoted to study the mechanics of continental extension and break-up at non-volcanic margins. Different aspects of the extensional process in continental lithosphere have been studied using several geophysical techniques. The first main topic investigates the tectonic, velocity structure and extensional history of the Galicia Interior Basin, an abandoned rift located between the continental platform and the Galicia Bank (Figure 2). This encompasses chapters 1, 2 and 3. The work includes processing and interpretation of multichannel seismic reflection (MCS) lines and modelling of wide angle data. This is supplemented with petrological and chronological information provided by ODP drillings and a preexisting seismic stratigraphic study in the basin. The first chapter describes the acquisition, analysis and processing up to time migration of a set of MCS lines (AB, and GAP 14, 106 and 15) acquired in the basin during the late seventies by the Western Geophysical Company.

Time migrated sections of lines AB and GAPs were used to identify the interesting areas of the Galicia Interior Basin and plan part of the Iberia Seismic Experiment which took place on July 1997 on board the R/V Maurice Ewing. This survey was a joint American-German project which involved the University of Rice (Houston, U.S.A.), the Institute of Geophysics (Austin, U.S.A), and Geomar (Kiel, Germany). During the cruise MCS and wide angle data were acquired at the Galicia Interior Basin, across the Galicia Bank and into the Deep Galicia Margin. The second chapter describes the processing (up to prestack depth migration) and modelling of a coincident MCS and wide angle line, line 17, acquired during this survey at the Galicia Interior Basin. The detailed image given by the pre-stack depth migration has allowed us to identify the post-, syn- and pre-rift units along the line. This, combined with the existent seismic stratigraphy (Murillas et al., 1990), constrain the age of the main extensional event along line 17 at the Galicia Interior Basin (Valanginian, 137-132 m.y.). An integrated interpretation of the MCS and the wide angle

data reveals the tectonic structure of the basin and its relationship with previous Variscan structures. The mode of deformation of the crust during extension is discussed based on results of the rheological evolution of the crust during extension (developed in chapter 4 and 5) and on the combined structural-velocity image along line 17. In addition, the velocity structure here is compared to that of the anomalous crust at the continental ocean transition zone of the margin and with other areas of highly extended continental crust, e.g. the Rockall Trough. The result of this study suggests that the basin formed along an ancient Variscan suture zone (Porto-Badajoz-Cordoba suture, Figure 2) which separates two different types of crust. The main phase of rifting is Valanginian. The crust at the centre of the basin is continental in nature, the high stretching factors (4-5) that were attained during extension and the low mantle velocity indicate that serpentinisation might have started here. The velocity structure can be explained by uniform pure shear. Based on reasonable initial thermal models for the lithosphere, and modelling results (Hopper and Buck, 1988) it seems unlikely that lower crustal flow occurred.

Chapter 3 presents an interpretation of the time migrated MCS industry lines (AB and GAPS). This, combined with the seismic stratigraphy of the basin (Murillas et al., 1990), reveals the 3D structure and extensional history of the Galicia Interior Basin and generalise the observations made along line 17. At the centre of the basin, the main episode of rifting is Valanginian. Towards the east flanks of the Galicia Bank a second generation of faults that dip westwards is observed to be superimposed in the Valanginian episode. These correspond to a Hautiverian to Aptian extensional phase (132-112 m.y., Murillas et al., 1990) which is coeval to the main rifting that led to continental break-up at the Deep Galicia Margin (Figure 2). We present a new compilation of the available structural and geochronological information at the margin together with the new results from the Galicia Interior Basin. This compilation is used as a basis to discuss the possible causes for rift abandonment at the Galicia Interior Basin.

The last two chapters are concerned with the mechanisms and style of break-up during the last stages of extension at non-volcanic margins. In chapter 4 a numerical model is developed which is motivated by observations made at non-volcanic margins of the west Iberia type. The predictions of the model are compared with the observations made at the Iberia Abyssal Plain and the Deep Galicia Margin segments of the west Iberia margin (Figure 2). The model studies the relationship between the rheological evolution of the crust during extension, the development of decollements during the last stages of rifting and the exhumation of serpentinised mantle at the continent-ocean transition. For this, a one dimensional code was developed (that tracks the temperature field and rheology during uniform stretching of the lithosphere) to calculate at which stretching factors the entire crust moves into the brittle deformation field. We found that the embrittlement of the crust is a key point controlling the onset of serpentinisation and the development of

detachments at the west Iberia margin. When the entire crust is brittle, faults can cut across the crust into the mantle and bring large amounts of seawater to serpentinise it. This may lead to the development of decollements at the base of the crust since serpentinites have a very low coefficient of friction and can develop high pore pressures (Escartin et al., 1997a). Because serpentinites form a weak zone at the base of the crust, extension may focus where serpentinites form which may lead to crustal separation and mantle exhumation along the serpentinite decollements. In the model, extension proceeds as uniform pure shear (Mckenzie, 1978) until the formation of decollements. After this stage, decollements decouple deformation in the crust from deformation in the mantle, producing a departure from pure shear and leading to a more *simple shear-like deformation* mode (Wernicke, 1985).

In chapter 5 we investigate the relative role of melting and serpentinisation in controlling the style of continental break-up at different non-volcanic margins. Non-volcanic margins such as the Woodlark basin, which is an active system located at the eastern tip of Papua New Guinea, do not have a wide transitional zone between continental and oceanic crust. In contrast, the continent-ocean boundary is sharp and the observed faults at the edge of the continental crust have dips only slightly lower than that predicted by fault mechanics. We suggest that the structural difference between this margin and those of the Iberia type lies on the thermal structure of the lithosphere at the onset of rifting. To show this we calculate the potential thickness of serpentinite and the thickness of melt produced by adiabatic decompression of the mantle during rifting. For cool initial thermal states (corresponding to ancient paleo-orogens: west Iberia, or cratons: south west Greenland) and longer rift durations serpentinite production is more important than melting. This leads to margins where serpentinite decollements may occur at the last stages of rifting and serpentinite mantle is exhumed at the continent ocean transition. In contrast, at margins where the initial lithospheric structure is warm (young orogens: Woodlark basin) the lithosphere has little strength, and the margin breaks away well before the temperature at the crustal mantle boundary is low enough to allow the formation of serpentinite. Furthermore more melting will occur than at the west Iberia type margins. Melt intrusions into the lower crust may produce a rotation of the stress field allowing faults to be active at slightly lower angles than those predicted by fault mechanics (Parsons and Thompson, 1993).

## **CHAPTER 1. ACQUISITION, PROCESSING AND ANALYSIS OF INDUSTRY MULTICHANNEL SEISMIC REFLECTION DATA.**

### **1.1 INTRODUCTION**

This chapter describes the processing sequence of a set of industry multichannel seismic reflection (MCS) lines is described. Lines AB, GAP 15, 106 and 14 were acquired by the Western Geophysical Company during 1977 and 1979. These lines were shot across the Galicia Interior Basin as part of a regional survey to investigate its hydrocarbon potential (Figure 1.1). At the beginning of the last decade, the first and only tectonic interpretation of the Galicia Interior Basin was carried out in basis of stack sections of these lines (Murillas et al., 1990). However, in stack sections the morphology of the basement and the faults within it are not well defined, specially if the basement is rough and strongly dipping as in an area that has underwent considerable tectonism. To obtain an image similar to the geological cross section along the seismic lines, these need to be migrated. This chapter describes the acquisition and processing up to time migration of this set of industry lines. Chapter 3 discusses the tectonic interpretation of the lines.

### **1.2 DATA ACQUISITION**

Line AB and GAPs 15, 106 and 14 were shot with a Maxipulse source. Line AB was recorded with a 48 channel, 2.4 km long streamer. Shots were fired at a 50 m interval yielding a 2400% stack. GAP lines 106, 14 and 15 were recorded with a 48 channel, 3.295 km long streamer. The shot interval was 70.1 m, yielding also a 2400% stack.

The Maxipulse system belongs to the dynamite era sources and was used until the 80's. The principle of the system is to let the bubble produced by the dynamite explosion oscillate and record it in an auxiliary channel for each shot. By letting the bubble oscillate all the energy produced by the explosion is used to obtain more penetration into the subsurface. The recorded bubble or source wavelet is used to compress these oscillations into a spike (Fitch, 1979).

In the Maxipulse system the explosive is propelled along a hose by the gun operator until the firing depth (~12 m below the sea surface). One second later the explosion occurs several meters away from the hose (Fig 1.2). The source wavelet of every shot is recorded by 2 hydrophones near the end of the gun hose, therefore each shot gather consists of 48



traces and 2 auxiliary channels where the source wavelet is recorded. The zero recording time is given by the instant at which the gun operator propelles the explosive along the hose. Since the time span that the explosive travels along the hose until it explodes is different for every shot, the zero time of the explosion is also different for every shot (See Fig. 1.3). Therefore the shots need to be brought to the same zero time, this is accomplished by deterministic deconvolution of every shot with its source (see next section).

### **1.3 DATA ANALYSIS**

Processing of the lines was aimed to image the morphology of the basement and deep structures within it. The main steps in the processing of the data were: deterministic deconvolution, statistical deconvolution, multiple attenuation, stacking and time migration (Figure 1.4). Deterministic and statistical deconvolution improve the temporal resolution of the seismogram, stacking yields a zero offset section, i.e. brings source and receiver to a coincident position. Multiple attenuation improves the image of deep structures within the basement. Finally, time migration moves deep reflections into their true subsurface positions and collapses diffractions improving the spatial resolution of the stack section. These steps are thoroughly explained in the next sections.

#### **1.3.1 Deterministic Deconvolution and Brute Stack**

To synchronise the shot gathers and collapse the source bubble oscillations into a spike every shot gather is deconvolved with its source wavelet. Using a two sided operator to perform the deterministic deconvolution, the zero time is moved to the time at which the explosion onset occurs in each shot (Wood and Riley, 1978) (Fig.1.5). Two shot gathers after deterministic deconvolution are shown in Figure 1.6. Although the shot gathers have been brought to the same zero time and reverberations have been compressed, a strong ringy noise that obscures the record at all travel times has been created through this process.

After deterministic deconvolution the traces within shot point (SP) gathers were reorganised into common mid point (CMP) gathers geometry. A CMP gather consists of all the traces within the profile with the offsets (SP-receiver distance) centred in one location and normally it is assumed that a particular arrival comes from the same reflecting point in the subsurface. In practice, the traces within a same CMP often do not come from the same reflecting point but from an area around the reflecting point, as for instance when the reflecting horizon is dipping. Nevertheless, the common reflection point assumption is used

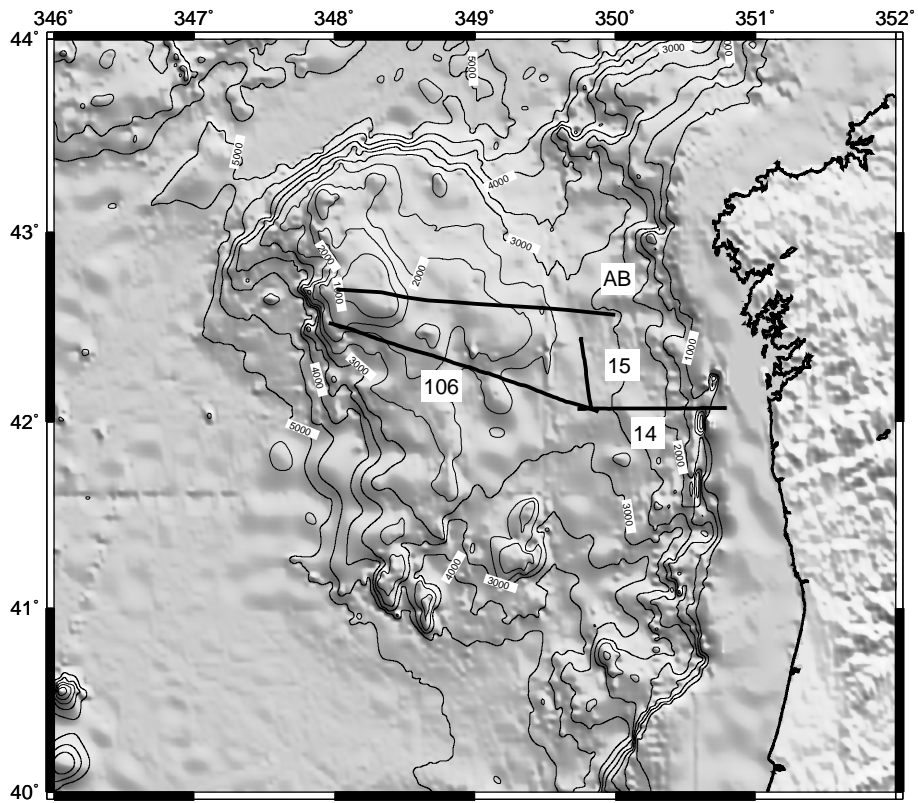


Figure 1.1. Bathymetric map of northwest Iberia. Tracks of multichannel seismic reflection lines AB, GAP 106, 14 and 15 are shown.

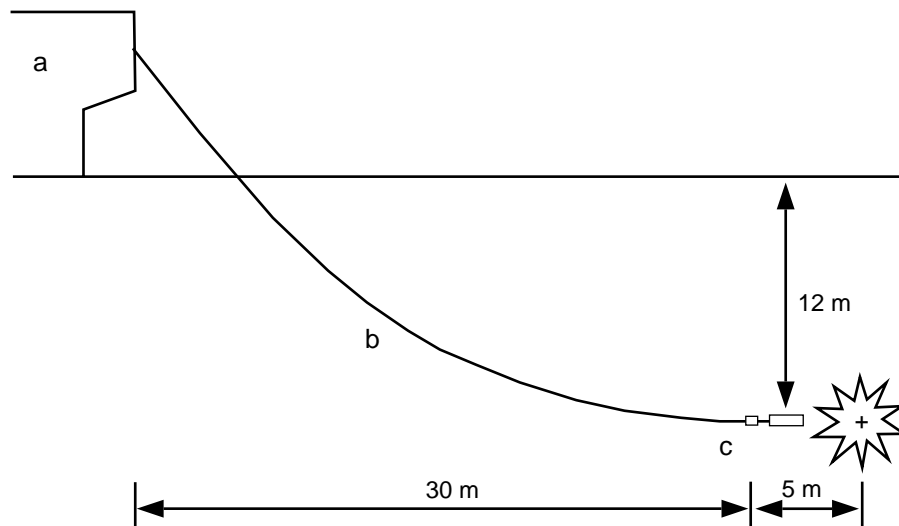


Figure 1.2. Schematic of Maxipulse system; a-shooting vessel, b-hose, c-gun transducer position. Gun transducer- -3db, 0.5 Hz to >10kHz.

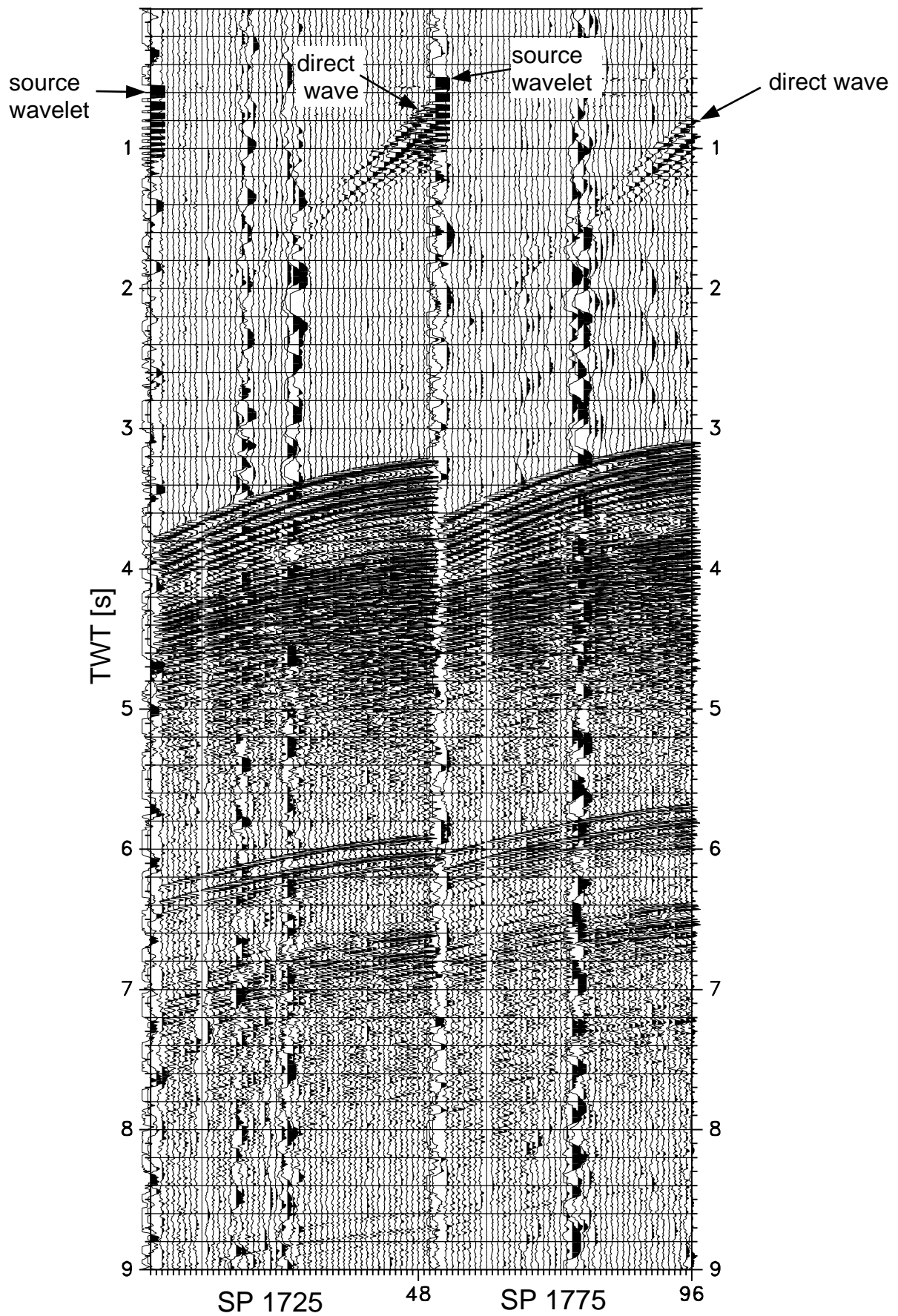


Figure 1.3. Raw shot point gathers 1725 and 1775 of line AB with their respective source wavelets. The shots are displayed in true amplitude and with no frequency filter. Note that the direct waves arrive at different two way times.

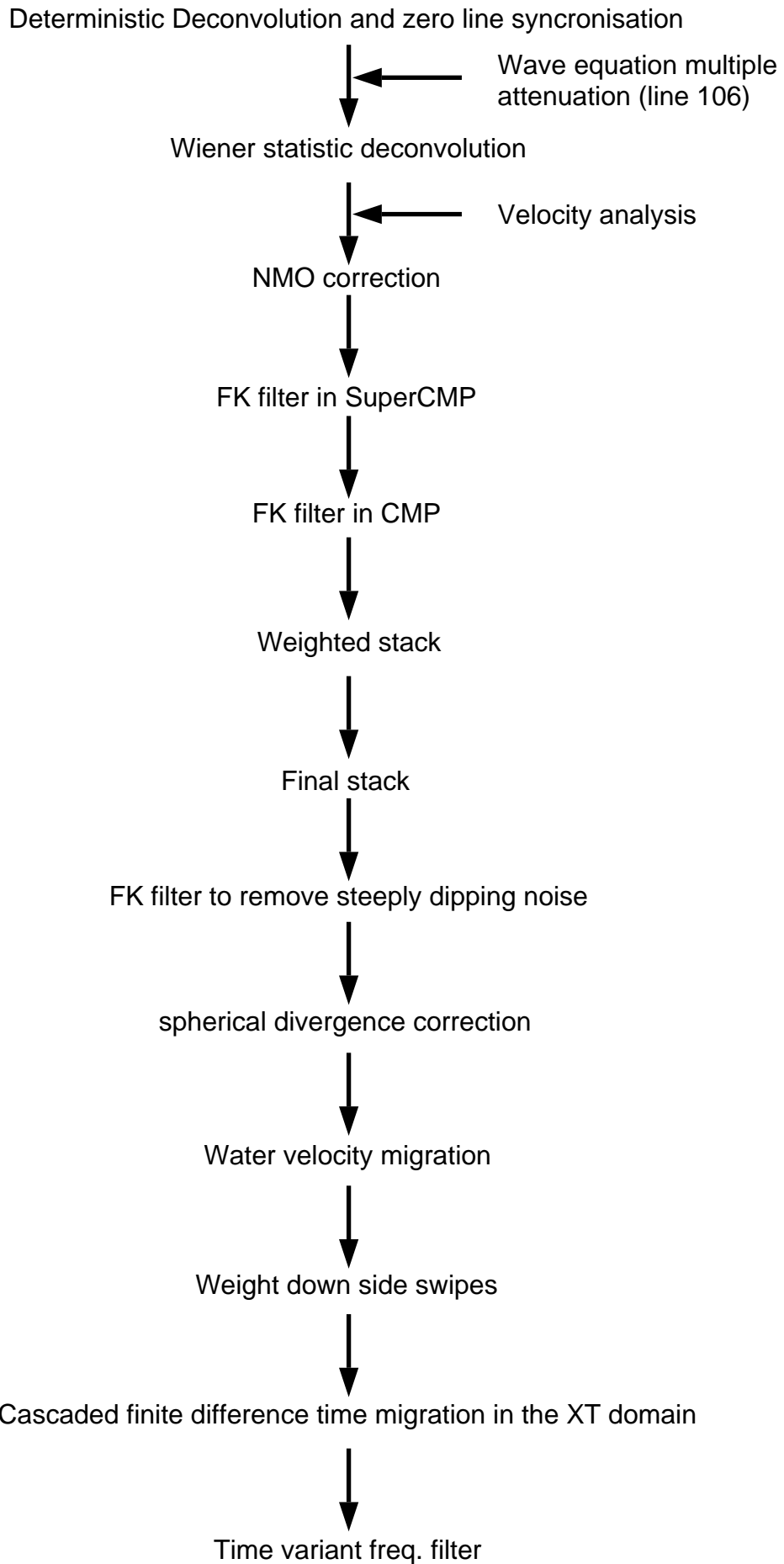


Figure 1.4. Processing flow for MCS industry lines.

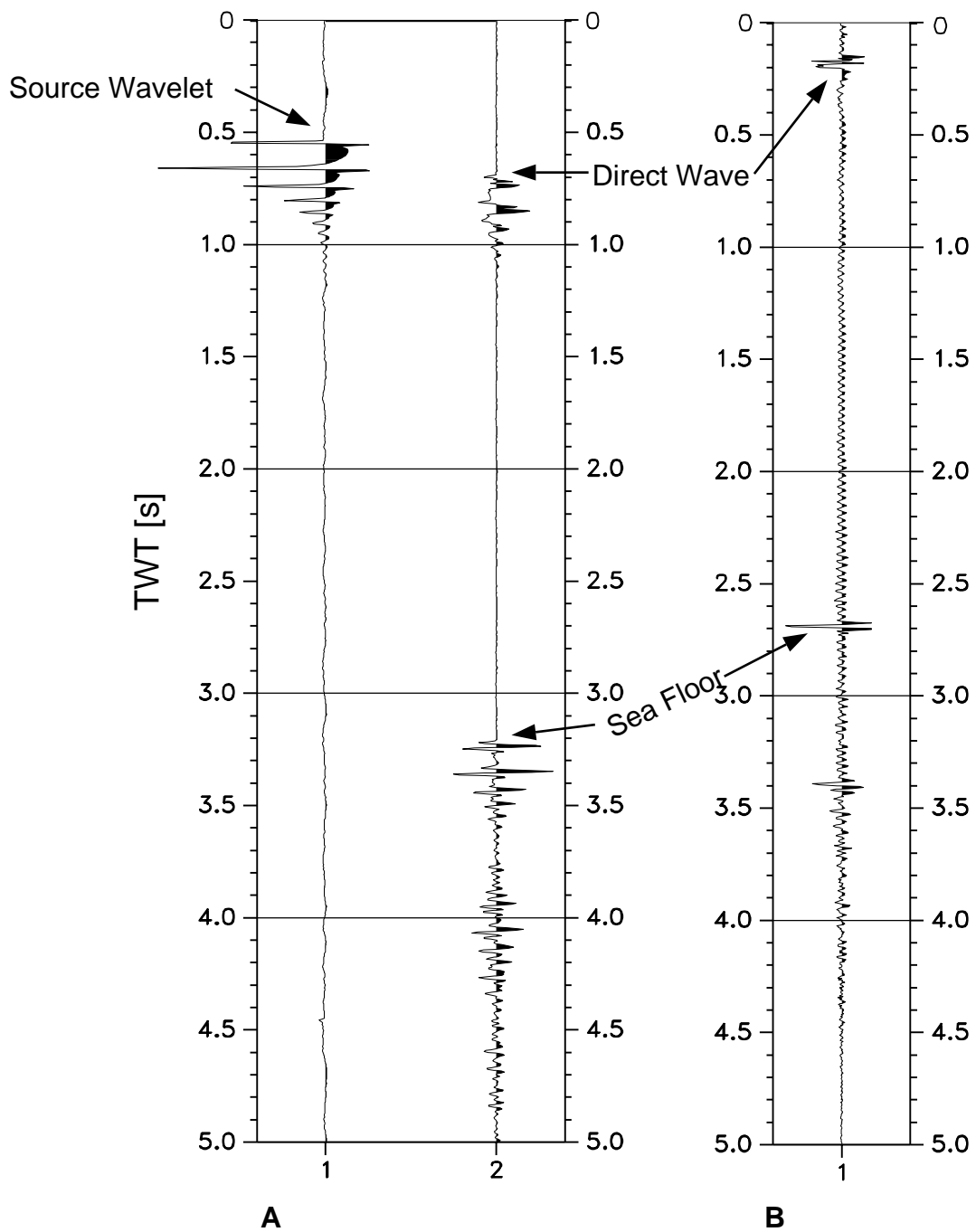


Figure 1.5. **A.** Source wavelet (left) and seismic trace (right). **B.** Deconvolved seismic trace. The deconvolution operator is the inverse of the recorded source wavelet. Note that after deconvolution the zero time is moved to the onset of the source wavelet.

to calculate the Normal Move Out (NMO) correction. This is applied to the traces within a CMP gather to bring at the same time level the reflections coming from the same point at depth, and requires information from the so called Normal Move Out (NMO) velocities (see section 1.3.3). The NMO velocities used in the processing carried out by the Western Geophysical Company were used to correct for NMO and produce the brutestack. Once the NMO correction is applied, the reflections coming from the same location in the subsurface are aligned horizontally and the traces within the CMP can be summed or stacked. Seismic signals coming from a true reflection point sum up coherently and random noise sum up destructively, in this way the signal to noise ratio is increased. The brutestacks of line AB, GAP 106, 14 and 15 are shown in Fig 1.7.

### **1.3.2 Analysis of the Noise**

After deterministic deconvolution two types of noise are present in the shot point gathers (Fig. 1.6):

1. A high amplitude low frequency noise with a frequency range from 1 to 10 Hz that is present through all the record length has been enhanced (Fig. 1.8). This noise was attenuated by statistical deconvolution and filtering

2. A ringy noise created by the deterministic deconvolution (at shot point gather 1725 and 1825). This noise was present in many shot gathers along line AB and has three frequency peaks at 2-3 Hz, 30 Hz and 56-57 Hz depending on the offset distance from source to receiver (Figure 1.9). The lowest and highest frequencies of the noise are outside of the seismic spectrum and could be filtered out. However the 30 Hz frequency is within the signal bandwidth and a band pass filter should not be used. Stacking and statistical deconvolution did not render good results and a thorough analysis was carried out in order to understand how this noise was produced and how to eliminate it. This is presented in the next sections.

#### *1.3.2.1 Analysis of the source wavelet*

The ringy noise observed at SPs 1725 and 1825 (Figure 1.6) is related to instabilities in the deconvolution operator since it only appears after this process. The deconvolution operator is the inverse of the recorded source wavelet, hence these instabilities have their origin in the form and frequency content of the source wavelet. Figure 1.10 shows the source wavelet of shot point gather 1725. Its first amplitude peak is clipped and its amplitude spectrum presents 3 notches at the frequencies that characterise the ringy noise. We analysed with synthetic data the effects that frequency notches and amplitude clipping of the source wavelet have on the deconvolution operator.

First, we tested that the deconvolution algorithm worked properly by deconvolving two identical synthetic traces, one representing a seismic trace and the other the source wavelet. Since the deconvolution operator is the inverse of the source wavelet, the result of the deconvolution is a spike (Figure 1.11).

To investigate the effect of notches in the source wavelet we created a monofrequent notch in the synthetic source wavelet and deconvolved it with the synthetic seismic trace. The result is that, as expected, the deconvolved trace presents a ringy noise of that same frequency (Figure 1.12). Since the real seismic traces also present a frequency notch (Figure 1.13A), we created also a notch in the synthetic seismic trace. After deconvolution the monofrequent ringy noise has been attenuated. The amplitude spectrum of the deconvolved trace is the multiplication of that of the seismic trace (which presents a frequency notch) with that of the inverse of the source wavelet (which presents noise of the same frequency). Ideally this multiplication results in a white amplitude spectrum, this corresponds to a spike in the time domain. In the practice we obtain a spike with a low amplitude monofrequent ringy noise (Figure 1.13B). Clearly, the low amplitude of this noise can not explain the amplitude of the noise observed after deconvolving our real data.

Clipping the amplitude of the source wavelet produces a high frequency notch in its amplitude spectrum. Thereby when deconvolving the synthetic seismic trace with a synthetic source wavelet whose amplitude has been clipped we obtain a spike with noise of high frequency content (Fig. 1.14A). However this frequency ( $\sim 105$  Hz) is much higher than that of the noise observed in the real data ( $\sim 30$  Hz).

To model a similar situation to our real data we deconvolved a synthetic trace with a 30 Hz notch, with a synthetic source wavelet also with a 30 Hz notch and additionally clipped. The result is that the 30 Hz ringy noise is superimposed on the high-amplitude, high-frequency noise (Fig 1.14B) yielding a noise pattern similar to that observed in our real data (Figure 1.6).

### *1.3.2.2 Attenuation of the noise*

To attenuate the noise produced by the deterministic deconvolution we applied a 1/105 Hz band pass filter to the source wavelets along the profile. This method removed the effect of clipping the amplitude of the source wavelet, but not the notch at 30 Hz. However, as previously shown (Figure 1.13B), the effect of the 30 Hz notch during the deconvolution cancels out with the effect of the same notch in the data (Figure 1.14C). Figure 1.15, shows that after filtering the source wavelet, the deterministic deconvolution does not generate noise.

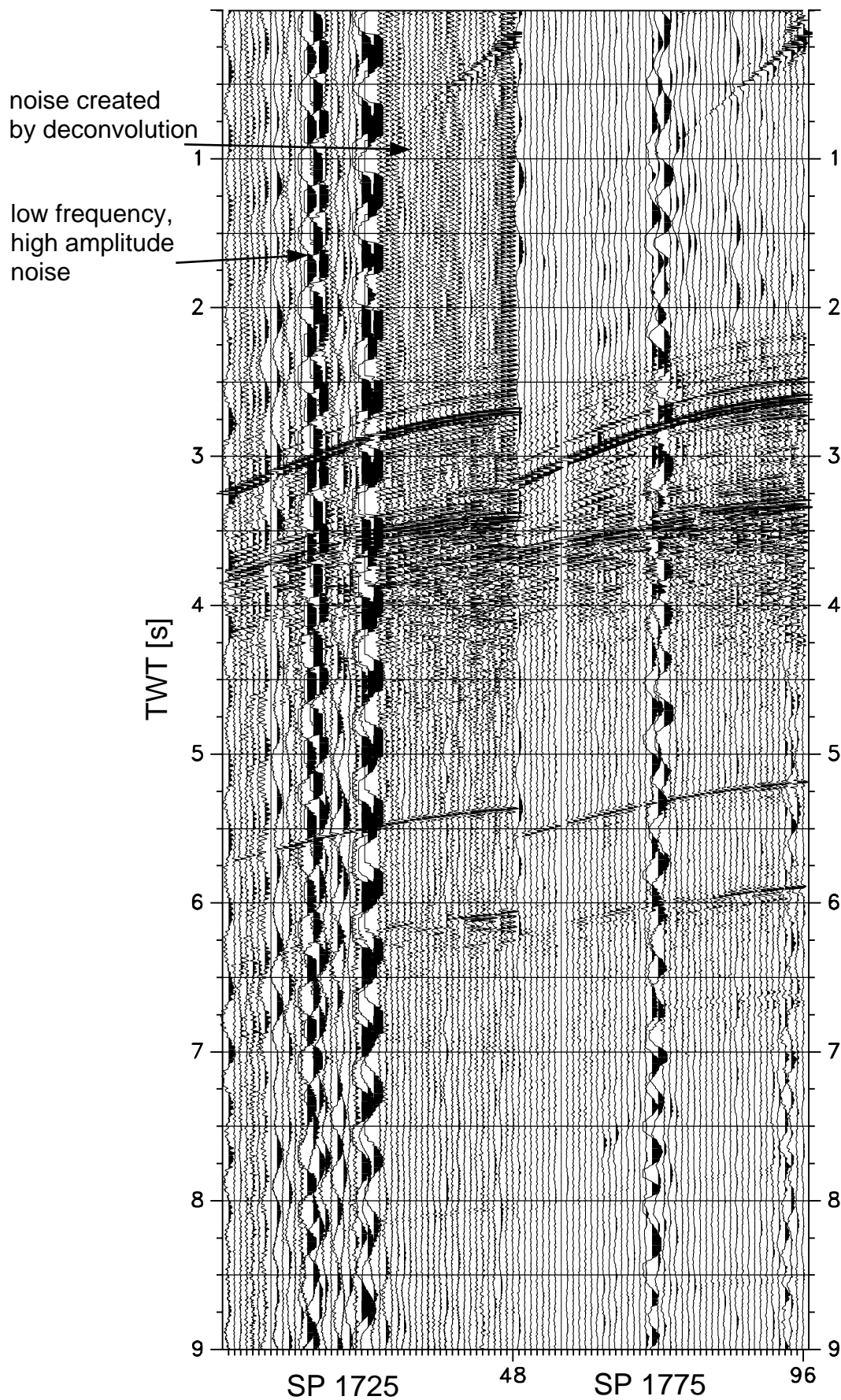


Figure 1.6 A. Shot point gathers 1725 and 1775 of line AB after deterministic deconvolution. The shots are displayed in true amplitude and without frequency filter in order to show the signal to noise ratio. Two types of noise are present: a low frequency high amplitude noise, and a higher frequency noise created by deconvolution. (Figure 1.6 continues in the back).



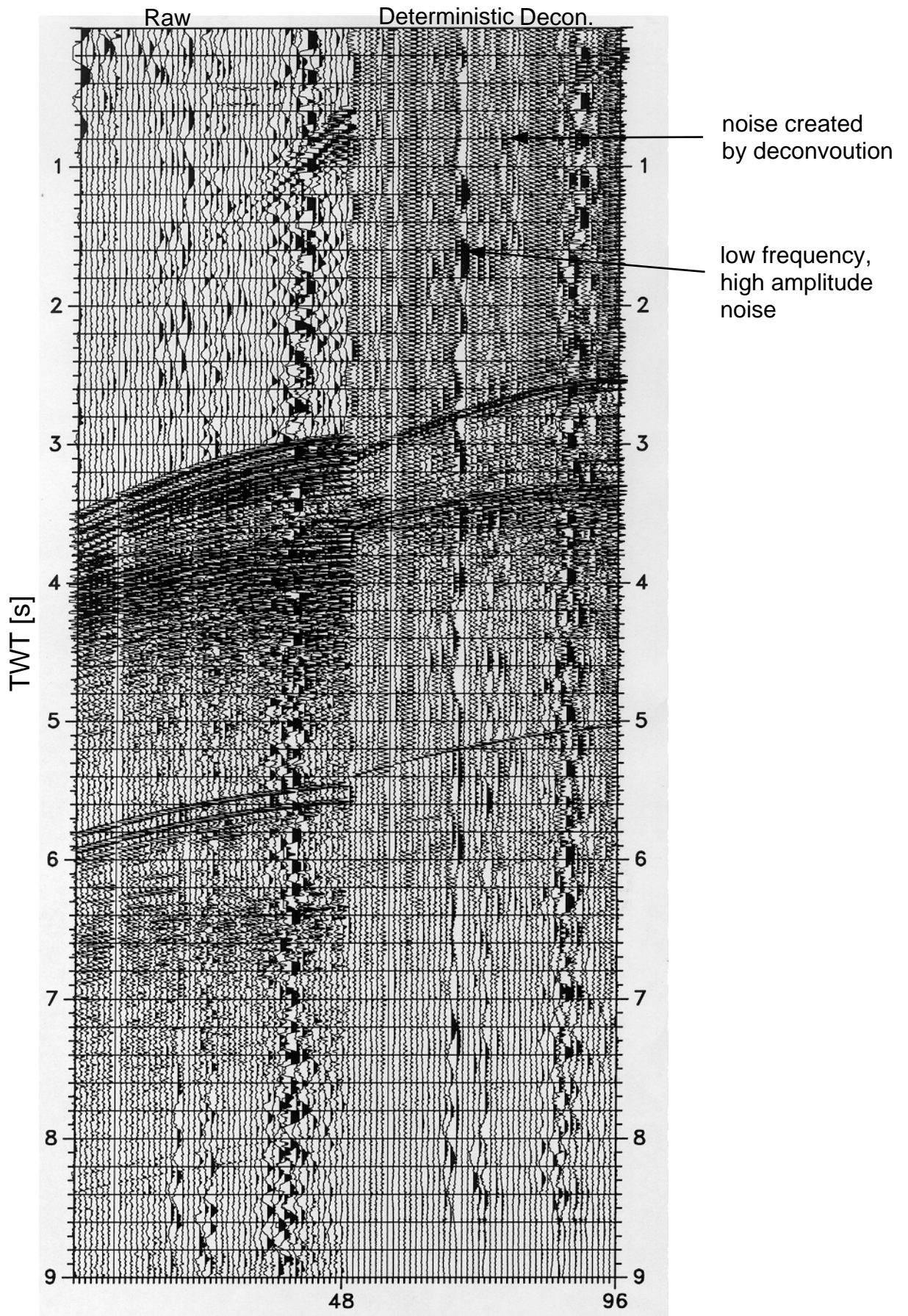


Figure 1.6 B. True amplitude display of shot gather 1825 of line AB before and after deconvolution. Also here the deconvolution process creates a ringy noise.

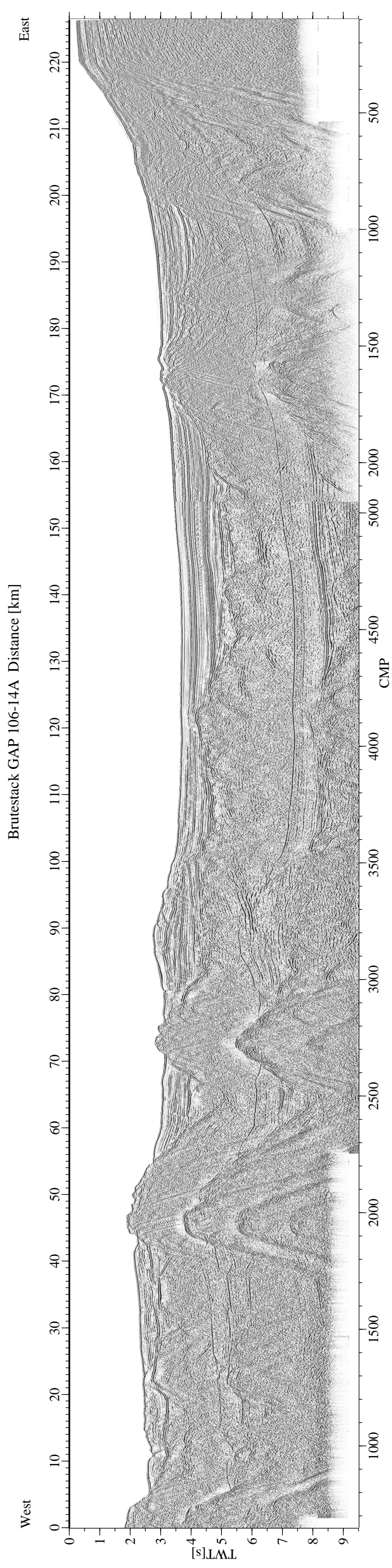
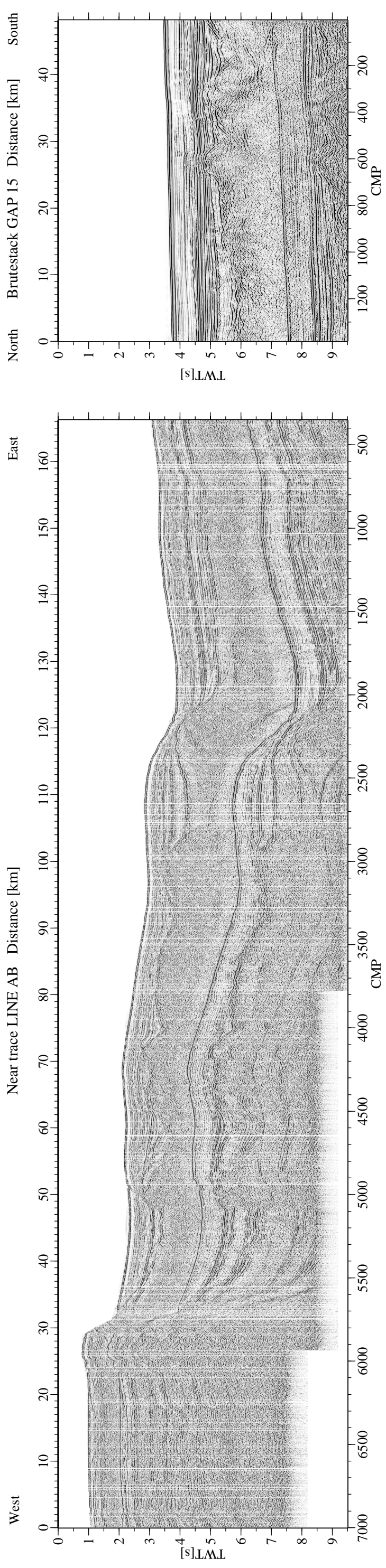


Figure 1.7. Brutestacks and neartrace of lines AB, GAP 106, 14 and 15.

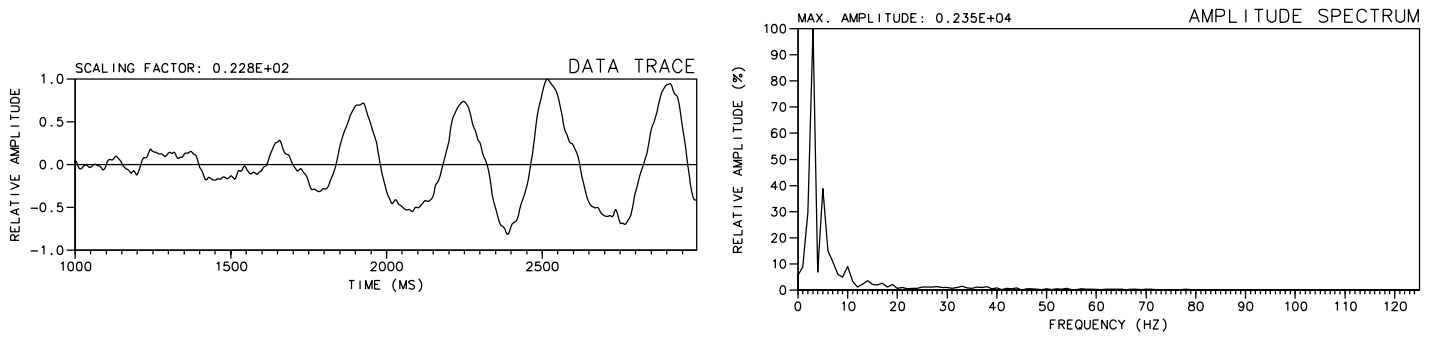


Figure 1.8. (Left) Portion of seismic trace of shot gather 1725 showing high amplitude, low frequency noise. (Right) Amplitude spectrum of the seismic trace shown at the left panel.

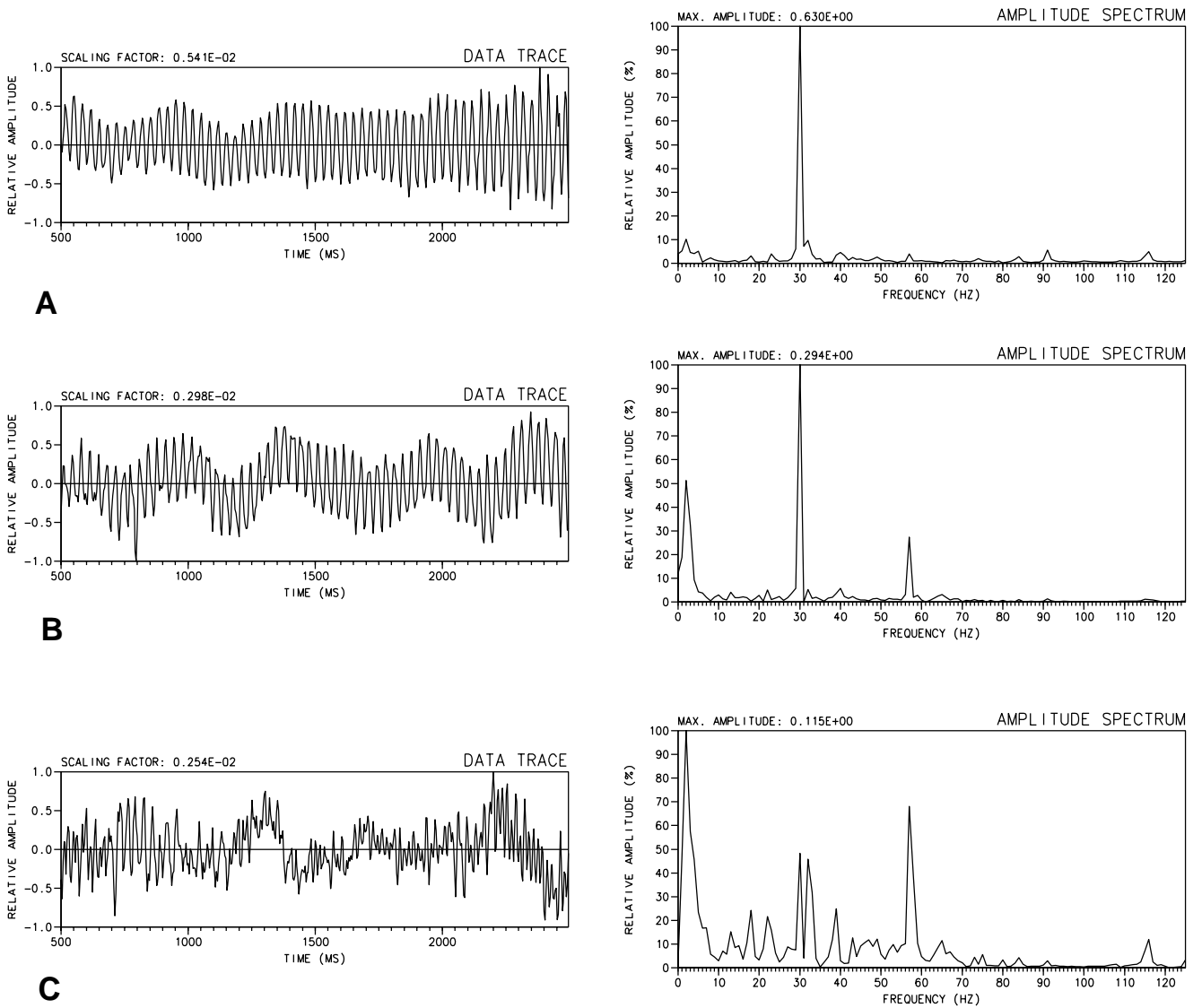


Figure 1.9. (Left) Seismic traces of shot point 1725 showing ringy noise created by deconvolution in a portion of the record above the seafloor. (Right) Amplitude spectrums of data shown at left. **A.** Near offset trace. **B.** Medium offset trace. **C.** Far offset trace. The noise has a high amplitude peak at 30 Hz. A 2-3 Hz and a ~56 Hz frequency picks appear as the distance to source receiver increases.

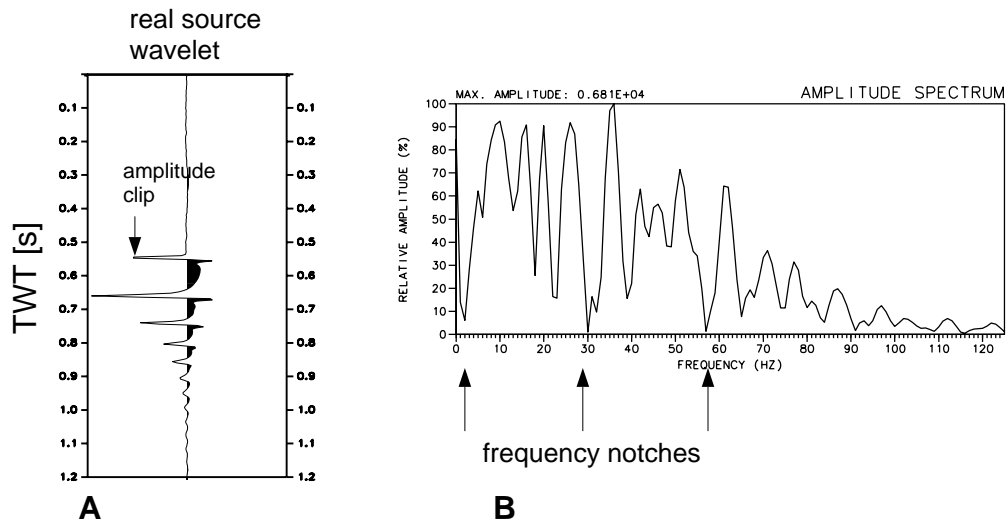


Figure 1.10. **A.** Seismic wavelet of shot gather 1725. Its first amplitude peak is clipped. **B.** Amplitude spectrum of the source wavelet. Frequency notches are present at the amplitude peaks of the noise created by deconvolution (see Fig. 1.9).

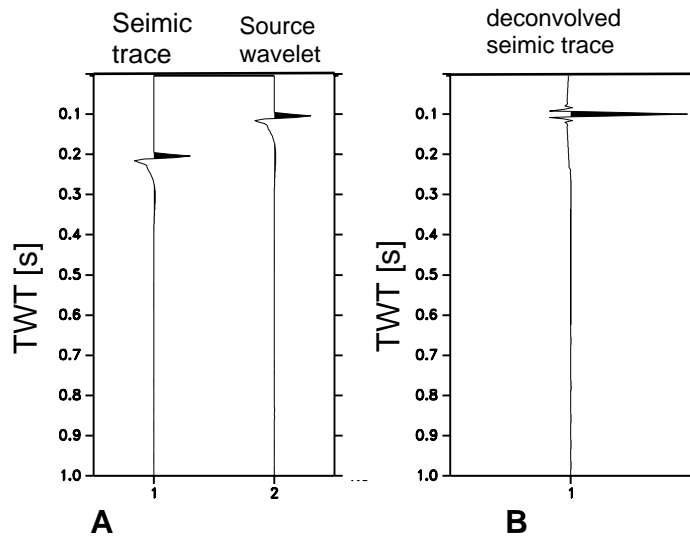


Figure 1.11. **A.** Example of deconvolution of a synthetic trace with a synthetic source wavelet. Both traces are identical but shifted in time. **B.** The result of deconvolution is close to a spike.

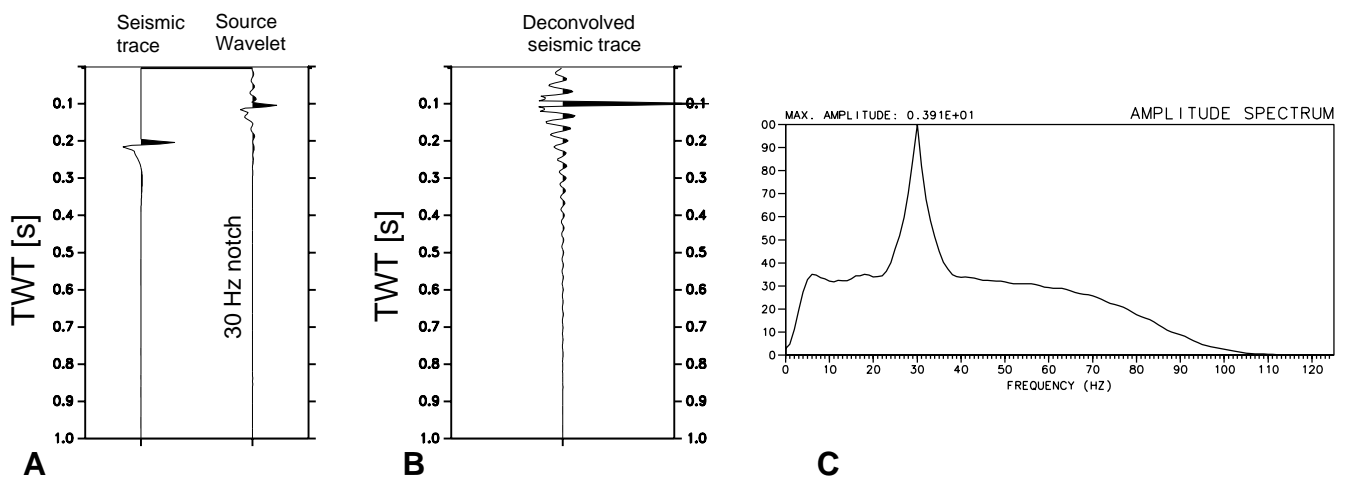
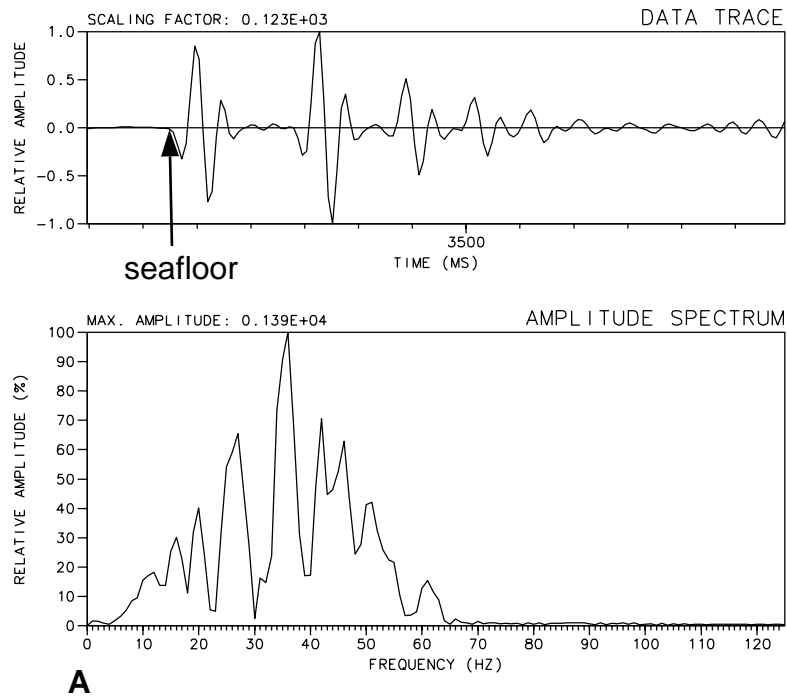
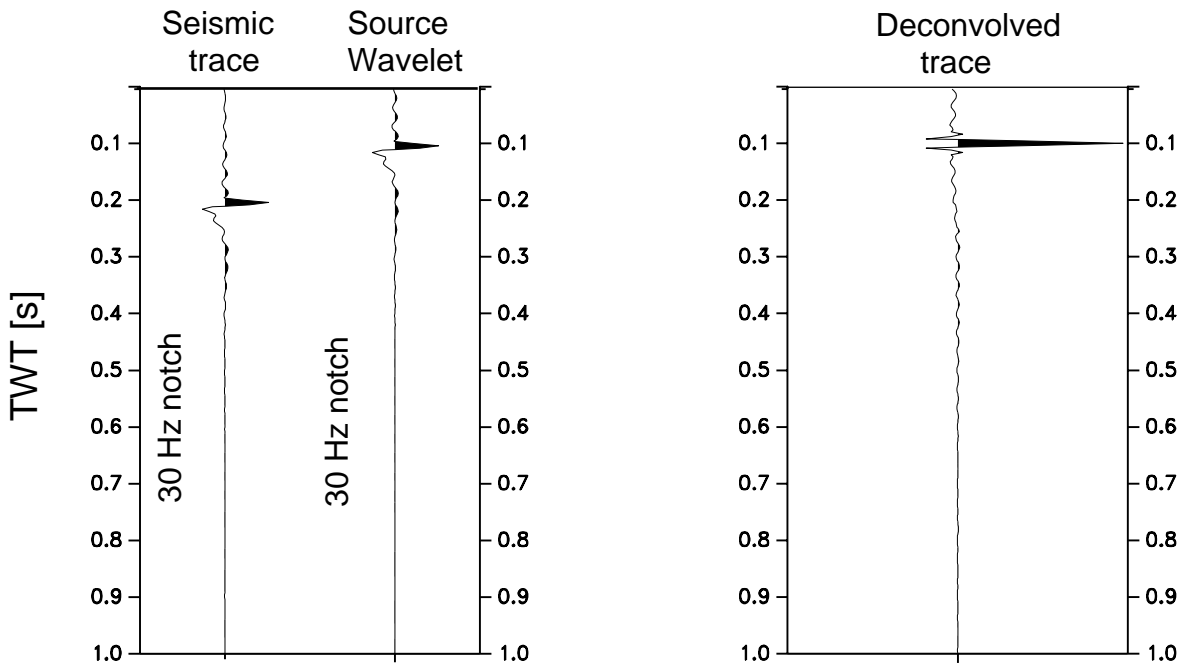


Figure 1.12. **A.** When a synthetic seismic trace (left) is deconvolved with a synthetic source wavelet that is identical but has a 30 Hz frequency notch (right), the result, **B.**, is a spike with ringy noise. **C.** Amplitude spectrum showing that the noise is 30 Hz i.e., the same of the notch in **A.**

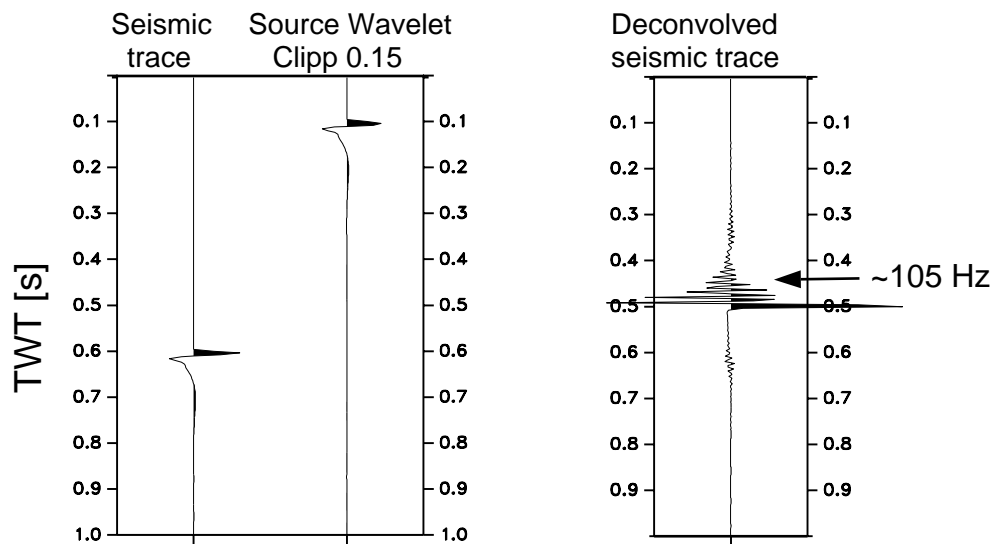


**A**

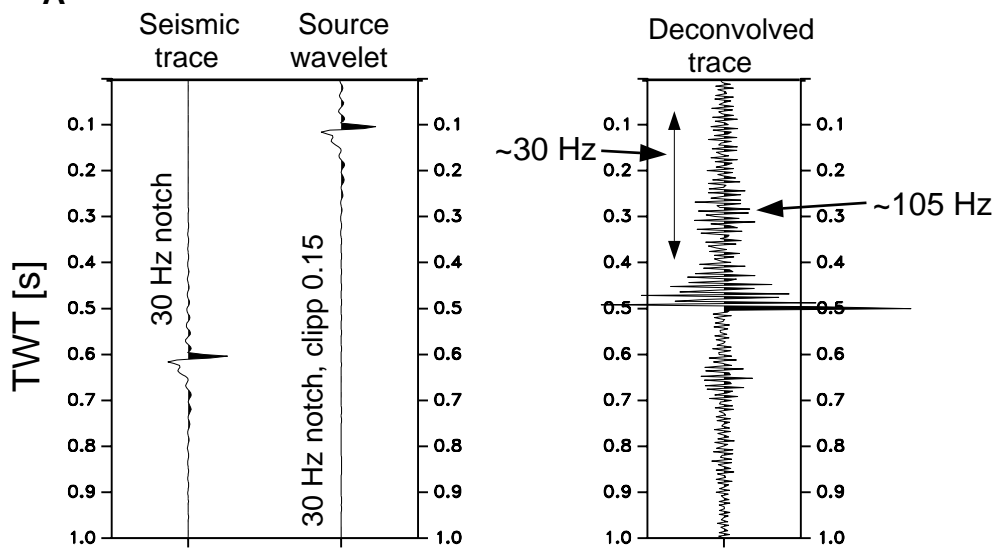


**B**

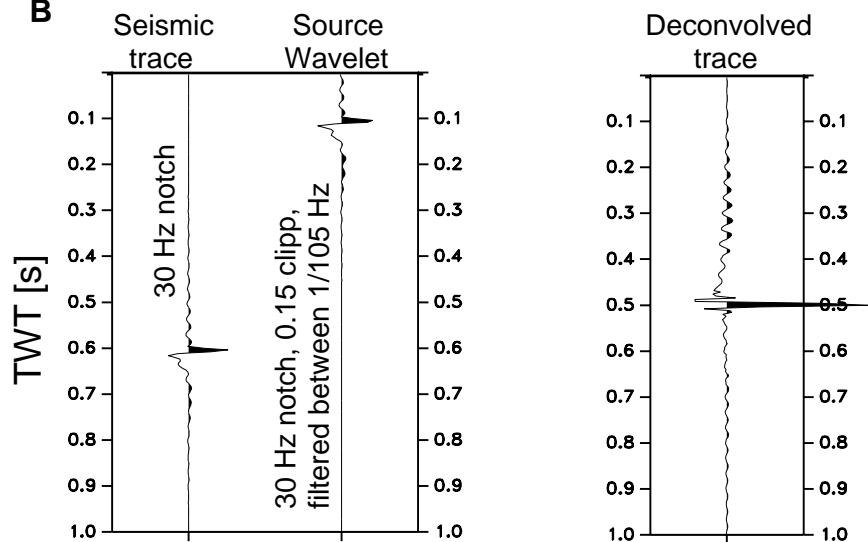
Figure 1.13. **A. (Top)** Seismic trace of shot gather 1725 displaying data near the seafloor. **(Bottom)** Its amplitude spectrum presents a frequency notch at 30 Hz. **B.** When a synthetic source wavelet is deconvolved with an identical synthetic source wavelet, also with a notch of 30 Hz, the result is a spike with low amplitude noise of 30 Hz (compare with Figure 1.12). This low amplitude noise can not explain the ringy noise observed in our real data (figure 1.6).



**A**



**B**



**C**

Figure 1.14. **A. (Left)** When a synthetic seismic trace is deconvolved with an identical source wavelet whose peak amplitude is clipped, the result is **(Right)** a spike with high frequency (~105 Hz), high amplitude noise. This high frequency noise does not explain the noise in our real data. **B. (Left)** The same as in **A**, but now the seismic trace and the source wavelet present a notch at 30 Hz. **(Right)** The result of the deconvolution is a spike with high amplitude and ~105 Hz noise superimposed on a 30 Hz wave train. This noise is similar to that observed in our data. **C. (Left)** The same as in **B**., but with the source wavelet filtered between 1 and 105 Hz, which removes the notch created by the amplitude clipping. **(Right)** The result from deconvolution is spike with very low amplitude, 30 Hz noise.

### 1.3.3 Velocity Analysis and NMO Correction

Within a CMP gather reflections coming from a single point in depth follow a hyperbolic travel time curve. To correct by NMO implies to transform the travel time hyperbola into a horizontal line at the travel time of its apex. Therefore the time difference between any point along the hyperbola and the apex must be calculated. Assuming that the crust is made up of layers of constant velocity, this time difference,  $\Delta t_{NMO}$ , is described, in first order approximation, as a function of the so called Root Mean Square velocity,  $V_{rms}$ , and the offset from the receiver to the source,  $x$ :

$$\Delta t_{NMO} = \frac{x^2}{2V_{rms}^2 t_0}$$

where

$$V_{rms}^2 = \frac{\sum_{i=1}^n V_i^2 \Delta t_i}{\sum_{i=1}^n \Delta t_i}$$

for  $n$  layers  $i=1, \dots, n$ .  $V_i$  is the velocity of each layer, or interval velocity,  $\Delta t$  is the time that the wave travels through the layer, and  $t_0$  is the time at the apex of the hyperbola.

However, the crust is usually not horizontally layered and the reflections do not align along a perfect hyperbola. The velocity which gives the best fit hyperbola to data which are not perfectly hyperbolic is the so called stacking velocity (Sheriff and Geldart, 1995). The stacking velocity is determined from velocity analysis. Velocity analysis are carried out in CMP gathers, where the assumption of hyperbolic alignment is often reasonable. We carried out the velocity analysis every 2.5 km along the profiles, and closer where the topography was rougher. Our velocity analysis consists of 2 series of panels that gives a function of the velocity with time for a single CMP location. The first series of panels shows a CMP gather corrected by NMO with different constant velocities. The second panel consists of constant velocity stacks of 100 consecutive CMPs, where the CMP showed in the first panel is the centre CMP. The stacking velocity at each travel time is the one which gives us a flat event in the CMP gather and the best image in the stacked section. Velocities in the shallow strata are picked on individual CMPs where small variations of velocities produce large NMO changes. Velocities for deep reflections are picked on stack panels where horizon continuity can be better determined. The events being picked were identified in the brute stack in order to pick primary arrivals and not multiples, which usually have lower stacking velocities, or diffractions.

The NMO correction increases with offset and with earlier times. After NMO correction the far offset traces corrected with low velocities (i.e. large NMO) appear stretched and their frequency content is unrealistically low. When stacking, those traces interfere destructively with the near offset traces which contain higher frequencies. To avoid this effect far traces distorted by stretching were muted.

### **1.3.4 Statistical Deconvolution**

To further compress the wavelet and try to recover the true subsurface reflectivity series a statistical deconvolution was applied using an optimum Wiener filter. Assuming that the seismogram,  $s(t)$ , is the convolution of the impulse response of the earth,  $e(t)$ , with the basic seismic wavelet,  $w(t)$ , plus random noise,  $n(t)$ :

$$s(t) = w(t) * e(t) + n(t)$$

then deconvolution tries to recover the reflectivity series, that is, the earth impulse response (Yilmaz, 1987).

Let  $s_k$  be the seismogram,  $f_k$  the filter to determine, and  $e_k$  the desired output: the earth impulse response. The optimum Wiener filter  $f_k$ , is the one that makes the difference between the desired output and the actual output, minimum in the least squares sense:

$$\frac{\partial}{\partial f_i} \sum_{k=0}^n (e_k - s_k * f_k)^2 = 0, i = 0 \dots n$$

developing this becomes:

$$\sum_{j=0}^n \phi_{ww}(i-j) f_j = \phi_{we}, i = 0 \dots n$$

where  $\phi_{ww}$  is the autocorrelation of the source wavelet and  $\phi_{we}$  the crosscorrelation of the source wavelet and the earth impulse response (Yilmaz, 1987). These equations are commonly named the Normal equations, and the number of unknowns they contain is bigger than the number of equations. Therefore some hypothesis need to be made in order to determine the system. Since the source wavelet is not known, its autocorrelation is approximated by that of the seismic trace. This is possible because the earth impulse response,  $e(t)$ , and the noise,  $n(t)$ , are random series and hence their autocorrelation is a



constant value. Thereby the autocorrelation of the seismic trace,  $\phi_{ss}$ , is that of the source wavelet multiplied by a constant value,  $\phi_0$ :

$$\phi_{ss} = \phi_0 \phi_{ww}$$

To compute a Wiener statistic deconvolution in practice requires to give as input the value for the prediction lag, the filter length, the time window for the computation of the filter. Additionally, it can be chosen whether the computation of the autocorrelation is a multichannel process, gather consistent or a single trace process.

Spiking deconvolution, i.e. zero prediction lag, was chosen after thorough testing. From the matricial form of the normal equations it is derived that the length of the filter is the same as that of the autocorrelation of the seismic trace. Therefore the length of the autocorrelation of the seismic trace should be long enough to include that of the source wavelet and short enough to avoid including information about multiples and noise. Commonly, the operator length is obtained by testing and chosen by visual inspection of the results. Since the source wavelets were recorded, we computed their autocorrelation and checked its length, which was 240 ms.

The convolutional model does not take into account the change of the source waveform caused by the attenuation of higher frequencies as it travels through the crust. To consider this effect, the operator was calculated in 3 different time windows: one centred at the sediments, the second at the top basement, and the third one at the last part of the seismic record. Each deconvolution operator was applied at 100% at the centre of each window and interpolated in between. The time windows were at least 10 times longer than the operator length in order to avoid that any strong event had more weight than the rest of the events. The deconvolution was accomplished by computing the operator for every single trace to take into account the change in the waveform with increasing offset. Figure 1.16 shows two shot gathers after statistical deconvolution, note that the seismic signal has been compressed and in addition the high amplitude, low frequency noise has been attenuated (compare with Fig. 1.15).

### **1.3.5 Multiple Attenuation - Final Stack**

Multiples are events that have undergone more than one reflection. Its amplitude is proportional to the product of the reflection coefficients of each reflecting interface. Interfaces with large impedance contrasts, as the water bottom, generate multiples that are strong enough to obliterate, in some cases, primary arrivals. Along lines AB, and GAP lines 106, 14 and 15 the seafloor is at about 3 s TWT and the multiple lies within the basement, where the amplitude of the primary reflections is weak. Since these lines were processed to

image the deep part of the basin which reveals its extensional style, especial attention was paid to multiple attenuation.

At line AB, and GAP lines 106, 14 and 15 multiple attenuation was carried out through dip filtering in the FK domain and weighted stack before stacking. Subsequently FK filtering was locally applied again to the stack sections. At Line 106 the seafloor was very rough and multiple attenuation was very difficult. Therefore, in addition, the wave equation method was applied in the raw shot gathers (after deterministic deconvolution). In the next sections a detailed description of the methods used in all profiles are first explained. Then the wave equation method is described even though it comes prior to the others in the processing sequence.

### *1.3.5.1 Dip Filtering in the FK Domain before Stack*

Dip filtering in the Frequency,  $\nu$ , wave number,  $K_a$ , domain is based on the fact that an event that has a particular dip  $\Delta t / \Delta x = 1 / V_a$ , where  $V_a$  is the apparent velocity of the wave (i.e. ratio of the real velocity to the angle of incidence at the receiver location), in the (x,t) domain, maps as a straight line with the inverse dip in the wave number, frequency domain, ( $K_a, \nu$ ) since:

$$\frac{\Delta t}{\Delta x} = V_a = \nu \lambda_a = \frac{2\pi\nu}{K_a}$$

Events with a positive apparent velocity map on the ( $K_a > 0, \nu$ ) quadrant, while events that have a negative apparent velocity map on the ( $K_a < 0, \nu$ ) quadrant.

Multiple attenuation through dip filtering in the ( $K_a, \nu$ ) domain takes advantage that after NMO correction in the CMP gathers the primaries dip horizontally and multiples dip downward in the (x, t) domain. This allows to differentiate the multiple in the ( $K_a, \nu$ ) domain, filter it out and transform back into the (x, t) domain.

In practice, before FK filtering, after NMO correction a second NMO correction is applied (also called Delta-T correction, Figure 1.17). This is designed in such a way that the primaries and multiples map in a different quadrant of the ( $K_a, \nu$ ) plane. The filter is designed to remove only the signal from the quadrant with multiple energy. The Delta-T correction is designed in such a way that the multiple dips downward but is almost flat in order to avoid spatial aliasing problems (Figure 1.17). When the spacing between traces within a CMP gather is large, the seismic signal might be spatially aliased, this means that its dip can no longer be determined and therefore maps in the two quadrants of the ( $K_a, \nu$ ) domain, making dip FK filtering no longer effective. If the multiple lies almost flat in the

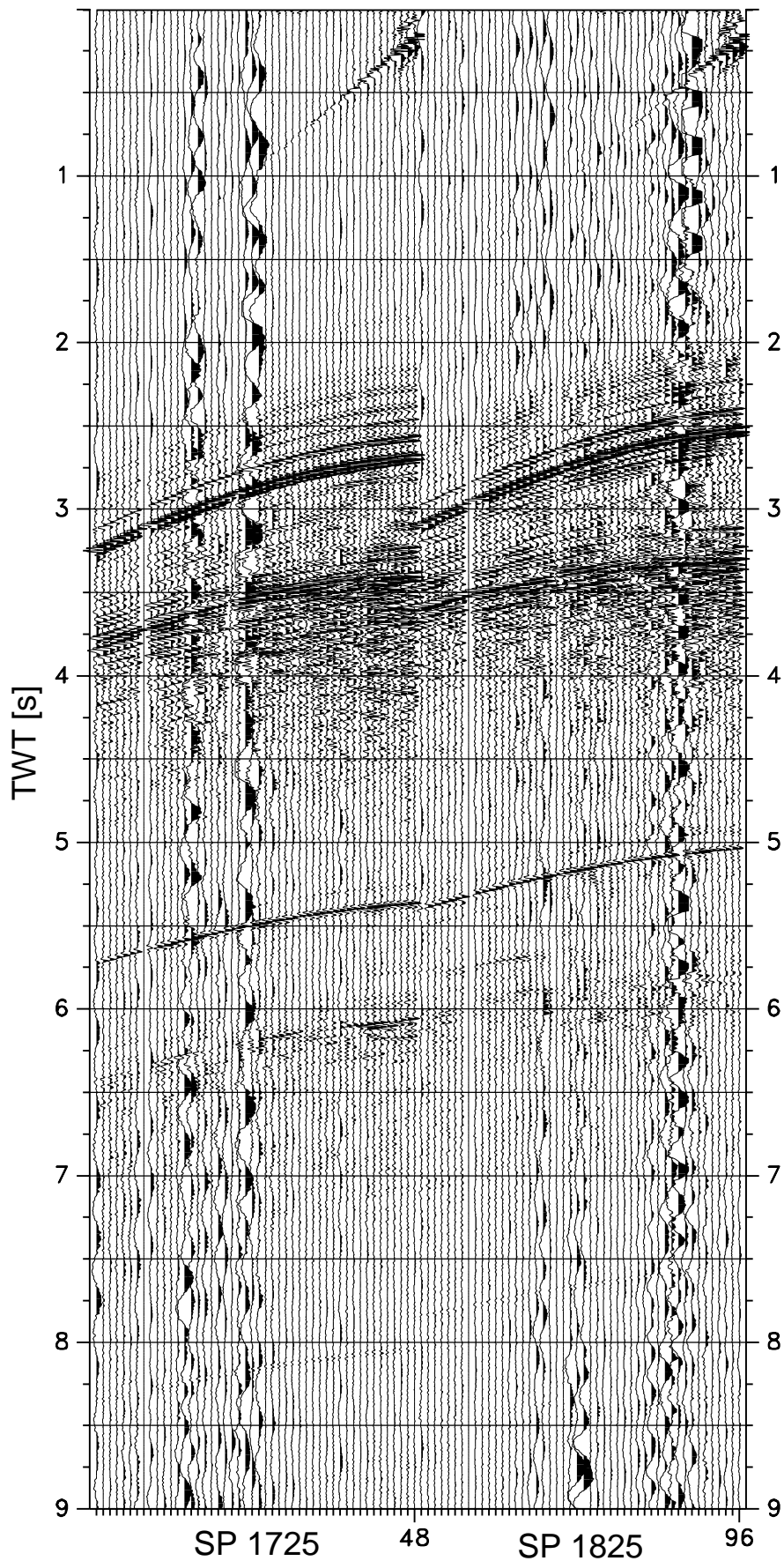


Figure 1.15. True amplitude display of shot gather 1725 and 1825 of line AB after deterministic deconvolution. A 1/105 Hz band pass filter has been applied to the source wavelets before calculating the operator for deconvolution. Note that deconvolution does not produce the ringy noise (compare with Fig. 1.6).

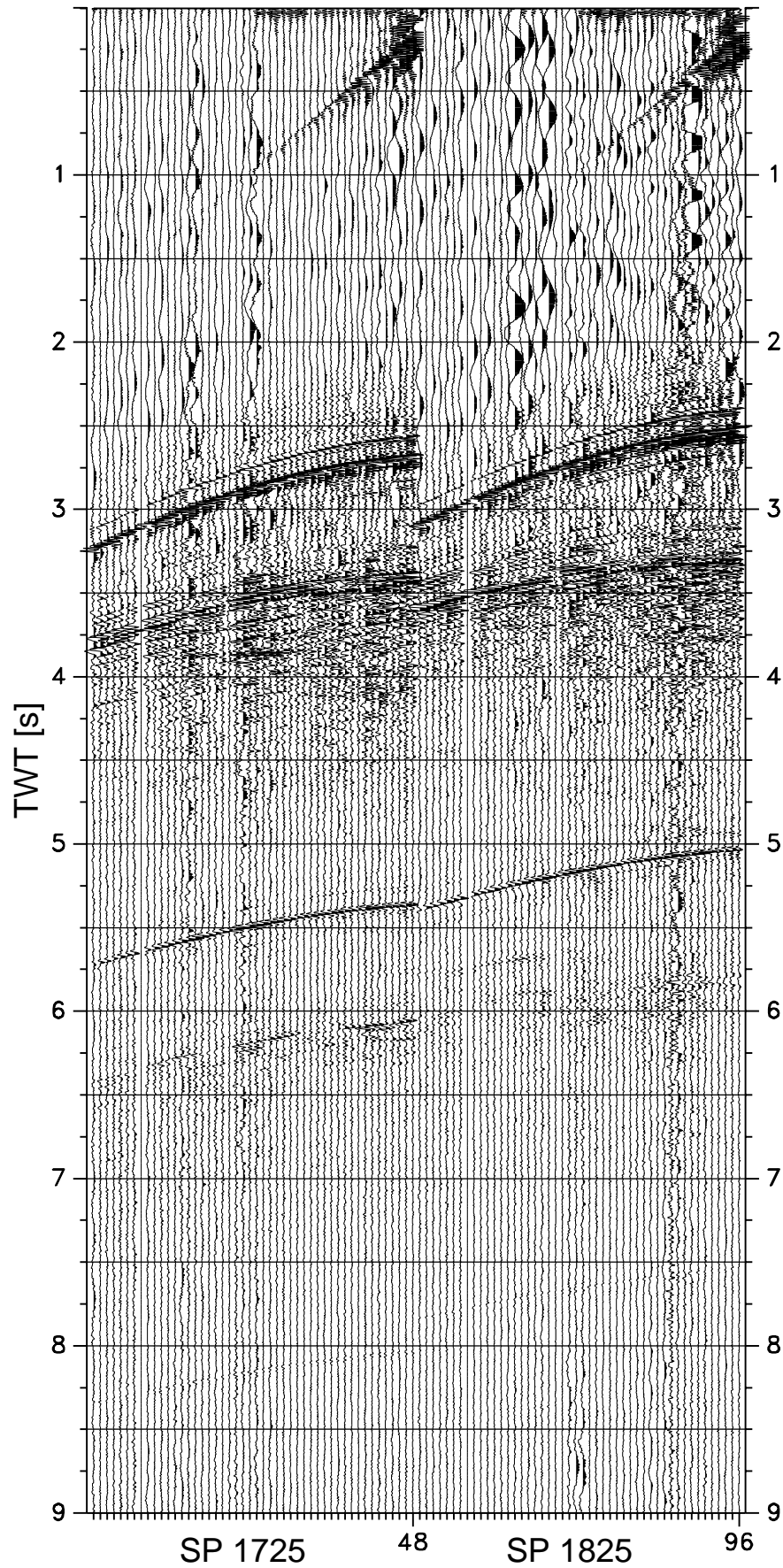


Figure 1.16. True amplitude display of shot gather 1725 and 1825 of line AB after deterministic and statistical deconvolution. Note that the seismic signal has been further compressed and the low frequency, high frequency noise has been attenuated (compare with Fig. 1.15).

(x,t) domain it maps as a near vertical line in the  $(K_a, v)$  domain, and this problem is avoided.

Figure 1.17 shows an example of the multiple of CMPs 1799 and 1800 of line AB. Here the sequence followed to apply the FK filter is shown. After the FK filtering there is still remaining multiple but it dips in the opposite direction than before. This occurs because the data is still spatially aliased. In line AB the spacing between traces within a CMP, 100 m, is too big to sample correctly the waves whose wave length is bigger than the Nyquist wave length,  $K_{aN}$ :

$$K_{aN} = \frac{1}{2 \times 50m} = 0.01m^{-1}$$

To diminish the effect of spatial aliasing we arranged two consecutive CMP gather in a SuperCMP gather (Figure 1.18). In doing so the distance between traces was halved and the Nyquist number doubled, allowing to have higher wave lengths without aliasing. After FK filtering the SuperCMP gather the remaining multiple was filtered out by a second FK filter in the CMP domain (Fig. 1.18), muting of the near traces and weighted stack.

#### 1.3.5.2 Weighted Stack

In the NMO corrected CMP gathers multiples are distinguished because usually they do not align horizontally. In particular, after FK dip filtering, they show little lateral coherency. The weighted stack calculates a measure of the lateral coherency at every time sample and for every trace, and weights down samples which have little lateral coherency. This measure of lateral coherency is calculated, at each time sample, by a Gaussian function which is centered at the amplitude of the pilot trace CMP (the CMP gather stacked trace) and its width is determined by the variance in trace amplitudes at that time. Hence, trace amplitudes which are least similar to the stacked trace are given smallest weights, and traces similar to the pilot trace bigger weights (Sheriff and Geldart, 1995). Figure 1.19 shows an example of multiple attenuation after applying FK filtering and weighted stack.

#### 1.3.5.3 FK Dip Filtering after Stack

Once the previous multiple attenuation techniques were applied multiple energy remained in some areas of the stack section. These were areas where the sea floor dips steeply and hence the multiple arrivals are not hyperbolic in the CMP gathers. Also, in areas where the topography is rough and the multiple of events from slightly outside the plane are difficult to remove. These multiples have usually large amplitudes and smear

across the section during migration obscuring primaries. Hence, a second FK dip filter was applied to attenuate the multiple with steep dips.

#### *1.3.5.4 Wave equation multiple attenuation*

This process was applied on GAP 106 because along this line the seafloor topography is very rough and the multiple beneath rotated basement blocks was very difficult to attenuate. This method is based in the so called wave equation datuming that consists in the extrapolation of the recorded wave field  $\psi = \psi(x, z = 0, t)$  to a new section  $\psi = \psi(x, z = z_1, t)$  which appears as if the sources and receivers had been moved to a different elevation  $z_1$ . This is achieved using a form of Huygen's principle useful in extrapolating seismic waves from one datum to another (Berryhill, 1979, Berryhill, 1984, Berryhill and Kim, 1986). Each receiver is seen as a small loudspeaker which plays back the signal recorded at that position, the signal at a certain point of another datum is the sum of all the signals played back by each receiver in the streamer.

Using wave equation datuming a seismic record can be extrapolated through a round trip traversal of the water layer, thus creating an accurate prediction of the sea floor multiples. In a second step, the record containing the predicted multiples is compared with and subtracted from the original (Figure 1.20).

The input data for the extrapolation process must be sorted in shot point gathers and it must be applied to the raw data. The time, phase and amplitude of the multiple are not well predicted by the extrapolation. Thus time, phase corrections, and amplitude matching are in practice accomplished by 2 different processes. For the time and phase correction the crosscorrelation of the observed and the simulated multiple is carried out. The time shift can be determined from the position of the envelope of the crosscorrelation. The phase shift from the value of the instantaneous phase at the position of the envelope maximum. The amplitude of the predicted multiple is subsequently multiplied by the quotient of the product of the amplitude of the real and predicted multiple to the square of the predicted amplitude for each time sample within a window centred in the sea floor multiple.

The final stacks of lines AB and GAP 106, 14 and 15 are shown in Figure 1.21.

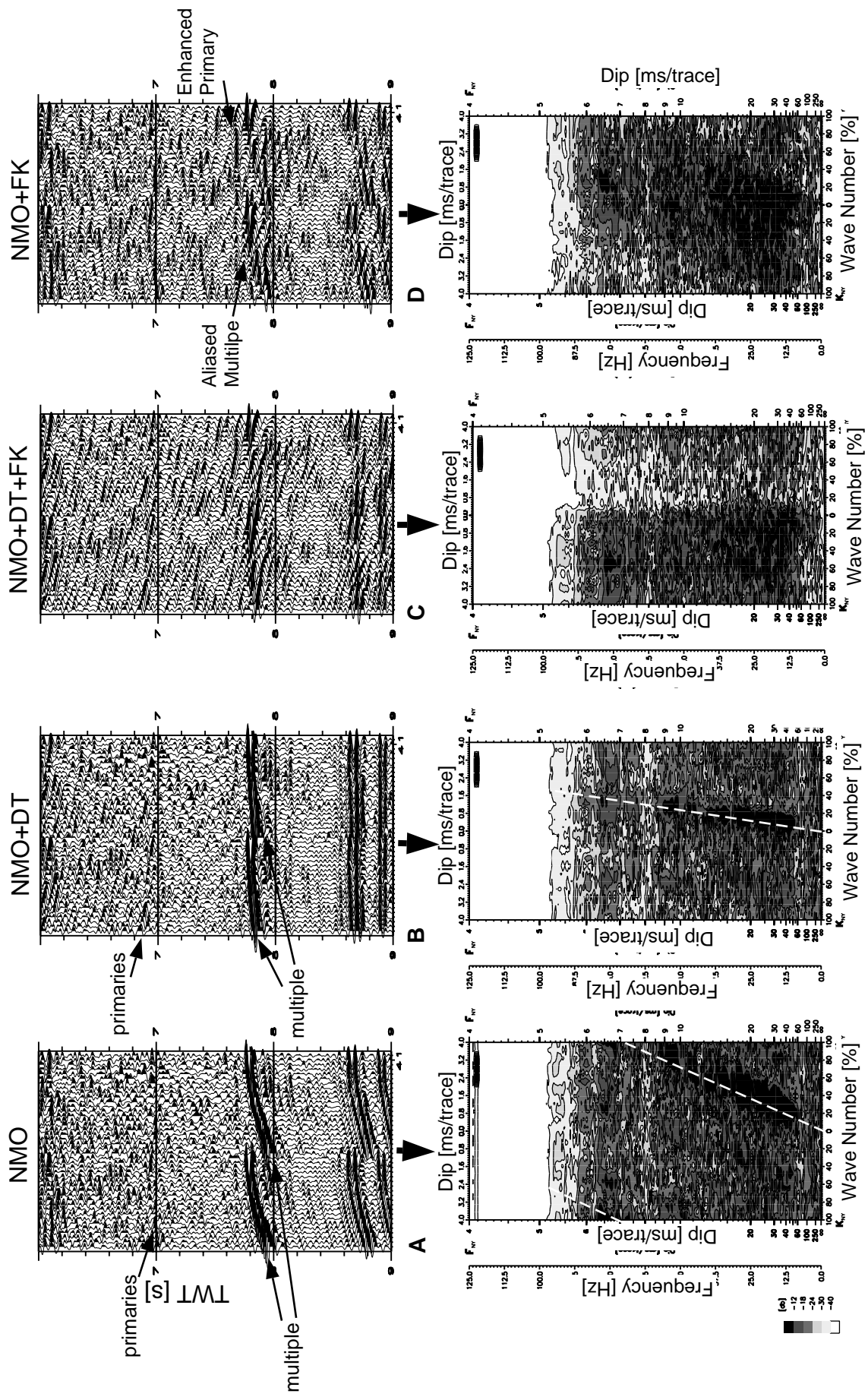


Figure 1.17. Example illustrating the effect of spatial aliasing of the multiple in FK filtering. **Top:** Multiple of CMPs 1799 and 1800 of line AB. **Bottom:** FK spectrum of the multiple, the white stippled line indicates the centre dip of the multiple **A.** CMPs after NMO correction. Note that the aliased multiple maps on the left quadrant of the spectrum. **B.** CMPs after NMO and Delta T correction (see text). The multiple dips shallowly and the primaries dip upward. The multiple maps now nearly vertical in the FK spectrum. **C.** The same as in **B.**, after filtering out the multiple. **D.** The same as in **C.**, after removing the Delta T correction. Part of the multiple is removed but there some aliased multiple is still present.

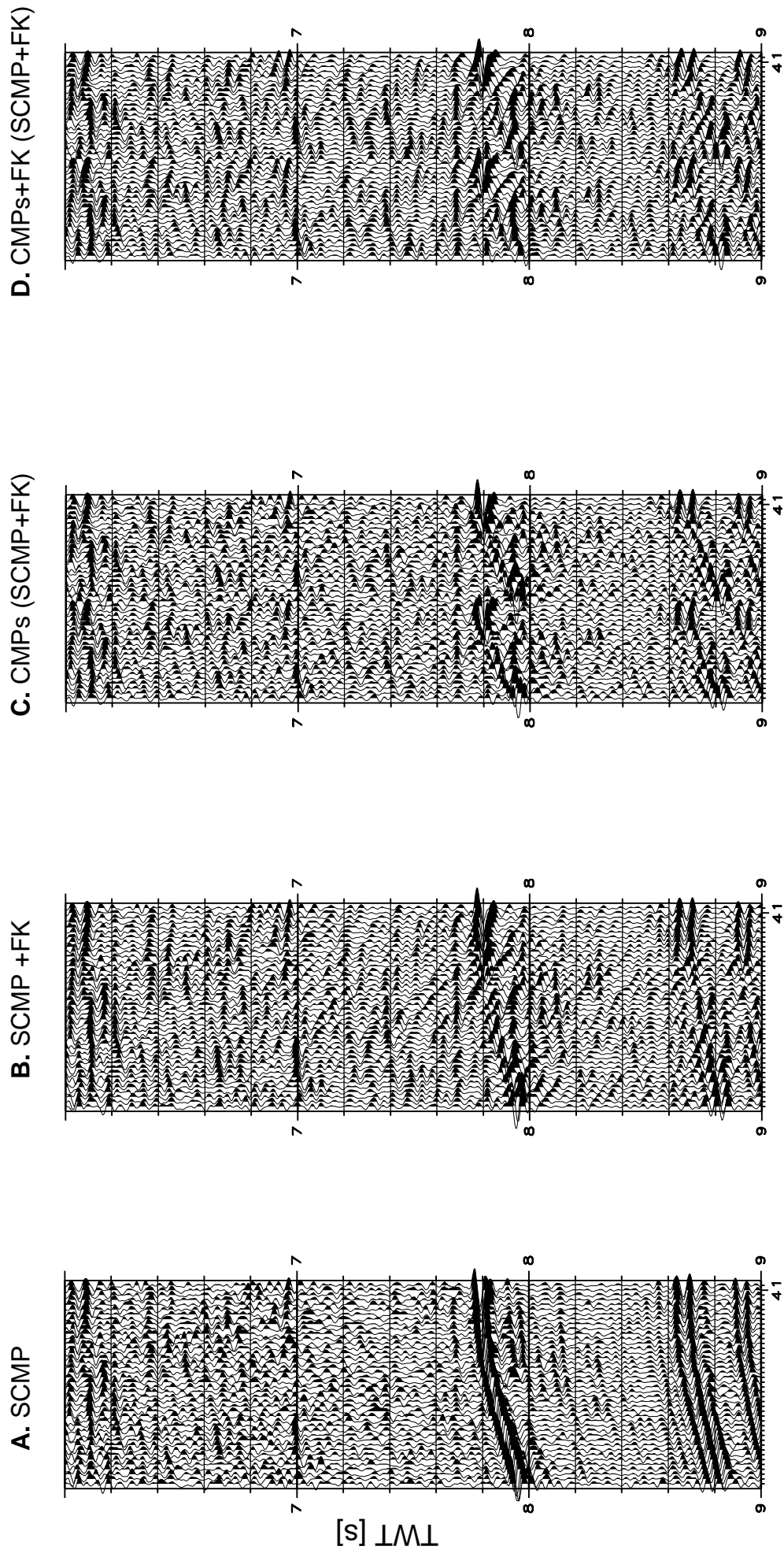


Figure 1.18. Example of FK filtering sequence followed in the processing of the seismic lines. **A.** SuperCMP gather of CMPs 1799 and 1800 of line AB corrected by NMO. **B.** Same as **A.** after FK filtering. **C.** Rearrangement of **B.** back to CMP gathers. **D.** Same as **C.** after second FK filtering in the CMP domain.



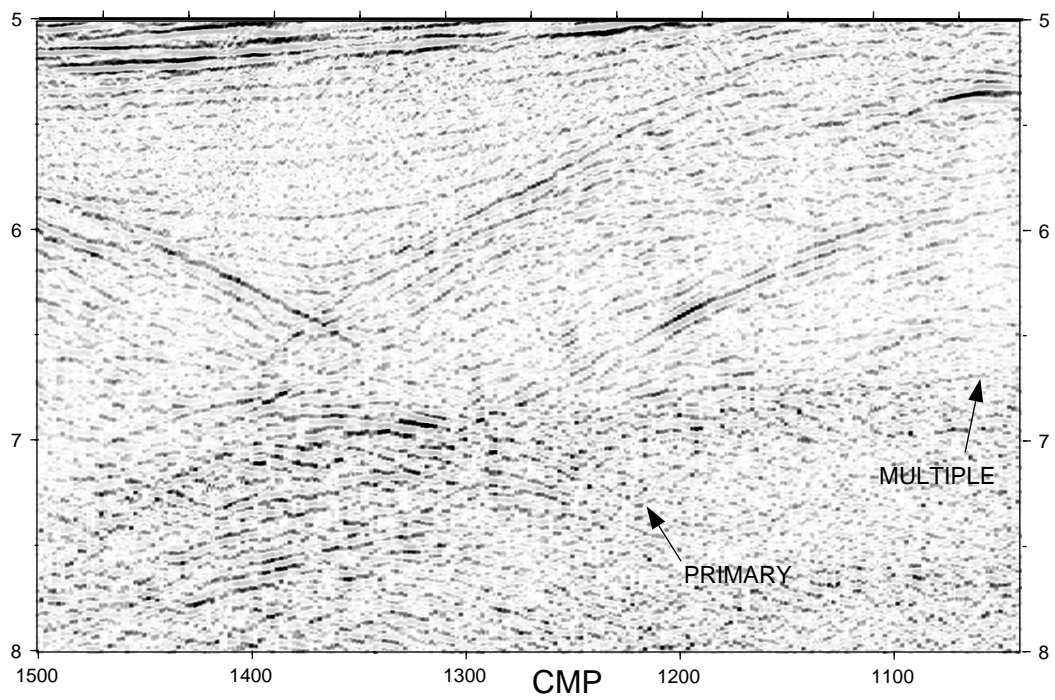
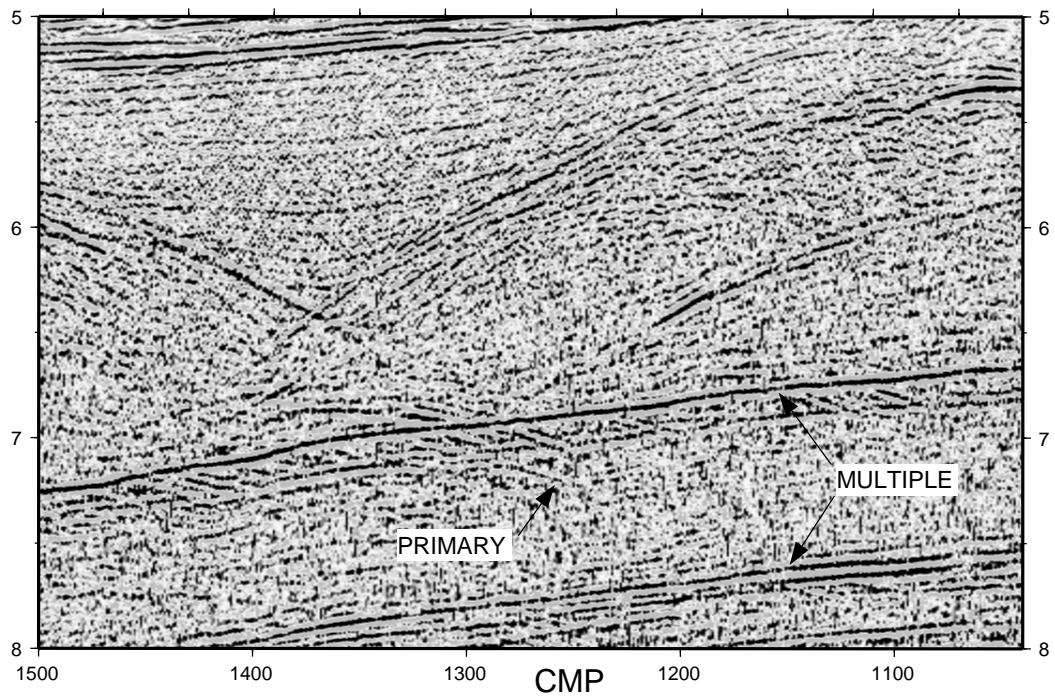


Figure 1.19. Example of multiple attenuation on line AB. **(Top)** Brute stack. **(Bottom)** Final stack.

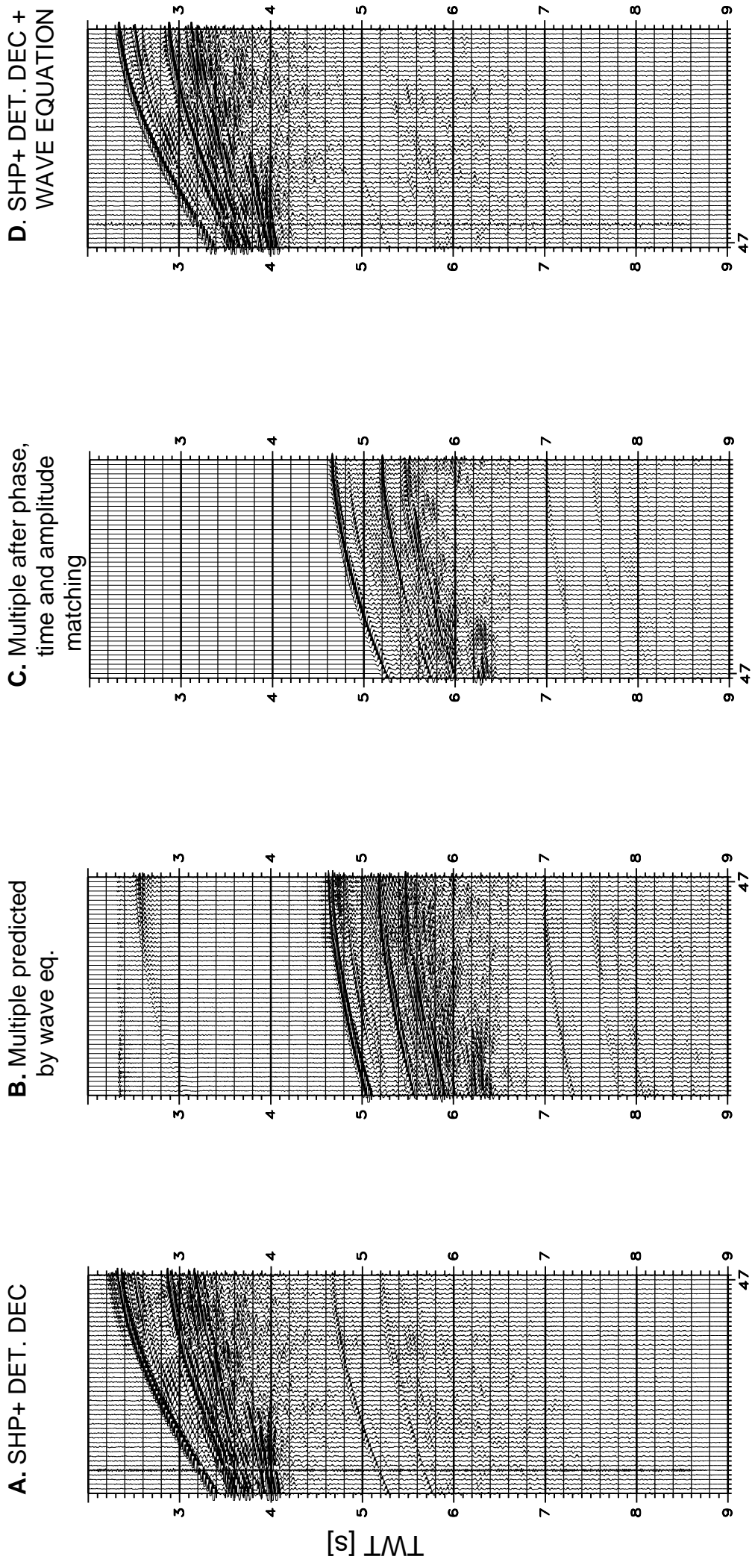


Figure 1.20. Example of the wave equation method to attenuate the water layer multiple in shot point gather 725 of line 106. **A.** Raw shot point with deterministic deconvolution. **B.** Multiple predicted by wave equation method. **C.** Predicted multiple after phase, time and amplitude matching with the real multiple. **D.** Final result of wave equation after subtraction of the predicted multiple from the shot gather.

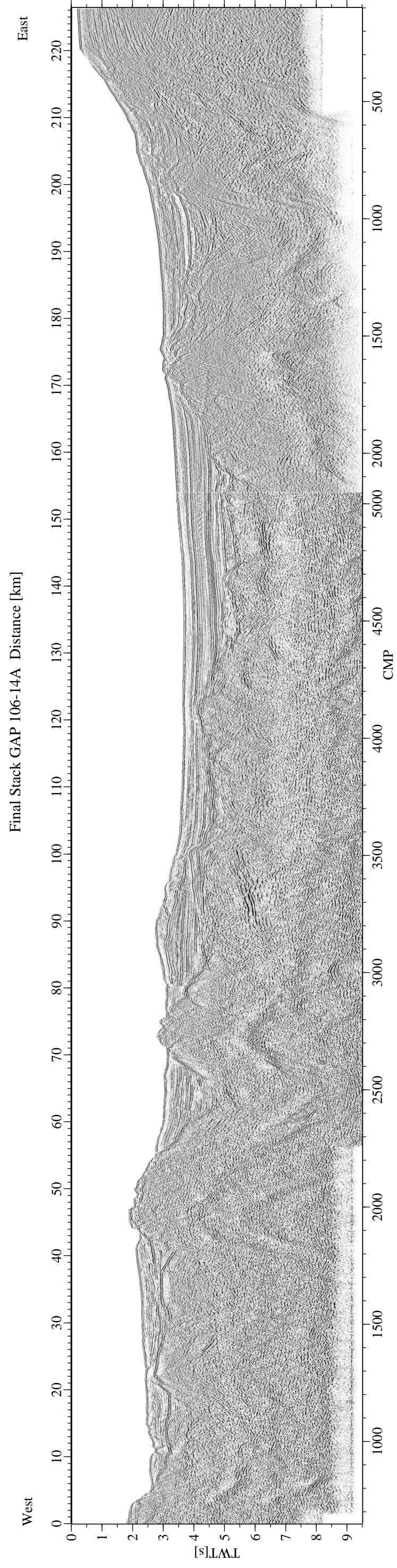
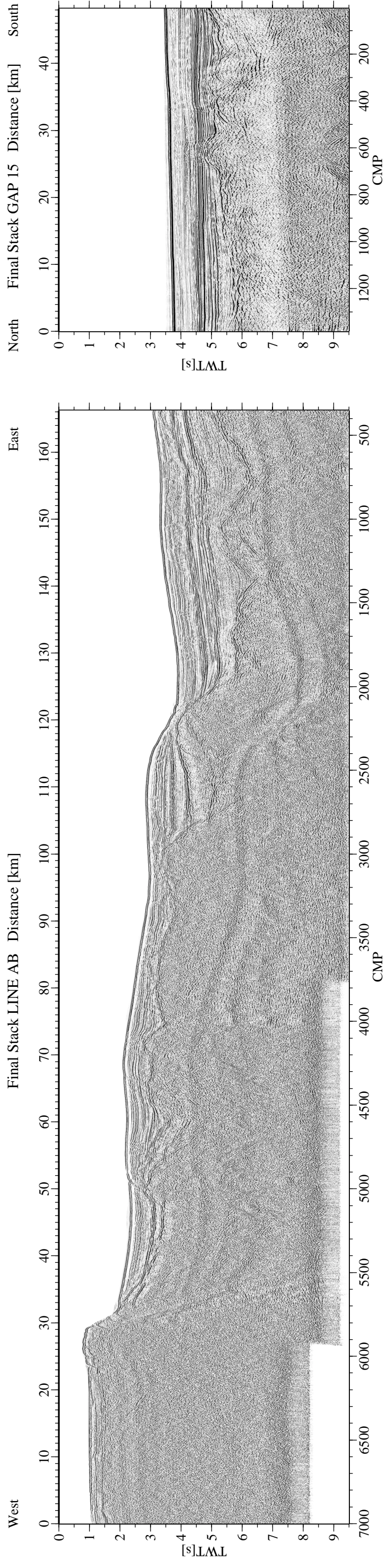


Figure 1.21. Finalstacks of lines AB, GAP 106, 14 and 15.

### **1.3.6 Time Migration**

The goal of migration is to make the stack section appear similar to the geologic cross section along the seismic line. We used a finite difference migration which is based in the zero-offset assumption, i.e. source and receiver positions are coincident, and in the Huygen's Principle, which will be explained in the next subsections. However, before migration the amplitudes within the stack section must be correctly balanced and a spherical divergence correction must be applied.

#### *1.3.6.1 Spherical Divergence Correction and Velocity Model for Migration*

As the seismic wave travels through the earth its amplitude is attenuated due to the spherical divergence of the energy of the wave front and to the increase of velocity with depth. Therefore a process must be applied that corrects for the attenuation of amplitude at late TWT, this is called spherical divergence correction.

A single shot can be considered as a point source that generates spherical waves. As the energy density of the wave has to be maintained, it has to be inversely proportional to the square of the distance to the source ( $r$ ), to  $1/r^2$ . Since the wave amplitude is proportional to the square root of the energy density, it turns out that as the wave front propagates its amplitude decreases proportionally to,  $1/r$  (Yilmaz, 1987, Sheriff and Geldart, 1995).

The foregoing holds for an homogeneous medium. In a non homogeneous medium the amplitude of the wave is further attenuated. This attenuation caused by the increase of the velocity with depth can be expressed as  $1/V_{rms}^2 t$ . Therefore, to correct the amplitudes for spherical divergence in a non homogeneous medium, we will have to multiply the amplitudes by a factor proportional to:  $V_{rms}^2 t$ . This is a first order approximation that does not take into account effects like focusing and defocusing but produces a reasonable amplitude balancing of a stacked zero offset section necessary for migration.

In order to get a geologically meaningful  $V_{rms}$  velocity function with depth, the stacking velocities are converted to interval velocities. The converted interval velocities are smoothed laterally and their value is brought to a geological meaningful value, where necessary. After that they are converted back to root mean square velocities.

#### *1.3.6.2 Cascaded time Migration*

In a stacked section events that dip do not map on their true subsurface position. Consider a constant velocity situation like the one shown in Figure 1.22. A reflection from

a reflector at point C underneath E is observed at A and maps on C' in the stacked section. Clearly,

$$\tan(\xi_\alpha) = \sin(\xi)$$

so that in the stacked section, the reflector seem to have a smaller dip than it really does, and appears longer than it is. Therefore a process of reposition of the data is needed. Migration steepens and shortens reflections, bringing them back to their true subsurface position. Migration uses the Huygen's Principle which states that any point in a wave front can be regarded as a new source of waves. Therefore, we can regard the reflector as composed by infinitesimal point sources exploding at time equal to half of the TWT to the reflector and at the reflector depth. The wave front generated at this particular instant,  $\psi = \psi(x, z_r, t = 0)$  takes the reflector shape, this is called the Imaging Principle. Because the seismic wave is continuous, it can be downward continued and traced backward to find  $\psi = \psi(x, z_r, t = 0)$  from the knowledge of the seismic wave at the receiver position,  $\psi = \psi(x, z = 0, t)$ , that is, the stacked section. The downward continuation is implemented using a finite difference approximation to solve the scalar wave equation.

In practice, we accomplished the migration in two steps through a cascaded migration (Larner and Beasley, 1987). First a water velocity migration was carried out implemented by a finite difference algorithm in the frequency space domain. This migration produced a sharp image of the sea floor and collapsed side swipes and remaining noise the amplitudes of which were carefully weighted down. The second step consisted in doing a residual migration of the water velocity migrated section, with a geological velocity model. The final migrated sections of line AB GAPS 106, 14 and 15 are shown in Figure 1.23.

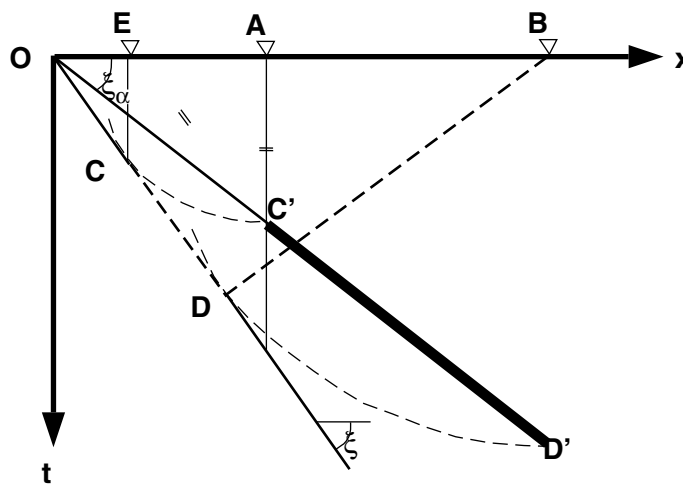


Figure 1.22. Migration of segment C D into CD increases the dip from  $\xi$  to  $\xi_\alpha$

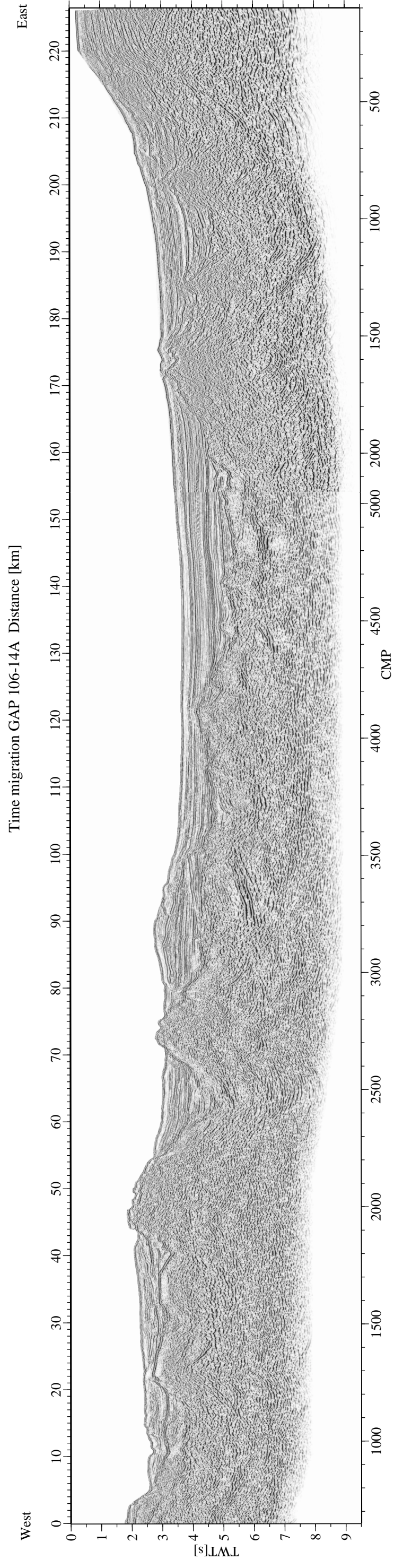
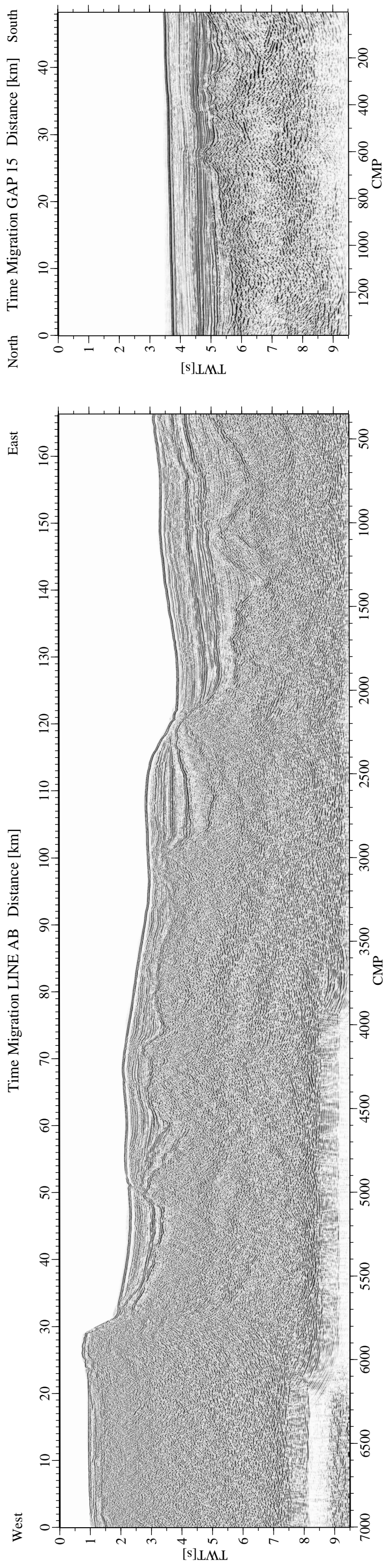


Figure 1.23. Time migrations of lines AB, GAP 106, 14 and 15.

## **CHAPTER 2. THE STRUCTURE OF THE GALICIA INTERIOR BASIN: CONTINENTAL EXTENSIONAL TECTONICS AND MECHANISMS.**

### **2.1 ABSTRACT**

In this chapter we present a transect from the continental platform, through the Galicia Interior basin to the Galicia Bank (Figure 2.1). Based on a coincident MCS near vertical reflection and wide angle seismic data and on the revision of previous studies of the seismic stratigraphy on the margin we constrain the onset of extension in the Galicia Interior Basin to Tithonian age much younger than previously proposed (Triassic, Montenat et al., 1988). The basin has an asymmetric structure and coincides with two different types of crust. It may have formed by reactivation of a Variscan suture separating the different terranes found beneath the continental platform and the Galicia Bank. At the centre of the Galicia Interior Basin the basement is extremely thinned reaching stretching values of 4 to 5. Uniform stretching of the upper and lower crustal layer explains the crustal structure modelled with wide angle data. Furthermore, estimations of the thermal structure of the crust at the beginning of rifting indicate that the base of the crust was probably too cold for lower crustal flow to occur. Hence, that differential stretching of the upper and lower crust might have been mechanically unfeasible. In contrast, numerical modelling indicates that progressive embrittlement of the entire crust at the centre of the basin might have allowed faults to cut to the Moho and facilitated low degree of serpentinisation of the mantle.

### **2.2 INTRODUCTION**

The Galicia Interior Basin is a deep (max. 3 km) and narrow bathymetric trough located offshore the northwest Iberia margin. From south to north, it extends along ~150 km between the continental platform and the Galicia Bank (Figure 2.1). The Galicia Interior Basin has been interpreted as the northward continuation of the Lusitanian Basin (Montenat et al., 1988, Wilson et al., 1989, Figure 2.1) which is thought to belong to a system of rifts basins which formed between Europe, North America and Africa in Triassic times prior to the opening of the Central Atlantic (Klitgord and Schouten, 1986). Basins such as the Porcupine or the Rockall Trough, and the conjugate basins of the Newfoundland margin (e.g. the Whale and the Jeanne d'Arc basins) are interpreted to belong to the same system (Lefort, 1984). Final seafloor spreading in the North Atlantic occurred oceanward

of all these basins, leaving them abandoned at the landward side of the final break-up margins.

Although the Iberia Abyssal Plain and the Deep Galicia Margin segments of the west Iberia margin have been intensively surveyed, the Galicia Interior Basin has been little studied. Only MCS stacked sections which were used to study the seismic stratigraphy of the basin were previously published (Murillas et al., 1990). This study correlated the seismic stratigraphy sequence within the Galicia Interior Basin with that determined at the Deep Galicia Margin during ODP 103 and at several wells of the continental platform (Figure 2.1), and suggested that the main extensional phase within the basin was Valanginian (137-132 m.y.). In this chapter we present the first coincident MCS and wide angle line along the Galicia Interior Basin (line 17, Figure 2.1). The processing of the MCS line up to prestack depth migration and the modelling of the wide angle data are first presented. Based on an integrated interpretation of both data and on the previous seismic stratigraphy study (Murillas et al., 1990) we discuss the phases of extension along the basin, the relationship with pre-existing Variscan structures, the amounts and mechanisms of extension and the nature of the crust at the centre of the basin.

### 2.3 DATA ACQUISITION

Coincident wide angle and MCS data were simultaneously acquired along profile 17 (Figure 2.1) during the Iberia Seismic Experiment aboard the R/V Ewing during July to August 1997. For the MCS data a 160 channels 4 km streamer was used along most of the line (line 17W in Figure 2.1). However, near the coast (east of 10°W) a 40 channels, 1 km streamer was used due to the heavy ship traffic (line 17E in Figure 2.1). The wide angle data were recorded on 7 Ocean Bottom Hydrophones from Geomar (Flueh and Bialas, 1996), evenly spaced at a distance of 22.5 km. OBH 241 located at the eastward slope of Galicia Bank did not record data due to tape drive failures. A 20 tuned air gun array source was used with a total capacity of 130 L. Shots were fired at a compromise time interval for MCS and wide angle data of ~ 40s, corresponding to a shot spacing of 100 m. This geometry yielded a 20 fold stack for MCS line 17W, and a 5 fold stack for MCS line 17E.



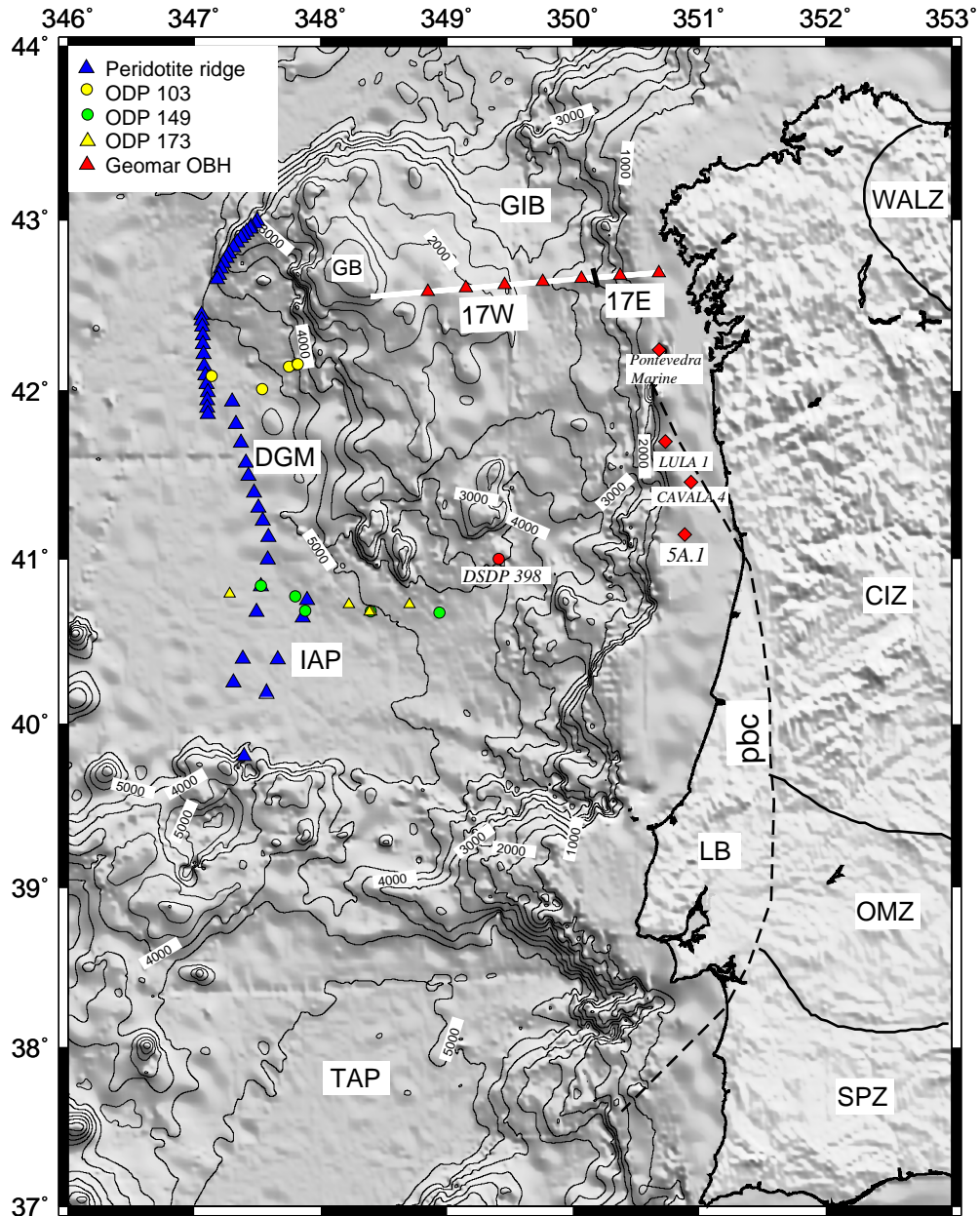


Figure 2.1. Bathymetric map of west Iberia. The margin is divided in three segments: the Tagus Abyssal Plain (TAP), the Iberia Abyssal Plain (IAP) and the Deep Galicia Margin (DGM). The Galicia Interior Basin (GIB) is located between the continental platform and the Galicia Bank (GB). The position of the coincident MCS and wide angle profile 17 is shown. Also the position of ODP drillings 103, 149 and 173, of the wells in the continental platform (Pontevedra Marine, LULA 1, CALVALA 4 and 5A.1) and of dredge Site DSDP 398 are shown. Onshore the terranes of the variscan massif are indicated (modified from Quesada et al., 1994): CIZ = Central Iberian Zone; OMZ = Ossa Morena Zone; SPZ = South Portugese Zone; WALZ = West Asturian Zone; LB = Lusitanian Basin. The Porto-Badajoz-Cordoba suture (pbc) runs from south to north separating different terranes of the variscan massif. Its northwards continuation is believed to run offshore along the GIB (Capdevila and Mougénot, 1988).

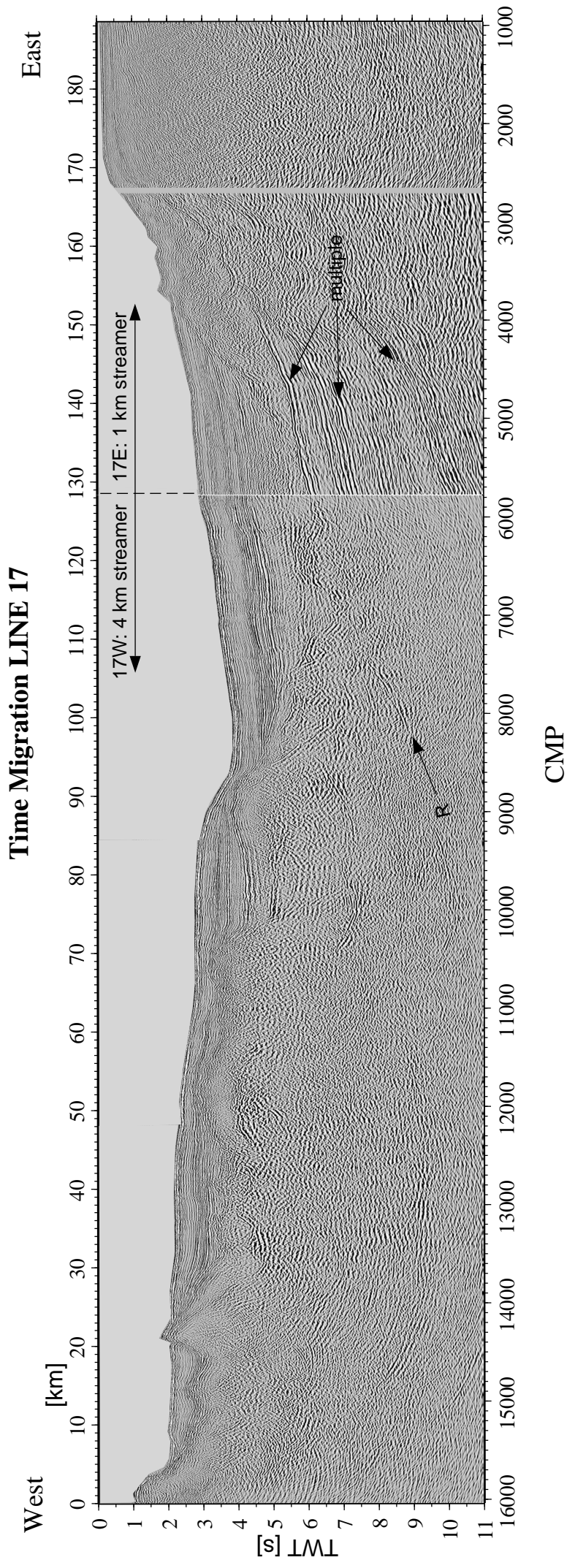


Figure 2.2. Time migration of line 17. Note that on line 17E the multiple was not removed because the short streamer and the shooting interval yielded a 5 fold stack.

## 2.4 ANALYSIS OF THE DATA

### 2.4.1 MCS data

The main steps in the processing sequence of the line 17 W data were statistical deconvolution, velocity analysis, multiple removal and time migration (see chapter 1 for details). The statistical deconvolution was computed using a single trace spiking Wiener filter operator. Within each trace two 2 s long overlapping windows were designed for the computation of the deconvolution operator. The first at the sediments and the second at the basement to account for the change in frequency with increasing travel time. The two operators were applied at 100% at the centre of each window and interpolated in between. Velocity analysis were performed twice, once after statistical deconvolution and the second after multiple removal.

Multiples in deep water are difficult to attenuate because usually the amplitudes of primary reflections at the multiple TWT are weak. Additionally, the shooting interval of 100m led to a distance between traces within a CMP of 200 m, which caused serious problems of spatial aliasing in the CMP gathers. To remove the multiple two FK filters and a weighted stack in the CMP gathers were applied. The first FK filter was applied to the CMP gathers NMO corrected with the water velocity in order to flatten the multiple of the seafloor. The flat multiple plots as a zero dip line in the FK domain avoiding spatial aliasing. A narrow FK filter was designed to filter out the 0 dip arrivals. The second FK filter was designed using the same strategy but using a velocity of 1700 m/s in order to filter out the multiple of the sediments. A weighted stack was applied to every CMP gather after NMO correction with stacking velocities. This process compares at every time sample the amplitude of every trace within a CMP gather with the amplitude of the stacked trace of the corresponding CMP gather. The samples with a very different amplitude from the stacked trace are weighted down. Hence, amplitudes that are not laterally consistent along the gather, in particular the remainders of the multiple are attenuated. An inner trace mute was applied to remove multiple at near offsets. After stacking, multiples of strongly dipping layers were still present and surgical FK filters were applied in the stacked section to further attenuate them.

The time migration was accomplished in two steps. First the data were migrated with constant water velocity using a finite difference algorithm in the frequency space domain. After water velocity migration, side swipes and remaining multiple collapsed and their amplitudes were carefully weighted down. The data were then migrated for second time using a finite difference algorithm on the time space domain. This migration was performed with a smoothed and geologically meaningful version of the stacking velocity model.

Along line 17E the 5 fold CMP gathers prevented FK multiple removal before stacking because the NMO was too small to discriminate primaries from multiples. The rest of the processing sequence is similar to that used for line 17W. The time migration of line 17W and 17E is shown in Figure 2.2.

At rifted margins faulting produces a complex basement topography and strongly dipping layers within tilted blocks are difficult to image by conventional processing techniques. Also structures underneath the tilted blocks suffer from pull up and pull down effects appearing domed beneath the fault blocks. To obtain a geometrically correct image in depth the data were pre-stack depth migrated. This method not only produces a section in depth but also corrects for raypath bending at velocity interfaces and gradients following Snell's Law (Hubral, 1977) and avoids CMP smearing. Such effects may be particularly important at rifted margins where faulting juxtaposes bodies of very different velocities and the basement has a complex structure.

For pre-stack depth migration a geological velocity model is necessary. The model is iteratively constructed by depth-focusing error analysis of reflected and diffracted energy at closely spaced intervals (80 m) along the profile and common reflection gathers (Sherwood, 1989, Denelle et al., 1986). The velocity model has to be built up one layer at a time, since the velocity of the overburden affect those determined for deeper levels. Thus we first determine the water velocity, then incorporate that velocity into the next iteration where we determine the velocity of the topmost sedimentary layer again through depth focusing analysis. The procedure is repeated until the entire section has been analysed for velocity resulting in an optimised depth migration and velocity model that is both detailed and geologically meaningful. However focusing analysis only give good velocity information where there are reflections to pick and also where the reflectors are not too deep so that offset dependent information about their velocity can be obtained. Beneath the basement and at the deep part of the section, sometimes no clear reflections are observed, and sometimes where clear reflections are seen they are too deep. Therefore beneath the basement where the velocity information given by focusing analysis was not accurate, wide-angle velocities were used as a guide to create the macrovelocity model for pre-stack depth migration. The pre-stack depth migration is shown in Plate 1.

#### **2.4.2 Wide angle data**

Wide angle data were copied and split into single shot records stored as common receiver gathers in SEG Y format. Subsequently the data were deconvolved and an offset and time dependent band pass filter was applied. The aim of the deconvolution was to increase the resolution to image the near offset reflections of sedimentary layers and top basement. A single trace statistical Wiener deconvolution was applied with a prediction length of 80

## LINE 17- Pre-stack depth migration

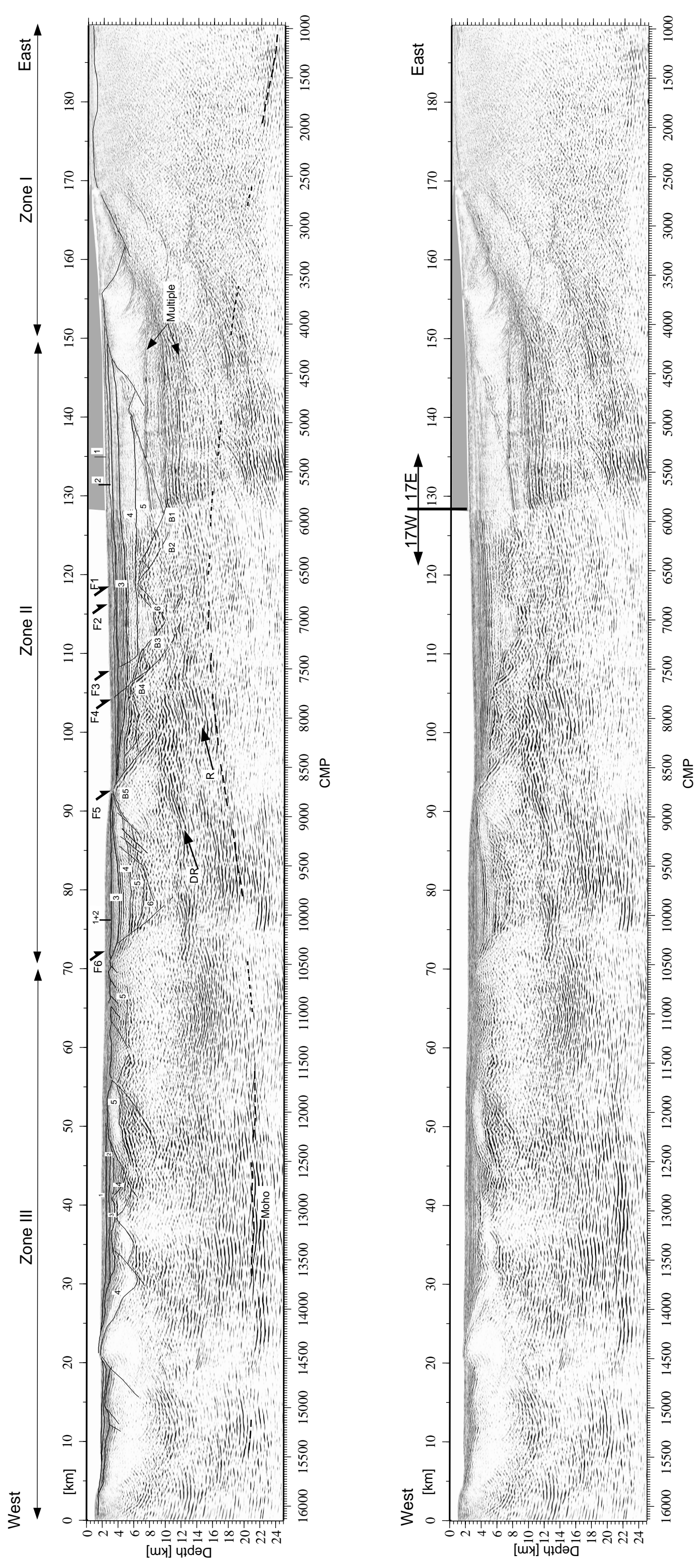


Plate 1. Pre-stack depth migration of line 17 (**Bottom**), overlaid with an interpretation (**Top**). At Zone I, II and III differ in their structural style and in their velocity structure (see Figure 5). Numbers indicate the sedimentary formations defined from a seismic stratigraphy study in the basin (see text). F1 to F6 are faults active during the main extensional episode at the centre of the basin. B1 to B5 are blocks rotated along these faults. Reflections DR and R are discussed in the text. Moho indicates the wide angle Moho.

ms. This value was chosen long enough to avoid changing the source wavelet shape but to attenuate the reverberations that obscure the primary reflections of sediment layers and top basement in the near offsets. The filter was computed using a 480 ms long operator designed on a 2 s long window, so that different operators were computed along the trace. The operators were applied at 100% within each window and interpolated in between. The frequency filter was designed to maintain relatively high frequencies (3/5 - 35/50 Hz) for near offsets and short travel times and progressively filter out high frequencies as the offset and travel time increased. The narrowest band pass filter applied was 3/5 to 10/20. After processing wide angle reflections can be identified more readily in the near offsets (Figure 2.3). Appendix 1 shows all the processed seismic record sections.

Picking the onset of far offset arrivals was accomplished using both the processed and the raw data. For the near offsets we used the processed data. Errors in travel time picking are about 50 ms in sedimentary layers reflections and refractions and basement reflections. The error is about 100 ms in refracted arrivals from the crystalline basement.

## 2.5 MODELLING OF WIDE ANGLE DATA

Wide angle data were interactively forward modelled using the program 'MacRay' (Luetgert, 1992). In addition, the coincident MCS data were used to constrain the depth to the sedimentary units and to the basement in between OBH positions. This was accomplished by identifying the reflections from the sediments and top basement in each of the OBHs seismic record. The recording time at the centre of each reflection was converted to TWT and the corresponding reflector was identified in the time migrated MCS profile. The sediment reflections were followed laterally along the MCS profile, digitised and converted to OBH geometry. This was done by subtracting at each position of the MCS profile one way travel time to the seafloor (Kopp, Phd Thesis). Figure 2.4 shows the OBH near offset reflections with the digitised horizons.

The wide angle model was constructed one layer up a time. First the depth and velocities of the shallow sedimentary layer were found by matching the near offset reflections and refractions in the wide angle data. Laterally the velocities of the layer were kept constant and its depth was found by setting imaginary sources in between OBHs and matching the depth to the digitised MCS horizons converted to OBH geometry. This was repeated for every sedimentary layer down to top basement. Below top basement only wide angle data information was used with exception of the MCS Moho which was also digitised in the MCS profile and converted to OBH geometry. This was used to extrapolate the wide angle Moho where there was no information from the wide angle data.

Finally, the wide angle model was cross checked against and partly rebuilt using the prestack depth migrated section. The detailed velocity model constructed by depth focusing analysis during prestack depth migration allowed to image structures that did not appear in the time migrated section (compare top basement at block B5 in the depth and time migrated sections, Figure 2.2 and 2.12 and Plate 1). Therefore where the depth migrated section yielded a better image, the sedimentary layers and top basement were digitised on the time converted depth migrated section and used to build the wide angle velocity model.

## **2.6 VELOCITY STRUCTURE FROM WIDE ANGLE DATA**

The resulting depth velocity model is shown in Figure 2.5. There are three areas with different velocity structure which also differ in their structural style (see next section). Zone I corresponds to the continental platform, Zone II is the deepest part of the basin, and Zone III corresponds to the eastern flank of Galicia Bank.

### **2.6.1 Sedimentary layers**

Zone I : the reflections from the sedimentary layers were observed neither on OBH 237 nor on OBH 236 since the reverberations were very strong. In this area the velocity and depth of the sedimentary layers was found by matching only the wide angle refractions from the sediments and they are not very well constrained. Towards the continental shelf the sedimentary cover thickness decreases to 300 m. However, two small subbasins (also observed in the MCS profile, Plate 1) are modelled (km 154-170, and 174-183 respectively) where the sedimentary cover locally thickens to around 2.3 and 0.8 km respectively

Zone II: 5 sedimentary units were identified with a maximum thickness of 6 km. The near offset reflections of this sedimentary layers coincide with unconformities that can be followed laterally along the MCS profile (Figure 2.8, 2.9 and 2.10). These unconformities correspond almost everywhere to the boundaries between the sedimentary formations defined by Murillas et al (1990) within the Galicia Interior Basin (see next section). The three uppermost units correspond to postrift Formations 1 + 2, 3a and 3b respectively (see next section and Figure 2.4) and altogether have a maximum thickness of 2.2 km. Their velocities increase gradually without strong velocity contrasts (1.8 to 2.9 km/s, 3.1 to 3.3 km/s, and 3.35 to 3.4 km/s). The bottom of the third unit coincides with the latest Aptian break-up unconformity observed in the MCS data (Plate 1, Figure 2.4). This corresponds to a strong velocity jump. Unit 4 corresponds to sedimentary Formation 4, at OBH 239 (Figure 2.9 and 2.4). This unit has a velocity that varies laterally from 3.8 to 4 km/s at

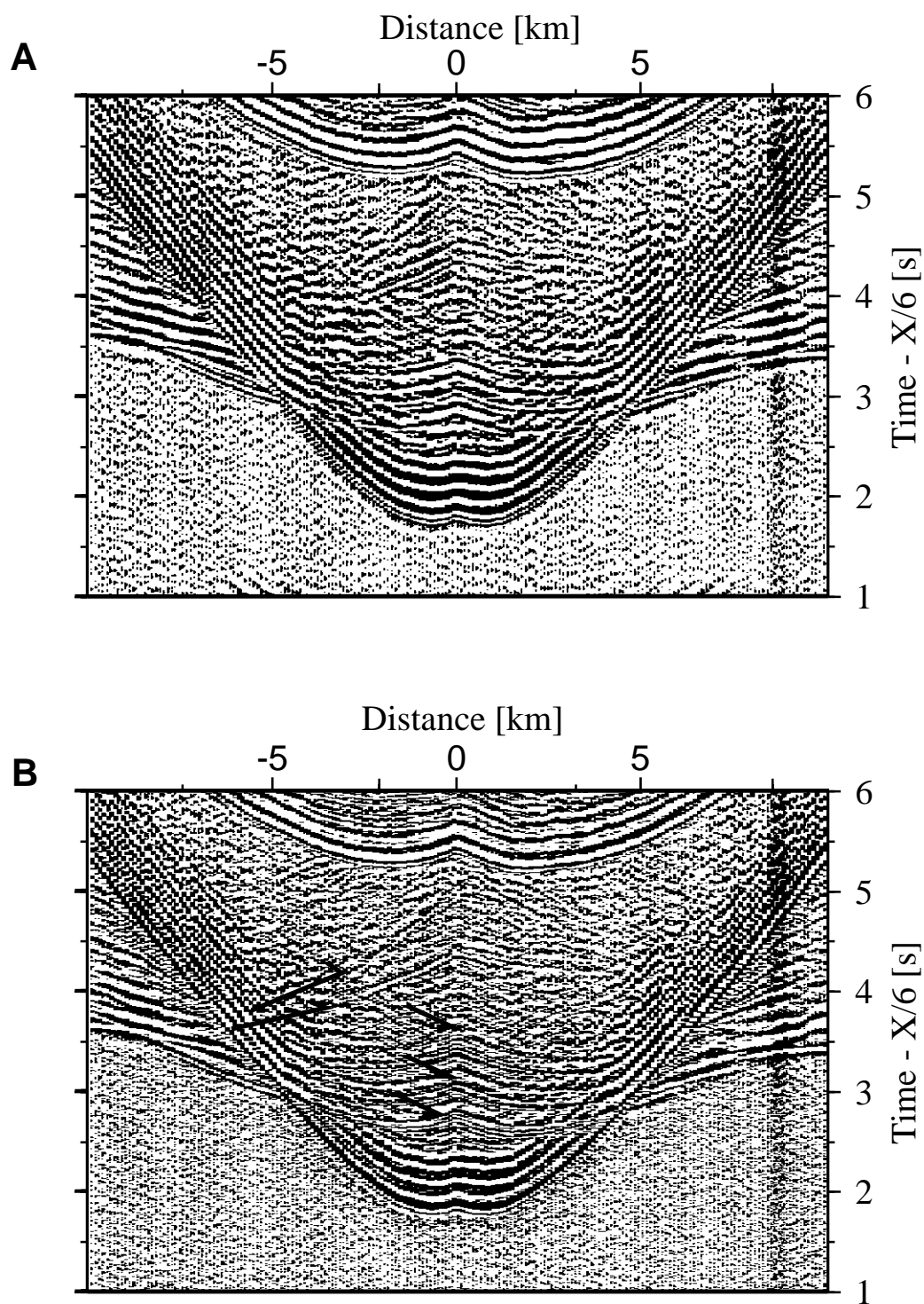


Figure 2.3. Seismic record of OBH 239. **A.**, before processing, **B.**, after deconvolution and offset dependent band-pass filtering. After processing reflections in the near-offset are easier to identify.



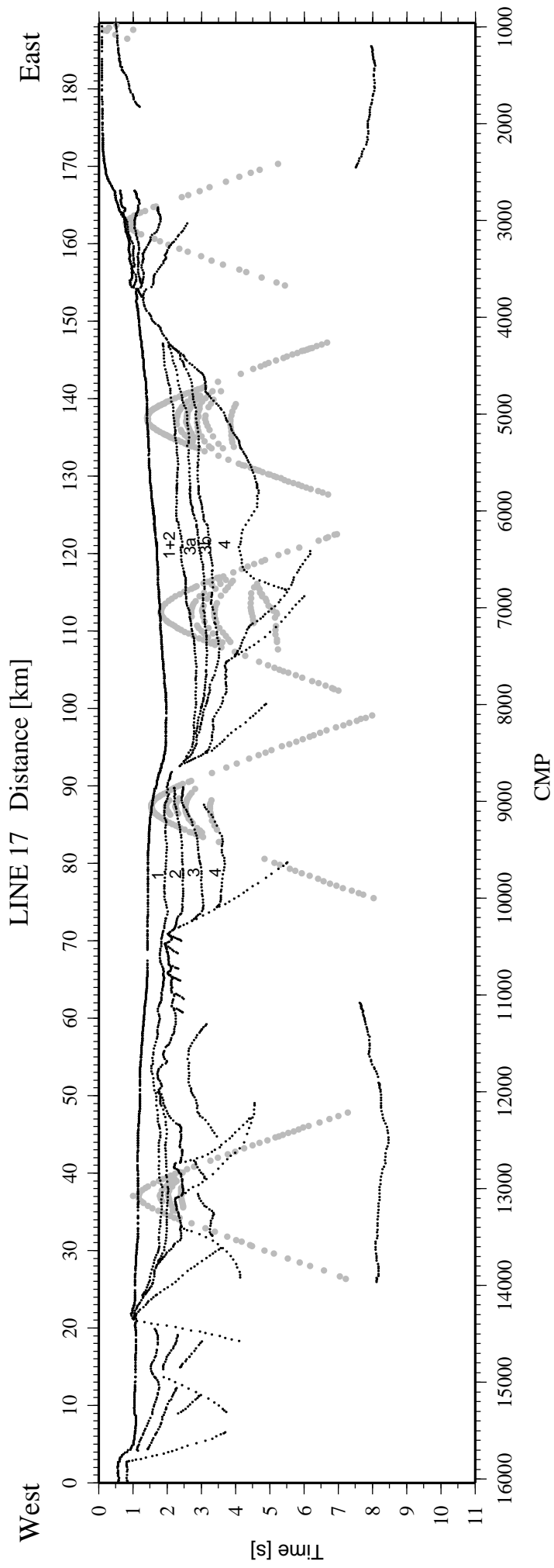


Figure 2.4. Direct water wave arrival and near offset reflections picks of OBHs along line 17. The digitized reflectors along the MCS profile converted to OBH geometry are also shown. The numbers indicate the seismic formations defined by Murillas et al. (1990), giving the correspondence between the seismic units interpreted from the OBHs records and that from the seismic stratigraphy.



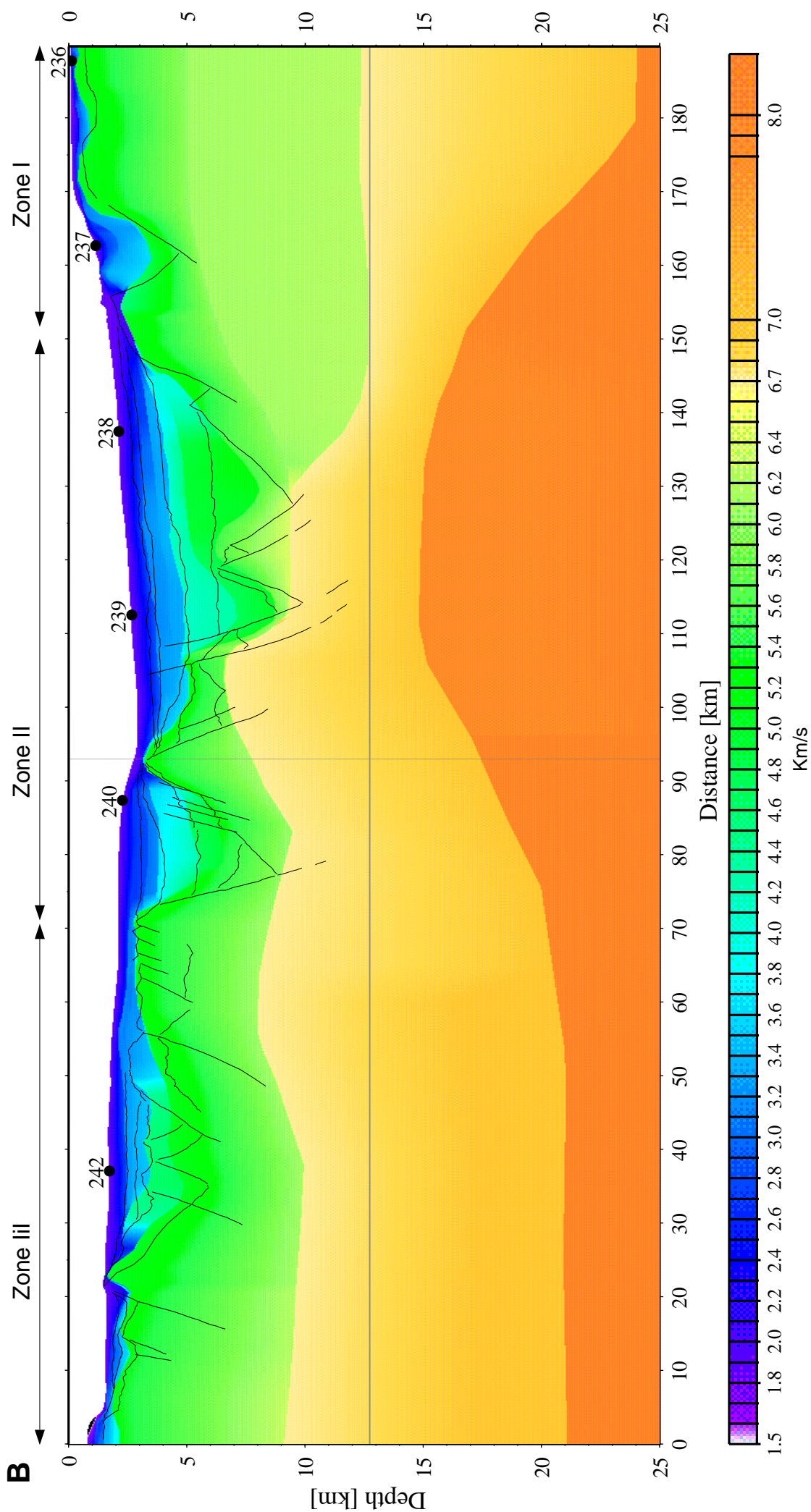


Figure 2.5 B. 2-D velocity structure from wide angle data overlaid by geological interpretation of the prestack depth migrated profile (Plate1).

OBH 238 to 4.1 to 4.3 at OBH 239. Unit 5 corresponds to sedimentary Formation 5, at OBH 239 and has a velocity from 4.7 to 5.1 km/s.

Zone III: Towards Galicia Bank, the sedimentary cover thins to 1 km, although it thickens locally in small basins formed above tilted blocks (Figure 2.5). In these subbasins the sedimentary cover is about 1.2 and 2.8 km thick respectively.

The velocity structure of the sedimentary layers is very similar to that obtained by depth focusing analysis and common reflection point gathers during prestack depth migration.

### **2.6.2-Basement**

Zone I: The basement consists of three velocity layers at the continental shelf and slope (Plate 1). Refractions through these layers are observed in OBH 236 and 237 (Pg1, Pg2 and Plc in Figure 2.6 and 2.7). Their velocities range from 5 to 6, 6.1 to 6.2 and 6.7 to 6.9 km/s respectively. Towards the centre of the basin the layers thin and their velocity gradient increases.

The depth of the Moho is controlled in this area by the PmP reflection observed on OBH 236 (Figure 2.6) and by matching the reflections from the Moho in the MCS profile (Figure 2.2 and Plate 1). The crust is 24 km thick at the eastern end of the profile and thins progressively towards the basin.

Zone II: In contrast to Zone I, west of km 130, the crust consists only of two velocity layers. This velocity structure is required to match the refraction arrivals from the crystalline crust of OBHs 238, 239 and 240 (Pg and Plc arrivals Figure 2.8, 2.9, 2.10). At the deepest part of the basin the basement reaches a minimum thickness of 6 km. The upper layer has velocities from 5.6 at the top to 6.4 km/s at the bottom, and a high velocity gradient ( $0.26 \text{ s}^{-1}$ ). This layer thins notably at km 112, this is constrained by the Plc arrival at OBH 240 (km 105-125, Figure 2.10). The second layer in the basement reaches a minimum thickness of 5 km in the deepest part of the basin (km 111 to 130, Figure 2.5) and has a velocity from 6.7 at the top to 6.9 km/s at the bottom. Both layers thicken and their velocity gradient decreases towards the west.

The depth of the Moho in this area is constrained by PmP arrivals interpreted in OBH 237, 239, and 240 (Figure 2.7, 2.9 and 2.10). The 7.8 km/s velocity of the uppermost mantle in this area is lower than that in Zones I and III. This is constrained by Pn refracted arrivals through the mantle in OBH 236, 239 and 240 (Figure 6, 9 and 10).

Zone III: the velocity structure of the eastern flank of Galicia Bank is modelled using refracted and reflected arrivals from OBH 240 and 242 (Figure 2.10 and 2.11). These indicate that the basement consists of two velocity layers. The first one has velocities ranging from 5 to 6 km/s, which increase towards the west to 5.3 to 6.3 km/s at the top and

bottom of the layer respectively. Its average thickness is 6 km, but thins locally below small subbasins. The second basement layer has an average velocity ranging from 6.7 to 6.9 km/s and an average thickness of 10 km. In this area the depth is controlled by a PmP arrival observed at OBH 240 (Figure 2.10) and reflections in the near vertical data and occurs fairly constant at 21 km depth.

## **2.7 INTEGRATED INTERPRETATION OF THE MCS AND WIDE ANGLE DATA**

Line 17 shows a cross section in depth along the continental platform, the deep Galicia Interior Basin and the eastern flank of the Galicia Bank. These areas differ in their structural style and, as described above, in their velocity structure (Plate 1, Figure 2.5). In this section we review the seismic stratigraphy of the basin. Subsequently an interpretation of the crustal structure revealed by the MCS and the wide-angle data is given.

### **2.7.1 Sedimentary Formations**

The sedimentary formations of line 17 were identified by correlation of the seismic horizons with an intersecting MCS profile (line AB, see Figure 3.1 chapter 3) where the seismic stratigraphy of the Galicia Interior Basin had been previously defined (Murillas et al., 1990). This was carried out by means of seismic facies criteria, correlating an important set of MCS data, results of DSDP Leg 398 (Sibuet et al., 1979) and ODP Leg 103 (Mauffret and Montardet, 1988). Additionally they used information from several wells on the continental platform (see Figure 2.1 for location of wells, drill holes and dredges). Following Murillas et al. (1990) we have identified 6 sedimentary units along the profile, three postrift, two synrift and a synrift -prerift sedimentary unit. These are equivalent to those identified during Leg 103 on the Deep Galicia Margin (Mauffret and Montardet, 1988).

#### **Formation 1 (late Eocene to Recent)**

Unit 1 drapes conformably over the underlying topography along line 17. In the deepest part of the basin (Zone II, Plate 1) unit 1 thickens from east to west reaching its maximum thickness of 1.75 km and presents some evidence of tectonism in the form of slight normal faulting. Towards the continental platform (Zone I, Plate 1) Formation 1 is difficult to identify because it is obscured by the shallow sea bottom multiple. Nevertheless, the unit may be present in a small subbasin continental slope (CMP 2700 to 3700 in Plate 1). At the eastern flank of Galicia Bank (Zone III, Plate 1) Formation 1 presents a relatively constant thickness of about 1 km, increasing locally above half grabens of tilted blocks (CMP 12300 to 13700 and 14400 to 15700, Plate 1).

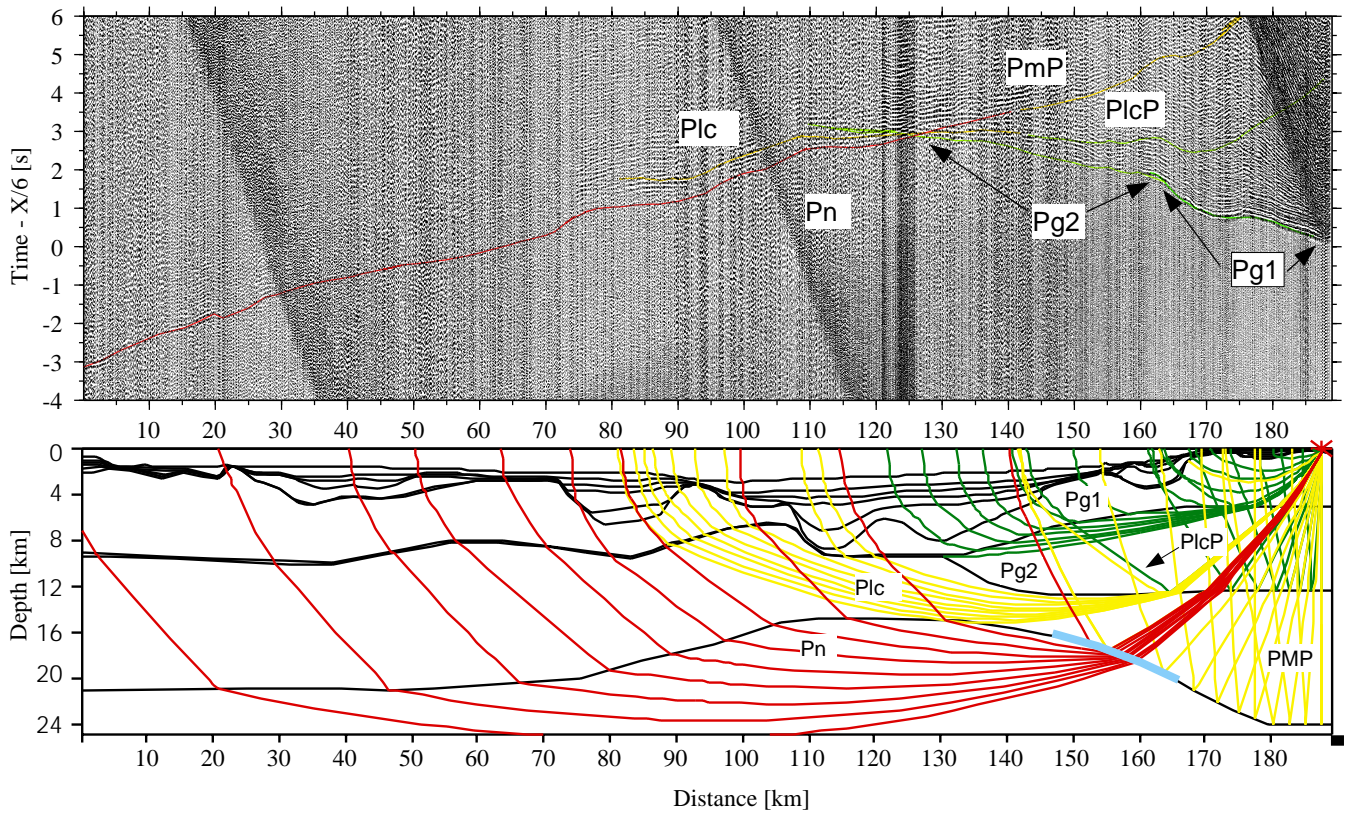


Figure 2.6. Processed record section from OBH 236 (**Top**) overlain by travel time arrivals calculated from the rays through the 2-D velocity-depth model (**Bottom**). Colors indicate rays travelling through different layers: upper crust (Pg1), middle crust (Pg2), lower crust (Plc) and mantle (Pn). PlcP and PmP indicate reflections from the lower crust and from the Moho. The same nomenclature is used for all the OBH record sections. The thick blue line at the Moho indicates the extent of it that is controlled by the data.

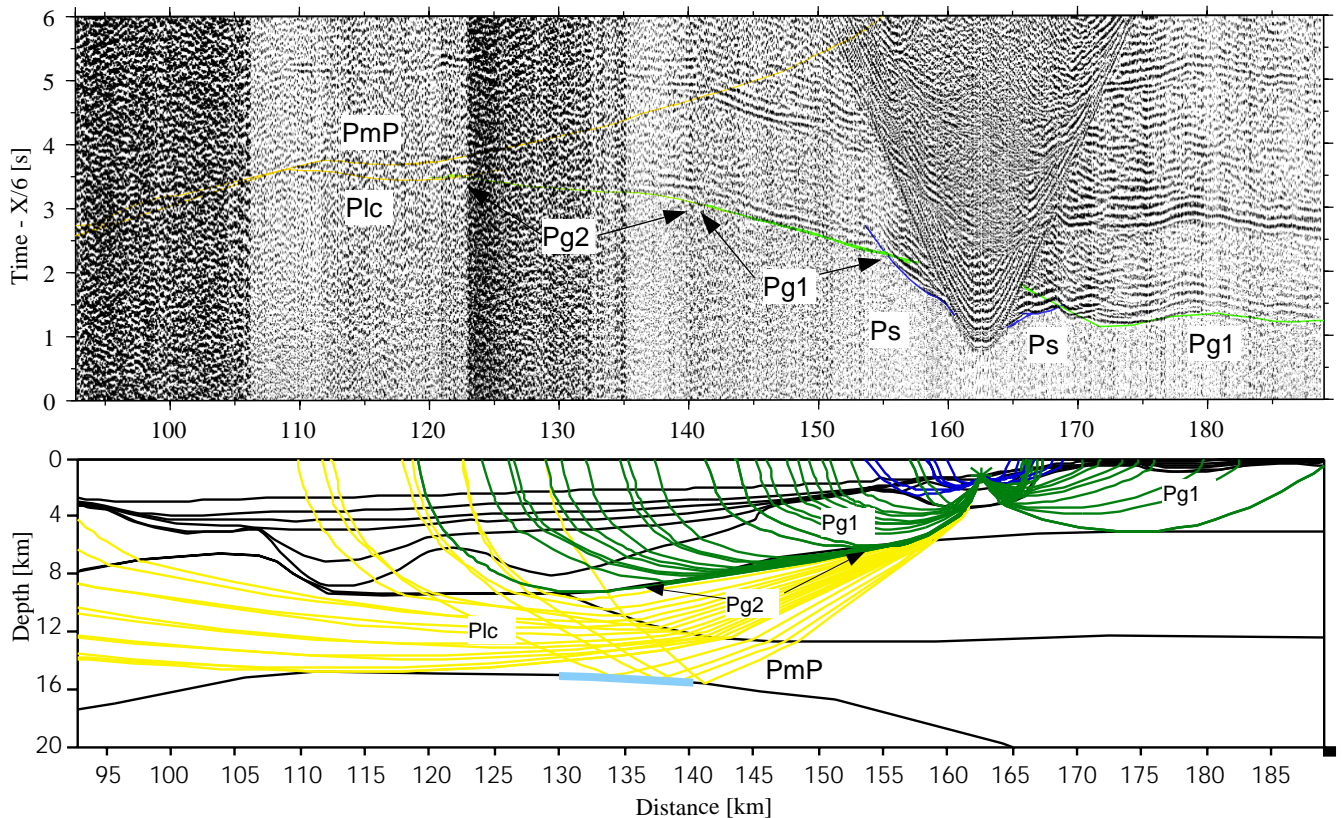


Figure 2.7. Processed record section from OBH 237 (**Top**) overlain by travel time arrivals calculated from the rays through the 2-D velocity-depth model (**Bottom**).

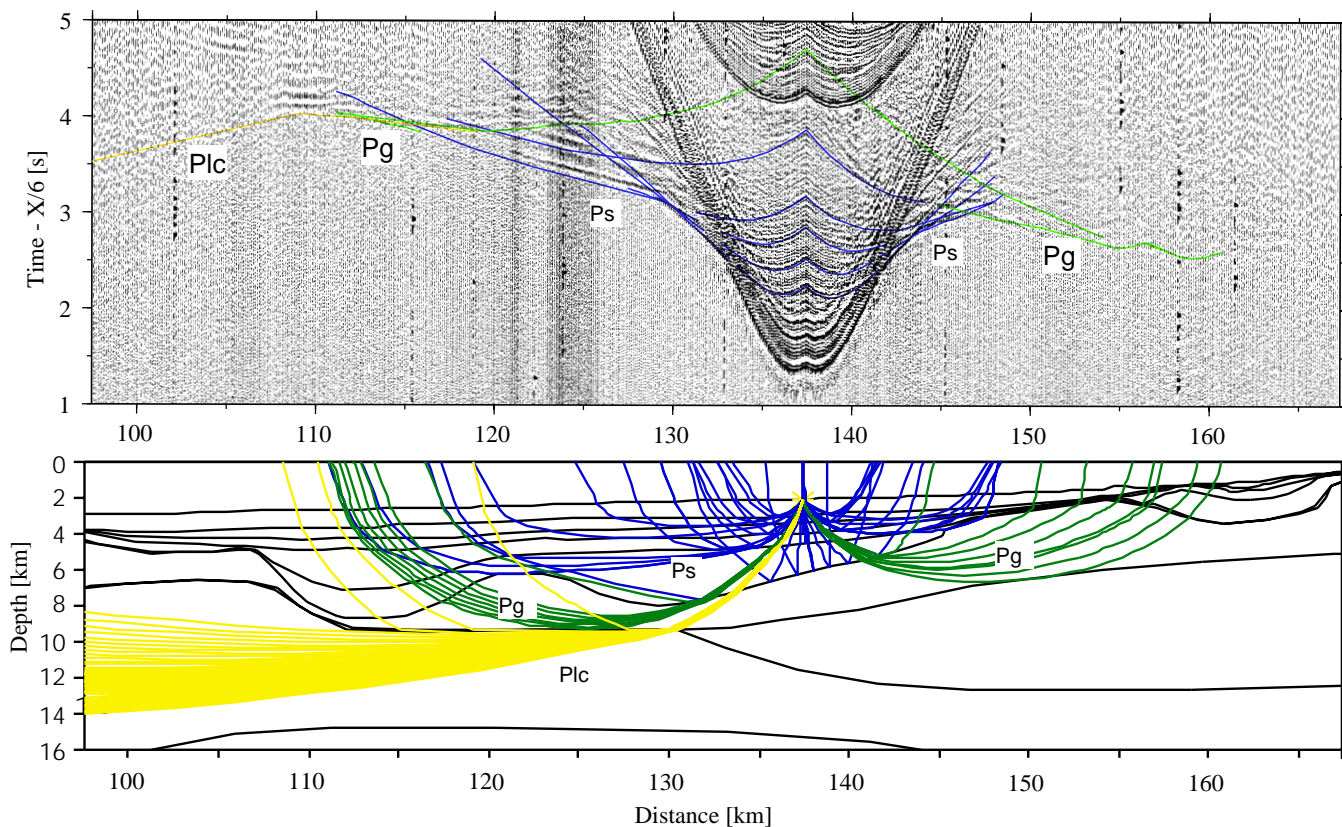


Figure 2.8. Processed record section from OBH 238 (**Top**) overlain by travel time arrivals calculated from the rays through the 2-D velocity-depth model (**Bottom**). Ps and Pg indicates rays refracted through the sediments and upper crust respectively. Note that west of km 130 the crust is modelled as consisting of two layers instead of 3.

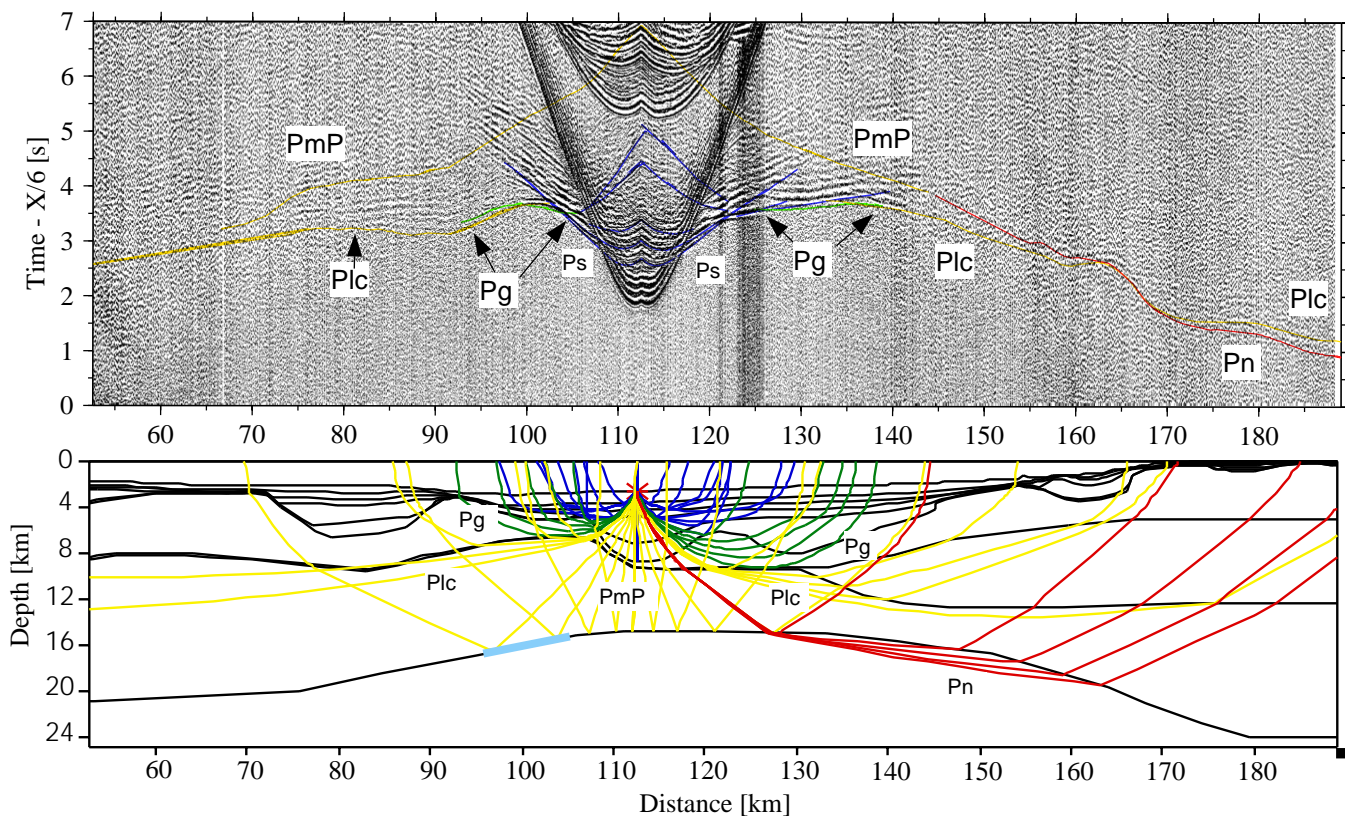


Figure 2.9. Processed record section from OBH 239 (**Top**) overlain by travel time calculated from the rays through the 2-D velocity-depth model (**Bottom**). The thick blue line at the Moho indicates the extent of it that is controlled by the data.

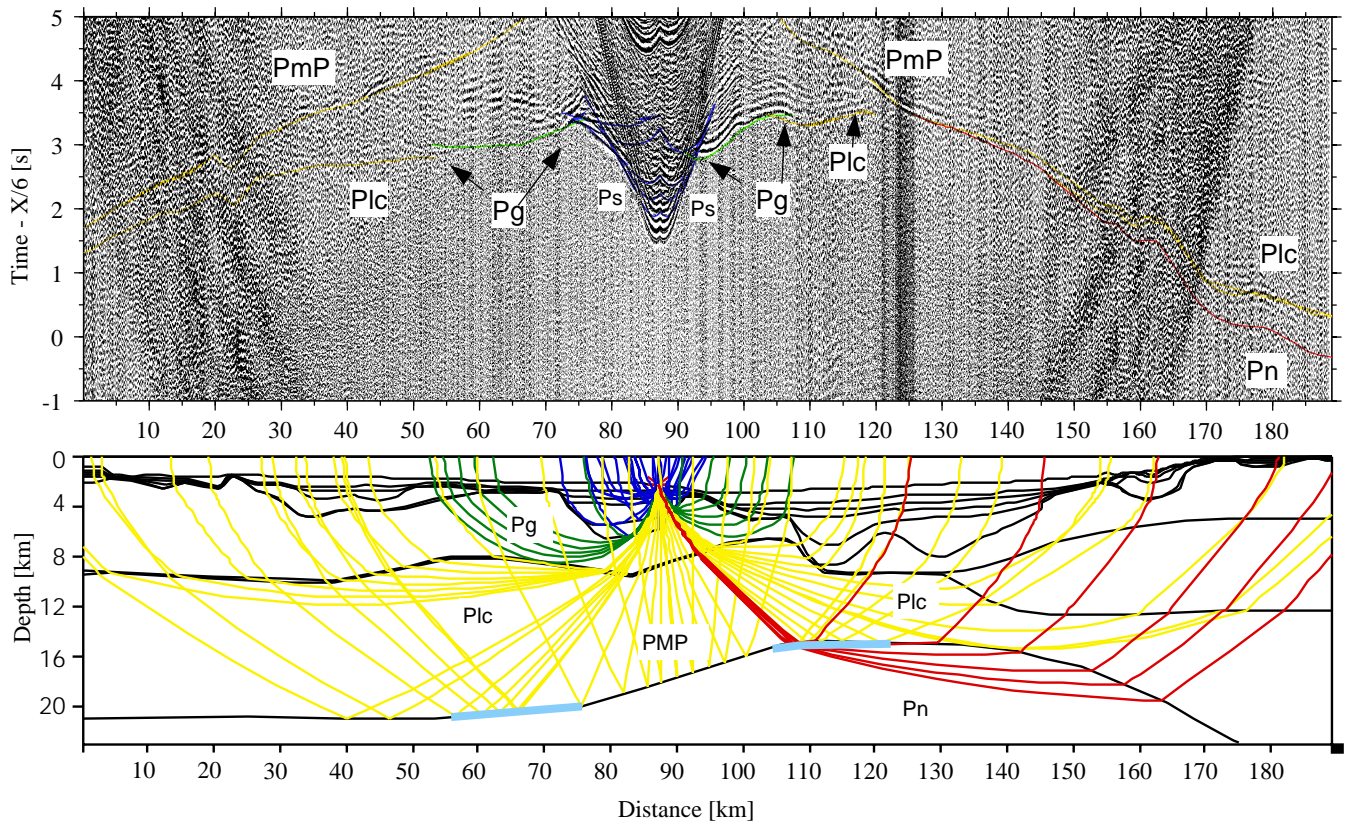


Figure 2.10. Processed record section from OBH 240 (**Top**) overlain by travel time arrivals calculated from the rays through the 2-D velocity-depth model (**Bottom**). The thick blue line at the Moho indicates the extent of it that is controlled by the data.

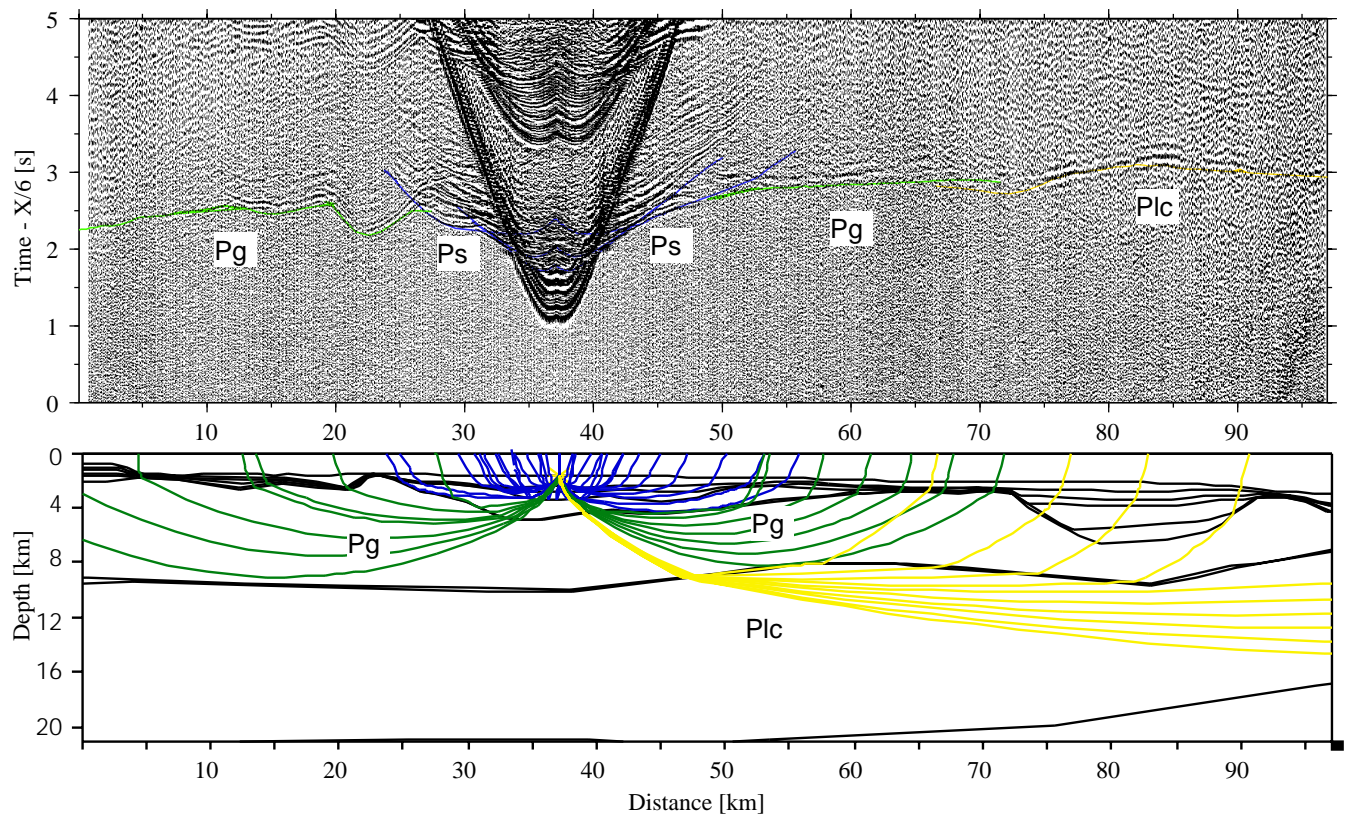


Figure 2.11. Processed record section from OBH 242 (**Top**) overlain by travel time arrivals calculated from the rays through the 2-D velocity-depth model (**Bottom**).



# Prestack depth migration Line 17

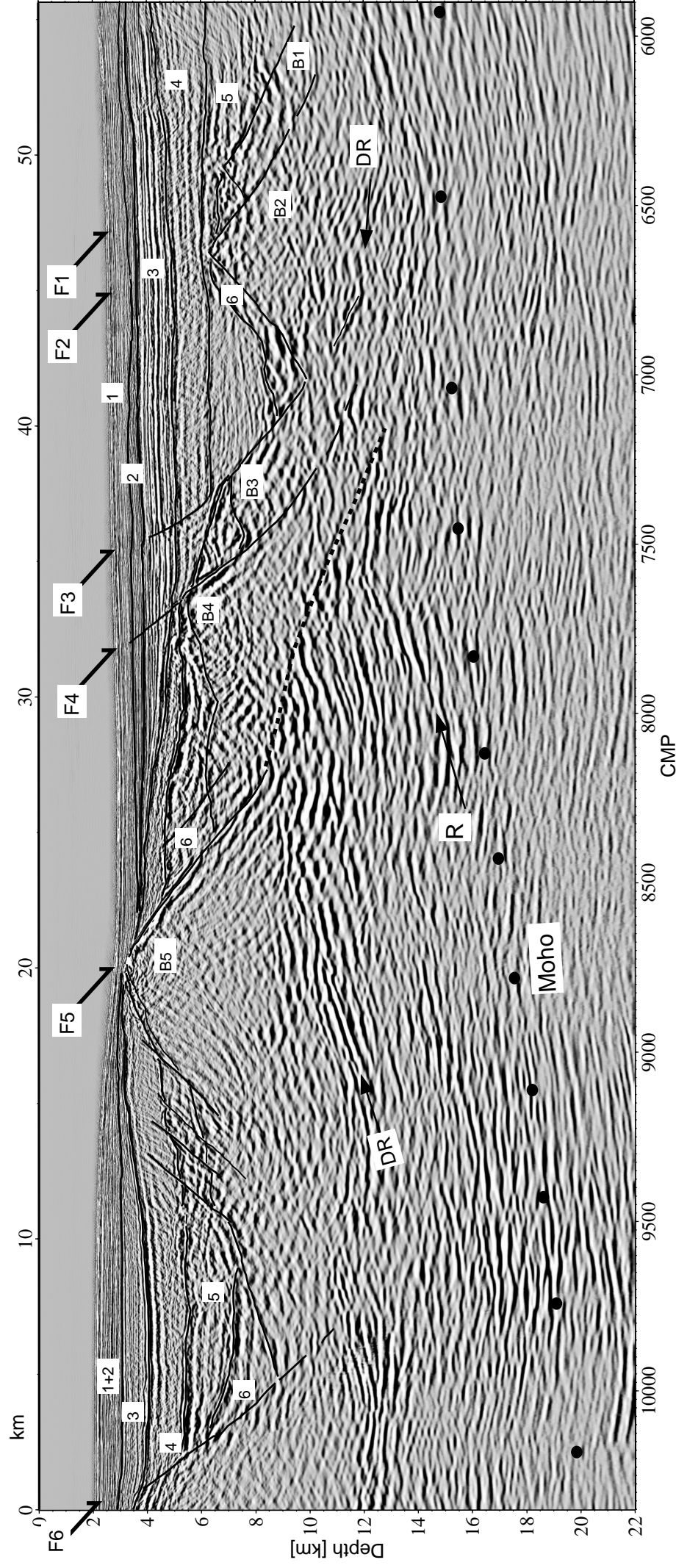


Figure 2.12. Detail of Zone II along the line 17. Numbers indicate sedimentary formations. F1 to F6 are faults active during the deposition of Formation 5 (Valanginian in age, 137-312 m.y.) and probably 6 (Tithonian to Berriasian, 151-137 m.y.). F6 might sole out at the set of reflections DR (solid line), or might continue as indicated by the stippled line. B1 to B5 are continental blocks rotated along faults F1 to F6. Westward dipping faults on block B5 offset top basement and top of Formation 5, but do not reach top of Formation 4 indicating that they were active while this last unit was being deposited (Hauterivian to late Aptian, 132-112 m.y.). The deep reflections DR and R are discussed in the text. The black dots (Moho) indicate the wide angle Moho.

**Formation 2 (Senonian to middle Eocene)**

Formation 2 is a group of high amplitude, good continuity reflections that lie conformably over the former topography. Average thickness is fairly constant along the line, around 0.75 km. This unit is also affected by slight normal faulting in the deepest part of the basin (Zone II, Plate 1).

**Formation 3 (Albian to Cenomanian)**

At DSDP Site 398 (Sibuet et al., 1979) an important stratigraphic gap, attributed to deep oceanic circulation separates the Albian “black shales” (Formation 3) from the Campanian to Eocene pelagic sediments (Formation 2) (Murillas et al. 1990). Formation 3 presents a strong layered character and is 1.75 km thick at the deepest part of the basin (Zone II, Plate 1). The onlap pattern of the base of this unit over the preexisting topography of the deep basin indicates deposition during the thermal subsidence of this area of the margin. In the eastern flank of Galicia Bank its facies are sometimes transparent and its thickness decreases towards Galicia Bank.

Within the deepest part of the Galicia Interior Basin we have divided Formation 3 in two subunits, 3a and 3b. The top of layer 3b is an intraformational unconformity whose near offset reflection is observed in OBH records 238 and 239 (Figure 2.4). The onlap pattern of formation 3a on 3b at the eastern flanks of the deepest basin (Zone II, Plate 1) indicates that there was also a depositional hiatus between Formation 3a and 3b.

**Formation 4 - Synrift I ( Hauterivian to late Aptian)**

This unit is synrift with the main extensional phase that led to the breakup along the Deep Galicia Margin to the west of Galicia Bank (Mauffret and Montardet, 1988, Murillas et al, 1990). Its upper limit is a strong reflection which corresponds to the latest Aptian break-up unconformity observed to the west of Galicia Bank (Murillas et al., 1990). In the wide angle data this unconformity is observed in the near offset reflections and is modelled as an abrupt velocity jump also observed on the prestack depth migration velocities (Figure 2.5). Within the deepest part of the Galicia Interior basin (Zone II, Plate 1) Formation 4 shows no evidence of synrift tectonism and was deposited during the period of thermal subsidence within this basin. Thus, this unit is postrift to the extension in the Galicia Interior Basin. Towards Galicia Bank (Zone III) Formation 4 shows a clearly synrift character with the westward directed extension that led to the continental breakup west of the Galicia Bank. Between CMP 13400 and 14700 (Plate 1) Formation 4 is a wedge with strata fanning formed by deposition during rotation of a block bounded by a large westward dipping fault.

### **Formation 5- Synrift II (Valanginian)**

This unit consists at ODP Site 638 in the Deep Galicia Margin (Figure 2.1) of sandstones and claystones Valanginian in age (Boillot et al., 1987). It is interpreted as an outer shelf progradational sequence to the west of Galicia Bank (Mauffret and Montardet, 1988). This unit is synrift with the first phase of extension that occurred to the west of Galicia Bank (Mauffret and Montardet, 1988). Along line 17 this unit lies at the top of tilted blocks bounded by eastward dipping normal faults and locally forms wedge like fans indicating that it is also synrift with the extension in the Galicia Interior Basin (e.g. CMP 6700 to 7200, Plate 1, Figure 2.12).

### **Formation 6: Synrift III (Tithonian to Berriasian)**

This sequence is thought to correspond to a large carbonate platform deposited across the margin during Tithonian to Berriasian times (Murillas et al., 1990, Mauffret and Montardet, 1988). It has been found on drill holes beneath the continental shelf and in the Deep Galicia Margin. We interpret that on line 17 corresponds to a unit characterised by large amplitudes and low frequencies deposited on top of the rotated blocks at the deepest part of the basin (on top of blocks B1 to B5, Plate 1, Figure 2.12). It also corresponds to a jump to velocities more than 5 km/s in the prestack velocity model. This unit probably indicates the first extensional phase of rifting in the Galicia Interior Basin, since carbonates only deposit in very shallow waters.

## **2.7.2 Basement**

The velocity structure as well as the structural style of the basement change along line 17. This change in the velocity structure corresponds also to a change in the morphology of the basement which together reveal the asymmetry of the basin. In the continental platform and slope area the basement is characterised by three velocity layers and a smooth deepening of the basement towards the center of the basin. Only a shallow slope basin interpreted to be bounded by a westward dipping fault offsets the basement (Plate 1). Westward of km 130, in Zones II and III, the basement has only two velocity layers (figure 2.5). Zone II, the deepest part of the basin where extension factors are largest (3.7 to 5.2), is characterised by large rotated blocks (B1 to B5 in Plate 1 and Figure 2.12) bounded by eastward dipping faults (F1 to F5 in Plate 1 and Figure 2.12). Block size decreases towards the centre of the basin where the basement lies deepest (>7 km deep at CMP 6500). The offsets of top basement on some of the faults in this area are up to 5 km. Block bounding faults started acting at high angle (~70 °) and have rotated up to ~35 °. Sediment wedges with internal stratal fanning indicate that Formation 5 was deposited when faults F1-F6 were active (e.g. CMP 6800-7300, Plate 1 and Figure 2.12). Thus, the main extensional

phase in the basin is Valanginian in age, which yields a minimum rift duration of ~5 m.y., although rifting may have extended up to 19 m.y. (Formation 5 and 6 synrift, see discussion in section 8.1). Note that the time scale used here is that published by Gradstein et al., 1996.

The area towards the Galicia Bank is characterised by a shallowing of top basement and also two velocity layers (Zone III, Plate 1, Figure 2.5). In this area, superimposed on the Valanginian extension, a second generation of faults dipping westward is observed. This extensional phase also extends into Zone II where west dipping faults cut the west flank of block B5 (Figure 2.12). Rotation on these faults was active while Formation 4 was being deposited, hence this extensional phase is younger than the one that formed the deep Galicia Interior Basin (Zone II). This extensional phase is interpreted to be Hauterivian to late Aptian in age and coincides with the extension that led to the final continental break-up to the west of the Galicia Bank at the Deep Galicia Margin.

The velocity structure combined with the MCS depth migrated section give insights into the mechanisms of deformation of the crust during extension. Seismic wide-angle velocities are normally interpreted in terms of petrology based on measurements of seismic velocities of different rock types at various pressures and temperatures at the laboratory. Experimental results indicate that the upper and middle crustal velocity layers of Zone I and Zone III, (where very little distortion of the seismic velocities produced by extension is expected), might consist of granites and granodiorites. The lower crustal velocity layer (velocities of 6.7 to 6.9 km/s) might be mainly made up of one or several composites like granulites, mafic granulites and anorthosites (Christensen and Mooney, 1995). The ductile strength of the lower crust is probably in between that of anorthosites and that of mafic granulites as within high grade metamorphic terranes exposing lower crustal rocks anorthosites are known to form low strain lozenges whereas mafic granulites and amphibolites are strongly deformed and sheared (e.g. South Harris shear zone, Reston, 1990; Portsoy complex of the Scottish Caledonides, Read, 1960). The interpretation of the MCS and the wide-angle data along profile 17 indicates that during the last stages of extension within the Galicia Interior Basin at least part of the lower crustal rocks moved from the ductile to the brittle deformation field. When the seismic reflection horizons are overlain on the wide angle profile (Figure 2.5) faults F1 to F6 reach the lower crustal velocity layer. Assuming that this velocity layer corresponds to the petrological lower crust, at least the upper part of the lower crust was cool enough to deform brittlely at the centre of the basin where extension factors are largest. Within the lower crustal velocity layer at the centre of the basin a set of bright, continuous, gently dipping reflections, DR, is observed (Plate 1, Figure 2.12). Fault F5 seems to mark the east limit to this reflectivity pattern. The extent of fault F5 is unclear, it may sole out at the top of the reflections DR, or it may cut through them, as indicated by the stippled line (Figure 2.12). This reflectivity does not coincide with

a clear wide-angle velocity limit, and we interpret that this reflectivity might be due to thin compositional layering. We speculate that the subhorizontal attitude reflects a ductile deformation fabric formed during extension of the lower crust. Towards the centre of the basin the crust thins to 6 km (Figure 2.5) and the DR reflectivity is truncated by faults F1 to F4, which might be interpreted as indicating progressive embrittlement of the crust with increasing extension. Rocks under ductile shearing yielding the DR fabric were brought to shallower levels as extension increased towards the centre of the basin (Plate 1, Figure 2.12). The rocks cooled and decompressed and eventually the yield strength required to deform brittlely was less than that to deform ductily (see chapter 5), and faults F1 to F4 cut deeper obliterating pre-existing ductile fabrics (CMP 6000 to 7000, Plate 1, Figure 2.12).

## **2.8 DISCUSSION**

### **2.8.1 Extensional history of the Galicia Interior Basin**

Drilling at the Deep Galicia Margin (ODP 103, Boillot and Winterer, 1988) and at the Iberia Abyssal Plain (ODP 149, Sawyer et al., 1994, and 173, ODP Leg 173 Shipboard Scientific party, 1998) recovered Tithonian to Berriasian shallow water carbonates. These were also encountered at dredge hauls around the Galicia Interior Basin (Dupeuble et al., 1987), and in several wells in the continental platform (Comas et al., 1988). Mauffret and Montardet (1988), associated these carbonates with a group of reflections characterised by high-amplitude, low frequency and moderate continuity observed in MCS profiles at the Deep Galicia Margin. Within the Galicia Interior Basin this seismic unit might form the top of the tilted blocks in the deepest part of the basin (see last section, and Murillas et al., 1990). These carbonates were deposited at depths that did not exceed few hundred meters (ODP Leg 173 Shipboard Scientific Party, 1998, Moullade et al., 1988). Thus assuming isostasy and in the absence of evidence for excessive volcanism at the margin or thermal uplift from plume activity, the shallow carbonates indicate that the margin (the Iberia Abyssal Plain, the Deep Galicia Margin and the Galicia Interior Basin) was underlain by only slightly thinned crust during the late Jurassic-early Cretaceous.

In the deepest part of the Galicia Interior Basin Formation 5 was deposited during the main phase of rifting indicating a minimum duration of 5 m.y. If Formation 6 (Tithonian-Berriasian carbonates) is also considered as a synrift sequence, then rifting lasted 19 m.y.. Our observations do not support previous phases of rifting in the Galicia Interior Basin that have been identified to the south in the Lusitanian Basin (Figure 2.1) (Montenat et al., 1988).

Within the deep basin, Zone II, Formation 4 (Hauterivian to Aptian, Murillas et al., 1990) onlaps onto Formation 5 (CMP 4500 to 8500, Plate 1, figure 2.12), indicating that it was deposited during the postrift thermal subsidence following the Valanginian extensional episode. However, towards Galicia Bank Formation 4 is synrift to a younger extensional phase characterised by westwards dipping faults. At block B5 the west dipping faults offset top basement and top of Formation 5, but do not reach the top of Formation 4 (Figure 2.12). This indicates that the faults were active during the deposition of Formation 4, during the Hauterivian to Aptian extensional episode that led to continental breakup in the Deep Galicia Margin.

The main extensional phase has led to a markedly asymmetric structure of the Galicia Interior Basin reflected in the change of the velocity structure along line 17 (Figure 2.5). We suggest that this change in the velocity structure is not due to asymmetric thinning of the crustal layers but reflects the pre-existing structure in the area. Beneath the continental platform and slope the basement consists of three velocity layers. This velocity structure is also typical for the Paleozoic Variscides terrane onshore NW Iberia: the central Iberian Zone (Cordoba et al., 1988, Figure 2.1). Figure 2.13a shows the correspondence between the crustal structure onshore and at the continental platform. The velocity and thickness of the mid and lower crustal layers are very similar. The upper crustal layers differ in that on the continental platform it is thinner and has lower velocities at the top and a higher velocity gradient. We attribute this to modification of the velocities to the inclusion of fluids in the upper crust at the continental platform. The three layers thin progressively towards the centre of the basin. From the centre of the basin towards Galicia Bank the basement has a two layer velocity structure. The velocity structure along line 17 close to Galicia Bank is very similar to that observed on the western side of Galicia Bank on Profile 6 (Whitmarsh et al., 1996, Figure 2.13a). Because the crust at the flanks of Galicia Bank is little extended (stretching factor  $\sim 1.5$ ), the change in velocity structure may reflect that the crust at the continental platform and slope (Zone I) is fundamentally different from that at the deep basin and towards the Galicia Bank (Zone II and III).

The asymmetry of the basin is also indicated by its structural style. Deepening of the continental platform is accomplished gradually, only the occurrence of a shallow slope basin offsets the basement. In the deep basin the major faults F1 to F6, that accommodated much of the extension, dip landwards (Zone I, Plate 1). We suggest that these faults formed along a major suture that separates two different terranes of the Variscan orogen (Figure 2.14). This structure might correspond to the offshore continuation of the Porto-Badajoz-Cordoba suture that runs from south to north separating different Variscan terranes (Figure 2.1, Capdevila and Mougénot, 1988, Quesada et al., 1994). The continental platform is within the Central Iberian domain of the Variscan orogen (Capdevila and Mougénot, 1988, Quesada et al., 1994), whereas studies of dredged samples from the Galicia Bank indicate

that the basement there is the northward continuation of the Ossa Morena domain (Capdevila and Mougenot, 1988, Mamet et al., 1991). We suggest that extension during the Tithonian-Valanginian event at the Galicia Interior Basin focused along the suture since it constituted a zone of pre-existing weakness separating the Central Iberian crust of the continental platform and slope from the Ossa Morena crust of the Galicia Bank (Figure 2.14). The change in velocity structure might reflect the change in crustal type from the Central Iberian Zone (Cordoba et al., 1988) to the Ossa Morena Zone.

Lateral changes from three crustal layers into two crustal layers have also been observed at the Rockall Trough (O'Reilly et al., 1996, Hauser et al., 1995). There it has been interpreted as due to differential stretching during extension leading to the amalgamation of three crustal layers into two. In this model, a decollement level at the top of the lower crust decouples the upper and mid crustal layers from the lower crust. This results in a large extension of the upper and mid crustal layers and subsequent amalgamation of both layers into one, while the lower crust extends by a smaller factor. This argument might explain the structure of the Rockall Trough where three layered structure is observed in the little extended crust at both sides of the basin but 2 layers are observed in the centre where extension is much larger (O'Reilly et al., 1996, Lowe and Jacob, 1989, Bunch, 1979). However, at the Galicia Interior Basin the velocity structure of the little extended Galicia Bank consists of two layers, and thus the two velocity layer structure might not be a product of extension. Furthermore, numerical modelling experiments impose a lower limit to the crust-mantle boundary (CMB) temperature for lower crustal flow and hence differential stretching to occur. Lower crustal flow towards the centre of the basin may only occur when the initial temperature at the CMB is in excess of 700°C to 800° C, for an initial 30 km thick crust and a rheological strength between anorthosite and dry quartz for the lower crust (Hooper and Buck, 1998). The crust onshore Iberia immediately east of the Galicia Interior Basin is 32 km thick (Cordoba et al., 1988), indicating a lower limit for crustal thickness before extension. Estimates of erosion onshore west Iberia since the Variscan based on the present depth of plutonic intrusions are on the order of 6 km (Vigneresse et al., 1999). Onset of rifting at the Galicia Interior Basin occurred around 100 m.y. after the Variscan orogen, and erosion was probably faster soon after the formation of the orogen, hence the crust onshore might have been  $\leq 35$  km thick at the beginning of rifting at the Galicia Interior Basin. Wide-angle velocities and observations of the distribution of the extensional strain in high grade deformation terranes indicate that a rheology for the lower crust in between that of anorthosite and dry quartz might be most appropriate to model its strength (see section 5.7.2, and also chapter 5). Thus it seems realistic that a temperature of 700 to 800 °C was needed for lower crustal flow at the Galicia Interior Basin. Assuming a crust of 32 to 35 km, reasonable values for the radiogenic heat

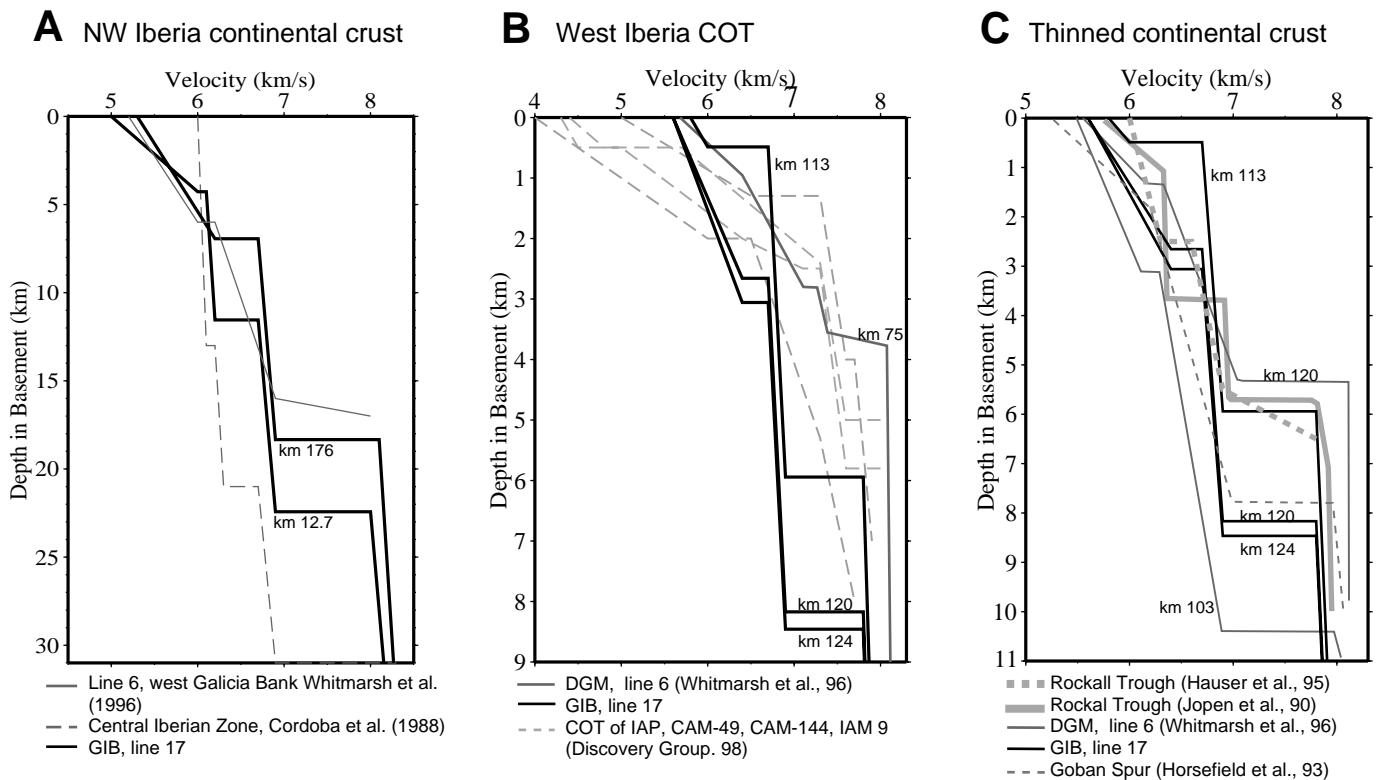


Figure 2.13. **A.** 1-D depth velocity profiles at slightly stretched continental crust: at the Galicia Bank and the continental platform along line 17. 1-D depth velocity profile of continental crust onshore west Iberia (Cordoba et al., 88) and on the west flank of Galicia Bank (Whitmarsh et al., 96) are shown for comparison. **B.** 1-D velocity profiles at highly stretched continental crust along line 17 ( Zone II, km indicate the position along line 17). Velocity profiles along the continental ocean-transition (COT) of the Iberia Abyssal Plain (IAP) and at the Deep Galicia Margin (DGM) are shown as an example of crust consisting of serpentinised peridotite. Velocity profiles at other rifts where the highly stretched crust is believed to be continental are shown. **C.** The same as in **B.** along line 17. Velocity profiles of other rifts where highly stretched crust is believed to be continental in nature are shown. Also velocity profiles of the continental crust at the west flank of the Galicia Bank are shown (the km indicate the position along line 6, Whitmarsh et al., 96, see Figure 3.1 and 3.5).



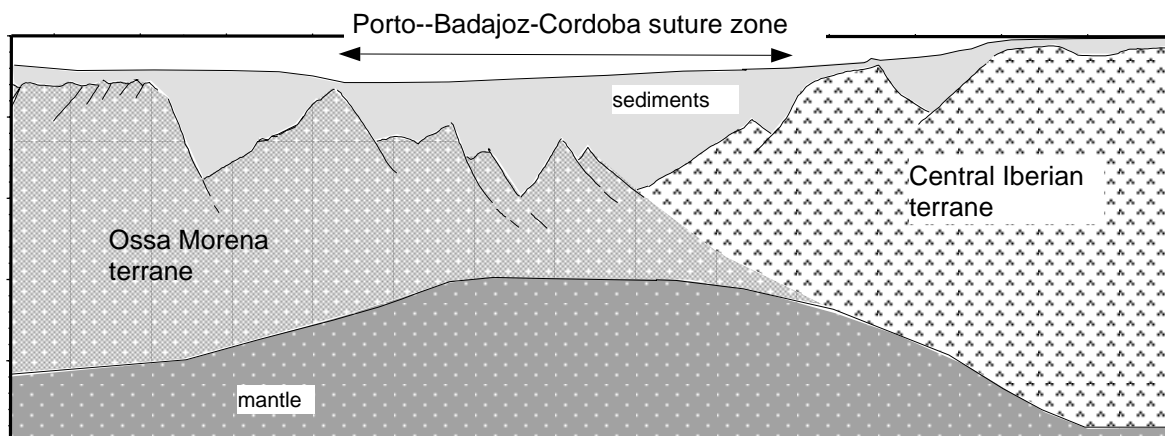


Figure 2.14. Geological cartoon explaining asymmetry in the velocity structure and in the morphology of the basement along line 17. (The line drawing is that interpreted on the depth migration but only the major faults are shown, Plate 1). The continental platform and slope belong to the Central Iberian terrane, whereas the Galicia Bank area belongs to the Ossa Morena terrane (Mougenot and Capdevila, 88). The Galicia Interior Basin might have developed along the Porto-Badajoz-Cordoba suture that separates these two different terranes. The asymmetry in the velocity structure might reflect the velocity structure of these two different types of crust.

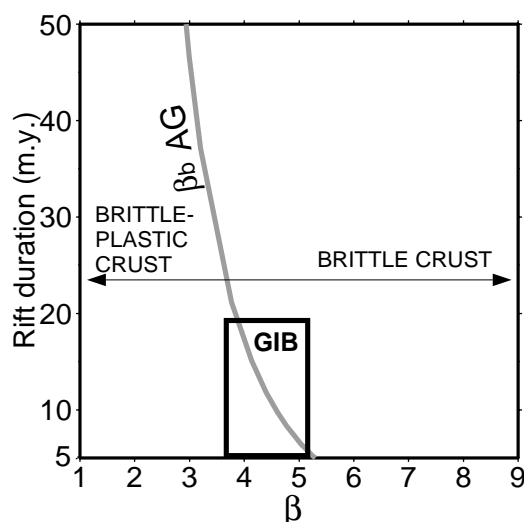


Figure 2.15. Line  $\beta$  AG indicates the stretching factors,  $\beta$ , at which the entire crust becomes brittle for different rift durations (for an aggregate rheology: 50% dry quartz, 50% anorthosite, see chapter 5 for details on the calculation). Stretching factors and possible rift durations at the center of the GIB (Zone II, Plate 1) are within the black box. At the centre of the GIB the entire crust had just entered or was in the point to move into the brittle deformation regime.

production in the crust and normal mantle temperature, yields a temperature at the CMB of around 450 to 600°C (see chapter 5). Since the temperature of the CMB only decreases during extension (see chapter 5), we suggest that lower crustal flow and differential stretching in the crust did not occur during extension at the Galicia Interior Basin. This conclusion supports the interpretation that rifting in the Galicia Interior basin developed along an older tectonic structure.

### **2.8.2 Nature of the crust in the deep Galicia Interior Basin (Zone II)**

The structure along line 17 shows that, assuming that the entire basement is continental in origin, extension factors at the centre of the Galicia Interior Basin (Zone II) attained a value of 3.7 to 5.2 (measured at CMP 6400 and 6700 respectively (Plate 1), assuming an initial 32 km thick crust, Cordoba et al., 1988). These high extension factors together with the widespread occurrence of serpentinised peridotite along the western Iberia margin (Boillot and Winterer, 1988, Whitmarsh and Sawyer, 1996, ODP Leg 173 Scientific Party, 1998) raise the question of whether the thin crust at the centre of the Galicia Interior Basin is only continental in nature, it consists of continental blocks on top of a progressively serpentinised mantle, or is mainly serpentinised peridotite.

Stretching factors of 4 to 6 are observed at the continental crust immediately landwards to the decollements S and H at the Deep Galicia Margin and Iberia Abyssal Plain (Chian et al., 1999, Whitmarsh et al., 1996, see chapter 4). Landward of these detachments the crust is continental in origin whereas seawards it has been interpreted to consist of serpentinised mantle (Boillot et al., 1989, Pickup et al., 1996, Chian et al., 1999). Continental blocks detach onto these decollements which are interpreted to be floored by serpentinised peridotite (Chian et al., 1999, Boillot et al., 1989, Reston et al., 1996). This suggests that when the crust is thinned by a factor of 4 to 6 a fundamental change in the mode of deformation might occur leading to the development of decollements and the exhumation of serpentinised mantle. Numerical modelling (see chapter 5) of the rheological evolution of the lithosphere during extension indicates that the entire crust moves into the brittle regime of deformation when these stretching factors are reached. This allows faults to cut down to the mantle and bring large amounts of seawater to serpentinise it. In addition, serpentinites have a low coefficient of friction (Escartin et al., 1997) and they may form a decollement at the base of the crust through which crustal separation and mantle exhumation occurs (see chapter 5). Figure 2.15 shows the stretching factors at which the entire crust moves into the brittle regime of deformation as a function of rift duration and for an aggregate (50% dry quartz, 50% anorthosite) lower crustal rheology. The stretching factors observed at the deep Galicia Interior Basin (Zone II) and the possible duration of the rifting there, 5 to 19 m.y., are indicated by a rectangular box. These are

calculated assuming an appropriate thermal state for the lithosphere at the beginning of rifting (see chapters 5 and 6 for discussion). This graphic shows that the entire crust was entering the brittle regime when faulting ceased at the centre of the basin. We infer that the crust at the centre of the Galicia Interior Basin (Zone II, Plate 1) may have been in a thermal and mechanical state appropriate for mantle serpentinisation to start. In this section we investigate, based on the wide angle and MCS data, if serpentinisation of the mantle took place and if eventually this led to crustal separation and mantle exhumation. If mantle was exhumed at the Galicia Interior Basin or part of the crust we observe consists of serpentinised mantle then the stretching factors must have been higher than 5.3 at the centre of the basin.

If the crust at the centre of the Galicia Interior Basin consists entirely or partly of serpentinised peridotite its velocity structure should resemble those of areas where there is strong evidence that the basement is made of serpentinised peridotite as for instance at the continent ocean transition zone of the Iberia Abyssal Plain (ODP Leg 173 Scientific Party, 1998, Dean et al., 2000, Discovery Group, 1998, Chian et al., 1999). The continent-ocean transition zone is defined at the west Iberia margin as the area between the most oceanward continental block and the first geophysically inferred oceanic crust. The velocity structure at the continent-ocean transition zone of the Iberia Abyssal Plain is characterised by a 2 to 4 km thick upper layer with velocities ranging from 4.5 to 7 km/s and a generally high velocity gradient ( $1 \text{ s}^{-1}$ ), and a lower layer up to 4 km thick with a velocity of  $\sim 7.6 \text{ km/s}$  and a low velocity gradient (Dean et al., 2000, Discovery Group, 1998, Chian et al., 2000, Figure 2.13b). The velocity of the lower layer increases progressively to reach a normal mantle velocity of 8 km/s at around 10 km depth (Chian et al., 1999). Moho reflections are rarely observed (Chian et al., 1999, Dean et al., 2000). Both layers are interpreted to consist of serpentinised upper mantle (Chian et al., 1999, Dean et al., 2000). The upper high velocity gradient layer is interpreted to reflect the depth extent of synrift hydrothermal circulation, yielding a 100% to 25% degree of serpentinisation. The velocities of the lower layer are interpreted as indicating a bulk serpentinisation of less than 25 %, probably concentrated along faults (Dean et al., 2000). This contrasts with the velocity structure at Zone II along line 17 (Figure 2.13b). Here the crust consists of two velocity layers, the upper layer has a maximum thickness of 3 km and the lower layer a of 5.5 km. The velocities in the upper layer range from 5.6 to 6.4 km/s, indicating that, most probably, it does not consist of serpentinite. When mantle is exposed at the top of the basement it is heavily serpentinised and has a lower velocity at the top. The velocity can be as low as 3 km/s at the top of the peridotite ridges (Chian et al., 1999) and is generally  $\sim 4.5 \text{ km/s}$  on top of the subdued basement of the continent ocean transition at the southern Iberia Abyssal Plain (Chian et al., 1999, Dean et al., 2000).

The lower crustal layer presents velocities of 6.7 to 6.9 km/s and a low velocity gradient. No gradual increase towards velocities of 8 km/s is observed and Moho reflections are seen in this area at OBH 240 (Figure 2.10) and OBH 237 (Figure 2.9). This velocity structure is typical for lower continental crust and very different to that observed at the Iberia Abyssal Plain (Figure 2.13b). Hence, from the velocity structure, it seems unlikely that this lower layer consists of serpentinised mantle.

The velocity of the mantle where this is shallowest (Zone II) is as low as 7.8 km/s. This contrasts with the velocities of 8 and 8.1 km/s observed at the mantle of Zone I and Zone III. The low mantle velocities at the centre of the basin may indicate a low degree of serpentinisation due to faulting across the entire crust at the centre of the basin, and hence might give an indication for the embrittlement of the entire crust at Zone II (Plate I, Figure 2.5).

In the MCS profile a very bright reflection that dips towards the basin, R, lies about 1 km above the wide angle Moho (Plate 1, Figure 2.2). R does not correspond to a velocity contrast in the wide angle data. The strong reflectivity of R may be due to several causes: i) R has the same origin as the reflectivity, DR, interpreted to be a ductile fabric, ii) R is a crust-mantle boundary, CMB, reflection but it does not coincide with the wide angle data Moho. This might be due to anisotropy of the velocities in the crust, or to lateral displacement of OBH 240 off Line 17, iii) R separates continental lower crust from a 1 km thick layer consisting of highly serpentinised peridotite of velocity  $\sim 6.9$  km/s which lies above the less serpentinised mantle, of velocity 7.8 km/s. If interpretations ii) or iii) are assumed then the continental crust is 1 km thinner as previously suggested, and stretching factors reach a value of about 6 when compared to the 32 km thick crust onshore.

We interpret the velocity structure of the crust at the deep Galicia Interior Basin to be the result of extension of the continental crust similar to Galicia Bank. The velocity structure of the upper layer is very similar to that of the thinned continental crust at the Deep Galicia Margin (Whitmarsh et al., 1996, Figure 2.13c). The lower crustal layer presents typical lower crustal velocities for continental crust as they are observed in our profile at the east flank of Galicia Bank (Zone III, Figure 2.13a) and are also similar to the lower crustal layer velocities in the western side of the Galicia Bank (Whitmarsh et al., 1996).

### **2.8.3 Comparison with other failed rifts**

The velocity structure of the deep part of the Galicia Interior Basin is very similar to that observed at the Rockall Trough, where the crust has been interpreted to be continental in origin (Hauser et al., 1995, O'Reilly et al., 1996, Figure 13c). However the Rockall Trough presents slightly higher stretching factors, 5 to 6, than the Galicia Interior Basin

and is much wider (O'Reilly et al., 1996). Below the lower crust of the Rockall Trough a 1 km thick layer with velocities of 6.9 to 7.8 km/s is observed which is interpreted to consist of a serpentinised peridotite (Hauser et al., 1995, O'Reilly et al., 1996). It has been proposed that the whole crust in the Rockall Trough entered the brittle regime after attaining this large extension factors and that fluids going down the mantle through brittle faults serpentinised it forming the transition layer at the base of the crust (O'Reilly et al., 1996). This agrees with our modelling results (see chapter 6). However, it is difficult to understand how a ~6 km thick continental crust extended without breaking along the ~200 km width of the Rockall Trough (Reston et al., 2000, chapter 6). When the crust enters the brittle regime it behaves as a single strong layer, reducing the toughness of the crust or its resistance to break (Dunbar and Sawyer, 1989, Bassi, 1993). This suggests that it is mechanically difficult to extend a 6 km thick crust over such a large area without breaking it and exhuming serpentinised mantle. As extension proceeds along the 200 km wide basin the stretching factors should increase and the crust should thin to less than 6 km. In contrast, the Galicia Interior Basin is much narrower and stretching factors did not exceed a value of 6. When stretching factors of 5 or maybe 6 were attained extension ceased and jumped to the west of the Galicia Bank, at the Deep Galicia Margin, where final continental breakup occurred. In the next chapter we speculate about the causes for rift cessation at the Galicia Interior Basin taking into account the geodynamic context of the west Iberia margin.

## 2.9 CONCLUSIONS

The conclusions of the integrated interpretation of a coincident MCS and wide angle seismic line along the northern part of the Galicia Interior Basin are:

(1) The Galicia Interior Basin has an asymmetric structure reflected in the morphology of the basement and the velocity layering in the crust. This suggests that it may have formed by reactivation of a Variscan suture, the Porto-Badajoz-Cordoba suture, separating different terranes found beneath the continental platform: the Central Iberian Zone, and the Galicia Bank: the Ossa Morena Zone.

(2) Along line 17 two different extensional phases are observed:

- At the centre of the Galicia Interior Basin large eastward dipping faults bound rotated continental blocks. Movement along this faults took place during deposition of sedimentary formations which are Tithonian to Berriasian (151-137 m.y.) and Valanginian (137-132 m.y.) in age, constraining the duration of rifting to 19 m.y.. The Tithonian to Berriasian formation may correspond to a large carbonate platform deposited in shallow waters over

the whole margin, implying that the main extensional phase took place during Valanginian times and was only 5 m.y. long.

- Towards the east flank of Galicia Bank a second generation of faults which dip westwards is observed. Movement along these faults took place during deposition of a sedimentary formation which is interpreted to be Hauterivian to Aptian in age (132 to 112 m.y). This phase is coeval with the main extensional phase that led to continental break-up in the Deep Galicia Margin.

3) At the centre of the basin the basement is extremely thinned reaching stretching values of 4 to 5. The velocity structure is typical for highly stretched continental crust.

4) Uniform stretching of the upper and lower crust explains the crustal structure modelled with the wide angle data. Furthermore, estimates for the initial thermal lithospheric structure and numerical modelling results (Hopper and Buck, 1988) indicate that the base of the crust was probably too cold for lower crustal flow to occur. This might imply that differential stretching of the upper and lower crust might have been mechanically unfeasible. In contrast, numerical modelling indicates that progressive embrittlement of the entire crust at the centre of the basin might have allowed faults to cut to the Moho and facilitated low degree of serpentinisation of the mantle.

**CHAPTER 3. STRUCTURE OF THE GALICIA INTERIOR BASIN FROM MCS  
INDUSTRY LINES AND EVOLUTION OF THE WEST IBERIA MARGIN.**

**3.1 INTRODUCTION**

Lines AB, GAP 106, 14 and 15 were acquired during the late 70's as a part of a regional reconnaissance survey in the Galicia Interior Basin carried out by the oil company REPSOL. These lines were acquired and processed by Western Geophysical Company. Murillas et al. (1990) published the first study of the seismic stratigraphy in the Galicia Interior Basin using paper copies of stack sections of these lines. We have studied three lines that run from the continental platform across the deep Galicia Interior Basin to the shallow Galicia Bank (line AB, GAPs 106 and 14, Figure 3.1). Line GAP 15 runs from south to north along the depocentre of the basin (Figure 3.1). We processed these lines up to time migration (chapter 1), to improve the image of the complex basement structure and deep sedimentary units which was unclear in the sections used by Murillas et al. (1990). These time migrated sections were also used to choose where to shot line 17 during the Iberia Seismic Experiment (1997) carried out by the R/V Maurice Ewing. In this chapter we review the seismic stratigraphy of the basin and present an interpretation of the MCS lines based on the new images in the time migrated sections. These images have allowed us to recognise accurately the sequence of synrift-prerift sediments and the structure of the rotated blocks bounded by extensional faults. We have also imaged a sequence of bright reflectors within the basement which seem to be distributed within the entire basin and were not clearly imaged in the stack sections interpreted by Murillas et al. (1990). However, recording of the lines stopped before the Moho TWTs. Nevertheless, many features observed in line 17 (chapter 2) are also imaged on the older and lower quality GAP and AB lines, indicating that some of the crustal features extent along a large portion of the basin. To understand the variation of the amount of extension along the basin we have used the crustal thickness constraints given by line 17 (chapter 2) in the north of the basin, and those given by line 1 (Zelt et al, 1999), and line IAM 11 (Gonzalez et al., 1999) in the southern part of the basin (Figure 3.1). Finally, we speculate about the causes for rift failure at the Galicia Interior Basin based on the distribution of crustal extension and the timing of the main extensional events at the different segments of the west Iberia margin.

**3.2 INTERPRETATION OF TIME MIGRATED SECTIONS**

Murillas et al. (1990) used the stacks of the MCS lines presented here to define the seismic stratigraphy of the Galicia Interior Basin. Since the image of the flat lying, shallowest sediments does not change much with time migration, in this chapter we will focus in the new aspects brought by the reprocessing. We have obtained new information on the deep lying synrift-prerift sedimentary sequences and the morphology of the basement. Section 2.7.1 of chapter 2 reviewed the facies, character, lithology and age of the sedimentary formations defined by Murillas et al. (1990) and we will refer to it when necessary. Line AB, GAP 106, 14 and 15 reveal a 3D image of the Galicia Interior Basin (Figure 3.1, and 3.2). To the north, line AB runs from the depocentre of the basin to the shallowest area of Galicia Bank. It crosses line 17 at a small angle at about CMP 2800 (Figure 3.2). Thereby most of the structures observed on line AB can be easily correlated with those on line 17. To the south, GAP 14 shows a cross section perpendicular to the margin from the continental platform to the deepest part of the basin. Here it ties with GAP 106 that runs obliquely to the margin up to the southern flank of Galicia Bank. GAP 15 is a transect along the deepest part of the basin in its strike direction. Using these lines we have identified three zones which differ in their structural style and also probably in the timing of the main extensional events (Figure 3.2). These coincide with Zone I, II and III identified along line 17, namely the continental platform and slope domain, the deep basin, and the east flank of Galicia Bank (see chapter 2).

### **3.2.1 Sedimentary cover**

Along the lines Formations 1 and 2 drape over the underlying topography indicating deposition without significant tectonism nor thermal subsidence. Formation 3 shows an onlap pattern on the previous sedimentary units indicating that it was deposited during a thermal subsidence period (Figure 3.2). At the deepest part of the basin (Zone II) and at the continental slope (Zone I) Formation 4 also onlaps on the basement topography and does not show evidence of synsedimentary tectonism indicating that it was also deposited during thermal subsidence of the basin and therefore is postrift to the main extensional event in the Galicia Interior Basin (Figure 3.2 and 3.3). Towards Galicia Bank Formation 4 shows rotation and fanning of the strata formed by movement along westward dipping faults (Zone III, CMP 4500-4900, line AB, CMP 1400-1500 and 1700 to 1900, GAP 106, Figure 3.2 and 3.3). This tectonism is coeval with the Hautiverian to Aptian phase (132-122 m.y.) that led to final continental break-up west of Galicia Bank, at the Deep Galicia Margin. Within the deepest part of the basin the postrift sedimentary



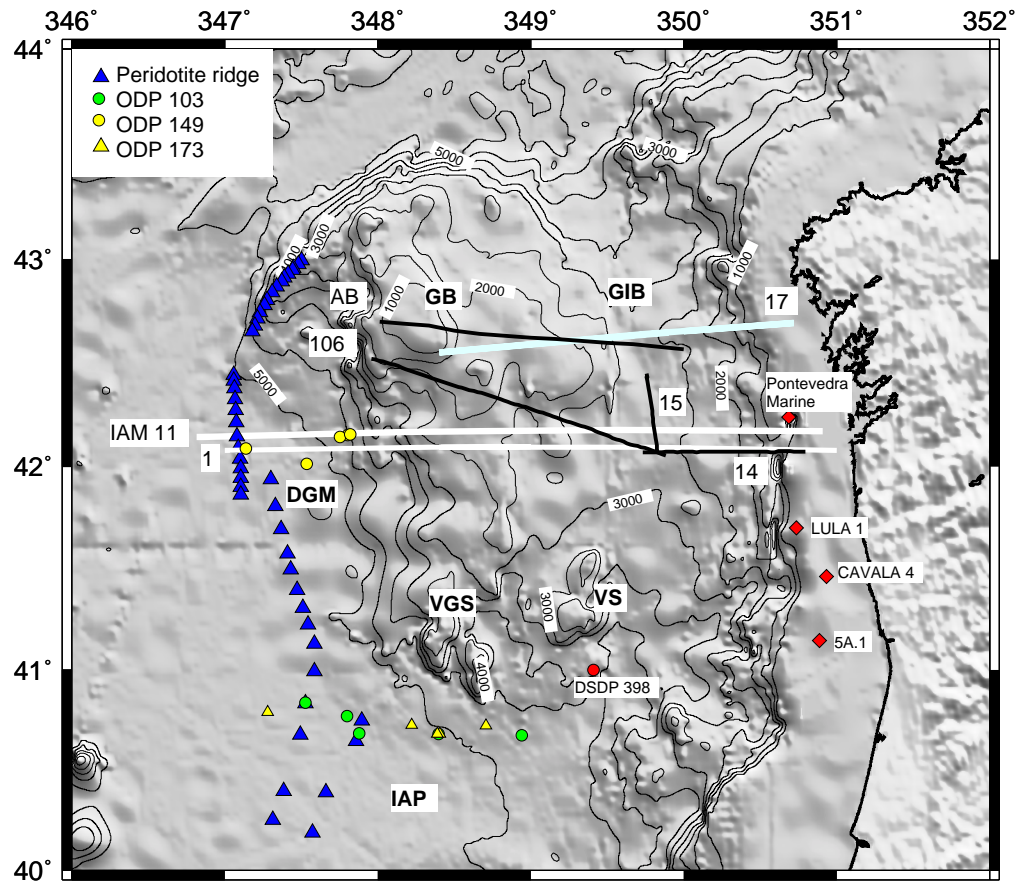


Figure 3.1. Bathymetric map of west Iberia showing tracks of industry lines AB, GAP 14, 106 and 15. Lines 17 (chapter 2), Line 1 (Zelt et al., 99) and IAM 11 (Gonzalez et al., 99) which are also used for the interpretation of the industry lines are also shown. Diamonds indicate the platform wells used by Murillas et al. (90) to define the seismic stratigraphy of the Galicia Interior Basin (GIB). ODP drilling locations and DSPD dredge 398 to the south of Vigo Seamount are also shown. **DGM**: Deep Galicia Margin, **GB**: Galicia Bank, **GIB**: Galicia Interior Basin, **IAP**: Iberia Abyssal Plain, **VSG**: Vasco da Gama Seamount, **VS**: Vigo Seamount.

sequences, Formations 1 to 4, thin towards the south at expenses of Formation 3 and 4 (Figure 3.2).

Based on the improved image after time migration we have redefined the location and extent of Formations 5 and 6 with respect to that given by Murillas et al. (1990). On the continental platform and slope Formation 5 lies on top of rotated blocks bounded by westward dipping faults (Zone I, GAP 14, Figure 3.2). However, is difficult to identify clearly the depth extent of the small basins formed on top of the rotated block and hence the depth extent of this Formation in this area; MCS data with deeper penetration would be needed to clarify this. At the deepest part of the basin, along line AB (Zone II, Figure 3.2), we have interpreted that Formation 5 fills the gap between rotated blocks (B1 to B5) bounded by eastward dipping faults (F1 to F6). On this line Formation 5 does not portray the clear synrift character that shows along line 17 (Figure 2.12). Nevertheless, since these lines are very close we interpret that this is due to imaging problems and that here this unit was also deposited during movement of the eastward dipping faults being synrift to the main extensional phase of the basin. Note that on the time migrated section of line 17 strata fanning within Formation 5 is not observed (CMPs 6700-7200, Figure 2.2), whereas in the depth migrated section this becomes clearer (CMPs 6700-7200, Figure 2.12). This is due to the very detailed velocity information obtained by depth focusing error analysis and common reflection points during prestack depth migration (see section 4.1, chapter 2). Along GAP 106 Formation 5 seems to form sedimentary fan like wedges on top of block B7 and B10 formed by deposition during rotation of faults F8 and F11 (GAP 106, Figure 3.2 and 3.3). This indicates that also here the main extensional phase took place during deposition of this unit, i.e. during Valanginian times (137-132 m.y.).

On line AB we have interpreted, similarly to line 17, that Formation 6 lies on top of the rotated blocks B1 to B6. Also here as in line 17, this unit does not show strata fanning formed by deposition during rotation of the main faults F1 to F6 and we interpret it to be a carbonate platform deposited during the first stages of extension of the Galicia Interior Basin (Tithonian to Berriasian, 151-137 m.y.) (see section 7.1).

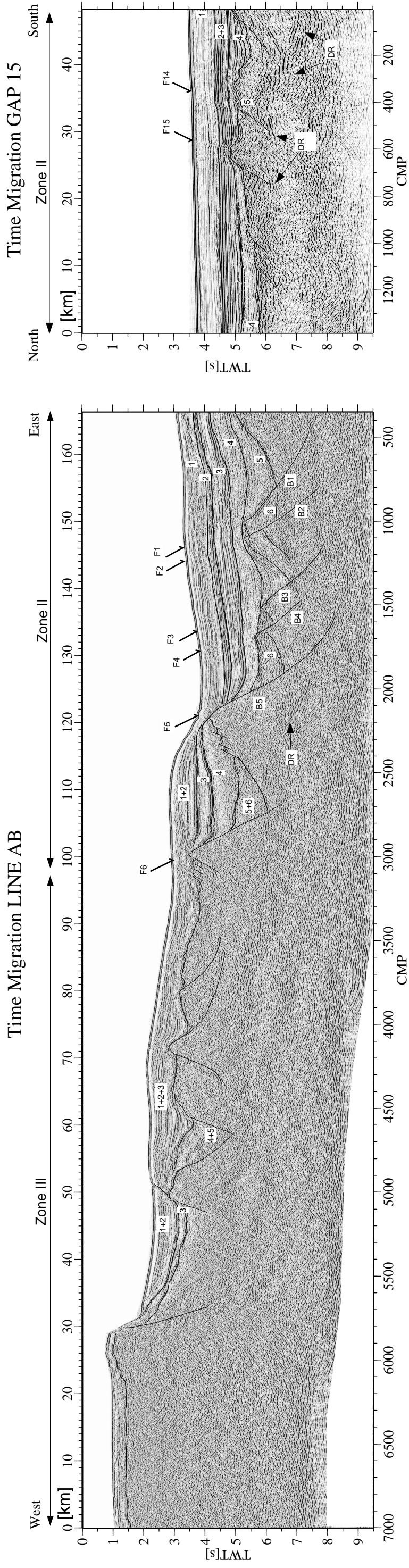
### **3.2.2 Basement**

The basement of the continental slope deepens smoothly towards the centre of the basin along line AB (CMP 375-700, line AB, Figure 3.2). In the south, the basement of the continental slope (Zone I, GAP 14, Figure 3.2) is very rough and is offset by westward dipping faults on top of which small half graben basins are observed. The continental slope area (Zone I) is separated from the deep basin (Zone II) by a roughly symmetric basement high or ridge which does not have the appearance of a block rotated along an extensional faults (CMP 11000-2000, GAP 14, Figure 3.2). This ridge might be a local feature since on

line IAM 11 (Banda et al., 1995, unpublished MCS data), which lies just north of GAP 14 (Figure 3.1), this ridge is not observed. Therefore we interpret that the ridge has no regional significance for the extensional evolution of the basin.

At the deep basin, (Zone II), extension is accommodated by eastward dipping faults bounding rotated blocks whose size decreases towards the centre of the basin where basement lies deepest (Zone II, Figure 3.2). These faults rotated during deposition of Formation 5, i.e., during Valanginian times (137-132 m.y., Figure 3.2 and 3.3). On line AB the morphology of the blocks and the faulting pattern is very similar to that on line 17 and we interpret that faults, F1 to F6, bounding the blocks, B1 to B5, correlate with those on line 17 (Figure 2.12). Along GAP 106 the rotated blocks, B7 to B12, present a complex structure which might be due to the obliquity of the line and are not readily correlated with those observed along lines AB and 17 (Figure 2.12, 3.2 and 3.3). We interpret the blocks on GAP 106 to be bounded by eastward dipping faults which also offset a set of high amplitude, low frequency, deep reflections, DR (Figure 3.2, 3.3). A similar reflectivity pattern is also observed on line AB, below block B5, and along most of line 15 (DR on Figure 3.3). The DR reflections appear as a set of gently dipping, continuous reflections on block B12 (GAP 106, Figure 3.2 and 3.3) and B5 (line AB, Figure 3.2). However, towards the centre of the basin where the basement lies deepest the DR reflections appear discontinuous and offset by faults (F7 to F11 on GAP 106 and F14 to F15 on GAP 15, Figure 3.2). The seismic facies of the DR reflections, the variation of its continuity pattern with increasing amounts of extension and the TWT at which is observed is analogous to a set of reflectors observed on line 17 (DR, Plate 1, Figure 2.12). Therefore, in these lines we interpret also that the continuous subhorizontal attitude of DR (observed on block B5 on line AB and B11 on GAP 106) reflects a ductile deformation fabric formed during extension of the lower crust that extends across most of the deep basin in our data (see discussion on section 7.2). Towards the centre of the basin the crust thins to 6 km in the north (along line 17, Figure 2.5) and to 8 km in the south (line 1, Figure 3.1, Zelt et al., 1999), and the DR reflections are truncated by faults F11 to F7 (GAP 106, Figure 3.2), and F14 to F15 (GAP 15, Figure 3.2). DR are not observed at the centre of the basin on line AB, probably because of pervasive brittle faulting that has obliterated the subhorizontal reflectivity. In line 17 faults F1 to F5 offset the DR reflections at the centre of the basin (Plate 1, Figure 2.12, in chapter 2). We interpret that also on the lines presented here, as in line 17, the truncation of the continuous reflectivity at the centre of the basin is due to the progressive embrittlement of the crust with increasing extension and the truncation of fossil ductile deformation fabrics by deep penetrating brittle faults (see discussion on section 7.2.).

Towards the Galicia Bank (Zone III) top basement shallows and a second generation of faults is observed superimposed on the Valanginian episode (Zone II, line AB and GAP 106). Movement along these faults took place during deposition of Formation 4



Time migration GAP 106-14

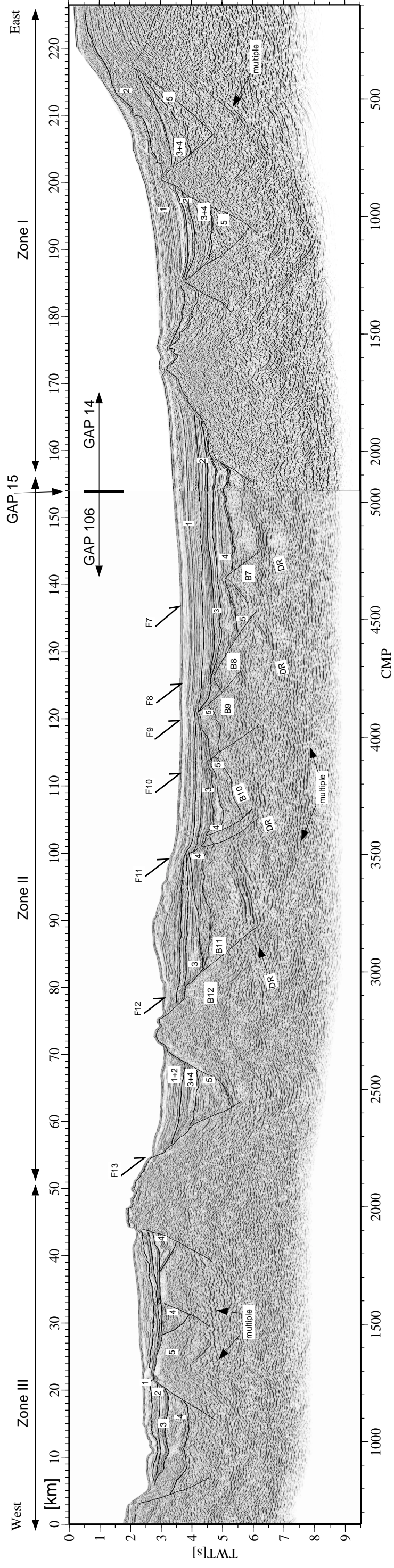


Figure 3.2. Time migrations of lines AB, GAP 106, 14 and 15 with interpretation. 1, 2, 3, 4, 5 and 6 indicate different sedimentary Formations (see text). F1 to F13 indicate extensional faults and B1 to B12 continental blocks rotated by these faults. For comparison see Figure 1.23 for time migrations without interpretations.

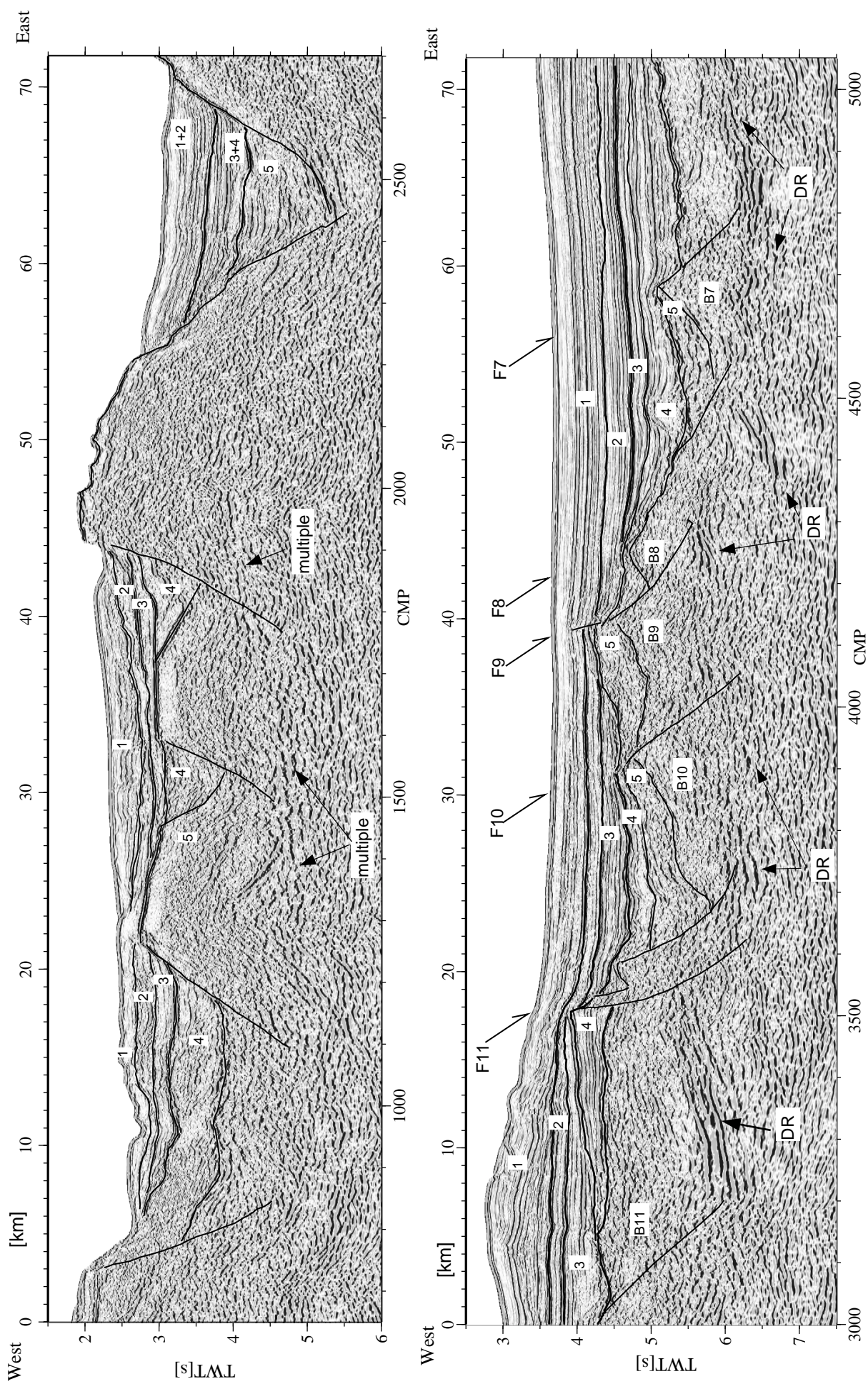


Figure 3.3. Detail of time migration of GAP 106 (Figure 3.2) showing two phases of extension. **(Top)** A Hautiverian to Aptian extensional phase (132-112 m.y.) characterised by continental block rotation along seaward dipping faults during deposition of Formation 4. This phase is coeval with the one that led to continental break-up at the Deep Galicia Margin. **(Bottom)** A Valanginian extensional phase (137-132 m.y.) characterised by continental block rotation along landward dipping faults during deposition of Formation 5.

(Hautiverian to Aptian, 132-112 m.y., Figure 3.2 and 3.3) when the focus of largest extension shifted to the Deep Galicia Margin where final continental break-up took place in Aptian times (Boillot and Winterer, 1988).

### **3.3 DISCUSSION**

#### **3.3.1 Variation of crustal thickness and timing of the extensional phases along the west Iberia margin**

In this section we present a map of the extensional phases and distribution of thinnest crust at the different segments of the west Iberia margin. This map is based on a compilation of our results with other published data at the margin (Figure 3.4). The final break-up margin off west Iberia is divided in three segments: the Tagus Abyssal Plain, the Iberia Abyssal Plain and the Deep Galicia Margin. The Tagus Abyssal Plain is separated from the Iberia Abyssal Plain by the Estremadura Spur which stands out from the continental margin and may be of volcanic origin younger than the rifting at the margin; an alkaline basalt dated at 74 m.y. old was dredged from its western tip (Mougenot, 1988). The Deep Galicia Margin is separated from the Galicia Interior Basin by the shallow Galicia Bank. The Bank is an area of thicker crust than its surroundings (Figure 3.4, and 3.5), although its elevation may be partially explained by uplift related to postrift compression during the closure of the Bay of Biscay (Boillot et al., 1979).

Continental rifting along the west Iberia margin propagated from south to north (Figure 3.4). In the Tagus Abyssal Plain the main extensional event has been proposed to be Oxfordian to Kimmeridgian in age (155-151 m.y., Mauffret et al., 1989). This age was constrained by seismic stratigraphy analysis of MCS lines at the Tagus Abyssal Plain based on comparisons with results of DSDP Legs south of Vigo Seamount (Groupe Galice, 1979) and Gorrige Bank (Ryan et al., 1973), and the geology of the Portuguese margin (Mougenot, 1988). The Lusitanian Basin, located onshore Portugal, experienced several episodes of rifting from Triassic to lower Cretaceous, however its main rifting phase is interpreted to occur coeval to that in the Tagus Abyssal Plain (Wilson et al., 1989, Rasmussen et al., 1998, Figure 3.4).

At least part of the main phase of rifting at the Iberia Abyssal Plain occurred synchronously with the main extensional event at Galicia Interior Basin during Valanginian times (137-132 m.y., Dean et al., 2000, 1988, Murillas et al., 1990). However, after this period, rifting ceased at the Galicia Interior Basin while extension continued at the Iberia Abyssal Plain up to Barremian times (125 m.y., Whitmarsh and Miles, 1995). The main rifting period in the Deep Galicia Margin occurred after cessation of rifting at the Galicia

Interior Basin, during Hautiverian to Aptian times (132-120 m.y., Boillot and Winterer, 1988).

Seafloor spreading along the west Iberia margin began from south to north in a time transgressive fashion (Figure 3.4). Offshore the Grand Banks and West Iberia the most prominent magnetic anomaly is J. This anomaly, although not a single seafloor spreading isochron, has been shown to be formed of anomalies M0 and M2 in the Central Atlantic (Rabinowitz et al., 1979, Tucholke and Ludwig, 1982). The J anomaly exists only off the southern parts off west Iberia and the Grand Banks (Figure 3.4), thereby implying a south to north propagation of seafloor spreading. Although still under debate (Srivastava et al., 1998), modelling of magnetic anomalies indicates that seafloor spreading might have occurred as far back as the M11 anomaly (132 m.y) at the Tagus Abyssal Plain (Pinheiro et al., 1992), and at the M3 anomaly (early Barremian, 125 m.y.) at the Iberia Abyssal Plain (Whitmarsh and Miles, 1995). No seafloor spreading anomalies appear to exist immediately west of the Galicia Bank because seafloor spreading began during the Cretaceous constant polarity interval (Ogg, 1988). However, based on the age of the break-up unconformity at the Deep Galicia Margin, seafloor spreading is thought to began during the late Aptian (112 m.y., Boillot and Winterer, 1988). Along the Iberia Abyssal Plain and the Deep Galicia Margin the first geophysically inferred oceanic crust occurs immediately west of a series of elongated peridotite ridges that run from south to north, and mark the oceanward limit of the continent-ocean transition zone (Figure 3.4, Beslier, 1993).

Based on wide angle data we have delineated the areas of thinnest continental crust from the Estremadura Spur to the northern end of the margin. At the Galicia Interior Basin constrains of crustal thickness are given by line 17 (Figure 3.5) and line 1 (Zelt et al., 1999, Figure 3.4). The crust in the continental platform is ~24 km thick, and thins towards the centre of the basin to 8 to 6 km (hatched area in Figure 3.4, Figure 3.5). The bathymetric data indicates that the Galicia Interior Basin continues to the south between the continental platform and Vigo Seamount, however no wide angle data are available in this area to constrain the crustal thickness. At the final break-up margin, along the Iberia Abyssal Plain and the Deep Galicia Margin, the hatched area indicates where the crust is 6 to 3 km thick (Figure 3.4). Crustal thickness constrains are given by wide angle data along IAM 9 (Dean et al., 2000), a depth migrated MCS line LG12 along the ODP 149 and 173 transects (Krawzyck et al., 1996, Figure 4.2), and line 6 along the ODP 103 transect (Whitmarsh et al., 1996).

Wide angle data (Dean et al., 2000, Chian et al., 1999, Whitmarsh et al., 1996) and results from ODPs 103, 149 and 173 (Boillot and Winterer, 1988, Whitmarsh and Sawyer, 1996, ODP 173 Scientific Party, 1988) have allowed to locate the position and extent of the continent-ocean transition zone along the Iberia Abyssal Plain and the Deep Galicia Margin segments of the west Iberia margin (Figure 3.4, Figure 3.5). This zone, which

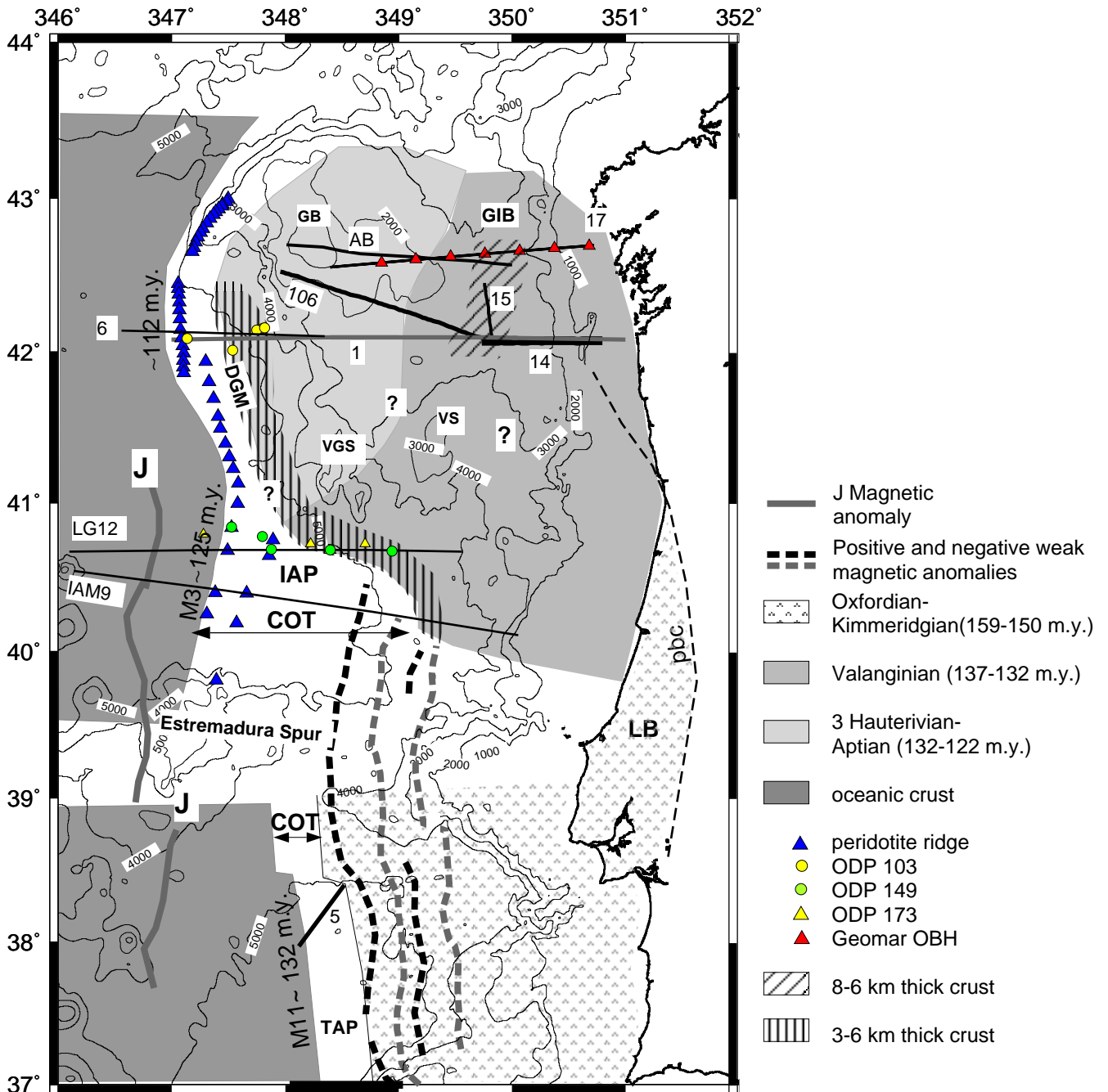


Figure 3.4. Bathymetric map of west Iberia. **COT**: continent-ocean transition, **DGM**: Deep Galicia Margin, **GB**: Galicia Bank, **GIB**: Galicia Interior Basin, **LB**: Lusitanian Basin, **IAP**: Iberia Abyssal Plain, **TAP**: Tagus Abyssal Plain, **pbcc**: Porto-Badajoz-Cordoba suture, **VGS**: Vasco de Gamma Seamount, **VS**: Vigo Seamount. The main extensional phases at each segment of the margin are color and pattern coded (see legend). The extent of the continental, the COT and the oceanic crust are also shown (see legend). At the continental platform of the IAP and GIB the crust is around 25 km. The diagonal lines in the GIB indicate the area of maximum extension, i.e. thinnest crust here (8-6 km). Question marks indicate that no information about the timing of the extensional phases and the crustal thickness is available. At the DGM and the IAP the area of thinnest crust (6-3 km) is indicated by vertical lines. Information about the timing of extension, nature and thickness of the crust is given by the seismic lines presented in this work (AB, GAPs 106, 14 and 15), existent lines in the literature (1, 5, 6, LG12 and IAM9) and ODP drillings (dredges and wells used to define the seismic stratigraphy at the GIB and TAP are not indicated here). The dashed north-south lines are weak, linear magnetic anomalies. Note that these are within the continental crust at the TAP, suggesting that at this segment the COT might extend further to the east. Seafloor spreading propagated from south to north, the age of seafloor spreading initiation is indicated at the landward edge of the oceanic crust.



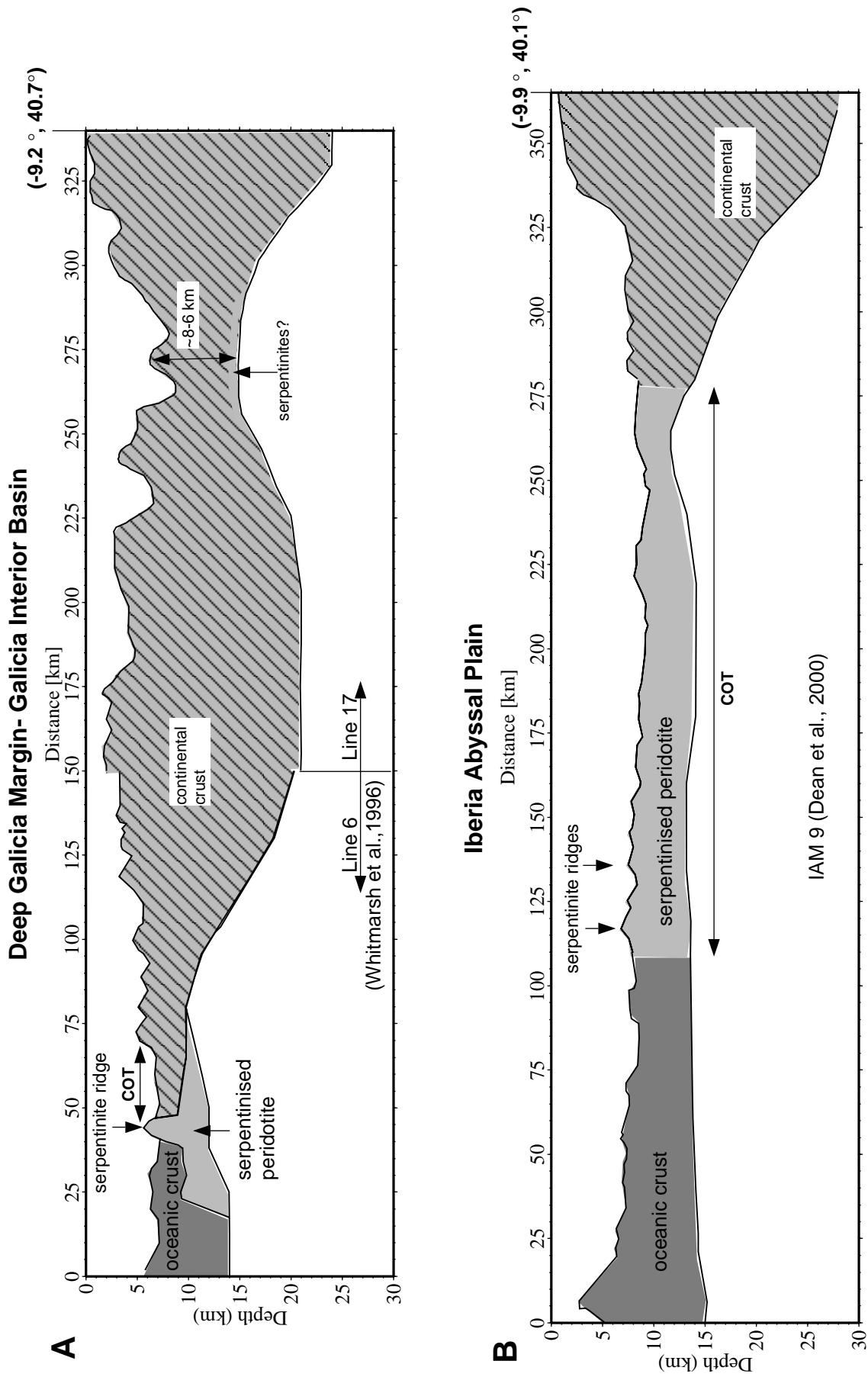


Figure 3.5. Interpreted wide angle sections along **A.**: the Galicia Interior Basin (GIB) and the Deep Galicia Margin , and **B.**: the Iberia Abyssal Plain (IAP). The width of the offshore continental crust increases to the north as opposite to the width of the ocean-continental transition zone.

extends from the most oceanward continental block to the first geophysically inferred oceanic crust, narrows to the north: from 170 km at the Iberia Abyssal Plain (line IAM 9, Dean et al., 2000), to ~20 km along the Deep Galicia Margin (line 6, Whitmarsh et al., 1996, Figure 3.4 and 3.5). The offshore width of the extended continental crust increases to the north as the width of the continent-ocean transition zone decreases. Thereby the overall width from the continental platform to the first geophysically inferred oceanic crust remains relatively constant along the margin (Figure 3.5).

The position and extent of the COT at the Tagus Abyssal Plain was defined by Pinheiro et al. (1992) using wide angle data recorded along a 80 km long reversed profile (line 5, Figure 3.4) and modelling of magnetic anomalies. However a new magnetic anomaly map off west Iberia (Miles et al., 1996) might suggest that the COT could extend further to the east. A series of alternating positive and negative, weak magnetic anomalies extend continuously along ~350 km from the Tagus Abyssal Plain to the south of the ODP 149, 173 area (Figure 3.4). These anomalies are within the previously defined continental crust (Pinheiro et al., 1992). Although the magnetic anomalies are weak when compared to normal seafloor spreading anomalies, their extent and continuity suggests that they might have formed by a similar process. Thereby the origin of the crust east of the continental ocean transition at the Tagus Abyssal Plain remains an open question (Figure 3.4).

In the next section we speculate about the mechanisms for rift failure at the Galicia Interior Basin and its relationship with the extensional strain along the margin and the northward propagation of the seafloor spreading centre.

### **3.3.2 Mechanisms for rift abandonment in the Galicia Interior Basin**

The way that extensional strain is distributed in the continental lithosphere forming wide rifts or narrow ones, and the relationship between extension of the continental lithosphere and initiation and/or propagation of a seafloor spreading ridge is a matter of continuous debate. Studies of extension of the continental lithosphere have focused on the influence that the extension velocity (England, 1983, England and Sonder, 1989), the existence of offset weaknesses in the crust and mantle (Dunbar and Sawyer, 1989), and the initial thermal state of the lithosphere (Buck, 1991, Bassi, 1993, Hooper and Buck, 1996) has on the formation of narrow versus wide rifts. Narrow rifts are those where extension is focused in a narrow area (< 100 km). At wide rifts extension is distributed over a larger area and the focus of maximal extension jumps laterally as rifting proceeds. In this sense, the rifted continental crust at the Iberia Abyssal Plain can be regarded as a narrow rift while the rifted continental crust at the Galicia Interior Basin and the Deep Galicia Margin constitutes a wide rift. Here the locus of maximal extension has jumped laterally through time (Figure 3.4 and 3.5). Observations at active rifts where initiation of seafloor spreading is occurring,

such as the Woodlark, and the Red Sea (Taylor et al., 1999, Bonatti, 1985), concentrate on why oceanic spreading initiates at certain locations, and how it propagates through rifted continental lithosphere. These observations have shown how, very often, the final shape and morphology of the margins are not only a consequence of the process of continental rifting itself but result from the feedback of synchronous continental rifting and seafloor spreading propagation. Furthermore, the direction along which spreading centres develop, leaving well developed basins at the landward sides of the final continental margins (e.g., Porcupine basin, Rockall Trough, Jeanne d'Arc basin, Galicia Interior Basin), may be linked to a more global tectonic framework in which large transform faults, spreading centres and accommodation zones connect different tectonic environments. Reconstruction of the exact position of Iberia with respect to Africa and Eurasia at the time of break-up along the margin and the interaction of spreading along the margin with subduction at the Thetys ocean is poorly constrained (Malod and Mauffret et al., 1991). In this section we suggest that none of the mechanisms invoked to explain widening of the rifting zone during rifting of the continental lithosphere explains rift abandonment at the Galicia Interior Basin. The ultimate cause for rift abandonment here might be related to the organisation of the tectonic stresses in a more global framework. To understand this the relative movement of the Iberia plate, the Newfoundland Margin and Eurasia as well as the timing and amounts of extension in the conjugate abandoned basins of the Newfoundland margin (e.g., the Jeanne d'Arc Basin) should be known with accuracy.

England (1983) first suggested that when the mantle rises up to fill the gap left behind by the extended crust, it cools down and strengthens. The overall strengthening of the lithosphere where the crust is thinnest makes it easier to extend an adjacent area where the crust has not yet been thinned. This eventually leads to a lateral shift of the locus of maximal extension. However, for this process to be effective extension must occur very slowly, at a strain rates less than  $10^{-15}\text{s}^{-1}$  (Sonder and England, 1989). Given that the rifting period in the Galicia Interior Basin (Tithonian to Valanginian) lasted from 5 to 19 m.y. (strain rate of  $5 \times 10^{-15}\text{s}^{-1}$ ) we discard this hypothesis as the cause of rift abandonment at the Galicia Interior Basin.

Buck (1991), Bassi (1995) and Hooper and Buck (1996) suggested that the initial thermal state of the lithosphere is what controls the width of the extended area. When the crust thins, higher density mantle is brought to shallower levels resulting in a compressional buoyancy force that inhibits extension. This crustal buoyancy force is only important when the lithosphere is thin so that the amount of possible weakening due to lithospheric necking is small. A thin lithosphere corresponds to a thick and warm crust. In the case of Iberia the crust onshore might have been 35 km thick at most, and the temperature at the base of the crust in between 450-600°C (see discussion on chapter 4 and 5). Therefore, we suggest that

the crust at the onset of rifting was neither thick nor warm, so that this hypothesis also does not apply in the case of the Galicia Interior Basin.

Finally, Dunbar and Sawyer (1989) have studied what might occur when at the onset of extension a weakness in the crust and a weakness in the mantle which are offset laterally exists. They suggest that rifting initiates where the crustal weakness is located but shifts progressively towards the location of the mantle weakness. The crustal weakness might have been the Porto-Badajoz-Cordoba suture along which the Galicia Interior Basin developed. The mantle weakness might have been the broad serpentinite zone at continent ocean transition at the Iberia Abyssal Plain. However, the weakness at the continent ocean transition of the Iberia Abyssal Plain develops as a product from rifting and clearly it did not exist at the beginning of extension. Furthermore, in the model of Dunbar and Sawyer (1989) strain is transferred from the upper crust weakness to the mantle weakness through flow in the lower crust. Hopper and Buck (1998) suggest that for a 30 km thick crust this occurs when the crustal mantle boundary is as hot as 700°-800°C degrees (for a rheology in between dry quartz and anorthosite). For a 50 km thick a temperature of 650°- 750° C is required at the crust mantle boundary assuming the same rheology. As discussed above (and also in section 2.8.1 of chapter 2 and in chapters 5 and 6) the initial thermal structure of the crust at the West Iberia margin was most likely colder than what is required for lower crustal flow to occur.

### 3.4 CONCLUSIONS

The conclusions of the interpretation of a set of industry multichannel lines at the Galicia Interior Basin and compilation of the available information about crustal thicknesses and timing of the phases of extension in the west Iberia margin are:

1. The Galicia Interior basin experienced its main extensional episode during the Valanginian (137-132 m.y.). This episode is characterised by eastward dipping faults and is coeval with at least part of the main extensional phase at the Iberia Abyssal Plain.
2. Towards the Galicia Bank a younger rifting episode which is characterised by westward dipping faults is observed. This episode is coeval to the main extensional phase that led to break-up at the Deep Galicia Margin.
3. At the deepest part of the basin, between ~42°N to ~42.7°N the crustal thickness ranges from 8 to 6 km. The basin might continue to the south between the continental platform and the Vigo Seamount.
4. Rift failure at the Galicia Interior Basin might not result from the changing strength or forces involved during continental rifting but may be a product of the global organisation of the tectonic stresses. More detailed plate reconstructions at the time of rift propagation along the margin are needed to understand this problem.

## **CHAPTER 4. RHEOLOGICAL EVOLUTION DURING EXTENSION AT PASSIVE NON-VOLCANIC MARGINS: ONSET OF SERPENTINISATION AND DEVELOPMENT OF DETACHMENTS LEADING TO CONTINENTAL BREAK-UP.**

### **4.1 ABSTRACT**

Several non-volcanic rifted margins exhibit within the continent-ocean transition a zone of partially serpentinized peridotites which continue under the thinned and faulted continental crust, and are thought to represent sub-continental lithosphere serpentinized by contact with hydrous fluids. As water in the volumes required can only come from the surface, we suggest that a major condition for the onset of serpentinisation is the embrittlement of the entire crust during progressive extension and hence the development of crustal penetrating faults to act as fluid conduits. We investigate this by modelling the rheological evolution of the lithosphere during extension and hence determining when the lower crust enters the brittle regime for a variety of different strain rates and lower crustal rheologies. Using an initial thermal structure appropriate for non-volcanic margins, we find that the entire crust becomes brittle at stretching factors of between c. 3 and 5, depending on the strain rate. This compares well with the thickness of the crust observed just landward of the onset of partially serpentinized peridotites west of Iberia. The predicted thickness of the serpentinized peridotites (the depth of the thermal limit of serpentinite stability beneath the crust-mantle boundary) also compares reasonably well with their observed thickness. As serpentinites are characterized by low friction coefficients, we suggest that the onset of mantle serpentinisation controls the development of detachments at the CMB such as the S and H reflectors west of Iberia (leading to crustal separation). The development of thick serpentinites probably contributes to the weakening of the upper lithosphere and hence the localisation of final break-up.

### **4.1. INTRODUCTION**

At many non-volcanic margins multichannel seismic reflection profiles, especially when combined with wide-angle seismic data, show that the upper crust thins progressively by continental block rotation accompanying movement along high angle normal faults. As thinning progresses the thin continental crust gives way to the continent-ocean transition

(COT) characterised by basement typical of neither oceanic nor continental crust. In several cases this region has been interpreted as an expanse of serpentized peridotite (e.g. Labrador sea, Chian et al. 1995; Newfoundland, Reid 1994; West Iberia margin, Boillot and Winterer, 1988; Whitmarsh and Sawyer, 1996; Pickup et al., 1996; Discovery Working Group, 1998; Chian et al. 1999, Otway Basin, southeast Australia, Finlayson et al. 1998), which continues landward under the fault blocks of the thinned continental crust (Boillot et al., 1989, Chian et al. 1999).

The best studied of these margins is the west Iberian margin (Figure 4.1), which has been the subject of several drilling legs (Boillot and Winterer, 1988; Whitmarsh and Sawyer, 1996; ODP Leg 173 Shipboard Scientific Party, 1998) and of many seismic reflection and refraction cruises (Whitmarsh et al., 1996; Reston et al., 1996; Sawyer et al., 1998). Here the last stages of crustal thinning seem to have involved continental block rotation onto a detachment fault or decollement: the S reflector at the deep Galicia margin (DGM) west of the Galicia Bank (Reston et al, 1996 - Figure 4.2a), the H reflector (Krawczyk et al. 1996, Figure 4.2b) and other possible detachments (e.g. Dean et al., 1999) in the south Iberia Abyssal Plain (IAP). Although the evidence is incomplete for all the margins, it appears that at least in places, these low-angle detachment faults follow the boundary between the overlying continental fault blocks and the underlying partially serpentized peridotites (Figure 4.3). These serpentinites may thus form a decollement: even after only 30% serpentisation, the friction coefficient of peridotites is greatly reduced (Escartín et al., 1997a).

Although the presence of partially serpentized peridotites is well documented and their possible role as a decollement is already a matter of some discussion, the onset of mantle serpentisation during rifting is not well constrained. Serpentinization requires:

- sufficient water (or water vapour) to react with the peridotites. From the chemistry of the reaction, we calculate that for every  $\text{km}^3$  of peridotite converted to serpentine,  $0.64 \text{ km}^3$  water (or volumetrically more water vapour) is required; this is proportionally reduced if serpentisation does not proceed to completion. The mantle itself does not contain water in sufficient volumes, so this must come from above and is most likely to be seawater that has passed to depth along conduits. The main conduit for fluids within the crust are connected networks of faults and fractures (e.g., Sibson et al., 1975; Finkbeiner et al., 1997), both of which form by brittle processes. Thus a major condition for mantle serpentisation (through the penetration of significant volumes of hydrous fluids to mantle depths) is the presence of brittle structures throughout the crust and hence that the entire crust is in the brittle regime.

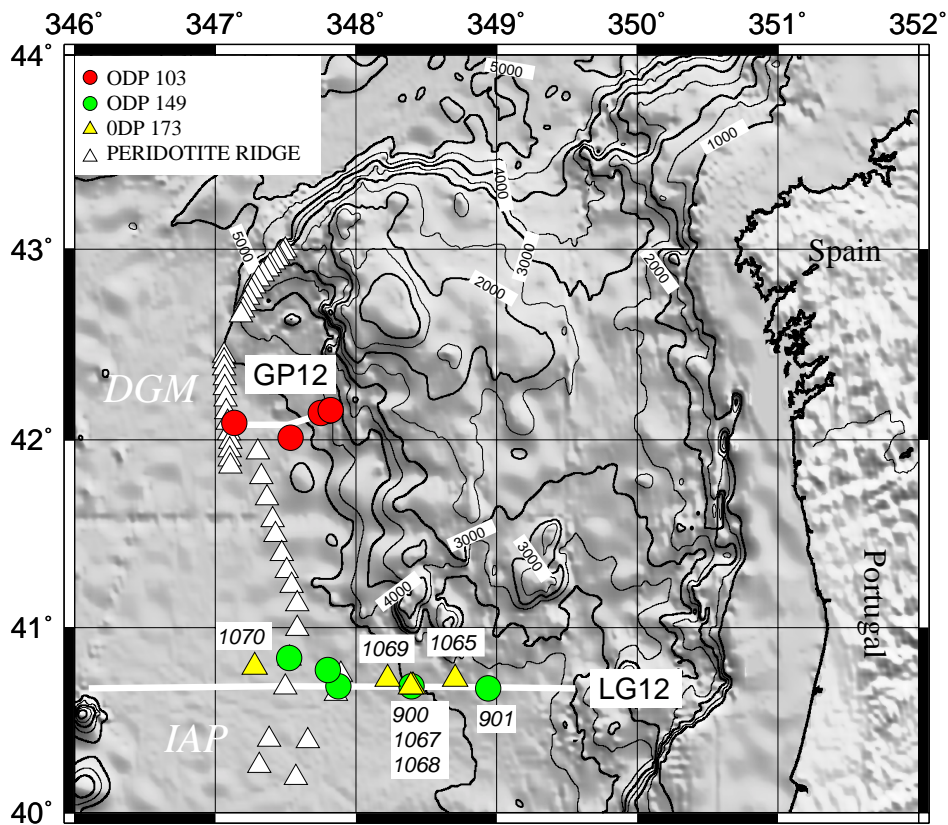


Figure 4.1. Shaded relief bathymetric chart of the West Iberia margin (Smith and Sandwell, 1995 - contour interval 500m), showing position of seismic lines GP12 and LG12, ODP boreholes (Legs 103, 149 and 173) and peridotite ridges. One such ridge runs along the deep Galicia margin (DGM): further south in the southern Iberia Abyssal Plain (IAP), the ridge are only part of a larger expanse of serpentinized peridotites forming top basement.

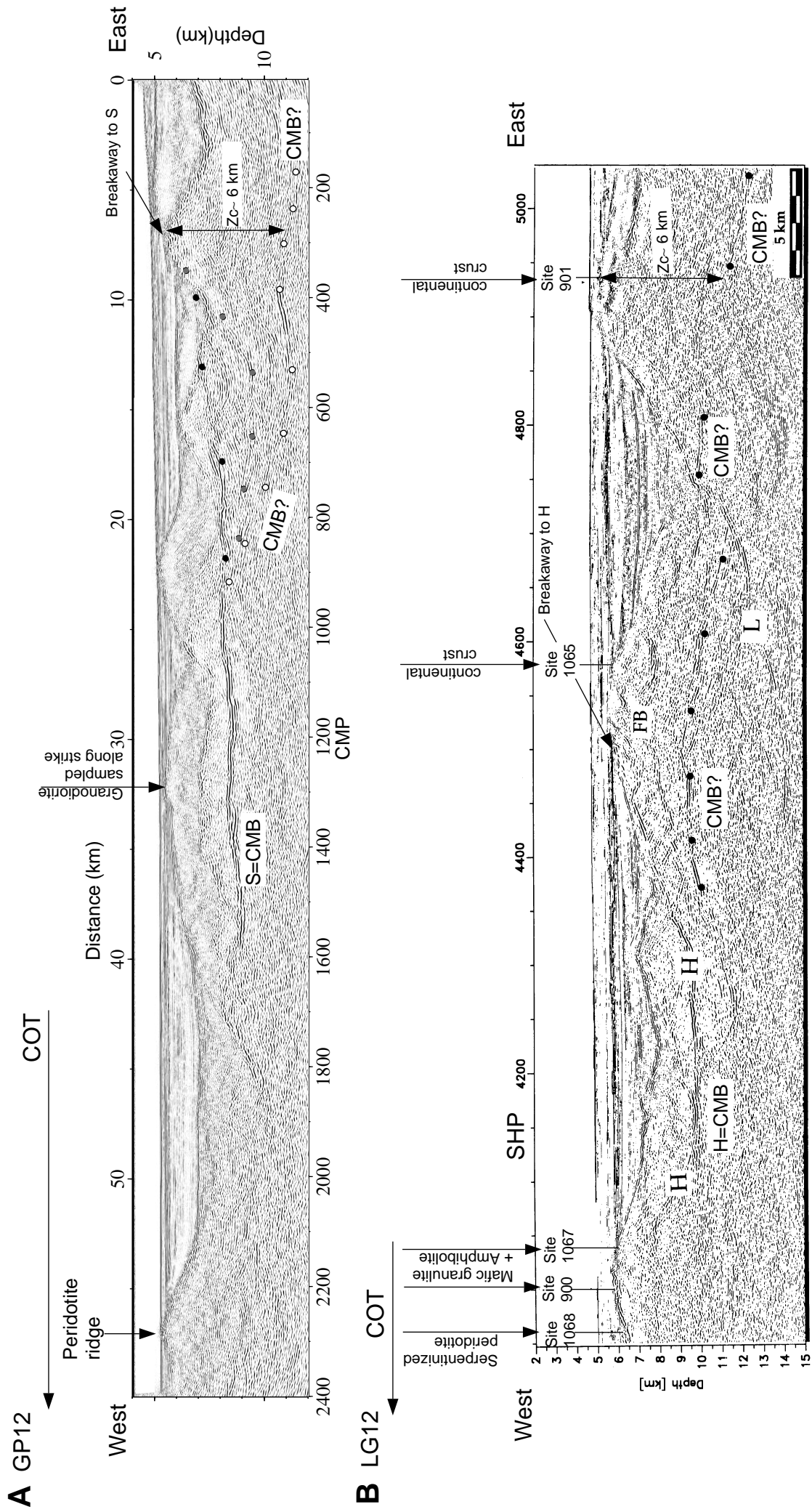


Figure 4.2. Prestack-depth migration of profile: a) GP12 (after Reston et al., 1996) in the deep Galicia margin (DMG), and b) LG12 (after Krawczyk et al., 1996) in the Iberia Abyssal Plain (IAP) (see Figure 4.1. for location). Drilling results are shown with an arrow above the drill sites. COT is the continental ocean transition and is defined as the area between the last continental crustal block and the first geophysically inferred oceanic crust (ODP Leg 173 Shipboard Scientific Party, 1998). In the COT serpentinized peridotite became exposed during rifting (Boillot and Winterer, 1988, Whitmarsh and Sawyer, 1996, ODP Leg 173 Shipboard Scientific Party, 1998). The brightest part of the detachment faults is inferred (Chian et al., 1999; Whitmarsh et al., 1999) We suggest that the detachments developed where hydrous fluids could pass down crustal penetrating faults to serpentinize the mantle: landward of the breakaway to these detachments, the crust never entirely entered the brittle regime. Black, white and grey dots highlight features discussed in section 4.4.1.



- peridotites at appropriate temperature conditions. The maximum temperature at which serpentine can develop varies somewhat depending on the serpentine mineral under discussion and the study carried out: for instance lizardite is variously described as stable only below 250°C (Agrinier et al., 1996), 350-500°C (O'Hanley, 1996) and 400-500°C (Ulmer and Tromsdorff, 1995); antigorite, the second most common serpentine mineral, is stable at temperatures up to 400-500°C (Ulmer and Tromsdorff, 1995).

In this chapter we model the thermal and rheological evolution of the lithosphere during extension at different strain rates. We investigate at what stretching factors the entire crust moves into the brittle regime, when the temperature of the uppermost mantle enters the serpentinite stability field, and hence when serpentinisation is likely to commence. Finally we discuss the effect of the serpentinisation on lithospheric strength and the implications of this for the development of detachments or decollements leading to continental break-up. Our approach is based on

- 1) numerically modelling the thermal evolution of the lithosphere.
- 2) using these results to investigate the evolution of crustal and upper mantle rheology during progressive extension.
- 3) determining at which stretching factors the entire crust becomes brittle for several strain rates and different lower crustal rheologies.
- 4) checking that at these stretching factors the upper mantle is within the temperature field for the development of mantle serpentinites.
- 5) finally, we estimate the maximum thickness of the layer of partially serpentinitized mantle beneath the crust and compare it to published estimates of melt thickness produced by decompression melting during extension.

We compare our results with the west Iberia margin as this is best constrained by ODP drilling and numerous seismic studies.

#### **4.1.1 Lithospheric rheology during progressive extension - principles**

The principles of lithospheric strength depth curves are well known (e.g., Brace and Kohlstedt, 1980). At the temperatures and pressures within the uppermost crust, the yield stress for brittle failure is less than that for failure by plastic deformation mechanisms such as dislocation creep. However with increasing pressure (depth), the brittle strength increases, whereas with increasing temperature (hence depth), the plastic yield stress for a given strain rate and rheology will decrease. The point at which the plastic and brittle yield

stresses are equal is the brittle-plastic transition. Above this transition deformation occurs by brittle failure; below it plastic deformation is favoured.

The yield strength required for brittle failure is independent of the temperature, rheology (except as noted below if the friction coefficient varies) and strain rate. Thus the depth of the brittle plastic transition as extension proceeds is controlled by the dependence of plastic yield strength on temperature, rheology (i.e. mineralogy) and strain rate. Of these, the evolution of the temperature field is controlled by the initial thermal state of the lithosphere and the extension rate.

During progressive extension, the crust thins and any rock within it cools. Both the decrease in pressure as the crust thins (facilitating brittle failure) and the drop in temperature (increasing the plastic yield stress) mean that an increasing proportion and eventually all of the crust will lie within the brittle regime. In investigating the onset of mantle serpentinisation, the stretching factor  $\beta$  when the crust moves entirely into the brittle deformation regime is of critical interest as then faults can carry fluids from the surface down into the mantle. This occurs when the depth to the brittle-plastic transition equals the depth of the crust mantle boundary. Although it is accepted that there is a zone of semibrittle behaviour between the brittle and plastic deformation mechanisms (Scholz, 1988, Kohlstedt et al., 1995), the thickness of this zone is narrow in comparison to the thickness of the brittle and plastic layers. We have ignored this transition zone for the sake of simplicity, because its precise thickness is poorly understood (Kohlstedt et al., 1995).

#### 4.2. MODEL DESCRIPTION

We consider a simple model in which the lithosphere undergoes extension by uniform pure shear (Figure 4.4). This is a reasonable approximation of the style of lithospheric stretching at least at moderate amounts of extension (e.g. McKenzie, 1978; White, 1989), but the pure shear assumption may limit the applicability of our model to the deformation occurring prior to the development of detachment faults as discussed below.

We consider that the lithosphere extends at a constant strain rate. Therefore the velocities, strain rate and stretching factors are related by:

$$\begin{aligned} v &= -\dot{\epsilon}^* z \\ u &= \dot{\epsilon}^* z \\ \beta &= L/L_0 = z_{CMB0}/z_{CMB} = \exp(\dot{\epsilon}^* t) \end{aligned} \quad (1)$$

where  $v$  is the vertical velocity,  $u$  the horizontal velocity,  $\dot{\epsilon}$  is the strain rate,  $b$  the extension factor,  $L$  and  $L_0$  are the width of the extending region after a certain time and at the beginning of rifting, and  $z_{CMB}$  and  $z_{CMB0}$  the thickness of the crust after a certain time and at the beginning of rifting respectively (Figure 4.4). Maintaining a constant strain rate implies that if the rift does not focus, the velocity of plate separation increases with time as the area of extension increases. This may occur within a broad runaway rift leading to continental break-up. However, if the region undergoing extension were to become focused during progressive extension, the constant strain rate assumption would be compatible with a constant rate of plate separation.

#### **4.2.1 Thermal Calculation**

The evolution of the temperature of the lithosphere is obtained by solving the one dimensional heat transport equation :

$$\partial T / \partial t = \kappa * \partial^2 T / \partial z^2 - v * \partial T / \partial z + H(z) / \rho * C \quad (2)$$

where  $T$  is the temperature,  $t$  is time,  $v$  is the vertical velocity,  $H(z)$  is the radiogenic heat production,  $\rho$  the density and  $C$  the specific heat. The values used for these constants are shown in Table 4.1.

Numerical modelling results show that the width and geometry of the rifts are mainly controlled by their initial thermal state (Buck, 1991, Bassi 1995, Hopper and Buck, 1996). We suggest that non-volcanic margins where serpentinized peridotite forms the COT may form from initially cold lithosphere (in the classification of Buck, 1991 and Bassi, 1995). Bown and White (1995) show that stretching such cool lithosphere (basal temperature 1300°C) does not produce significant melt except at very high stretching factors (at which the uniform pure shear assumption may not be valid - see below). Furthermore, the absence of voluminous magmatism at these "non-volcanic" margins implies that little melt is generated and hence that heat advected by melt will not significantly affect the temperature at the CMB. Consequently, melt generation is not included in our calculations.

Our starting model (Table 4.1 and Figure 4.4) is thus similar to previous cool/cold models (e.g. Bassi, 1995). We assume a distribution of radioactive elements that decreases exponentially with depth in the crust and is zero in the mantle:

$$\begin{aligned} H(z) &= H * \exp(-z / h_r), z < z_{CMB} \\ H(z) &= 0, z > z_{CMB} \end{aligned} \quad (3)$$

where  $z_{\text{CMB}}$  is the depth to the crust mantle boundary at every time during extension.  $H$  is the radiogenic heat production and  $h_r$  the radiogenic heat production scale (Table 4.1). This type of distribution maintains the observed linear relationship between the heat flow measured at the surface and the surface radioactive heat production even under differential erosion (Lachenbruch, 1970). The initial thermal state is calculated from the steady state heat transport equation setting the advective term to zero.

To solve the time dependent heat equation the temperatures at the top of the lithosphere and at 125 km (the initial thickness of the lithosphere) are kept constant throughout the calculations at 0 and 1300°C respectively. The heat transport equation is solved by finite differences, by center differencing the diffusion terms and upwind differencing the advective terms.

TABLE 4.1. Thermal parameters

Symbol	Name	Value
Kc	thermal conductivity in the crust	2.5 W m <sup>-1</sup> °K <sup>-1</sup>
Km	thermal conductivity in the mantle	3.4 W m <sup>-1</sup> °K <sup>-1</sup>
k	thermal diffusivity	8*10 <sup>-7</sup> m <sup>2</sup> s <sup>-1</sup>
$\rho_c$	crustal density	2800 kg m <sup>-3</sup>
l	hydrostatic pore pressure factor	0.35
g	acceleration of gravity	10 m s <sup>-2</sup>
H	radiogenic heat production	4.4 μW m <sup>-3</sup>
$h_r$	radiogenic heat production length scale	10 <sup>4</sup> m
Cp	specific heat	1250 J kg <sup>-1</sup> °K <sup>-1</sup>
R	universal gas constant	8.3143 J mol <sup>-1</sup> °K <sup>-1</sup>

### 4.2.2 Rheology

Brittle deformation (by sliding on pre-existing faults) in the upper crust is described by Byerlee's Law and is independent of the rock type and temperature. In terms of principal stresses and assuming hydrostatic pore pressure Byerlee's Law is (Brace and Kohlstedt, 1980):

$$\begin{aligned} \sigma_{zz} - \sigma_{xx} &= 14.4 * z(\text{km})\text{MPa}, \sigma_{zz} < 550\text{MPa} \\ \sigma_{zz} - \sigma_{xx} &= (12.2 * z(\text{km}) + 67.4)\text{MPa}, \sigma_{zz} > 550\text{MPa} \end{aligned} \quad (4)$$

We consider that the hydrostatic assumption is most reasonable for faults within the continental crust (Kohlstedt et al., 1995).

The plastic behaviour that materials exhibit under pressures and temperatures appropriate for the lower crust can be described by the plastic flow law for dislocation creep.

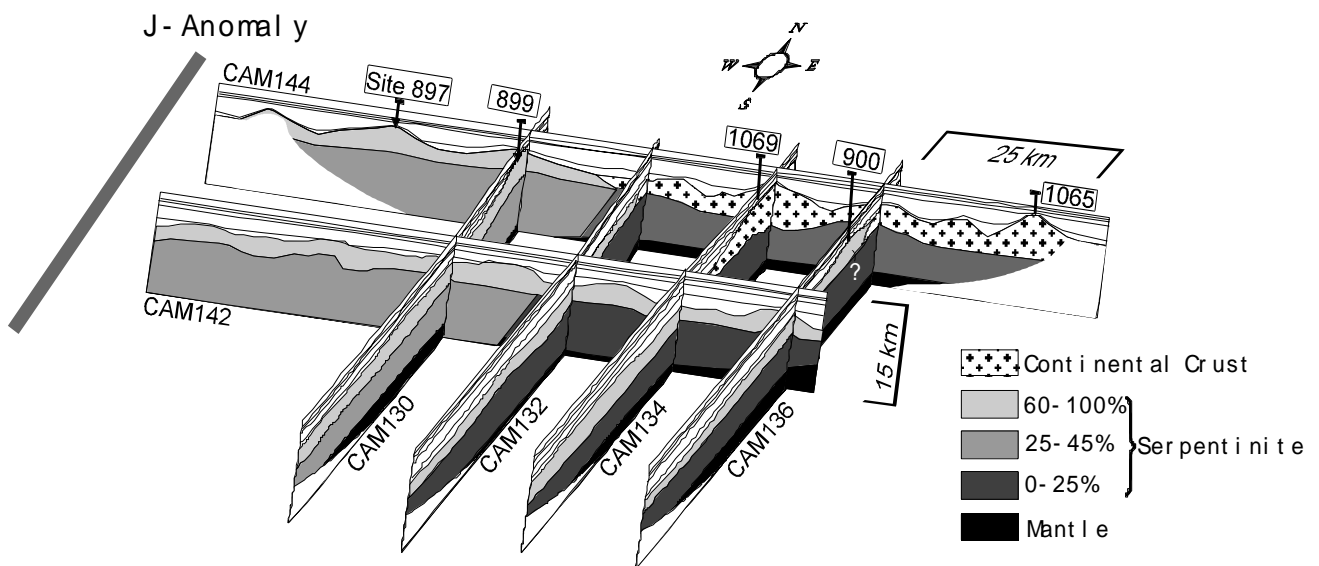


Figure 4.3. Three-dimensional interpretation, constrained by results of ODP drilling (Legs 149 and 173 - see Figure 4.2.B), of wide angle velocity profiles (Chian et al., 1999) in the southern IAP (Figure 4.1). The structure of the crust and mantle and inferred degree of serpentinization are shown.

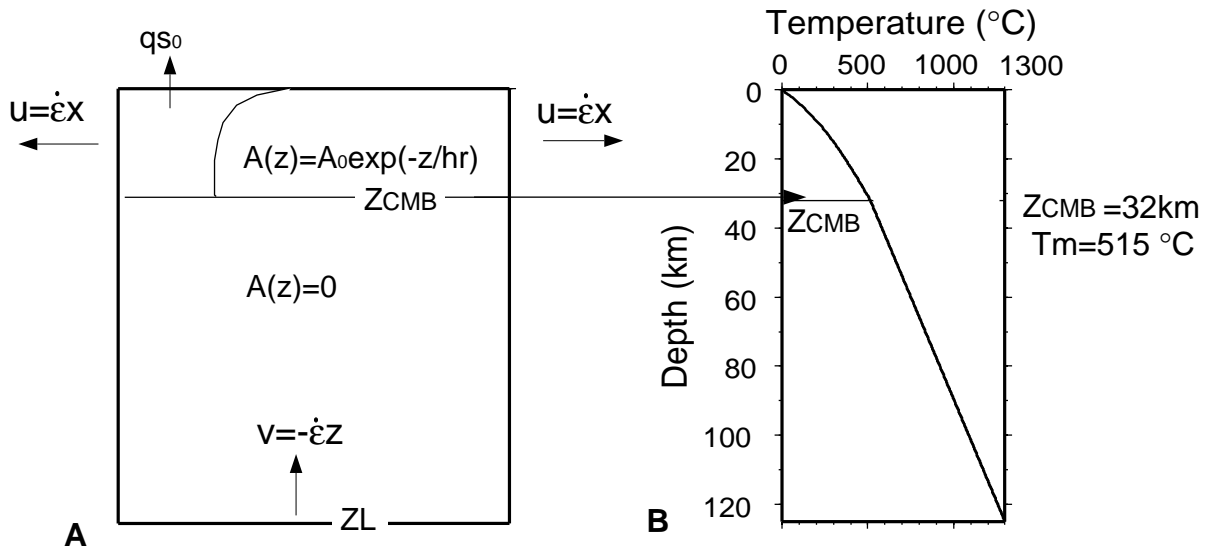


Figure 4.4. **A.** Initial model lithosphere used for the temperature calculations.  $v$  is vertical velocity,  $u$  is horizontal velocity. The velocity in any direction is the strain rate,  $\dot{\epsilon}$ , times the coordinate in that direction. Radioactive heat production,  $H(z)$ , is exponential in the crust and zero in the mantle. **B.** Initial thermal profile for this model lithosphere. The crust-mantle boundary (CMB) lies at a depth of 32 km ( $Z_{CMB0}$ ) and has an initial temperature of 515°C. The temperature at the top of the lithosphere is 0°C and at its base,  $Z_L=125$  km, 1300°.

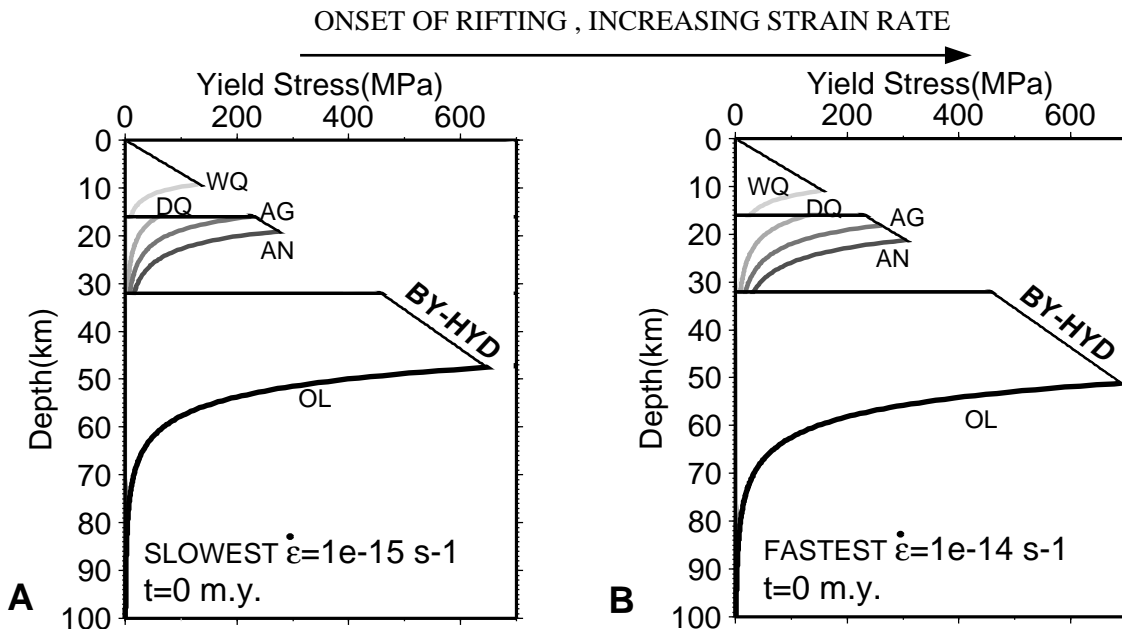


Figure 4.5. Lithospheric yield strength envelopes at the onset of rifting,  $t=0$  m.y. **A.** At a strain rate of  $10^{-15} \text{ s}^{-1}$ , **B.** at a strain rate of  $10^{-14} \text{ s}^{-1}$ . BY-HYD is brittle yield strength corresponding to Byerlee's law assuming hydrostatic pore pressure, WQ denotes the plastic yield strength for wet quartzite and DQ, AG, AN correspond to possible lower crust rheologies of dry quartzite, aggregate (50% dry quartzite, 50% anorthosite) and anorthosite respectively. OL is the plastic yield strength for olivine, which is assumed to control mantle rheology. For a given strain rate the zone of plastic deformation in the lower crust assuming dry quartzite rheology is thicker than assuming anorthosite rheology. For the slowest strain rate, **A.**, plastic deformation zones are thicker than at the fastest strain rate, **B.**

$$\sigma_{zz} - \sigma_{xx} = (\dot{\epsilon}/A) * \exp(E/nRT) \quad (5)$$

where  $A$ ,  $n$  and  $E$ , the activation energy, are material constants (Goetze and Evans, 1979),  $R$  is the gas constant and  $T$  the absolute temperature. Table 4.2 gives the values of  $A$ ,  $n$  and  $E$  used for the different minerals and aggregates used in the modelling.

Most previous workers have assumed a wet quartz rheology for the upper crust and a dry quartz rheology for the lower crust (e.g. Buck, 1991), so we too model this. However, the composition and hence rheology of the lower crust is still a matter of much debate and may well vary with tectonic province (Zandt and Ammon, 1995). In general, studies of exposed deep crustal sections (Salisbury and Fountain, 1990) and of lower crustal xenoliths (Griffin and O'Reilly, 1986) suggest that the lower crust contains little quartz. Furthermore, the comparison of wide-angle seismic velocities with those obtained from laboratory experiments indicate that whereas the upper and middle crust consists mainly of granites and granodiorites, which are likely to be dominated by quartz rheology (wet or dry), the lower crust is more mafic and may contain little quartz (Christensen and Mooney, 1995). Thus the dominant minerals in the lower crust are expected to be plagioclase, pyroxene and amphibole. Of these, the rheology of plagioclase and in particular of massive anorthosites has been the most intensively studied, and has been used as a proxy for lower crustal rheology (e.g., Kuszniir and Park, 1987); it is modelled here in addition to the dry quartz.

Anorthosites may however overestimate the plastic strength of the lower crust as within high grade terranes such as the Kapuskasing zone (Percival, 1986), the South Harris shear zone (Graham, 1980; Reston, 1990) and the Portsoy complex of the Scottish Caledonides (Read, 1960), anorthosites are known to form low strain lozenges whereas mafic granulites and amphibolites are strongly deformed and sheared. In contrast, dry quartz is not only unlikely to be a major component of the lower crust, but also is almost certainly too weak to represent the lower crust rheologically as quartz tends to recrystallize before amphibole or pyroxene in high grade environments (Handy, 1990). Thus we suggest that the most realistic estimate of lower crustal rheology is between that of anorthosite and dry quartz. We thus also model the rheology of an aggregate (Tullis et al., 1991) consisting of 50% anorthosite and 50% dry quartz. We emphasise that this aggregate is not meant to simulate lower crustal composition but just to model an intermediate strength lower crust in the absence of well-established flow laws for pyroxenes and amphibole.

The rheology of the mantle is modelled with the plastic flow law for dry olivine (Table 4.2). The flow law parameters for olivine are the values that give the best fit to the observed data when modelling the stretching factor that intracontinental basins have

undergone versus the strain rate at which extension occurred (Newman and White, 1997). These are very similar to experimental values given by Kirby (1983).

TABLE 4.2. Rheological parameters

Material	n	A (Pa <sup>n</sup> s <sup>-1</sup> )	E (Kj mol <sup>-1</sup> )
Wet Quartzite <sup>(1)</sup>	2.4	1.3*10 <sup>-20</sup>	134
Dry Quartzite <sup>(2)</sup>	2.9	5*10 <sup>-25</sup>	149
Aggregate <sup>(3)</sup>	3	4.9*10 <sup>-24</sup>	192.4
Anorthosite <sup>(4)</sup>	3.2	5.6*10 <sup>-23</sup>	238
Olivine <sup>(5)</sup>	3	10 <sup>-13</sup>	500

<sup>(1)</sup>Kronenberg and Tullis [1984], <sup>(2)</sup>Koch [1983], <sup>(3)</sup>Tullis et al. [1991], <sup>(4)</sup>Shelton and Tullis [1981], <sup>(5)</sup>Newman and White [1997].

### 4.3. MODELLING RESULTS

#### 4.3.1 Onset of rifting

The yield strength of the lithosphere at  $t=0$  m.y. for strain rates of  $10^{-14}$  s<sup>-1</sup> and  $10^{-15}$  s<sup>-1</sup>, and 3 different rheologies for the lower crust (Figure 4.5) shows that for a given strain rate, the initial plastic layer in the lower crust is thinner for strong rheologies (e.g. an anorthositic model for the lower crust). As we shall see, this means that a strong lower crust would require less stretching to move the entire crust into the brittle field. It is also apparent that each lower crustal rheology is stronger at higher strain rates than at lower ones. Indeed, at higher strain rates than considered here, plastic deformation might initially require higher stresses than brittle failure even in the deepest crust so that there is no plastic zone at the base of the crust. One might therefore expect that the plastic layer will disappear at lower stretching factors for higher strain rates, but as discussed below, the effect that strain rate has on the plastic flow laws may be offset by the cooling that can occur during rifting at slow strain rates.

#### 4.3.2 Evolution of the brittle plastic transition during progressive extension

At the beginning of extension two plastic layers exist within the crust (Figure 4.6): the upper one corresponding to dislocation creep toward the base of the wet granite rheology (assumed to dominate the top half of the crust), the lower to dislocation creep of the modelled lower crustal rheology. As extension progresses and the crust thins, rocks originally within the plastic deformation zone are brought to lower pressures (reducing the stress required for brittle deformation) and also cool (increasing the stress required for



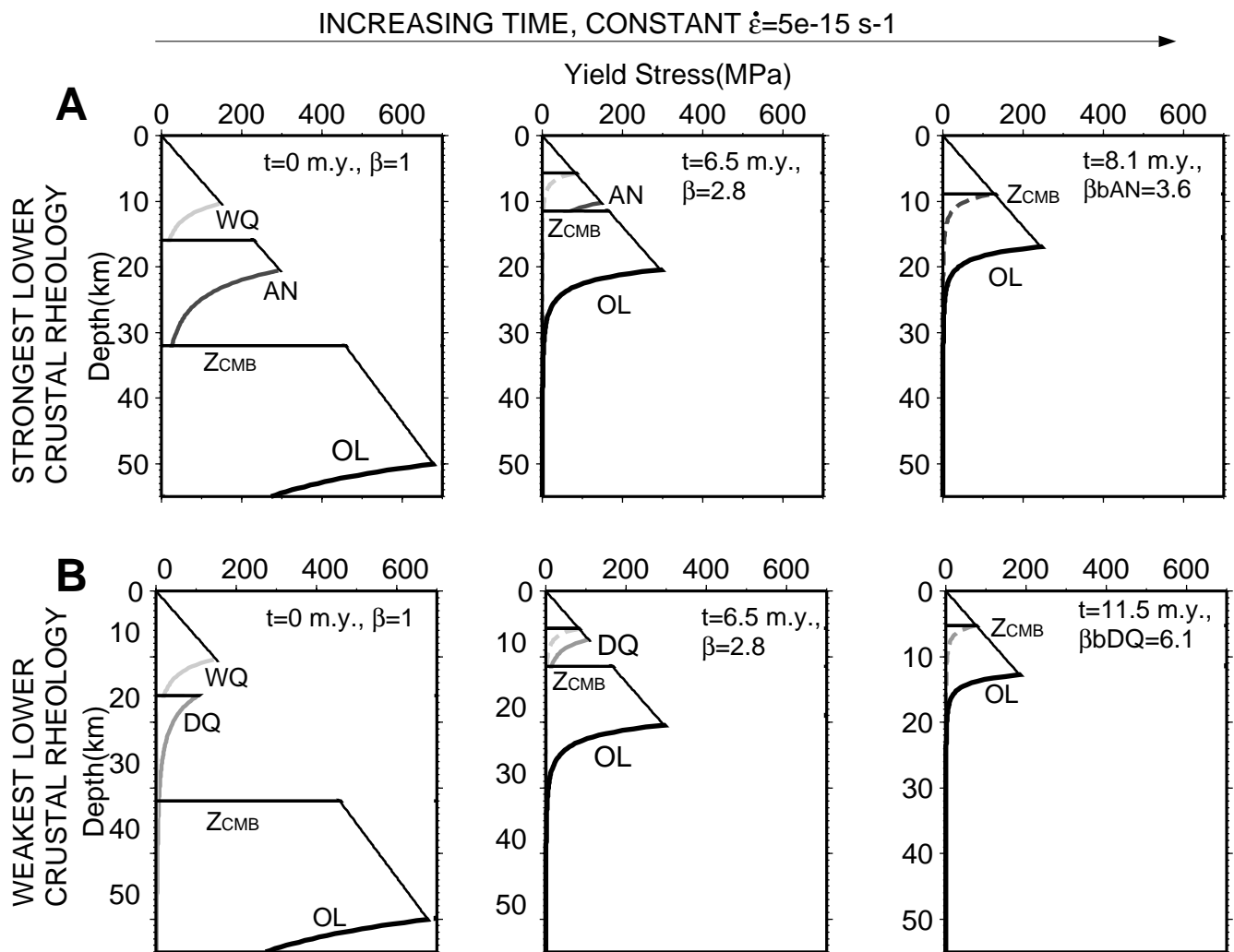
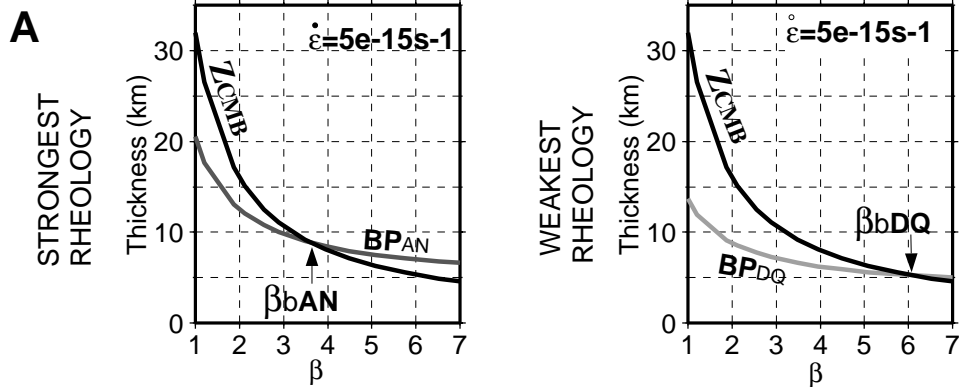


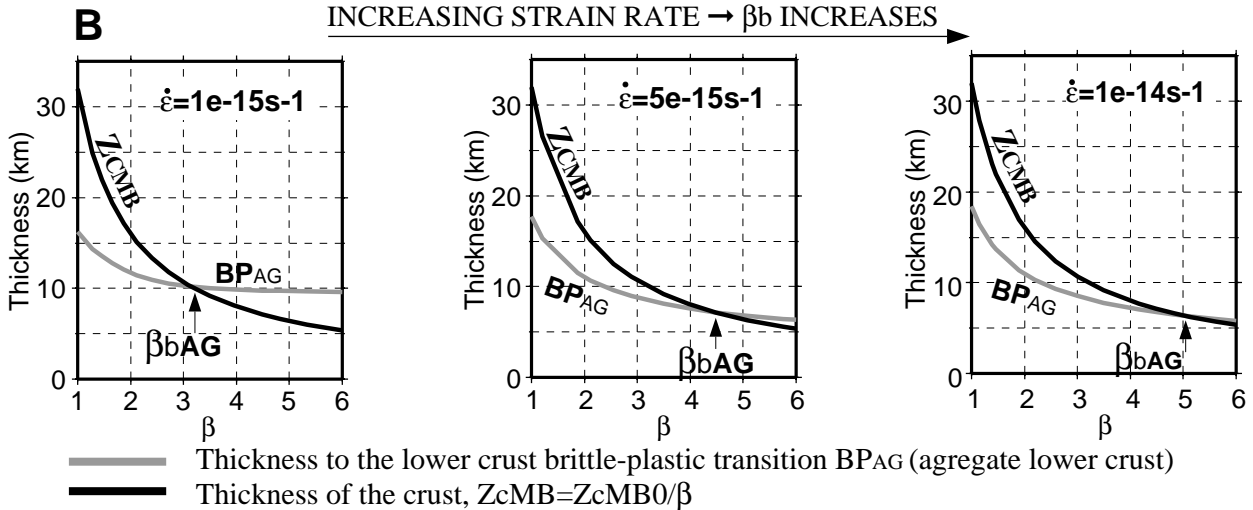
Figure 4.6. Temporal evolution of the lithospheric yield strength for a strain rate of  $5 \cdot 10^{-15} \text{ s}^{-1}$  from the onset of rifting up to the stretching factor ( $\beta_b$ ) at which the entire crust enters the brittle regime. Two different rheologies are assumed for the lower crust, **A.**, anorthosite, **B.**, dry quartzite. In each case the zone of plastic deformation at the middle crust enters the brittle deformation regime before the plastic zone in the lower crust does.  $\beta_b$  is bigger if a weaker (e.g. dry quartzite) rheology for the lower crust is assumed (compare **A.** and **B.**).

DECREASING LOWER CRUSTAL STRENGTH  $\rightarrow \beta_b$  INCREASES  $\rightarrow$



- Thickness to the lower crust brittle-plastic transition,  $BP_{DQ}$  (dry quartz lower crust)
- Thickness to the lower crust brittle-plastic transition,  $BP_{AN}$  (anorthosite lower crust)
- Thickness of the crust,  $Z_{CMB} = Z_{CMB0}/\beta$

INCREASING STRAIN RATE  $\rightarrow \beta_b$  INCREASES  $\rightarrow$



- Thickness to the lower crust brittle-plastic transition  $BP_{AG}$  (aggregate lower crust)
- Thickness of the crust,  $Z_{CMB} = Z_{CMB0}/\beta$

Figure 4.7. Depth to the lower crustal brittle-plastic transition (grey lines) and to the CMB (black lines) during progressive extension. **A.** Variation with rheology for a given strain rate  $5 \cdot 10^{-15} \text{s}^{-1}$ .  $BP_{AN}$  and  $BP_{DQ}$  indicate the depth to the brittle-plastic transition for anorthosite and dry quartzite respectively. The crust moves entirely into the brittle regime when the thickness of the crust equals the thickness of the brittle layer, i.e. at  $\beta_b$ .  $\beta_b$  increases for weaker lower crustal rheologies (e.g. dry quartzite). **B.** Variation for a given rheology, AG (50:50 aggregate) at three different strain rates.  $\beta_b$  increases with increasing strain rate.

plastic deformation). Thus these rocks will eventually move from the plastic to the brittle field. As a result, the zones of the crust that deform plastically thin and eventually disappear at a value  $\beta b$  at which the crust has moved entirely into the brittle regime.

#### 4.3.2.1 Effect of the rheology of the lower crust

For all models of lower crustal rheology considered here, rocks near the base of the upper crust that were originally part of the "wet quartzite plastic layer" in the middle crust will become brittle before the lower crust does. For instance at a strain rate of  $5 \times 10^{-15} \text{ s}^{-1}$ , the wet quartzite plastic zone in the midcrust disappears at  $b = 2.6$  (Figure 4.6), whereas for both a dry quartz and an anorthositic lower crust higher stretching factors are required. Thus the rheology of the lower crust controls  $\beta b$ .

A convenient way of visualising the rheological evolution of the crust is to plot  $b$  against the thickness of the crust ( $z_{\text{CMB}}$ ) and the depth to the lower crustal brittle-plastic transition. As stretching factors increase, both the crustal thickness and the depth to the brittle-plastic transition decrease, but the former decreases more rapidly so that the two curves eventually intersect. Whereas  $z_{\text{CMB}}$  is simply controlled by initial crustal thickness and stretching factor (i.e.,  $z_{\text{CMB}} = z_{\text{CMB0}}/\beta$ ), the depth to the brittle-plastic transition varies as a function of  $b$ , rheology and strain rate (Figure 4.7). These parameters thus control the point at which the two curves intersect, this is the stretching factor  $\beta b$  at which the crust has become entirely brittle. As already inferred from Figure 4.5, Figure 4.7a shows that for a given strain rate the factor  $\beta b$  is smaller if the rheology of the lower crust is strong than if it is weak.

#### 4.3.2.2 Effect of strain rate

For a given rheology the strain rate influences  $\beta b$  in two opposite ways. As noted above, at the onset of extension the strength of the lower crust increases with strain rate so that the initial zone of plastic deformation is thinner at higher strain rates (compare Figure 4.5a and 5b). Thus in principal high *instantaneous* strain rates lead to an increase in the depth to the brittle-plastic transition and hence to a decrease in the value of  $\beta b$ .

However as extension progresses, the depth of the brittle-plastic transition at any time during extension depends on the temperature structure of the crust. This is in turn controlled by the strain rate: a slow strain (extension) rate gives the lithosphere more time to cool so that at any depth and stretching factor, the temperature decreases with decreasing strain rate hence favouring brittle deformation mechanisms. Thus it is not immediately obvious whether  $\beta b$  will increase or decrease with strain rate, but for the

rheologies and strain rates we consider here, we find that the thermal effect dominates and that  $\beta_b$  increases with increasing strain rate (Figure 4.7b).

By similarly determining  $\beta_b$  for a variety of strain rates, we can plot the value of  $\beta_b$  vs. strain rate for the three model lower crustal rheologies (Figure 4.8). Overall the results can be summarised as follows:

- 1) for a given strain rate,  $\beta_b$  is larger for weaker lower crustal rheologies,
- 2) for a given rheology,  $\beta_b$  increases with increasing strain rate for all model rheologies.

The strain rate,  $\dot{\epsilon}$ , is related to the rift duration and stretching factor through

$$\beta = \exp(\dot{\epsilon} * t) \quad (6)$$

where  $\beta$  is the stretching factor at any given location and  $t$  is the duration of rifting at that given location. Therefore the values of  $\beta_b$  can also be shown as a function of rift duration (Figure 4.9). Longer rifting episodes imply slower strain rates and therefore smaller values for  $\beta_b$  for any given rheology.

#### 4.3.2.3 Dependence of the results on the initial thermal state of the lithosphere

The crustal temperature structure determines the depth of the brittle-plastic transition at any time, therefore the values of  $\beta_b$  depend on the initial temperature profile and in particular the temperature at the CMB at the onset of extension. To investigate this we have within the limits of our cool lithospheric model varied the initial temperature at the base of the crust between 470 and 560°C. Although some authors have suggested that a lithosphere with an initial temperature at the CMB below 500°C would need unrealistic high stress levels to strain appreciably (England, 1986), other authors use initial thermal models with such CMB temperatures (cold models of Buck 1991, and Hopper and Buck, 1996).

We find that cooler initial CMB temperatures (Figure 4.9a) shifts the  $\beta_b$  curves to lower values (that is the crust would become brittle at lower stretching factors) and reduces the influence of strain rate; conversely higher initial CMB temperatures increase  $\beta_b$  and increase the dependence on strain rate (Figure 4.9c). The change in  $\beta_b$  with the temperature at the CMB is in any case comparable to that resulting from a change in lower crustal rheology.

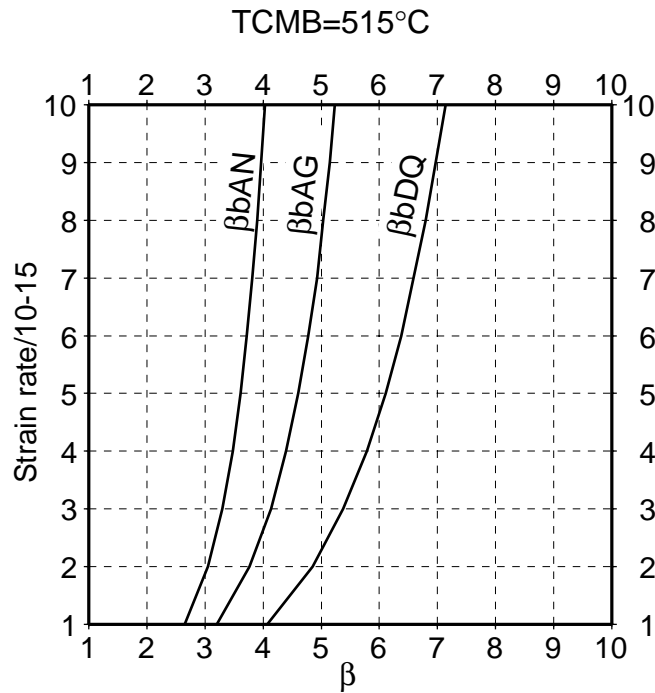


Figure 4.8. Variation of  $\beta_b$  with strain rate for the three different rheologies considered here. The strain rate values on the y-axis are divided by  $10^{-15} \text{ s}^{-1}$ . Curves  $\beta_b\text{AN}$ ,  $\beta_b\text{AG}$  and  $\beta_b\text{DQ}$  give  $\beta_b$  values for an anorthosite, an aggregate and a dry quartzite lower crustal rheology respectively.

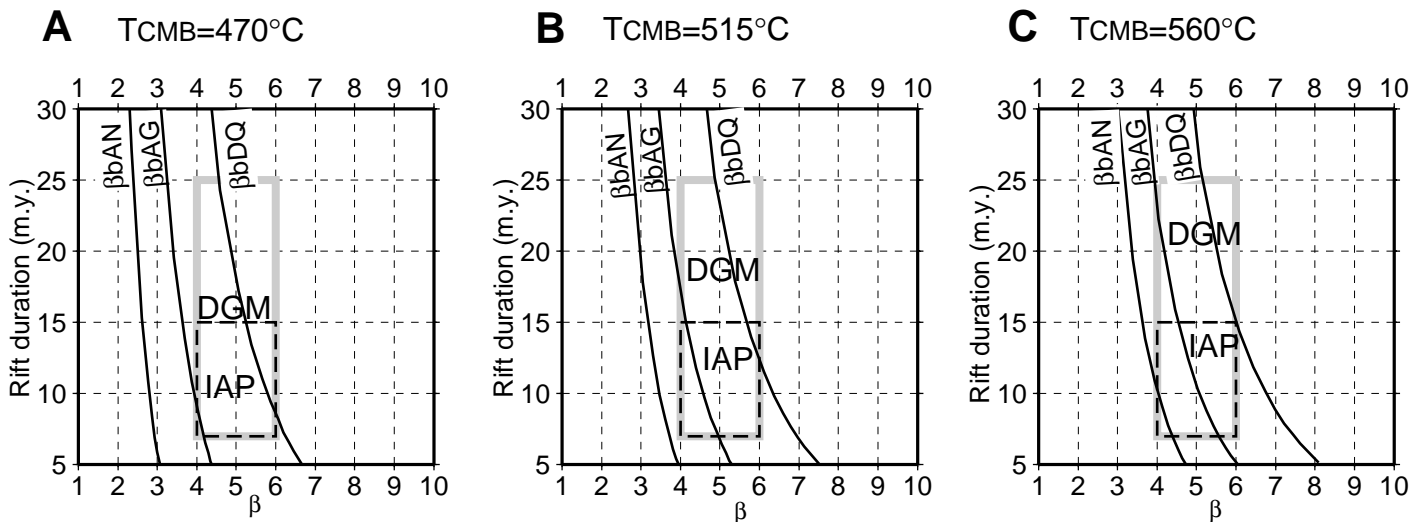


Figure 4.9. Variation for  $\beta_b$  with rift duration, for the three different rheologies considered here and for three different initial thermal models defined by the initial temperature at the CMB **A.**: 470°C, **B.**: 515°C, **C.**: 560°C. The model in **B.** is used in all other figures throughout this chapter. Superimposed are estimates of  $\beta$  and rift duration for the DGM and IAP margins just landward of the subcrop of serpentinized mantle (see Figure 4.2. and 4.3.).

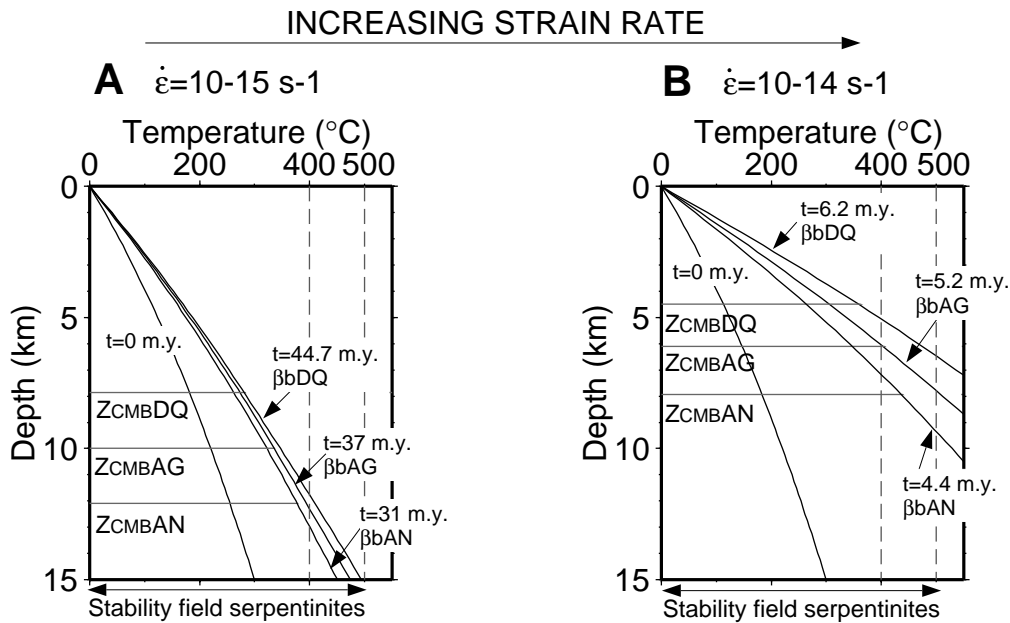


Figure 4.10. Geotherm at the onset of extension and at times corresponding to  $\beta$  for the three different rheologies considered here. **A.** Extension proceeds at a constant strain rate for  $10^{-15} \text{ s}^{-1}$ . **B.** Extension proceeds at a constant strain rate of  $10^{-14} \text{ s}^{-1}$ . In both cases  $Z_{\text{CMBAN}}$ ,  $Z_{\text{CMBAG}}$ ,  $Z_{\text{CMBDQ}}$  indicate the depth and temperature at the CMB when  $\beta_{\text{b}}$  is reached for anorthosite, aggregate and dry quartzite lower crust rheology respectively. The temperature at the CMB is in most cases below  $400^{\circ}\text{C}$  and in all cases below  $500^{\circ}\text{C}$  when  $\beta_{\text{b}}$  is reached. As these temperatures provide possible upper limits on the onset of serpentinitization, we infer that this is likely to begin as soon as the entire crust becomes brittle.

### **4.3.3 Stability field of serpentinites.**

So far we have determined for a variety of model parameters (lower crustal rheology, strain rate, initial thermal structure) the stretching factors at which the entire crust becomes brittle. As described in the introduction we consider an entire brittle crust a condition for the onset of serpentinitisation of the upper mantle: faults and fractures passing through the entire crust can act as conduits for the volumes of hydrous fluids required.

A further condition for the development of serpentinites during progressive extension is that the upper mantle lies within the serpentinite stability field. Lizardite and antigorite the most abundant polytypes of serpentinite are stable below c. 400°C to 500°C (Ulmer and Tromsdorff, 1995). In Figure 4.10 we plot the geotherms at the time corresponding to  $\beta_b$  for the three model lower crustal rheologies at the two end member strain rates we have considered. At the slowest strain rate, the temperature at the base of the crust when  $\beta_b$  is reached is for all lower crustal rheologies below 400°C, implying that when hydrous fluids could penetrate down into the mantle (through brittle faults) serpentinites would indeed form. At the fastest strain rate considered here, the temperature at the CMB when the entire crust becomes brittle is below 400°C for a dry quartz lower crustal rheology ( $\beta_b$  reached after  $t=6.1$  my), is very close to 400°C for the aggregate rheology ( $\beta_b$  reached after  $t=5.1$  my), and is well above 400°C for an anorthositic lower crustal rheology ( $\beta_b$  reached after  $t=4.3$  my). Thus if serpentinitisation only occurs below 400°C, at high strain rates, extension may (depending on lower crustal rheology) have to continue beyond  $\beta_b$  before serpentinitisation can commence. Note however that in all cases the temperature at the CMB is below 500°C when  $\beta_b$  is reached: if serpentinites can form at temperatures up to 500°C, then for all strain rates and lower crustal rheologies considered here, serpentinitisation will begin directly at  $\beta_b$ .

If the initial temperature at the CMB were lower than that used here (515°C) the temperature at the CMB when  $\beta_b$  is reached would also be reduced, thus favouring serpentinitisation. On the other hand as the initial temperature at the CMB increases, the temperature at the CMB for  $\beta_b$  will also increase and will eventually inhibit the formation of serpentinites.

### **4.3.4 Serpentinite thickness**

So far we have investigated at what stretching factors mantle serpentinitisation is likely to begin. We can also consider the maximum thickness of the serpentinitizing zone during rifting by determining the depth of the 400°C or 500°C isotherm below the CMB. However for a number of reasons, this comparison is somewhat qualitative. First, the penetration of fluids into the mantle peridotites may be restricted to the walls of fractures and faults.

Second serpentinisation may be limited by the volume increase of the serpentinisation process and the resulting tendency for fractures to seal; it is possible to predict the maximum depth of fluid penetration into the mantle but not how much fluid actually reaches this.

Third, it is possible that the extension of the upper lithosphere beyond  $\beta_b$  cannot be approximated by uniform pure shear. Once  $\beta_b$  is reached, the passage of hydrous fluids along crustal faults to the upper mantle will generate a serpentinized layer just below the CMB. This layer is likely to have implications for the mechanics of subsequent extension: as discussed in more detail below, even partially serpentinized peridotites are extremely weak and are likely to form a decollement at the base of the crust. Both the S reflector (deep Galicia margin) and the H reflector (southern IAP margin) are candidates for such decollements: the brightest portion of both appear to correspond to the boundary between crust and partially peridotites just oceanward of the onset of mantle serpentinisation. As these reflectors are not offset by movement along the block-bounding faults (although the underlying mantle was probably brittle at the time), it appears that they may have acted as detachments transferring the extension of the overlying upper plate laterally through local simple shear.

Thus after the onset of mantle serpentinisation, crustal extension may be controlled by newly developed detachment faults, and may differ substantially from that deep in the mantle leading to a departure from uniform pure shear. Specifically, we suggest that extension may localise in the crust above the decollement, leading to a narrow region of extension in the crust (and eventually to crustal separation through simple shear) above a broader region of extension in the mantle. Certainly immediately oceanward of H is the onset of complete crustal separation (infinite crustal stretching factors) (Whitmarsh and Sawyer, 1996, and ODP Leg 173 Shipboard Scientific Party, 1998) but without the voluminous magmatism expected if the whole lithosphere was so thinned.

Because we do not know the degree to which strain localisation in the crust occurs, we follow England and Jackson (1987) and consider two end-member situations between which "reality" probably lies:

- 1) extension proceeds as uniform pure shear where the strain rate in the crust and mantle remains the same (Figure 4.11a). This almost certainly underestimates the rapidity and localisation of crustal thinning and hence underestimates the thickness of the serpentinizing zone (Figure 4.12a and c).

- 2) extension in the brittle crust occurs by simple shear along a detachment, cutting through the crust and detaching on the serpentinite decollement; extension in the underlying mantle occurs by distributed pure shear. We follow England and Jackson (1987)



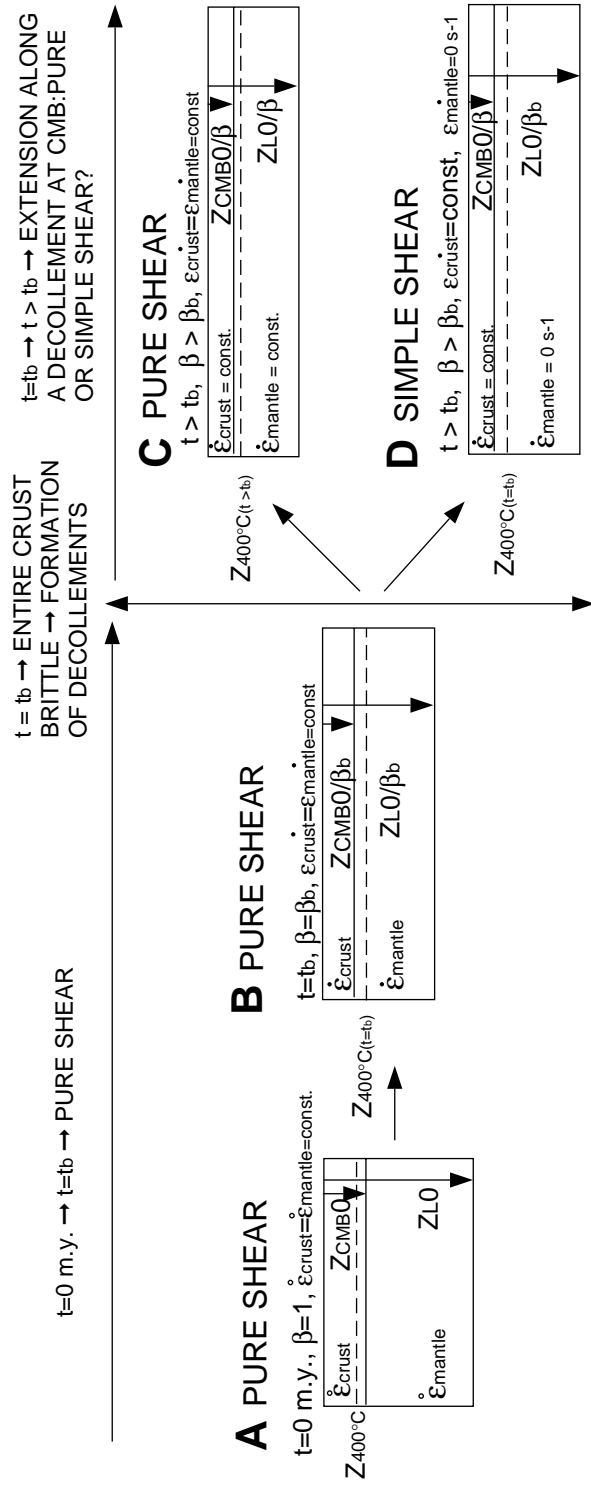


Figure 4.11. Cartoon illustrating changes in the way we model lithospheric deformation with ongoing extension. **A.** At the beginning of extension we model deformation as uniform pure shear with constant strain rate. The  $400^\circ\text{C}$  isotherm is within the crust. **B.** Extension proceeds as uniform pure shear until  $\beta_b$  is reached. The entire crust enters the brittle field and the  $400^\circ\text{C}$  isotherm is within the upper mantle therefore serpentinites can be formed. Because the low frictional strength of serpentinites and possible high local pore pressures, a decollement may form at the CMB and extension may proceed as a combination of: uniform pure shear **C.**, or "simple shear", which we model as non-uniform pure shear **D.**. In the latter model, the strain rate in the crust remains constant, but that in the mantle is set to zero, so that after  $\beta_b$  is reached, the depth to the  $400^\circ\text{C}$  and  $500^\circ\text{C}$  isotherms remain almost constant while the CMB rises in response to ongoing crustal thinning. The "simple shear" model thus predicts a thicker serpentinite zone thickness than the uniform pure shear model (Figure 4.12.).

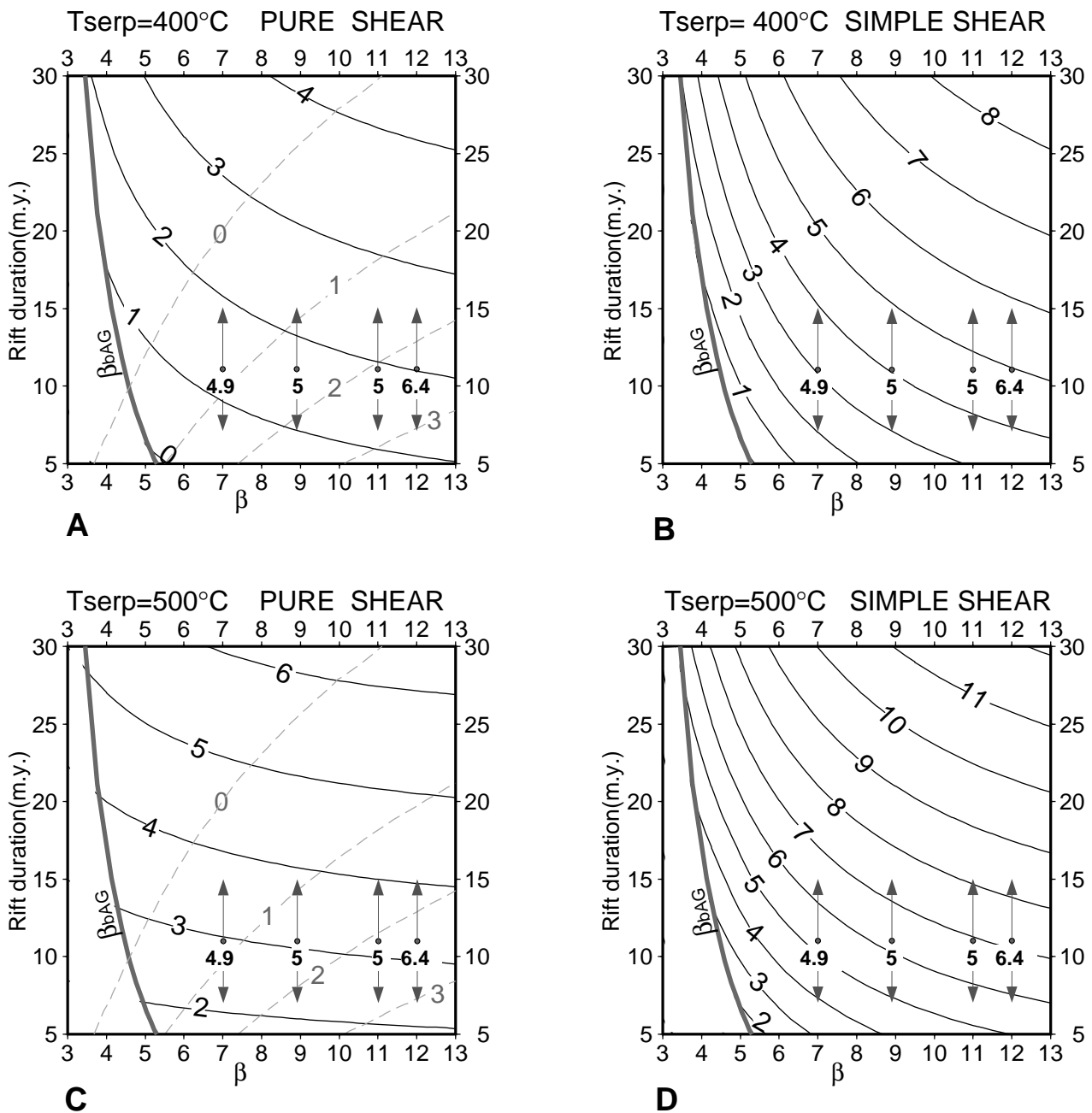


Figure 4.12. Contours (solid black lines) of the predicted thickness of the serpentinizing zone in km (vertical distance between the CMB and the controlling isotherm) for two values of this isotherm (**A.**, **B.** -  $400^{\circ}\text{C}$ ; **C.**, **D.** -  $500^{\circ}\text{C}$ ) and for two models of extension (Figure 4.11.) following the onset of serpentinization and the development of a decollement. The "pure shear model" (**A.**, **C.**) assumes uniform pure shear at all times - superimposed are contours of melt production (in km) after Bown and White, 1995 (grey dashes lines). Note that little melt is predicted prior to  $\beta_{bAG}$  (stretching factor when the entire crust becomes brittle for an aggregate rheology lower crust). The "simple shear" model (**B.**, **D.**) assumes extension in the crust is localized along a detachment after  $\beta_{bAG}$ , and is modelled as non-uniform pure shear (see text). Variation in thickness of partially serpentinized periodites (in km) with crustal stretching factors along line CAM 144 from the IAP (Chian et al., 1999), are shown below grey circles in bold font. Arrows indicate error bars for the duration of rifting, from 7 to 15 m.y.. Crustal stretching factors are averaged over the length of each fault block measured from average crustal thicknesses over each fault block length from Site 1065 to the oceanward tip of the continental crust along this line (see Figure 4.3.).

and model the end-member case here as non-uniform pure shear, which we will call simple shear, by maintaining a constant strain rate in the crust but setting it to zero in the mantle after  $\beta_b$  is reached (Figure 4.11b). This end-member underestimates the amount of extension in the mantle beneath the decollement and hence overestimates the depth to the controlling isotherm and thus the thickness of the serpentinizing zone (Figure 4.12b and d).

Thus, these two different approaches set bounds on the possible depths of the 400°C/500°C isotherms after the crust becomes entirely brittle and thus provide minimum and maximum estimates for the thickness of the potential serpentinizing zone (Figure 4.12).

For uniform pure shear extension as the stretching factor increases for any given strain rate, the thickness of the mantle shallower than the 400°C/500°C isotherm increases (Figure 4.10), implying that the potential thickness of serpentinized mantle developed during rifting also increases with stretching factor (Figure 4.12a, 12c). If simple shear extension occurs the increase of the serpentinizing zone thickness with stretching factor is more dramatic, since the depth of these isotherms remain constant after  $\beta_b$  is reached while the depth of the CMB decreases (Figure 4.12b, 12d).

#### 4.4. DISCUSSION

Using a cool lithospheric model, we have modelled the stretching factors at which the entire crust becomes brittle and at which the underlying mantle peridotites may start to serpentinize. We have briefly touched on the implications this might have for the rheological and tectonic evolution of the margin. In this section, we develop this further, by considering the rheological consequences of mantle serpentinisation and then how this may influence the evolution of the rift leading to break-up. We then compare the predictions of our model with observations from the West Iberia margin.

##### **4.4.1 Effect on lithospheric rheology, strain localisation and the development of detachment levels**

Experimental results indicate that the frictional strength of serpentinite is considerably lower than that predicted by Byerlee's law, its coefficient of friction being 0.3-0.45 (Escartín et al., 1997a, Escartín et al., 1997b). Thus conversion of upper mantle peridotites to serpentinisation would produce a decrease in the strength of the upper mantle (Figure 4.13). The weakening may have two effects:

1. the development of a weak zone in the center of the rift which will serve as a focus for continuing extension. Thus extension in the rift is likely to be localized where the mantle serpentinites first form. This has not yet been considered in 2-D finite element modelling and is clearly a subject for future investigations

2. the development of a horizontal weak zone at the base of the crust. This is likely to act as a decollement, especially as serpentinites can develop high local pore pressures during ongoing deformation (Escartín et al., 1997a; 1997b) and may explain the development of detachment faults such as S (Figure 4.2a) and H (Figure 4.2b). We note that these are found close to the landward limit of mantle serpentinites as inferred from the existing data and are underlain by probable serpentinites (Figure 4.3, Chian et al., 1999). The presence of serpentinites may allow faults to remain active at dips as low as  $23^\circ$  (Figure 4.13b): including the effects of high pore pressure and/or cohesion in the overlying section will reduce this further.

The seismic data support the idea that the serpentinitized peridotites act as a decollement. On GP12 for instance, the block-bounding faults appear to detach onto S (Hoffmann and Reston, 1992). S can be traced from a breakaway in the east, at CMP 400, to CMP 1600 as a gently west-dipping reflection (Reston et al., 1996, Figure 4.2a). At c. CMP 900, S cuts across and truncates deeper east-dipping reflections (Reston et al., 1996 – white dots of Figure 4.2a), which flatten at approximately the depth of the Moho (Whitmarsh et al., 1996) and are thus interpreted as the CMB. To the west of the truncation of these CMB reflections (i.e. between CMPs 900 and 1600), S is especially bright and corresponds to a major jump in velocity (Reston et al., 1996): the lower plate to S here exhibits velocities in excess of 7 km/s (Whitmarsh et al., 1996; Sawyer et al., 1998), best interpreted as partially serpentinitized peridotites. Thus over much of its length, S appears to follow the top of a weak zone at the CMB.

Between CMPs 400 and 900, S cuts at a low-angle through the crust (black dots on Figure 4.2a) and cuts but barely offsets top basement and pre-rift sediments at CMP 500 just to the west of the breakaway (see Reston et al., 1996, and Figure 4.2a). We suggest that this portion of the S reflector might be a late structure as this offset is far smaller than the topography of the fault blocks. We interpret deeper reflections (grey dots in Figure 4.2a) as the original fault that cut through the crust and reached the mantle (leading to mantle serpentinitisation and hence the development of a decollement). We speculate that these early structures were rendered inactive both by footwall rotation accompanying unloading and by the propagation of a low-angle fault from the decollement zone (Lister and Davis, 1989; Reston et al., 1996) to the surface (S between c. CMPs 900 and 400, Figure 4.2a).

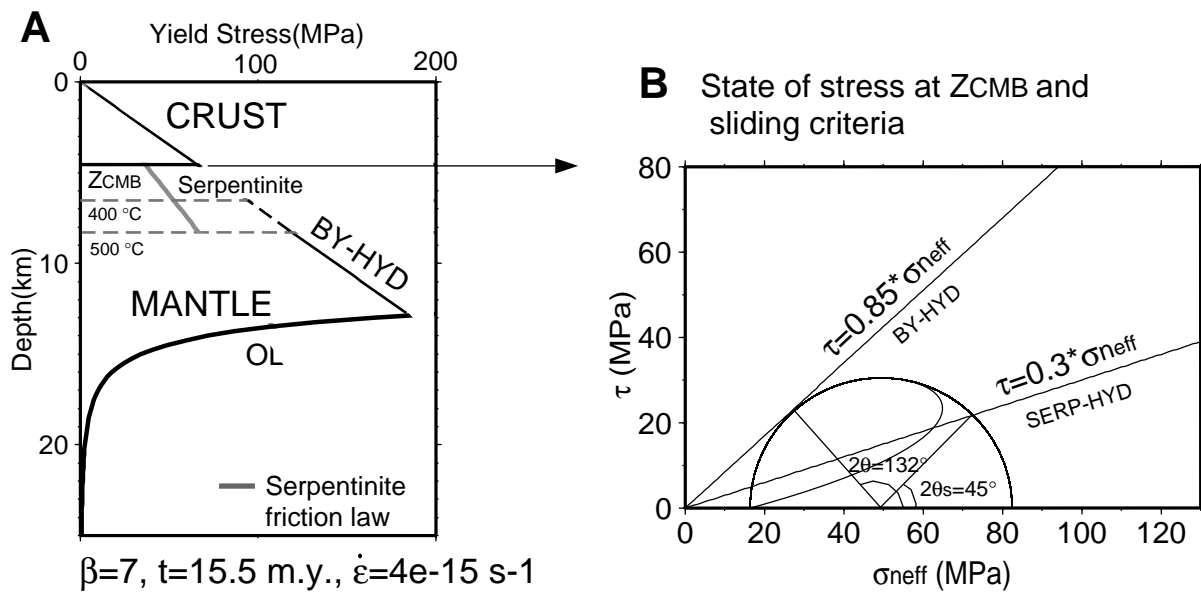


Figure 4.13. **A.** Yield strength envelope, assuming an aggregate rheology for the lower crust, after 15.5 m. y of extension.,  $\beta=7$ , at a constant strain rate of  $4 \cdot 10^{-15} \text{ s}^{-1}$ . Because the entire crust is in the brittle field and the upper mantle within the serpentinite stability field serpentinites can form. Potential serpentinization zone goes from the base of the CMB up to the  $400^\circ\text{C}/500^\circ\text{C}$  isotherm. In this area the serpentinite friction law ( $\mu=0.3$ ) is shown with a grey line. BY-HYD indicates Byerlee's friction law for hydrostatic pore pressure. OL: plastic flow law for olivine. Serpentinites at the base of the crust reduce the strength of the upper mantle and may contribute to rift localization. **B.** Mohr circle for this state of stress.  $\tau_{\text{BY-HYD}}$  indicates Byerlee's sliding criteria along preexisting faults,  $\tau_{\text{SERP-HYD}}$  indicate als Byerlee's sliding criteria but with a coefficient of friction of 0.3 appropriate for serpentinite.  $\sigma_{neff}$  indicates effective normal stress to the fault surface,  $\sigma_{neff} = \sigma_n - P$ , where P is pore pressure. The angle of sliding on preexisting fractures is reduced to  $23^\circ$  if serpentinite friction law is used.

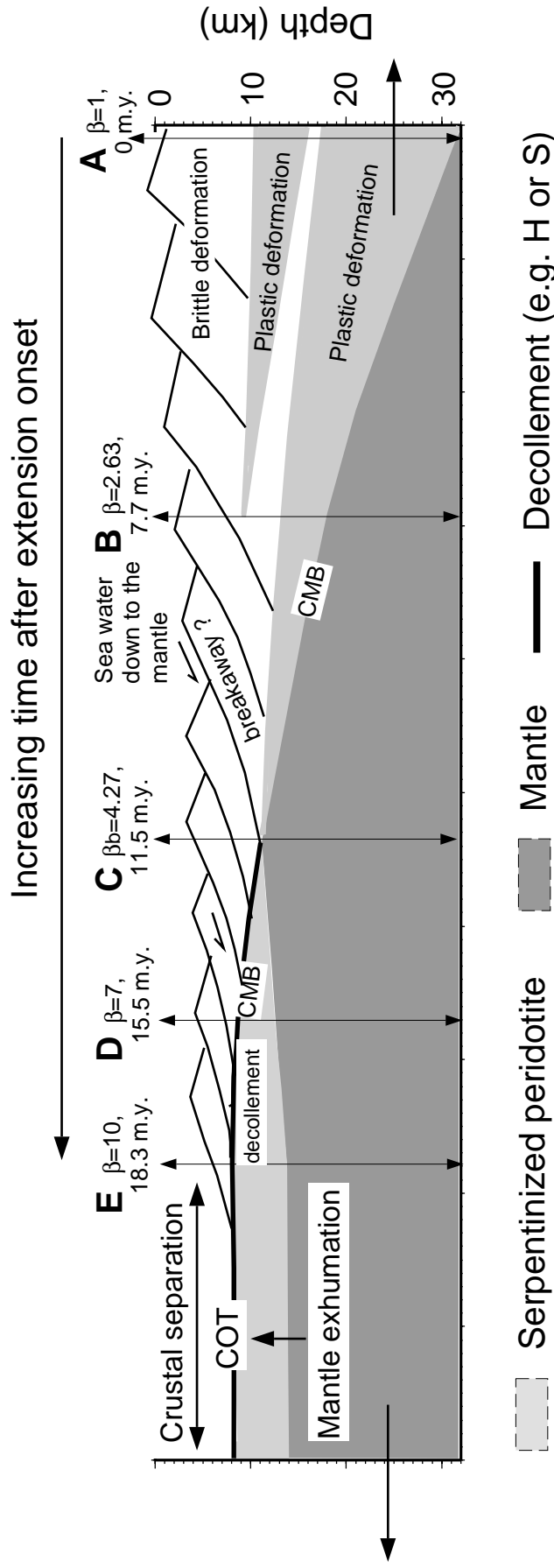


Figure 4.14. Temporal evolution of the center of the rift of a passive non-volcanic margin, from the onset of extension up to crustal separation. Extension is assumed to occur at a constant strain rate of,  $4 \cdot 10^{-15} \text{ s}^{-1}$ , as uniform pure shear. **A.** At the beginning of extension two plastic layers exist in the crust. The middle crustal layer is modelled assuming wet quartzite rheology, the lower crustal layer assuming an aggregate rheology. **B.** As extension progresses rocks are brought to shallower levels and thus cool. The wet quartzite layer in the middle crust enters the brittle regime after  $\beta=2.6$ . **C.** Extension continues and when  $\beta$  reaches 4.2 ( $\beta_b$ ) the entire crust enters the brittle regime. Faults cut across the crust and bring seawater to the mantle; because the CMB is within the serpentinite stability field, serpentinization begins. **D.** As extension progresses the thickness of the serpentinization zone increases. Serpentinites create a weak zone at the base of the crust, forming a decollement such as S at the DGM (Figure 2), and H at the IAP (Figure 3). **E.** Extension proceeds along this decollement are progressively pulled apart and rotated until crustal separation occurs and partially serpentinized mantle is exhumed.

#### **4.4.2 Comparison with west Iberia**

We can also compare the predictions of our modelling with observations from the west Iberia margin where serpentinitized peridotites are well known (Figure 4.2 and Figure 4.3). The parameters used in our model are compatible with those known for West Iberia: crustal thickness immediately onshore is currently c. 32 km (Córdoba et al., 1988), heat flow is between 60 and 80 mWm<sup>-2</sup> (Fernández et al. 1998), and seismic velocities (Córdoba et al., 1988; Pérez-Gussinyé, 1998) suggest that the upper crust is granitic whereas the lower crust is more mafic. Indeed ODP Legs 149 and 173 (Sites 900, 1067 - Whitmarsh and Sawyer, 1996; ODP Leg 173 Shipboard Scientific Party, 1998) cored anorthosites, mafic granulites and mafic amphibolites at the toe of tilted fault blocks (Krawczyk et al., 1996) immediately landward of serpentinitized peridotites (Site 1068).

The duration of rifting is surprisingly rather poorly constrained for the west Iberia margin, partly because of doubts raised about whether the sediment infilling the half-grabens of the margin is truly synrift (Wilson et al., 1996). Furthermore, it is not clear if rifting in any one place occurred during the extension of the whole margin or if rifting was diachronous across the margin (Reston et al., 1996). For instance, the duration of rifting at the landward edge of the serpentinite zone may correspond to that of the entire margin (i.e. the lithosphere there thinned up to the onset of seafloor spreading), or, as rifting progressed, thinning may have become progressively focused seaward and therefore the rift duration landward of the serpentinites would be less than the overall duration of rifting.

Because of these uncertainties, we consider a range of rift duration for both margin segments (Figure 4.9): between 25 my (Boillot and Winterer, 1988) and 7 my (Wilson et al., 1996) for the deep Galicia margin, and between 15 my (Whitmarsh and Miles, 1995) and 7 my (Wilson et al., 1996) for the southern IAP margin.

##### *4.4.2.1 Onset of serpentinitisation*

If the point at which the entire crust enters the brittle regime does mark the initiation of serpentinitisation and the development of detachment faults along the CMB, the intracrustal faults that mark the breakaway to S (km 5, figure a2) and the breakaway to H (shot point 4300 approximately, Figure 4.2c) might have been the first faults (or at least one of the firsts) to cut across the crust and hence bring sea water down to the mantle. Therefore the stretching factors just landward of these faults (Figure 4.2 shows the location where these were measured) place lower bounds on that needed to move the entire crust into the brittle deformation regime and should agree with the  $\beta_b$  calculated with our model. In so doing, we are comparing the temporal evolution of our model with the spatial variation observed west of Iberia.

At the Deep Galicia Margin, the thickness of the crust just landward of S is around 6 km (CMP 275 of GP12, Figure 4.2a and Line 6, Whitmarsh et al., 1996). In the southern IAP the crust landward of the breakaway to H (at about shot point 4900 of LG12, Figure 4.2b and lines CAM of Chian et al, 1999, Figure 4.3) is also around 6 km. When compared to the 32 km thick crust onshore these lead to stretching factors of 5.3. To allow for variations along and across the DGM and IAP we assume possible stretching factors of 4 to 6 just landward of S and H.

These ranges of stretching factors and rift durations compare remarkably well with the predictions of the model (Figure 4.9): our estimates of rift duration and stretching factor at the spatial onset of the serpentinites occur at similar values of  $b$  within the bounds predicted by our calculations. Thus in this respect our model matches well the observations from west Iberia.

#### *4.4.2.2 Comparison of serpentinite thickness*

We can also compare the thickness of serpentinite that our models predict will develop during rifting with that observed along the West Iberian rifted margin. It could be argued that after rifting has ceased, postrift cooling will lead to a deepening of the controlling isotherms and hence to a thickening of the serpentinitized zone. Results from ODP drilling (Legs 149 and 173) west of Iberia have found that the serpentinites, sampled at the basement highs (hence probably exposed longer at the sea floor), formed at low temperatures (c. 200°C) probably during the postrift phase. However, as pointed out by Agrinier et al (1996), these are unlikely to be representative of the deeper zone of anomalous velocity generally interpreted as partially serpentinitized peridotite but rather represent continued serpentinitisation of exposed mantle rocks under retrograde conditions. Although the depth to the 400°C and 500°C isotherms will increase as the lithosphere cools down after extension, this may not necessarily mean that the thickness of the serpentinitized layer will increase. First active faulting may be required to pump sufficient hydrous fluids through the system to lead to significant mantle serpentinitisation (e.g. Sibson et al., 1975). Second, serpentinitisation along pre-existing fractures may be self-limiting in that serpentinitisation involves a significant volume increase and is likely to result in the sealing of the fractures transporting the fluids. Only while deformation continues are the fractures likely to remain open or will new ones develop. Thus we suggest that the partially serpentinitized peridotites inferred at depth beneath the west Iberia margin formed during the rifting rather than subsequently.

The thickness of partially serpentinitized peridotites is best constrained for the southern IAP, beneath, oceanward and south of the H reflector, where a grid of wide-angle seismic data (Chian et al., 1999) has allowed the three-dimensional velocity structure to be



determined (Figure 4.3). The thickness of the partially serpentized layer varies from c. 5 km beneath H to more than 12 km further to the west where complete crustal separation has occurred. Over the same region, the crustal thickness varied from c. 7 km at the crest of tilted fault blocks to c. 2 km beneath the deep half-grabens, to zero where complete crustal separation has taken place. However, we are aware that the local variation in fault block thickness may not affect deeper temperature structure and hence the likely depth of serpentisation. Hence we use the average crustal thickness over distances of 10 km to estimate crustal stretching factors. Again a major uncertainty is the duration of rifting which is estimated between 7 and 15 my.

In Figure 4.12 we overlay the observed thickness of the partially serpentized layer on the contours predicted by the pure and simple shear models for two controlling temperatures (400 and 500°C). In general the plot shows that as the stretching factor increases, so does the thickness of the serpentized layer, as predicted by all four models. The best fit between the observed and the predicted serpentinite thickness is for the 500°C limit to serpentinite stability and for the "simple shear" model. However, assuming a lower initial CMB temperature would improve the fit for the 400°C isotherm and/or for the "pure shear" model. Thus this figure should only be read qualitatively since the initial temperature at the CMB is very poorly constrained. It gives however the order of magnitude of the thickness of the observed serpentinite layer.

#### 4.4.2.3 *Serpentinite vs. melt thickness.*

The potential thickness of the serpentizing zone during rifting can be compared with the melt thickness produced during extension (Bown and White, 1995, Figure 4.12a and c). The comparison is not exact as the starting thermal initial profiles are not the same for both calculations: Bown and White, 1995 assumed a linear geotherm (i.e., no radioactive heat production in the crust) so their initial temperature at the CMB is 365°C rather than 515°C. However, since the key parameters for melt production (lithospheric thickness and the temperature at the base of the lithosphere) are the same for both models, we expect that the melt thickness calculated using our starting model would be similar to the results of Bown and White shown in Figure 4.12.

As the melting model assumes uniform pure shear, this comparison is strictly only valid for the early evolution of the margin where uniform pure shear is likely to be a reasonable approximation. For the strain rates considered here, little or no melt production is predicted prior to the onset of mantle serpentisation at  $\beta\beta$ . The resulting development of serpentinite decollements just below the CMB may lead to significant departure from uniform pure shear. It is thus unlikely that the degree of crustal thinning observed at margins where decollements have developed at the CMB can be used to predict melt

volumes: the observation of complete crustal separation (west of S, west of CMP 2000 Figure 4.2a, and west of H, west of shot point 4000 Figure 4.2b) with little magmatism bears this out.

In Figure 4.12 we overlay melt thicknesses predicted by Bown and White on our predicted serpentinite thickness for the pure shear model (Figure 4.12a and c). The thickness of the serpentinitizing zone increases with rift duration whereas that of melt decreases (Figure 4.12a and c). For the simple shear model melt thickness (predicted by Bown and White) is not shown as the two models are not compatible: the simple shear model predicts far less melt for a given amount of stretching and rift duration than uniform pure shear (Latin and White, 1990). However, the little melt predicted by a simple shear model should also (for a given stretching factor) decrease with increasing rift duration, whereas the thickness of the serpentinitizing zone increases with rift duration (Figure 4.12b and d). Thus rift duration may help distinguish between geophysically similar high velocity mafic underplate and partially serpentinitized mantle.

#### **4.4.3 Development of passive non-volcanic margins, a case example: the western Iberia margin**

The results presented above can help to understand the temporal evolution of passive non-volcanic margins from the onset of rifting to crustal separation. These results are integrated in Figure 4.14 that shows the temporal evolution of the centre of the rift. Particular emphasis has been put to simulate conditions of the rifting episode in the western Iberia margin, the lithosphere is extended at a constant strain rate of  $4 \cdot 10^{-15} \text{ s}^{-1}$ ; a quartz rheology is used for the middle crust and a dry quartz/anorthosite aggregate rheology for the lower crust. The sequence for the evolution of the margin is as follows (Figure 4.14):

1) At the beginning of extension ( $b = 1$ ,  $t = 0$  m.y.) the crust deforms by brittle and plastic mechanisms. Two weak zones of plastic deformation exist at the middle and the lower crust (Figure 4.5 and Figure 4.6).

2) As extension progresses rocks are brought to shallower levels and thus cool. The decrease in temperature and pressure as extension progresses mean that the crust behaves increasingly brittly. After some amount of extension ( $b = 2.6$ ,  $t = 7.7$  m.y.) only the lower crust is still deforming plastically (Figure 4.6).

3) After  $\beta b$  is reached ( $\beta b = 4.2$ ,  $t = 11.5$ ) the entire crust is in the brittle (Figure 4.6, Figure 4.9) regime. Faults can cut across the crust and allow hydrous fluids to reach the upper mantle.

3) Since the upper mantle is within the serpentinite stability field (Figure 4.10), serpentinisation occurs.

4) The low coefficient of friction of serpentinites, perhaps in combination with localised high pore pressure may allow the CMB to act as a decollement between crust and mantle (Figure 4.13), such as S (Figure 4.2a) and H (Figure 4.2b).

5) Final crustal extension occurs along these new formed decollements (e.g. S or H). These decollements may have led to continental break-up by promoting crustal separation and mantle exhumation. During this phase the deformation of the lithosphere is likely to resemble non-uniform pure shear with local simple shear above the decollement.

The section shown in Figure 4.14 is a summary of the temporal evolution of the west Iberian margin. We note that it is also a good approximation of the large-scale spatial variation in the margin structure. This suggests that the idealised temporal evolution may have been recorded in the structure of the margin by the progressive focusing of the rift towards the region of final break-up. However, some of the detailed structure of the margin differs from that of our temporal model. For instance, the S reflector dips to the west (Reston et al., 1996) and is overlain by faults blocks that locally increase in size to the west: the comparison between the temporal and spatial evolution needs to be made with caution.

Finally, an important result of this modelling is the illustration that the boundary between brittle and plastic domains are not fixed markers within the crust, but rather migrate. Portions of the crust that were plastic at the start of rifting become brittle as the crust "anneals" during continued thinning. This contrasts strongly with analog modelling (Brun and Beslier, 1996) which assumes that the boundaries between brittle and plastic layers are fixed markers and that the whole crust becomes brittle because of the intense thinning of the plastic layer by differential crustal stretching as the stretching factors approach those of the deep margin. Our numerical modelling shows that such differential stretching is not necessary as even in a uniform pure shear model, the entire crust becomes brittle at stretching factors far less than observed at the deep margin as a result of the change of the P-T conditions within the crust; when  $\beta_b$  is reached the ratio of the thickness of the lower crustal rocks to the upper crustal rocks is the same as when extension began but the lower crustal rocks behave in a brittle manner.

#### 4.5. CONCLUSIONS

We have investigated the conditions at which the crust becomes brittle under progressive extension and the onset of serpentinisation at non volcanic margins using a one

dimensional model. Although our modelling is necessarily simplified, it does provide some insights into the development of non-volcanic margins and in particular the development and unroofing of serpentinitized peridotites at such margins. We have found that:

1. The entire crust moves into the brittle field after stretching factors  $\beta_b$  of 2.6 to 7.1 depending on the rheology of the lower crust and the strain rate. For our most realistic estimate of rheology this range is somewhat narrower ( $\beta_b = 3.2-5.2$ ).

2. When the entire crust becomes brittle the upper mantle is within the serpentinite stability field. Thus hydrous fluids brought to the upper mantle through brittle faults that cut across the crust can initiate serpentinisation.

3. The predicted onset of serpentinisation matches well with the spatial onset observed at the west Iberian margin: decollements such as S and H observed at the western Iberia margin formed just after the entire crust entered the brittle deformation regime.

4. The serpentinite thickness predicted by our model compares reasonably well with that observed below H at the IAP.

5. Both the potential thickness of the serpentinitizing zone and the thickness of melt generated increase with increasing stretching factor. However, the serpentinite thickness increases with increasing rift duration (for a given stretching factor), whereas the melt thickness decreases. At those passive margins where no significant melt is observed, serpentinites might be present and have played an important role in the later stages of extension.

6. The low frictional strength of serpentinites creates a weak zone at the base of the crust. This may have two effects: 1) localisation of the rift where first form, 2) formation of decollement levels at the base of the crust through which final continental break-up occurs.

## **CHAPTER 5. RHEOLOGICAL AND MAGMATIC EVOLUTION AT NON-VOLCANIC MARGINS DURING EXTENSION: THE EFFECT OF THE INITIAL THERMAL STRUCTURE**

### **5.1 ABSTRACT**

Several non-volcanic margins are characterised by the presence of partially serpentinitised peridotites within the continent-ocean transition (COT) and beneath the feather edge of the continental crust. However, other margins such as the Woodlark Basin are not. We investigate the thermal, magmatic and rheological evolution of margins during progressive extension as a function of initial lithospheric structure, strain rate (rift duration) and stretching factor. We find that for cratonic and old orogen models, the entire crust should become brittle at stretching factors of c. 4. The resultant crust-cutting faults allow water to reach and serpentinitise the mantle, leading to the development of weak serpentinite decollements at the crust-mantle boundary. Our predictions agree reasonably well with the onset and thickness of serpentinitisation at the SW Greenland margin (initial craton model) and the West Iberia margin (initial paleo-orogen model). They also explain the absence of serpentinites at the margins of the Woodlark Basin: here the crust was too thick and hot for serpentinites to form there prior to breakup. Instead, pressure release melting of the upwelling asthenosphere is predicted to occur in place of active mantle serpentinitisation. We suggest that the contrast between the initial thermal structure at serpentinite margins and somewhat magmatic margins such as Woodlark may lead to observed differences in structural style. At the West Iberia and SW Greenland margins, serpentinite decollements formed and may have been active at very low angles. In contrast, “detachment faults” associated with the Woodlark Basin were active at angles only slightly lower than predicted by fault mechanics, which may reflect the distortion of the stress field by igneous intrusions.

### **5.2 INTRODUCTION**

Although many rifted margins are characterised by voluminous magmatic activity at or close to breakup, others exhibit little or no magmatic activity and are termed non-volcanic (e.g., papers in Banda et al., 1995). Well-known examples of such margins include the west Iberian-Newfoundland conjugate margins (Boillot et al., 1988; Reid, 1994; Whitmarsh et

al., 1996; Whitmarsh et al., 1998), (Figure 5.1), the south Australian-Antartica conjugate margins (Lister et al., 1991), and portions of the west Greenland-Labrador conjugate margins (Chalmers, 1997; Srivastava and Roest, 1995; Chian et al., 1995), (Figures 1 and 2). All these margins formed by the rifting of cool, normal thickness post-orogenic orocratonic crust, and appear to be characterised by the presence of serpentinised peridotites within a broad continent-ocean transition (COT - Figure 5.2). However, the Woodlark Basin, another margin described as “non-volcanic” (Taylor et al., 1995; Mutter et al., 1996), (Figure 5.1), is not characterised by serpentinites, does not exhibit a broad continent-ocean transition, and formed relatively quickly in thick orogenic crust and hot, weak lithosphere. In this chapter we investigate whether the observed differences between these margins, and in particular the presence or absence of partially serpentinised peridotite within the continent-ocean transition (COT), can be related to differences in their rheological and magmatic evolution. These, in turn, arise from differences between the initial lithospheric structure of the margins and variations in duration, and amount of extension of each margin’s rifting.

### **5.2.1 Effect of progressive extension**

As extension proceeds two main processes take place:

1) the upwelling mantle starts to partially melt when the geotherm intersects the mantle solidus (McKenzie and Bickle, 1988). Bown and White (1995) showed that the stretching factor at which melting starts and the amount of melt produced are both controlled by the rate of extension; for typical non-volcanic margins such as west Iberia, stretching was slow enough for little melt to be formed.

2) the deep crust is gradually brought to shallower depths, and, depending on the rate of extension, cools (Jarvis and McKenzie, 1980). Both effects tend to move rocks that were originally in the plastic (commonly termed ductile) field into the brittle deformation field: the reduction in pressure reduces the brittle yield stress; the decrease in temperature increases the required plastic yield stress. As a result, the originally plastic portions of the lower crust will eventually move into the brittle field and the entire crust will become brittle. When this happens, faults can cut across the entire crust and allow hydrous fluids to penetrate to the mantle. Under appropriate P-T conditions serpentinisation will begin (see chapter 4).

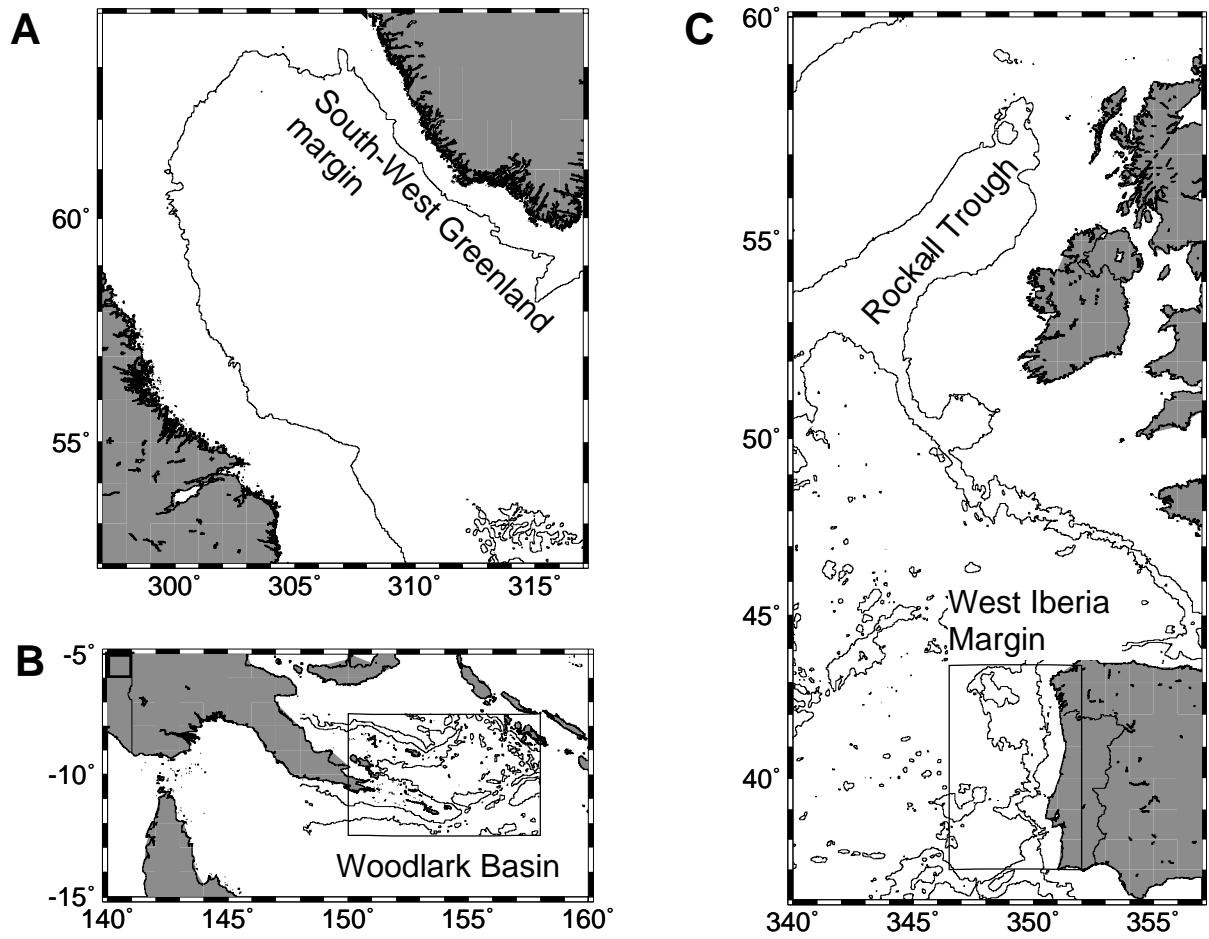
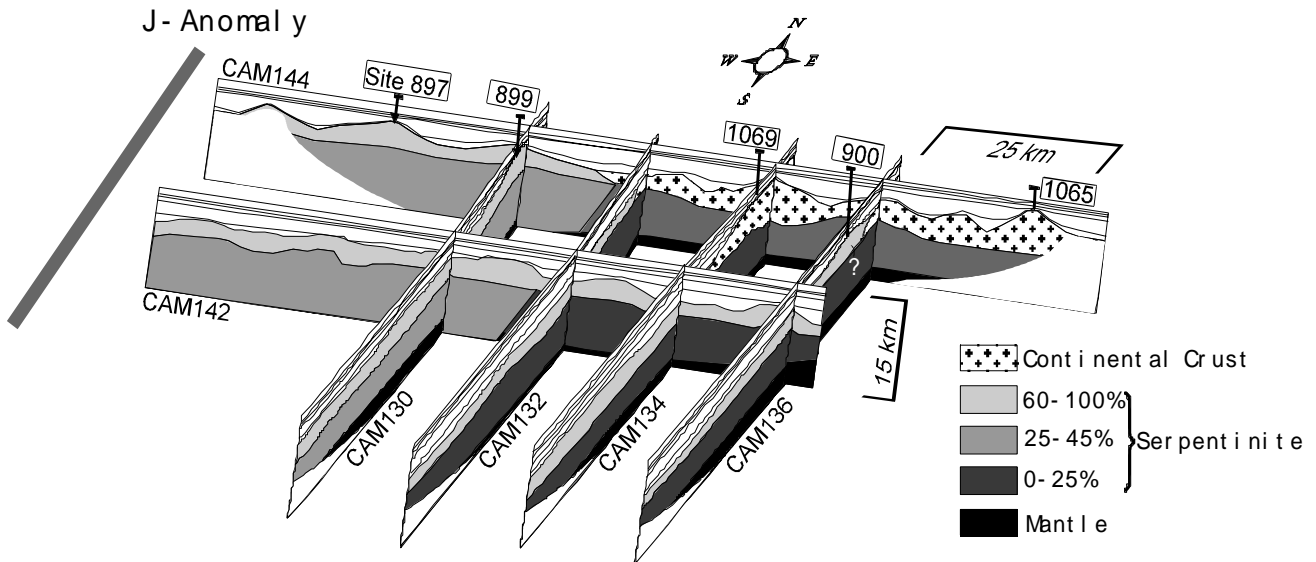


Figure 5.1. Location of the four margins discussed here: **A.** SW Greenland margin; **B.** Woodlark Basin and **C.** Rockall Trough and West Iberia Margin.

**A** WEST IBERIA (Iberia Abyssal Plain), lines CAM (Chian et al., 1999)



**B** SOUTH-WEST GREENLAND, line R2 (modified from Chian and Loudon, 1994)

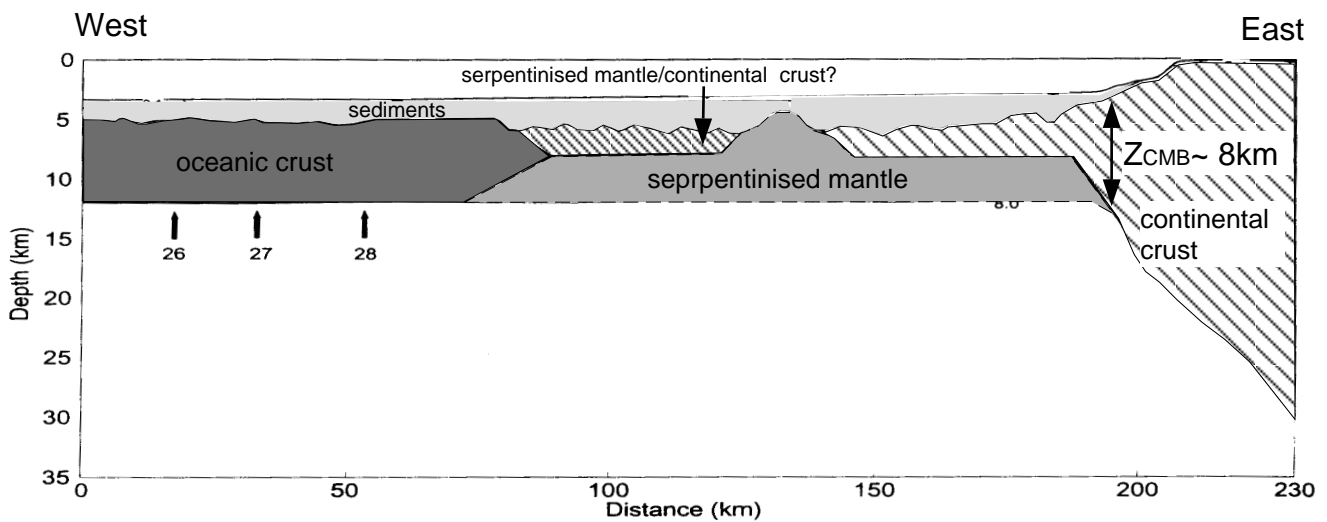


Figure 5.2. Cross-sections through **A.**, West Iberia margin (Galicia Bank segment - Reston et al., 1996) and **B.**, Greenland margin (after Chian et al., 1995), showing occurrence of serpentinized peridotites within the COT. Serpentinites both occur beneath thinned continental crust and as top basement where total crustal separation has occurred.



In this chapter, we consider the rheological evolution of non-volcanic margins with different initial thermal structures. In particular we investigate when the entire crust is likely to become brittle and when mantle serpentinisation may begin. In addition, we predict the thickness of the serpentinite layer and of the melt produced during extension, and compare the results to observations made at several margins.

### 5.3 MODEL DESCRIPTION

We consider a simple model in which the lithosphere undergoes extension by uniform pure shear at a constant strain rate. This seems to be a reasonable approximation at moderate amounts of extension (e.g. McKenzie, 1978). However, as discussed below, at high degrees of extension the serpentinisation of the mantle may lead to the development of decollements at the CMB and hence to a departure from uniform pure shear. The effect this has on the calculations of the potential thickness of the serpentinizing zone is discussed in chapter 4.

The temperature field must be determined in order to follow the rheological evolution of the lithosphere and to calculate the amount of melt produced during extension. This is calculated using a 1-D heat transport equation that takes into account the loss of the heat of fusion whenever decompression melting occurs during extension:

$$\partial T' / \partial t = \kappa * \partial^2 T' / \partial z^2 + v * \partial T' / \partial z + H(z) / \rho * C_p - L' * dF / dt$$

$T'$  is the temperature corrected for the adiabatic:  $T' = T^{true} - \gamma z$ , where  $T^{true}$  is the real temperature and  $\gamma$  is the adiabatic gradient ( $\gamma = \alpha g T / C_p$ ).  $t$  is time,  $v$  is the vertical velocity,  $H(z)$  is the radiogenic heat production,  $\rho$  the density,  $C$  the specific heat,  $dF/dt$  is the melt production rate and  $L'$  is the latent heat of melting (or heat of fusion) which we convert here into an effective 'superheat' of 600°K (Hess, 1989). The values used for these constants are shown in Table 5.1. Because the strain rate is constant, the upwelling velocity is related to strain rate by:

$$v = -\dot{\epsilon} * z$$

where  $\dot{\epsilon}$  is the strain rate and  $z$  is depth (defined to be positive downwards). The heat released by the freezing melt is not added in these calculations in large part because it is unclear at which depth melt will pond.

We assume a distribution of radioactive elements that decreases exponentially downward within the crust and which is zero in the mantle:

$$H(z) = H * \exp(-z/h_r), z < z_{CMB}$$

$$H(z) = 0, z > z_{CMB}$$

where  $z_{CMB}$  is the depth of the crustal mantle boundary (see Table 5.1 and 5.2 for the values of the parameters).

The development of the equations for the production of melt is described in Phipps Morgan, 2000, but will be outlined here for clarity. The melt production is calculated taking into account the increase in the solidus temperature,  $T_m$ , that is associated with progressive melt extraction or depletion of the ascending mantle: During ascent, pressure-release melting is likely to occur because the mantle solidus temperature decreases much more rapidly than the adiabatic curve with decreasing pressure (Figure 5.3). Peridotites have a solid-solution compositional change from melt extraction. After melt extraction, the residual material has an increased solidus (for a given pressure) (Figure 5.3). At any depth, the heat available to drive melting,  $dq$ , during an ascent  $dz$  is proportional to the temperature difference between the solidus and the adiabat at that depth:

$$\delta q = \rho C_p (dT^m / dz - \gamma) dz = \rho C_p (dT^m / dz) dz$$

where the first term within the parenthesis is the solidus gradient and the second the adiabatic gradient. ( $T^m$  is defined as the solidus temperature corrected for adiabatic effects).

The heat consumed by the generation of an increment  $dF$  of partial melt (at a given depth and time) is:

$$\delta q = -\rho(L + C_p dT^m / dF) dF$$

where the first term in the right hand side is the heat consumed by the latent heat of melting  $L$ , and the second term is the additional heat that can be stored in solid-state due to the melting-induced increase in the solidus temperature  $dT^m / dF$  (see Assimow et al., 1998, Phipps Morgan, 2000). The change in solidus temperature gradient due to increasing depletion,  $dT^m / dF$ , is assumed to be constant (see Table 5.1). Equating the heat available

to drive melting with the heat consumed by melting gives the melt productivity (at a given time during extension) :

$$dF/dz = -(dT^m/dz - \gamma)/(L/C_p + dT^m/dF) = -(dT^m/dz)/(L/C_p + dT^m/dF)$$

which is a constant value wherever melting occurs.

The rate of melt production  $dF/dt$  (at a given depth and time) is given by the product of the depth-dependent melt productivity by the upwelling velocity  $v$ :

$$dF/dt = v * dF/dz = \dot{\epsilon} z (dT^m/dz)/(L/C_p + dT^m/dF)$$

Because all the heat available for melting is consumed during melt generation, after partial melting the temperature in the melting region coincides with the solidus temperature (Figure 5.3). The change in temperature within the melting region is governed by the pressure- and depletion dependence of the solidus:

$$dT/dz = dT^m/dz - (dT^m/dF)dF/dz$$

where the first term of the right hand side of the equation is the slope of the solidus for zero depletion and the second term is the increase in the solidus temperature due to depletion, multiplied by the melt productivity. The temperature within the melting region is found integrating the previous equation over  $z$  :

$$T(z) = T^m(z) = (dT^m/dz) * z - (dT^m/dF) * \int_0^z (dF/dz) dz = (dT^m/dz) * z - (dT^m/dF) * p$$

where

$$p = \int_0^z (dF/dz) dz$$

is the depletion,  $p$ .

The heat transport equation is solved using an iterative finite difference scheme similar to Crank-Nicholson (Smith, 1985). As boundary conditions the temperature at the base and top of the region are kept constant throughout the calculations. The initial thermal state is obtained by solving the steady state heat transport equation setting the advective term to

zero. At every time step the temperature and the solidus are first calculated using the melt production rate and depletion of the previous time step. Once the temperature is known the new melt production rate and depletion for the actual time step are calculated and these are used to reevaluate the temperature field and solidus. This is done iteratively until a stable solution for the melt production rate is found.

The melt produced at a time  $t$  is obtained integrating over depth the rate of melt production:

$$F(t) = \int_0^z (dF/dt) dz'$$

Finally, the total thickness of melt,  $t_m$ , produced by a time  $t$  since the onset of rifting is:

$$t_m = 1/\beta_i \int_0^t F(t') \beta(t') dt'$$

### **5.3.1 Initial Lithospheric models**

We consider three initial lithospheric models to represent the rifting of a craton, of an old collapsed orogen, and of a young orogen (see Table 5.2 for key parameters and Figure 5.4). The cratonic model is based on the structure of West Greenland (e.g. Chian et al., 1995; Chalmers et al., 1997) prior to the opening of the Labrador Sea, and consists of a 35 km thick crust and a 155 km thick lithosphere (Figure 5.4a). The temperature at the Moho is 475°C. The old orogen model is based on the structure of West Iberia immediately prior to rifting as deduced from the current structure onshore Galicia (see chapter 4 and references therein). It consists of a 32 km thick crust, with a Moho temperature of 515°C, and a lithospheric thickness of 125 km. This is similar to many collapsed orogens (e.g. the Caledonides of the UK - Klemperer and Hoßbs, 1992). Finally, our young lithospheric model is based on the structure of Papua New Guinea immediately adjacent to the Woodlark Basin and on the P-T-t evolution of rocks exhumed from depth within the core complexes of the D'Entrecasteaux Islands (Hill et al., 1992). In this model, the crust is initially 50 km thick (Finlayson, 1976; Taylor et al., 1999), with a Moho temperature of 850°C (Hill et al., 1992), and the lithosphere is in total 95 km thick.

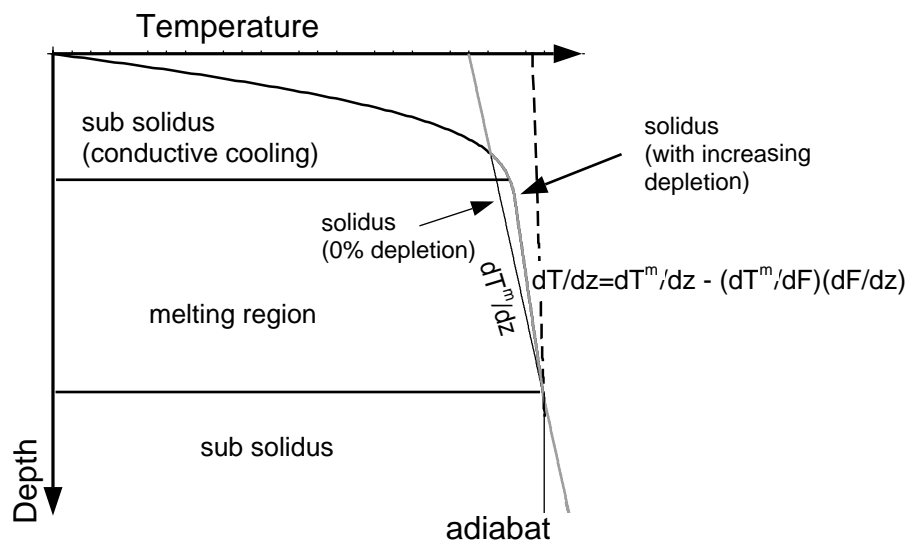


Figure 5.3. Model for pressure release melting accompanying mantle upwelling during lithospheric extension.

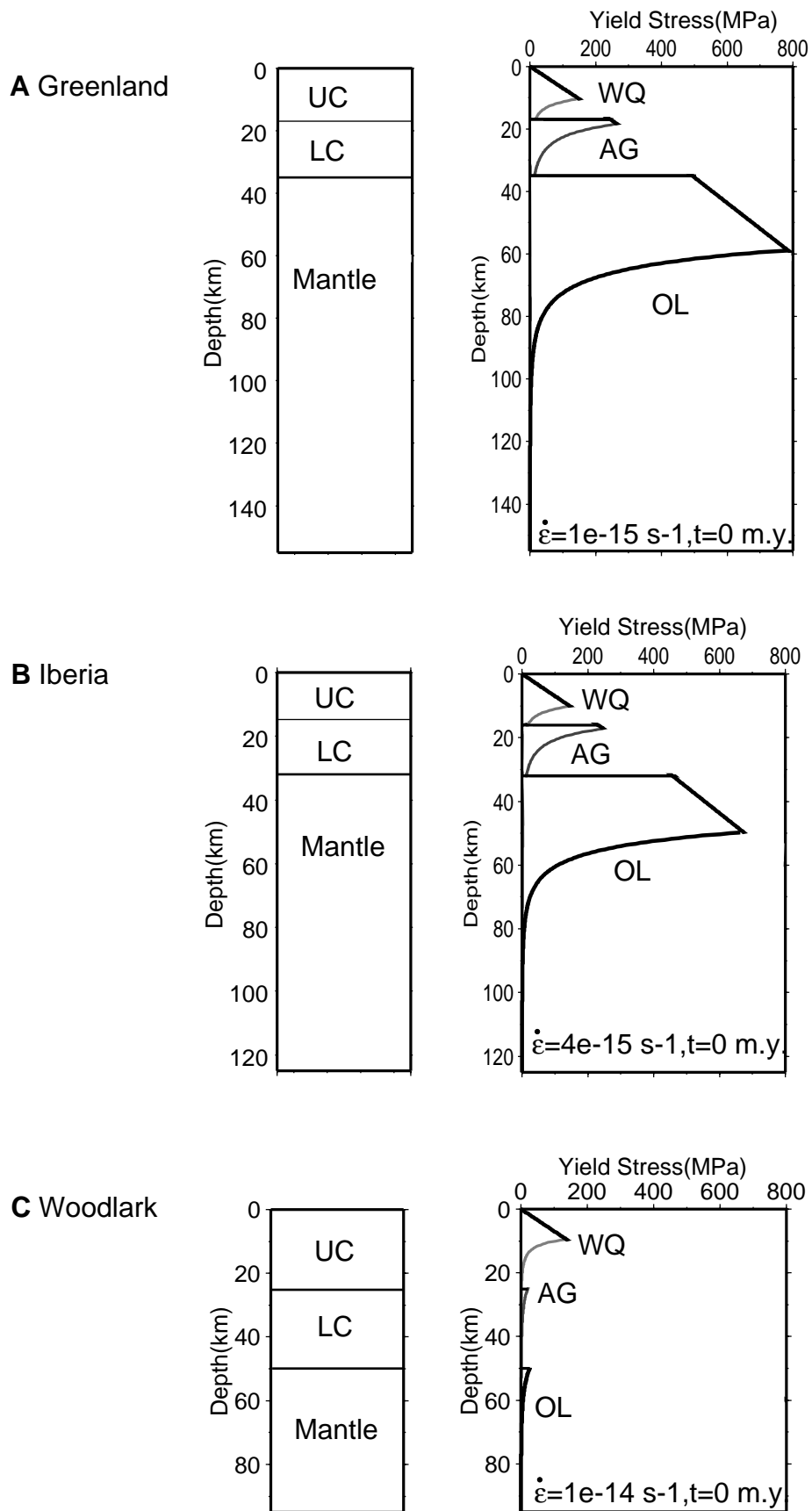


Figure 5.4. Initial lithospheric models and rheological profiles at the onset of rifting for **A.**, SW Greenland , **B.**, Iberia and **C.**,Woodlark. UC: upper crust, LC: lower crust, OL - olivine rheology assumed for mantle, WQ - wet quartz rheology assumed for the upper crust, and AG is aggregate rheology (50% dry quartz, 50% anorthsite) assumed for the lower crust.

TABLE 5.1. Thermal parameters

Symbol	Name	Value
K <sub>c</sub>	thermal conductivity in the crust	2.5 W m <sup>-1</sup> °K <sup>-1</sup>
K <sub>m</sub>	thermal conductivity in the mantle	3.4 W m <sup>-1</sup> °K <sup>-1</sup>
k	thermal diffusivity	8*10 <sup>-7</sup> m <sup>2</sup> s <sup>-1</sup>
r <sub>c</sub>	crustal density	2800 kg m <sup>-3</sup>
l	hydrostatic pore pressure factor	0.35
g	acceleration of gravity	10 m s <sup>-2</sup>
h <sub>r</sub>	radiogenic heat production length scale	10 <sup>4</sup> m
C <sub>p</sub>	specific heat	1250 J kg <sup>-1</sup> °K <sup>-1</sup>
R	universal gas constant	8.3143 J mol <sup>-1</sup> °K <sup>-1</sup>
L'	effective superheat	600 °K
dT <sup>m</sup> /dF	increase in solidus temperature due to melting	300 °K
dT <sup>m</sup> /dz	solidus gradient	3.25 °K/km

TABLE 5.2. Initial lithospheric models

Symbol	Name	Value
<b>Craton (e.g. SW Greenland)</b>		
z <sub>CMB</sub>	depth to crust-mantle boundary	35 km
z <sub>L</sub>	depth of the lithosphere	155 km
T <sub>CMB</sub>	temperature at the crust-mantle boundary	475 °C
T <sub>L</sub>	temperature at the lithosphere's base	1300 °C
H	radiogenic heat production	4.3 μW m <sup>-3</sup>
q <sub>So</sub>	initial heat flux at surface	65 mW m <sup>-2</sup>
<b>Old orogen (e.g. West Iberia)</b>		
z <sub>CMB</sub>	depth to crust-mantle boundary	32 km
z <sub>L</sub>	depth of the lithosphere	125 km
T <sub>CMB</sub>	temperature at the crust-mantle boundary	515 °C
T <sub>L</sub>	temperature at the lithosphere's base	1300 °C
H	radiogenic heat production	4.45 μW m <sup>-3</sup>
q <sub>So</sub>	initial heat flux at surface	71.4 mW m <sup>-2</sup>
<b>Young orogen (e.g. Woodlark)</b>		
z <sub>CMB</sub>	depth to crust-mantle boundary	50 km
z <sub>L</sub>	depth of the lithosphere	95.6 km
T <sub>CMB</sub>	temperature at the crust-mantle boundary	850 °C
T <sub>L</sub>	temperature at the lithosphere's base	1300 °C
H	radiogenic heat production	4.68 μW m <sup>-3</sup>
q <sub>So</sub>	initial heat flux at surface	80 mW m <sup>-2</sup>

### 5.3.2 Initial strength curves.

The strength of the lithosphere at constant strain rate is determined by the interplay between rheology, temperature and depth. Thick, hot crust leads to relative weakening; thin cold crust or thick cold lithosphere leads to relative strengthening. In each of the above models, a two layer crust is assumed, with the top half of the crust being rheologically modelled as wet quartz, and the lower half of the crust being modelled as an aggregate of 50% dry quartz and 50% plagioclase (Figure 5.4). Although we consider that dry quartz probably underestimates the strength of the lower crust, whereas anorthosites probably are too strong (see chapter 4), for completeness we also show results obtained assuming these two end-member rheologies (see Table 5.3 for rheological parameters).

Although we calculate the evolution of each model at a wide range of strain rates, we only show the strength curves at the average strain rates at which the different margins developed (Figure 5.4). Based on the duration of rifting at each margin (discussed further below), we use a  $10^{-14} \text{ s}^{-1}$  strain rate for Woodlark (Taylor et al. 1999), a  $4 \times 10^{-15} \text{ s}^{-1}$  strain rate for West Iberia and a  $10^{-15} \text{ s}^{-1}$  strain rate for West Greenland. Since the resistance to plastic rock deformation increases with strain rate, the higher strain rate for Woodlark should increase its initial strength profile. However, this effect is minor compared to the weakening effects of thick, hot crust: the integrated lithospheric strength (the total area to the left of the strength curve) is far less for the Woodlark starting model than for the other two cases.

Both the West Iberia and the West Greenland lithospheres initially exhibit marked weak zones at the base of the upper and lower crust and towards the base of the lithosphere (Figure 5.4a and 4b). The upper crust, the top of the lower crust and in particular the uppermost mantle are in contrast strong and initially brittle. The Woodlark Basin starting model is quite different. Despite higher instantaneous strain rates, the strength profile (Figure 5.4c) shows that beneath the brittle upper crust, the lithosphere has little strength. This model thus resembles models proposed for core complex formation in which the effective elastic thickness is small (Buck, 1988) and the lower crust can flow in response to buoyancy forces (Buck, 1991).



TABLE 5. 3. Rheological parameters,  $\sigma_{zz} - \sigma_{xx} = (\dot{\epsilon}/A) * \exp(E/nRT)$ 

Material	n	A (Pa <sup>-n</sup> s <sup>-1</sup> )	E (Kj mol <sup>-1</sup> )
Wet Quartzite <sup>(1)</sup>	2.4	1.3*10 <sup>-20</sup>	134
Dry Quartzite <sup>(2)</sup>	2.9	5*10 <sup>-25</sup>	149
Aggregate <sup>(3)</sup>	3	4.9*10 <sup>-24</sup>	192.4
Anorthosite <sup>(4)</sup>	3.2	5.6*10 <sup>-23</sup>	238
Olivine <sup>(5)</sup>	3	10 <sup>-13</sup>	500

<sup>(1)</sup>Kronenberg and Tullis [1984], <sup>(2)</sup>Koch [1983], <sup>(3)</sup>Tullis et al. [1991], <sup>(4)</sup>Shelton and Tullis [1981], <sup>(5)</sup>Newman and White [1997].

#### 5.4 RHEOLOGICAL EVOLUTION DURING PROGRESSIVE EXTENSION

As the lithosphere is extended, the crust thins and the depth of burial of deep crustal rocks is reduced. At the same time these rocks cool (see for instance the change in the temperature of the CMB in Figure 5.5). The reduction in the overburden pressure reduces the resistance to brittle faulting; the decreasing temperature results in increased resistance to plastic deformation. Thus during progressive extension the deformation mechanism of rocks changes, rocks that were initially behaving plastically will eventually switch to brittle behaviour. The stretching factor at which the entire crust becomes brittle will be called  $\beta_b$ . We consider that this amount of extension may be a key stage in the development of widespread serpentinites along and beneath non-volcanic margins. Serpentinisation requires aqueous fluids in considerable volumes (e.g., over 0.6 m<sup>3</sup> of water for each m<sup>3</sup> of peridotite to be fully serpentinitised). The most likely source of sufficient fluid to serpentinitise the uppermost mantle is from the surface along deeply penetrating brittle faults. As the depth extent of such faults is probably controlled by the thickness of the brittle layer, one condition for mantle serpentinitisation is that the entire overlying crust has become brittle, which occurs at  $\beta_b$ . Not only are serpentinitised mantle rocks a feature of many non-volcanic margins as discussed earlier, but also if developed beneath the crust (Boillot et al., 1989) during the rifting process may act as a decollement along which the crust can be pulled apart (see chapter 4). Thus the embrittlement of the entire crust may be a necessary condition for total crustal separation at some margins.

Figure 5.6 illustrates the rheological evolution of the three models, each evolving at a geologically appropriate strain rate. Both the West Iberia and the West Greenland cases show that at moderate stretching factors (2.7 and 2.3 respectively) the base of the upper crust becomes brittle while the lower crust remains plastic until slightly higher stretching factors. However at  $\beta_b=4.4$  and 3.2 respectively, the entire crust has become brittle. In contrast, the thick, hot crust of the Woodlark Basin model does not become entirely brittle

until stretched by more than a factor of 10. This reflects the initial lithospheric structure (thick, hot crust) and also the rapid strain rate (which means that deep crustal rocks do not have time to cool substantially by conduction during the rifting process).

For our three models we have generalised the results of Figure 5.6 by further considering for each model a wide range of possible rift durations (and hence a wide variety of possible strain rates). This allows our results to be compared with other margins and basins (Figure 5.7). We have also modelled two other rheologies for the lower crust - the end-member rheologies of dry quartz and anorthosite which probably under- and over-estimate the strength of the lower crust, respectively. As expected, the entire crust becomes brittle at lower stretching factors when a strong lower crustal rheology (anorthosite) is used, and at higher stretching factors if a weak lower crust is used (dry quartz). Furthermore, we find that if all other parameters are kept constant,  $\beta_b$  decreases with increasing rift duration (decreasing strain rate) because the lithosphere is given more time to cool during rifting.

A second condition for the onset of mantle serpentinisation is that the temperature of the uppermost brittle mantle lies within the stability field of serpentinites, which are stable up to 400-500°C (Ulmer and Trommsdorf, 1995), depending on the type of serpentinite. As we calculate the temperature structure of the lithosphere during extension (Figure 5.5), we can determine whether this condition is met. Furthermore, by determining the depth beneath the CMB of the isotherm marking the upper limit of the serpentinite stability during rifting, we can estimate the thickness of the serpentinising zone. In Figure 5.8, we contour the  $\beta_b$  curve (for the aggregate lower crustal rheology) as a function of rift duration and stretching factor, together with the thickness between the CMB and the 400°C and 500°C isotherms during rifting. The latter values are thus contours of the potential thickness of the serpentinising zone once the entire crust has become brittle. We only consider the thickness of this zone during rifting as we believe that active faulting (e.g. Sibson et al., 1975) is required to pump sufficient water into the mantle to cause serpentinisation (faulting is needed to keep the cracks open in face of the sealing tendency due to the volume increase associated with serpentinisation).

For all rift durations that were considered, after stretching factors at and beyond  $\beta_b$ , the 400°C isotherm is below the CMB for the SW Greenland and W. Iberia models, but not for the Woodlark Basin model (Figure 5.8). Indeed, at the short rift durations (4-6 Ma) that are most appropriate for the Woodlark Basin, the CMB temperature is above 500°C until stretching factors somewhat above  $\beta_b$ . Thus whereas for West Iberia and SW Greenland, serpentinisation should commence immediately after the entire crust becomes brittle, this is not predicted to be the case for the Woodlark Basin.

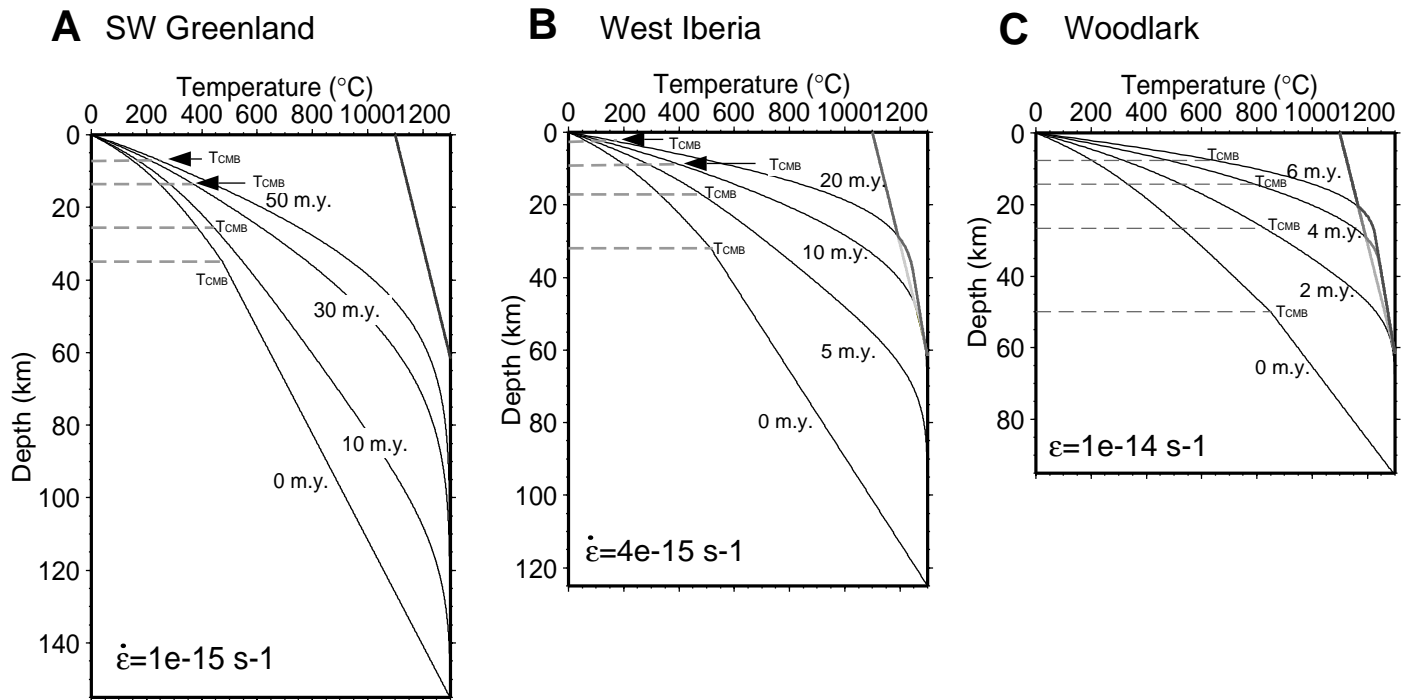
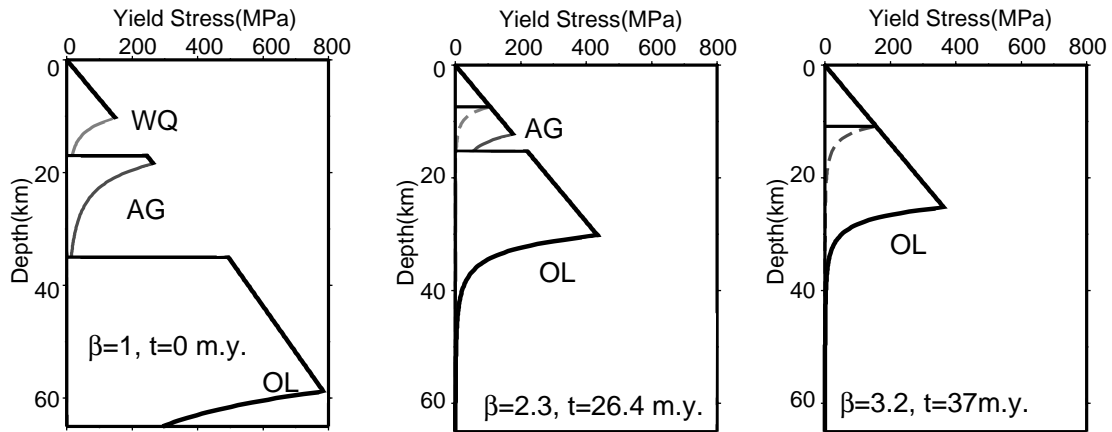
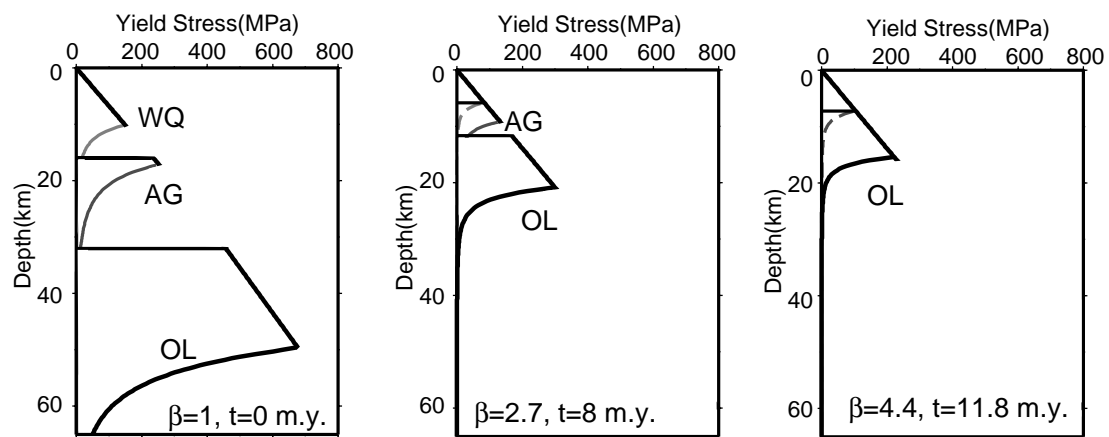


Figure 5.5. Evolution of the geotherm during rifting appropriate for **A.**, SW Greenland, **B.**, West Iberia and **C.**, Woodlark.  $T_{CMB}$  is the temperature at the crust-mantle boundary. Geotherm intersects solidus (grey line) after ~2my rifting for Woodlark and after ~10my rifting for West Iberia, but no melting is predicted during rifting SW of Greenland.

**A** SW Greenland,  $\dot{\epsilon}=1\text{e-}15\text{ s-}1$



**B** West Iberia,  $\dot{\epsilon}=4\text{e-}15\text{ s-}1$



**C** Woodlark,  $\dot{\epsilon}=1\text{e-}14\text{ s-}1$

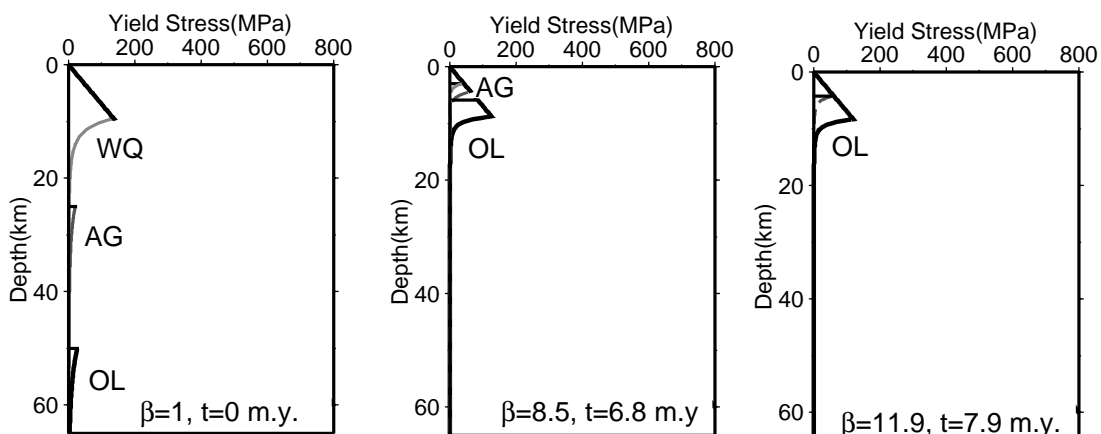


Figure 5.6. Rheological evolution of model lithospheres during progressive extension. Rheological profiles are shown at  $t=0$  (the onset of rifting), at the stretching factor when the upper crust becomes entirely brittle and at  $\beta_b$ , where the entire crust becomes brittle. **A.** SW Greenland: upper crust becomes brittle after 26.4 my rifting at a stretching factor of about 2.3, entire crust becomes brittle at  $\beta_b = 3.2$  after 37 my rifting. **B.** West Iberia: upper crust weak zone disappears at  $\beta \sim 2.7$ , and entire crust becomes brittle at  $\beta_b \sim 4.4$ . **C.** Woodlark Basin: upper crustal weak zone only disappears at  $\beta \sim 8.5$  and entire crust only becomes brittle at  $\beta_b \sim 12$ .

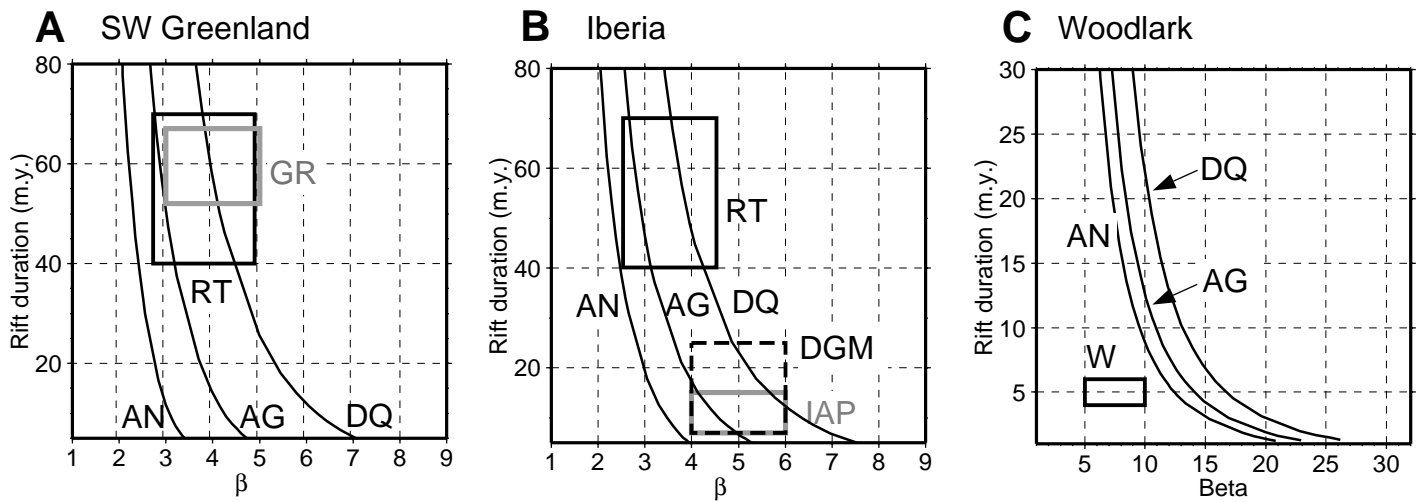
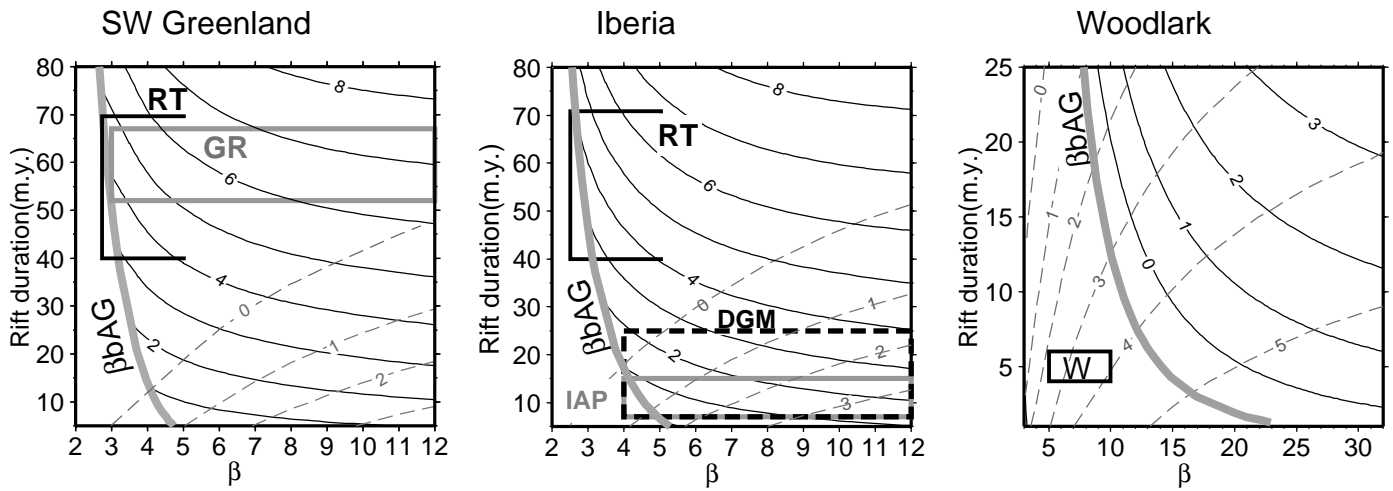


Figure 5.7. Plot of values of  $\beta_b$  as a function of rift duration for a range of possible lower crustal rheologies (AN=anorthosite, DQ is dry quartz, and AG is a 50:50 mixture of the two) for the **A.**, SW Greenland, **B.**, West Iberia and **C.**, Woodlark models. Boxes plotted on each are estimated rift durations and stretching factors at spatial onset of serpentinisation for Greenland (GR), Deep Galicia Margin (DGM), Iberia Abyssal Plain (IAP), Rockall Trough (RT) and Woodlark Basin (W - note that here no serpentinites have been reported so this box corresponds to the COT). Note general agreement between spatial onset of serpentinites and point at which the entire crust becomes brittle,  $\beta_b$ .

**A** Pure shear ,  $T_{serp}=400^{\circ}\text{C}$



**B** Pure shear ,  $T_{serp}=500^{\circ}\text{C}$

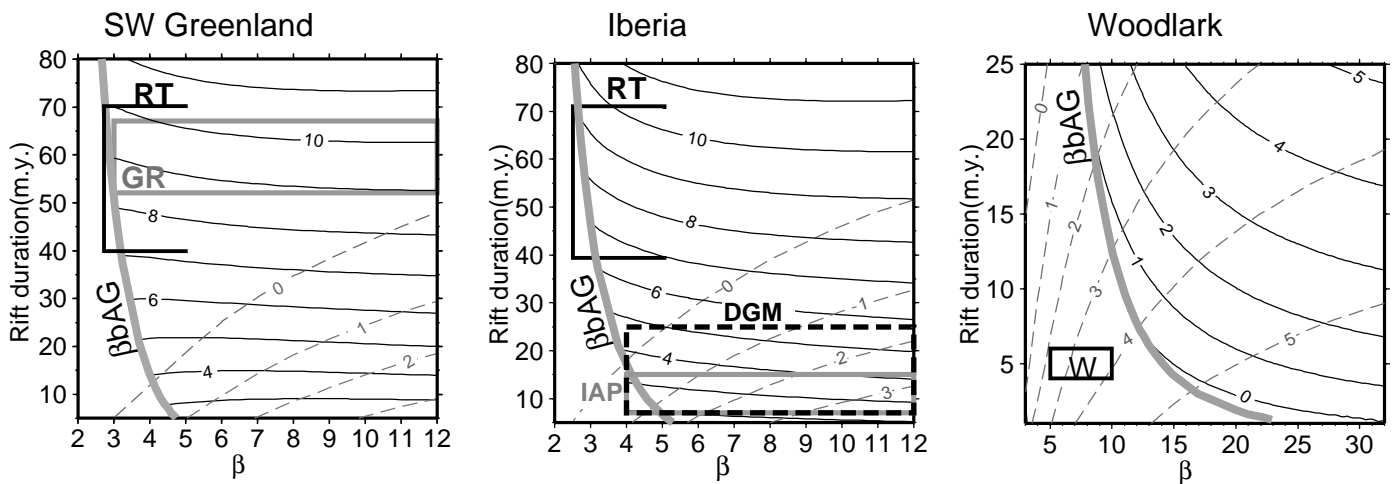


Figure 5.8. Plots of predicted thicknesses of serpentinites (thin solid contours) and of basaltic melt generated by pressure release melting (dashed lines). Boxes represent range of rift durations and stretching factors observed within the COT for margins (abbreviations as in Figure 7). Two possible upper temperature limits for serpentinite stability are considered: **A**.  $400^{\circ}\text{C}$  and **B**.  $500^{\circ}\text{C}$ .

Assuming uniform pure shear throughout, the thickness of the potential serpentinising zone increases with rift duration and stretching factor beyond  $\beta_b$ . Whereas both the West Iberia and the West Greenland models predict similar thickness of serpentinites for any given rift duration and stretching factor beyond  $\beta_b$ , the model predicts far thinner serpentinites for the young orogen model (Woodlark), where high temperatures inhibit serpentinisation, beyond a far higher value of  $\beta_b$ .

We compare the predicted thickness of the serpentinising zone with that of the basaltic magma produced by pressure release melting during rifting. In the old orogen and cratonic models for West Iberia and West Greenland, the thickness of total melt produced only exceeds that of the serpentinized zone at very high stretching factors and/or short rift durations (the bottom right-hand corner of the plots - e.g.  $\beta$  of 8, rift duration of c. 10 my). In contrast, in the range of rift durations investigated, the amount of melt produced during rifting of the young orogen model is generally greater than the thickness of the serpentinising zone.

The seismic signature of basaltic “underplate” and serpentinised uppermost mantle can be quite similar as both can be characterised by velocities in the range 7-7.4 km/s. However it is clear from our results that voluminous basaltic intrusion and mantle serpentinisation are likely to occur under quite different conditions. In particular, knowledge of the initial lithospheric model and the duration of rifting may thus help distinguish between serpentinites and mafic underplate.

## 5.5 COMPARISON WITH OBSERVATIONS

When we consider the actual rift durations observed for Woodlark, West Iberia and the West Greenland margins, we can compare the predicted thicknesses of new basaltic crust and of serpentinised mantle with the observations made at these margins.

### **5.5.1 Woodlark Basin**

Bathymetry and gravity data show that the crustal structure of the continental margins that surround the Woodlark Basin changes along the basin: the crust is thicker west of the Moresby Transform (approx.  $154.2^\circ$ ) (Martinez et al., 1999). This is believed to reflect the different prerift histories of the margins of the western and eastern basin (west and east of the Moresby Transform respectively). Both originated as a volcanic arc because of north Coral Sea subduction but the western margin additionally experienced collision and underthrusting by continental plateaus (Martinez et al., 1999). The lithospheric structure of

our young orogen is meant to simulate that of the western basin, and thus the rift durations and stretching factors we use for comparison are those of this basin.

Rift onset at the Woodlark basin is believed to have begun synchronously at 6Ma along the length of its protomargins (Taylor et al, 1999). However seafloor spreading initiated in a time transgressive fashion from east to west (Taylor et al., 1999), reaching Moresby Transform at 2 Ma and 151.8° E at 0.7 Ma (Taylor et al, 1999). Thus the range of rift durations for the western basin spans 4 to 5.3 Ma: we use values from 4 to 6 Ma to allow for this variation.

Taylor et al (1999) estimate average strains along the margins of the basin and obtain a maximal value corresponding to a stretching factor of 4. However we have estimated the stretching factors at the edge of the continental crust by comparing crustal thickness estimates obtained from gravity data, 7-10 km, (Martinez et al, 1999) with our the initial crustal thickness from our young orogen model (50 km). This leads to a range of stretching factors at the continental edge of 5 to 7 approximately. We again use a larger span of stretching factors, 5-10, to allow for variations along the margin. At all these stretching factors, the crust is still partly (largely) plastic in our young orogen model (Figures 6c, 7c and 8), so we predict no mantle serpentinisation. However, the rapid rift duration implies that partial pressure release melting of the upwelling asthenosphere will have started, producing several km of new basaltic melt (Figure 5.8). Thus, although these margins are described as non-volcanic we would expect to see some evidence for magmatic activity during rifting. As discussed further below, the observed core complexes may be such evidence.

### **5.5.2 West Iberia**

The rift duration of the west Iberia margin is somewhat controversial as Wilson et al., (1996) question whether all the sequences previously interpreted as synrift truly are so. On the basis of their reinterpretation of many of these units as postrift sequences, they proposed that the rift duration on both the Deep Galicia margin (DGM) and the southern Iberia Abyssal Plain margin (IAP) may have been as short as 7 my. However, as this argument (based on the lack of synrift wedges seen on the profiles) would also reclassify as postrift sequences proven synrift units from Woodlark basin (discussion during the Society meeting), we consider the previous, longer rift estimates to be more likely. In these previous estimates, it is generally accepted that the rift duration increases from south to north (reflecting the northward propagation of the spreading centre), lasting c. 15 my on the Iberia Abyssal Plain (IAP) margin and c. 25 my on the Deep Galicia margin (DGM).



The thickness of the crust at the landward limit of mantle serpentinisation can be used to estimate the stretching factor at which serpentinisation commenced (Figure 5.2). This compares well for these margins with the predicted value of  $\beta b$  for the range of rift durations, bearing in mind that we favour the longer estimates of rift durations as discussed above. We note that the crust thins further above a region of serpentinised mantle before mantle is exposed, supporting our suggestion that serpentinisation must occur here before total crustal separation can take place.

The predicted thickness of the serpentinizing zone can also be compared with the thickness of partially serpentinized mantle at these margins (see chapter 4). Assuming that the 500°C isotherm marks the upper limit of serpentinisation, these estimates agree reasonably well. With increasing  $b$ , increasing amounts of melt are predicted especially at shorter rift durations, whereas little voluminous magmatism is observed. This may indicate that either the rift duration is longer than suggested by Wilson et al. (1996), or that the melt is trapped deep within the lithosphere. Alternatively, crustal stretching factors (as deduced from crustal thinning) may locally exceed those of the entire lithosphere (which control melts production) as extension departs from pure shear at stretching factors beyond  $\beta b$ . In particular, the formation of a serpentinite decollement may localise extension in the overlying brittle crust (see chapter 4), leading to subsequent non-uniform stretching. In this case, the volume of melt produced at high crustal stretching factors (above a broader region of less subcrustal extension) may only slightly exceed that predicted at values of  $\beta b$ .

### **5.5.3 West Greenland**

The rift duration of these margins is estimated to have been between 52 and 67my (e.g. Chalmers, 1997, ; Srivastava and Roest, 1995), depending on the interpreted position of the COT. The thickness of the crust at the spatial onset of serpentinisation can be estimated from the velocity model of Chian et al. (Figure 5.2) to be between 7 and 9 km. For an initial 35 km thick crust, this implies stretching factors of about 4-5. On the West Greenland margin, the crust appears thinner above the landward edge of the serpentinized zone, but here crustal delamination following the onset of serpentinisation may have removed the upper crust (Chian et al., 1995 - see below for further discussion of the consequences of crustal delamination). Thus we concentrate on the West Greenland side: the stretching factors above the landward edge of the serpentinites agree reasonably well with the  $\beta b$  predicted by our modelling.

Moving further oceanwards, the crust thins and the serpentinite thickness increases (e.g. Chalmers, 1997), reaching c. 7 km. This is consistent with the predictions of the model (Figure 5.8); at high stretching factors, the depth of the 400°C and 500°C isotherms beneath the base of the crust increases to about 6 and 9km respectively for a rift duration

of c. 50 my. In contrast, no melt is predicted until lithospheric stretching factors in excess of 12 - the volcanic margin further north along West Greenland may thus reflect the influence of the early Iceland plume.

The results from the three margins thus match the predictions reasonably well. This suggests that a fundamental control on the evolution of a margin is likely to be the relative importance of mantle serpentinisation, controlled by the embrittlement of the overlying crust, and of asthenospheric melting, controlled by the rate and amount of mantle upwelling that accompanies rifting. These in turn are controlled by the initial lithospheric structure, and by the rate and total amount of extension.

#### **5.5.4 Rockall Trough**

The analysis developed above can also be applied to deep basins such as the Rockall Trough (Figures 5.1 and 5.9). Although in the past thought to be floored by oceanic crust (e.g., Roberts et al., 1981), it is now generally accepted that the Rockall Trough is underlain by continental crust (e.g. O'Reilly et al., 1997), although the evidence is somewhat equivocal (Joppen et al., 1990).

The age of rifting in the Rockall Trough has also been the subject of much controversy, with some authors suggesting that it initiated in the Late Paleozoic (e.g. Smythe, 1988), although the consensus now appears that it is dominantly a Cretaceous rift (e.g. Musgrove and Michener, 1995) that perhaps overprinted an earlier Mesozoic structure (e.g. Nadin et al., 1999; Cole and Peachey, 1999). The rift duration is thus not fully clear but probably was at least 40 my and perhaps somewhat longer.

The Rockall Trough is situated near the Atlantic margin and the well-developed seaward-dipping reflectors of the Hatton Bank region. It is heavily intruded by Paleocene sills which may hinder the imaging of the Pre-Cretaceous structure, and is marked in several places by major igneous centres of Late Cretaceous to Early Tertiary age (Hitchen and Ritchie, 1993). However, this magmatic activity all took place after rifting and there is no evidence for synrift magmatism; the Rockall Trough appears to be a fundamentally non-volcanic rift, developed towards the foreland of the Caledonian orogeny in crust c. 30 km thick. The lithospheric structure was probably somewhat between that of west Iberia or West Greenland prior to rifting: we shall compare observations from Rockall Trough to the predictions of both models.

The Rockall Trough is crossed by several deep penetration seismic profiles (e.g. Joppen et al., 1990), such as the BIRPS Westline profile (England et al., 1997). None of these profiles clearly images the Moho, so that constraints on the crustal structure and thickness come almost exclusively from wide-angle data. The best quality of these show

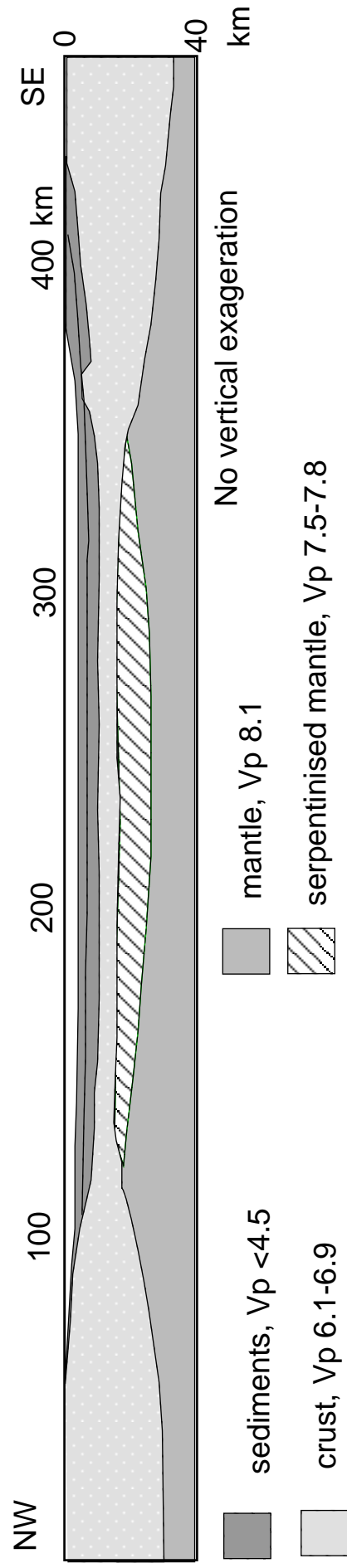
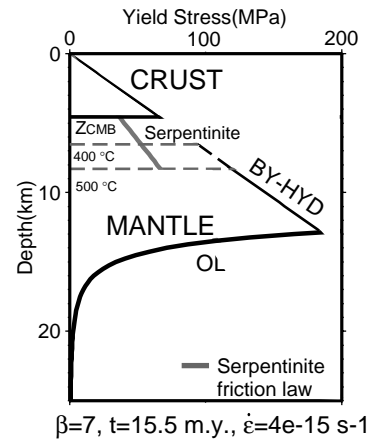
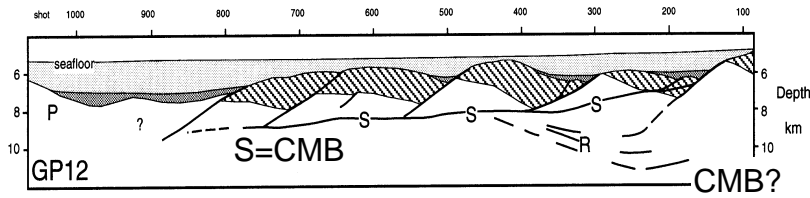


Figure 5.9. Interpreted wide angle line at the Rockall Trough (modified from O'Reilly et al., 1996). The 5 km thin continental crust extends along 200 km, below the mantle is serpentinised

### A S reflector



### B Low angle fault at Moresby Seamount

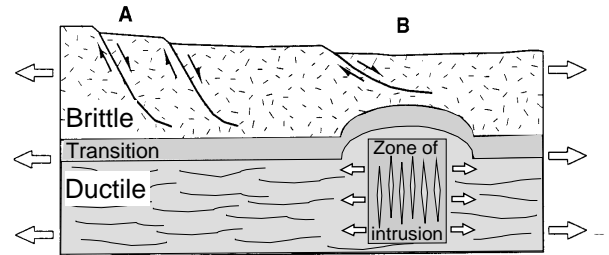
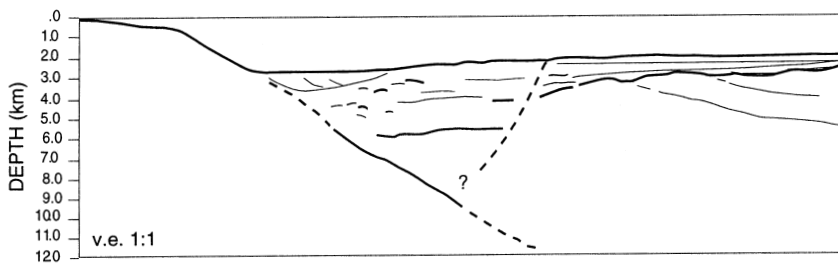


Fig 5.10. Two different types of detachment faults may form at rifted margins: **A.** Weak serpentinite decollements may develop at cool margins such as West Iberia and SW Greenland: here the low friction coefficient of serpentinites together with high local pore pressures generated (Escartin et al., 1997) allows faults to move at very low angles. **B.** At hotter margins, slight distortion of the stress field (due to igneous intrusion - Parsons and Thompson, 1993) allows faults to remain active to angles c. 10° lower than predicted by classical fault mechanics.

that the Central Rockall Trough (O'Reilly et al., 1997) has a crustal thickness of about 6 km (implying a stretching factor of  $\sim 5$ ) and is underlain by a layer 5-10 km thick with a velocity of 7.7-7.8 km/s, interpreted as partially serpentinised mantle.

We note that at such stretching factors and at a rift duration of c. 55 my, the entire crust should have become brittle, explaining the presence of serpentinized mantle beneath the rift. We also note that no melt is predicted at these stretching factors, although thicknesses of c. 6-10 km of partially serpentinized peridotite are predicted, depending on the upper temperature limit of serpentinite stability. Thus it appears that the Rockall Trough also fits the model developed here and could be a typical non-volcanic rift.

## 5.6 DETACHMENTS AND DETACHMENTS

It is clear from the above discussion that we envisage that the formation of serpentinites as one way that detachment faults or décollements can develop at rifted margins (Figure 5.10a). During rifting of cool lithosphere such décollements would develop at the crust-mantle boundary where the temperature would be below 400-500°C (as this is a necessary condition for serpentinization) when the entire crust becomes brittle. Good examples of detachments separating crustal rocks from partially serpentinised peridotites include the S reflector west of the Galicia Bank (Reston et al., 1996; Reston 1996) and the H reflector in the southern IAP (Krawczyk et al., 1996); such structures have also been inferred beneath the West Greenland margin.

However, the detachment faults associated with the core complexes of the Woodlark Basin region are unlikely to be formed in this way. First, thermal calculations suggest that widespread serpentinisation has not occurred because the temperature at the CMB is too high and the lower crust behaves plastically so that no crust-cutting faults exist. Second, the lower plate to the detachment does not consist of serpentinised mantle but rather of exhumed and ductilely deformed deep crustal rocks. Finally, the "detachment faults" here are not as low-angle as those associated with mantle serpentinisation: the fault traced to depth from the Moresby Seamount dips at c. 27°, little less than the 35° limit for normal fault reactivation predicted by classical fault mechanics (e.g. Sibson, 1985), whereas the S reflector can be shown to have been active at angles as low as c. 10° (Reston et al., 1996).

We suggest that the Moresby seamount "detachment fault" formed by relatively classical fault mechanics in crustal material stronger than serpentinites. The slightly low angle of this fault might be explained by the slight rotation of the stress field by intrusion into the lower plate (Parsons and Thompson, 1993 - Figure 5.10b), as observed in the D'Entrecasteaux Islands (e.g., Hill et al., 1992). In contrast, the very low angles of the serpentinite detachments can be partly explained by the low friction coefficient of partly

serpentinized peridotites ( $\sim 0.35$  - Escartin et al., 1997), but probably also require high fluid pressures along the decollement (Axen, 1992; Escartin et al., 1997; see chapter 4). The two types of "detachment" are thus markedly different and reflect the relative importance of mantle serpentinisation and igneous activity.

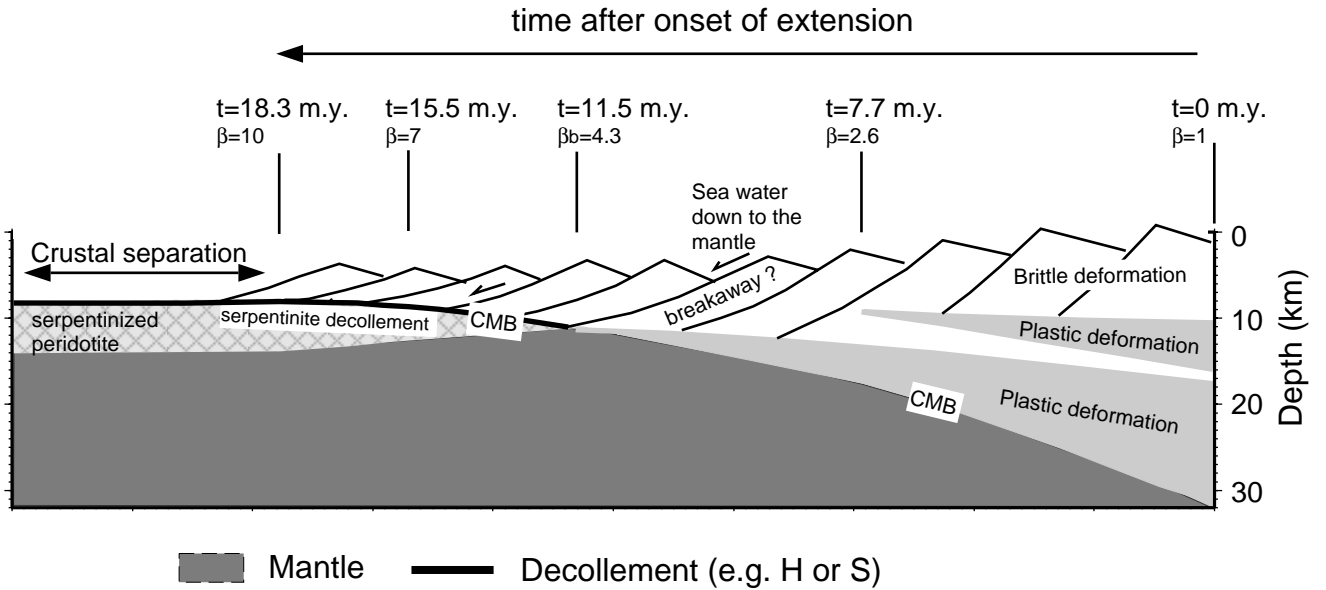
## 5.7 TEMPORAL EVOLUTION AT NON-VOLCANIC MARGINS

In this chapter we have described two fundamentally different types of "non-volcanic" margins: the west Iberia type where slow rifting of a cool crust leads to the formation of mantle serpentinites and the development of a decollement at the CMB, and the Woodlark Basin where more rapid stretching of hot, thick crust does not lead to mantle serpentinisation but instead to the partial melting of the mantle and the subsequent intrusion of melts into the base of the extending crust.

We can summarise the temporal evolution of such margins that is expected from our sequence of 1-D "snapshots" of rheological and thermal evolution (Figure 5.11). These "sections" illustrate the temporal evolution of the centre of the rift rather than the spatial variation from the unstretched continent to the COT, but do provide some insight into how such margins develop. In the West Iberia type (Figure 5.11a), the extending crust originally exhibited two plastic zones corresponding to the mid-crust and the lower crust. During progressive extension, the upper plastic zone disappeared and the upper and mid-lower crustal levels became tightly coupled above a weak plastic zone at the base of the crust. Eventually at stretching factors of about 4-5, the entire crust became brittle and faults cut deep into the mantle. Continuing rifting and movement along these faults pumped large volumes of water through the brittle crust and into the mantle, initiating mantle serpentinisation and leading to the development of a decollement at the base of the crust. This weak zone localised crustal extension, leading to complete crustal separation and mantle exhumation.

In contrast, at the onset of extension the Woodlark Basin crust had only a thin brittle carapace over a largely plastic crust. Although these plastic zones thinned during progressive extension, at no time did the entire crust become brittle (Figure 5.11b). Instead, at stretching factors greater than about 3-4, the upwelling asthenosphere underwent partial melting, leading to the intrusion of the hot, ductile lower crust by dense basaltic magmas that were "trapped" in the deep crust. Continued intrusion however led to local modification of the stress field, allowing normal faults to remain active at angles as low as c.  $25^\circ$ . In this case, as virtually all of the strength of the Woodlark Basin lithosphere was within the crust (e.g., Figure 5.6), crustal separation is synchronous with total lithospheric failure, resulting in no exposure of the subcrustal lithosphere.

### A West Iberia type



### B Woodlark type

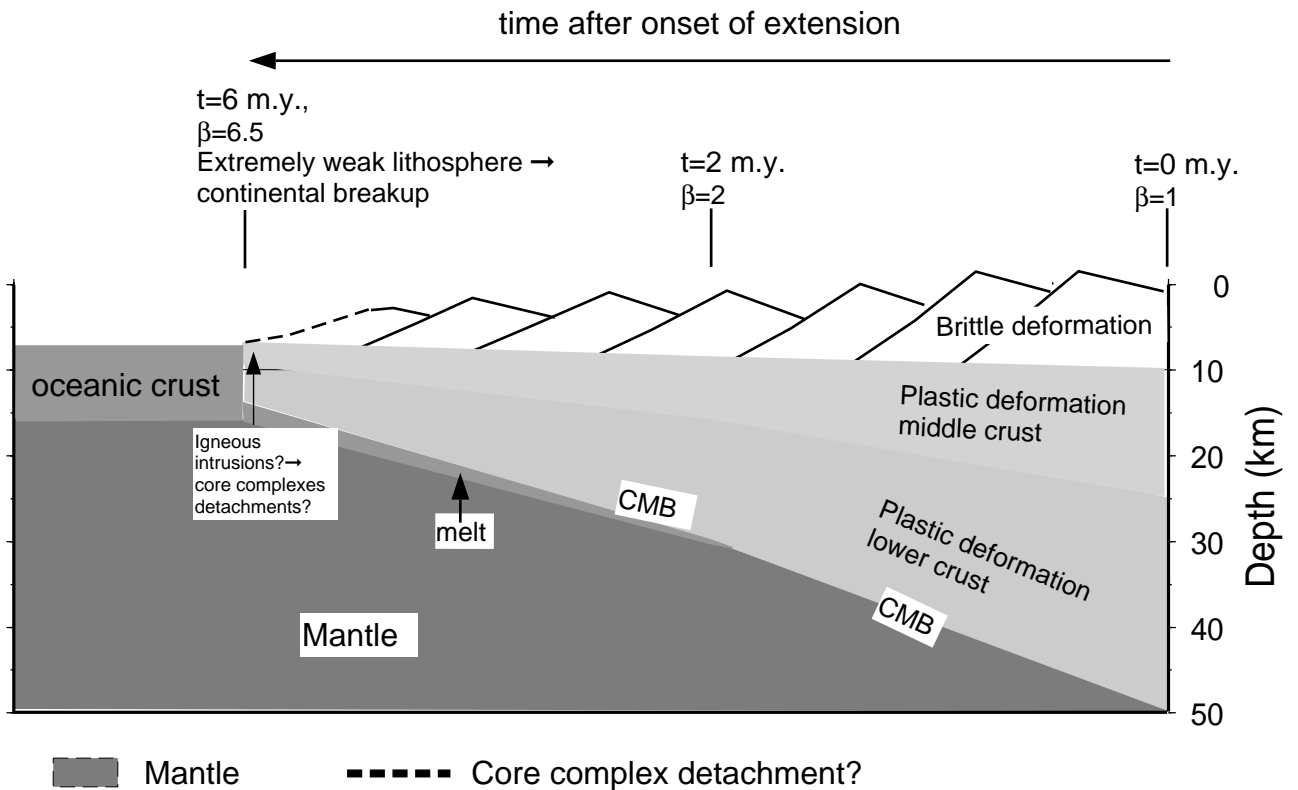


Figure 5.11. Diagram of the temporal evolution of the centre of the rift for the **A.**, West Iberia margin, uplift (pressure reduction) and cooling moved progressively more of the crust into the brittle regime until the entire crust became brittle at stretching factors of about 4. At this point, faults cut down through the crust, allowing hydrous fluids to reach and serpentinize the upper mantle, leading to the development of a decollement at the CMB (e.g. S) and hence to crustal separation prior to the onset of seafloor spreading. In contrast, during the rifting of hot lithosphere and thick crust to form the **B.**, Woodlark Basin, the entire crust did not become brittle and no serpentinites were formed. Instead, pressure release melting of the upwelling and mafic intrusion preceded lithospheric separation and may have led to core complex formation.

## 5.8 CONCLUSIONS

This study has shown that fundamental differences between the west Iberia / SW Greenland type of non-volcanic margin and the Woodlark Basin can be explained by the rheological and magmatic evolution of different lithospheric types during progressive extension. The thin crust and cool lithosphere of West Iberia and SW Greenland became completely brittle at moderate stretching factors, at which point fluids reaching the cool uppermost mantle could initiate serpentinisation. The weak serpentinites subsequently formed a weak layer, which acted as a decollement allowing complete crustal separation well before the lithosphere failed and seafloor spreading started. The result was the exposure of a broad expanse of serpentinised sub-continental mantle lithosphere within the COT at these margins.

In contrast, during rifting of the the thick crust and hot, weak lithosphere of the Woodlark Basin, partial melting of the upwelling asthenosphere was more pronounced, and the weak lithosphere failed once stretching factors of about 5 were exceeded, long before the crust could become entirely brittle. Thus serpentinites were never formed, and no mantle peridotites were exposed in the COT.



## CHAPTER 6. OUTLOOK

The aim of this thesis has been to study the processes of continental extension and break-up at non-volcanic passive margins. The conclusions have been presented in each chapter. However, several open questions remain that are discussed in this chapter and might represent potential topics of future research.

### **6.1 Differential versus uniform stretching in the crust - or how to reconcile extension factors on faults with overall extension factors in the crust.**

The first part of this thesis (chapter 2 and 3) has been devoted to study the extensional history of the Galicia Interior Basin, the mechanisms of extension in the basin and its relationship with the rest of the margin. We have proposed that the basin formed from Tithonian to Valanginian times along an ancient suture zone that separates two different types of crust. The velocity structure obtained by modelling of the wide angle data indicate that the crust is extremely thin at the centre of the basin (8 to 6 km, stretching factors up to 5.3). Numerical results (Hopper and Buck, 1988) and estimations of the initial thermal state of the crust at the beginning of rifting indicate that lower crustal flow might have been mechanically unfeasible during extension at the basin. This suggests that no differential stretching occurred during rifting in the basin. In contrast, uniform stretching of the upper and lower crustal layers explain the velocity structure if one assumes that prior to rifting at both sides of the basin the crust was fundamentally different. This interpretation is supported by the analysis of dredge samples at the Galicia Bank and at the continental platform which show that the Galicia Bank belongs to the Ossa Morena Zone, whereas the continental platform belongs to the Central Iberian Zone (Capdevila and Mougenot, 1988). However, when crustal extension factors exceed 2, it becomes difficult to reconcile uniform stretching with estimations of extension on brittle faults. Stretching factors along brittle faults assuming a domino model for faulting function up to  $\beta \sim 1.7$  (Jackson, 1987, Sclater and Shorey, 1989). This limit is restricted by the condition that normal faults cannot remain active at angles lower than  $35^\circ$  (assuming friction coefficients of around 0.8-0.6). If a listric fault model (Sclater and Shorey, 1989) and additionally the fractal dimension of faulting is taken into account (Marret and Allmendiger, 1992), the extension factor that can be attained by brittle faulting is at most 2. Two different explanations have been offered to explain how deformation in the crust occurs when crustal stretching factors exceed 2:

1. One mechanism invokes differential stretching of the upper and lower crust: the ductile lower crust thins more than the upper crust and thus higher crustal stretching factors are attained than by brittle faulting. However, for this to occur the lower crust has to flow

outward of the rifting zone. Hopper and Buck (1988) have shown that lower crustal flow, if it occurs, is directed towards the centre of the basin to fill the void produced by brittle faulting. Hence, if differential stretching occurs, it implies that at the centre of the basin the lower crust is less stretched than the upper crust, opposite as it is needed to explain crustal stretching factors in excess of 2. Therefore we suggest that this mechanism cannot reconcile the stretching factors measured on faults with the overall stretching factors in the crust.

2. The second explanation calls for several extensional phases (Jackson, 1987). In each of them the highest stretching factor attained by brittle faulting is 2. When the extensional phases are superimposed the maximum stretching factor through faulting is roughly 2 multiplied by the number of extensional phases occurred. For instance two phases of extension would yield a maximum stretching factor in brittle faults of 4, reconciling estimates of whole crustal thinning with extension in the brittle layer. This explanation although plausible in many other basins, does not appear to hold for the Galicia Interior Basin.

In the Galicia Interior Basin the first extensional phase took place during Tithonian to Berriasian times. During this phase shallow water carbonates were deposited, implying that the crust was only slightly thinned (see chapter 3). For instance, let's suppose that the crust was originally 32 km thick (this is the current crustal thickness onshore, Cordoba et al., 1988, see chapter 3, 4 and 5 for discussion on initial crustal structure) and that it thinned to 25 km during this period (this is the crustal thickness at the continental platform, see Figure 2.5 in chapter 2). This implies a stretching factor during this first rifting phase of  $\sim 1.3$ . However, during the Valanginian the crust was further thinned from 25 km up to 8 to 6 km. This implies stretching factors of about 3.1 to 4.1 during this second extensional phase. Low angle faults that might explain larger stretching factors through brittle faulting are not observed in the basin. On the contrary, faults in the deepest part of the basin (along line 17), started acting at an angle of  $\sim 70^\circ$  and rotated up to  $\sim 35^\circ$ , as predicted by fault mechanics (see Plate 1, chapter 2). Extension through brittle faulting using the classical domino model is measured dividing the original horizontal extent of an unrotated basement block, by the current horizontal distance after rotation. This model assumes that the thickness of the brittle layer remains constant throughout extension, implying that the amount of rocks which are faulted is always the same. However, as extension progresses the relative proportion of rocks in the crust that deform by brittle failure increases (chapters 2, 4 and 5). This implies that stretching in the deep levels of the crust is taken up by faulting. We suggest that it should be explored how the progressive embrittlement of the crust influences the stretching factors attained through brittle faulting. Estimations of stretching factors attained by faulting and whole crustal stretching may be reconciled when taking this into account.

## **6.2 Development of decollements and extension at the continent ocean transition zone of the West Iberia margin**

In chapters 4 and 5 we developed a numerical model to study the relationship between the rheological evolution of the crust during extension, the occurrence of detachments at the last stages of rifting, and the exhumation of serpentinitised mantle at the continent ocean transition of the west Iberia margin. Using a one dimensional code that tracks temperature and rheology during extension we found that the embrittlement of the crust is a key point in the structural development of the margin. When the entire crust is brittle, faults can cut across the crust into the mantle and bring large amounts of seawater to serpentinitise it. This may lead to the development of decollements at the base of the crust since serpentinites have a very low coefficient of friction and can develop high pore pressures (Escartin et al., 1997a, Figure 4.13, chapter 4). We have suggested that because serpentinites form a weak zone at the base of the crust extension may horizontally focus where serpentinites form. This may lead to crustal separation and mantle exhumation along the serpentinite decollements (Figure 4.14, chapter 4). However, because we used a one dimensional model we could not actually test these two hypotheses. Modelling in 2-dimensions is needed to explore these possibilities. Additionally, to make the temperature calculations more realistic than in the first approximation developed in chapter 4 and 5, these calculations should include:

1. The heat released by serpentinitisation, as this is a highly exothermic process and might influence the position of the 400/500°C isotherm which controls the thickness of the potential serpentinite layer.
2. The heat released by melting when it ponds and freezes. To calculate this, first the depth of magma ponding should be defined. Most calculations of the amount of melt produced during rifting assume that as melt is produced it rises up to the crust and accumulates as intrusives or extrusives (Bown and White, 1995, chapter 5). However, at mid-ocean ridges the depth of magma ponding is controlled by its buoyancy (Ryan, 1987) and/or the depth of its freezing horizon (~1200°C, Phipps Morgan and Chen, 1993). We propose to apply these restrictions to magma ascent during rifting of the continental lithosphere. Since during most of the continental rifting the 1200°C isotherm is deeper than the base of the crust, some of the melt produced may pond at intermediate levels in the lithosphere (Figure 5.5, chapter 5). This might partly give an explanation for the lack of significant synrift magmatism during rifting at the west Iberia margin.
3. Hydrothermal circulation is expected to occur along faults throughout rifting, making heat transport more efficient. Thus the temperature at the base of the crust will be reduced and might facilitate serpentinitisation. The effect of hydrothermal calculation

in the temperature field can be included as an enhanced thermal conductivity within the temperature and depth range where it occurs (Phipps Morgan et al, 1987).

Additionally, the mechanism by which an area of around 100 km in width consisting of serpentinised mantle can be exposed at the surface without significant synrift magmatism (Whitmarsh and Sawyer, 1996, ODP Leg 173 Shipboard Scientific Party, 1998) is not understood. Bown and White (1995) and in chapter 5 (Figure 5.8) it is shown that, for a normal temperature asthenosphere (1300°C) and extension rate appropriate for West Iberia, little melt is generated for moderate extension factors. However where crustal separation occurs, crustal stretching factor might be infinite: if the lithospheric stretching factor were also infinite (i.e. assuming uniform pure shear), several km thickness of melt would be expected (Figure 5.8, chapter 5, Bown and White, 1995). However, none of the ODP Legs carried out at the West Iberia margin have found significant products of synrift magmatism within the continent ocean transition. As recent wide angle surveys indicate that at least the uppermost 10 km consist mainly of serpentinised peridotite over widths greater than 100 km (Chian et al, 1999, Discovery Group, 1999, Dean et al, 1999), this anomaly cannot be dismissed as a local effect, but rather indicates that simple one dimensional models as that of Bown and White (1995) or the one presented in chapter 5 do not function at the continent ocean transition. First, it is possible that lithospheric extension deviates markedly from the uniform pure shear that is assumed in these calculations (Bown and White, 1995, chapter 5). Second, as explained previously, these melt production calculations assume that when melt was produced it rose vertically up to the crust and accumulated there as intrusives or extrusives. This need not be true. Lateral melt migration, perhaps due to rifting induced pressure gradients, and the further possibility that melt ponds at intermediate levels in its way to the surface (as explained previously), may both account for the discrepancies between the observations and the simple model predictions. Two dimensional finite element modelling is necessary to investigate the importance of these effects.

### **6.3 Interplay between continental rifting and seafloor spreading propagation: the chicken or the egg?**

One question remains, when does seafloor spreading begin at the West Iberia margin. This question can be treated from the continental rifting point of view or from the seafloor spreading propagation point of view:

1. Continental point of view. Martin (1984) proposed that as two continental plates move apart, oceanic spreading will initiate along the rift when continental extension has reached a threshold value. However at the West Iberia Margin it is

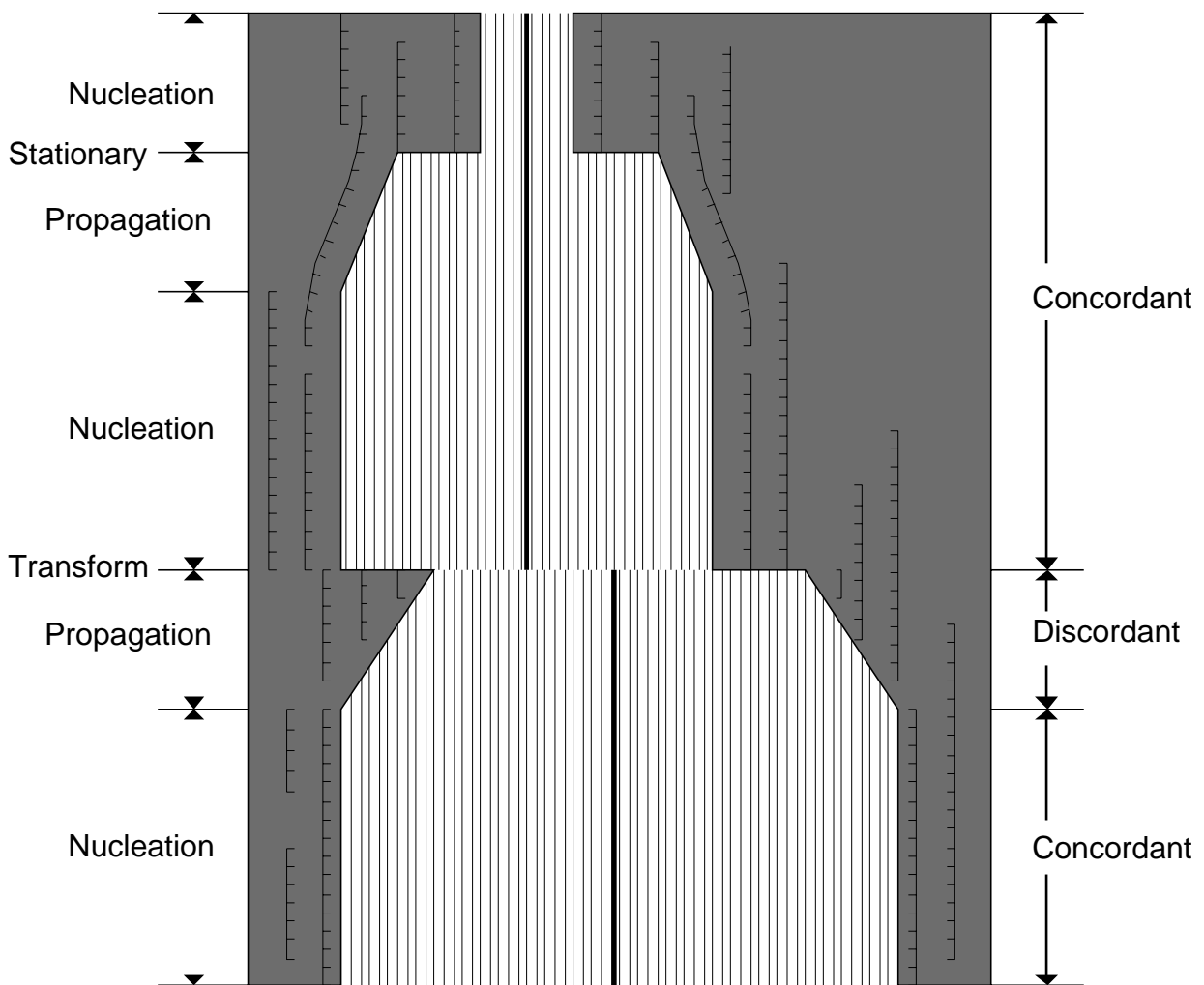


Figure 6.1. Idealized model of continent/ocean boundary evolution in the Woodlark Basin (Figure 3.4 of Andrew Goddlife's Phd.). Gray represents continental lithosphere. Black lines represent oceanic isochrons that are seen to be concordant with the margin when a spreading centre propagates, and perpendicular to the margin when propagation stops.

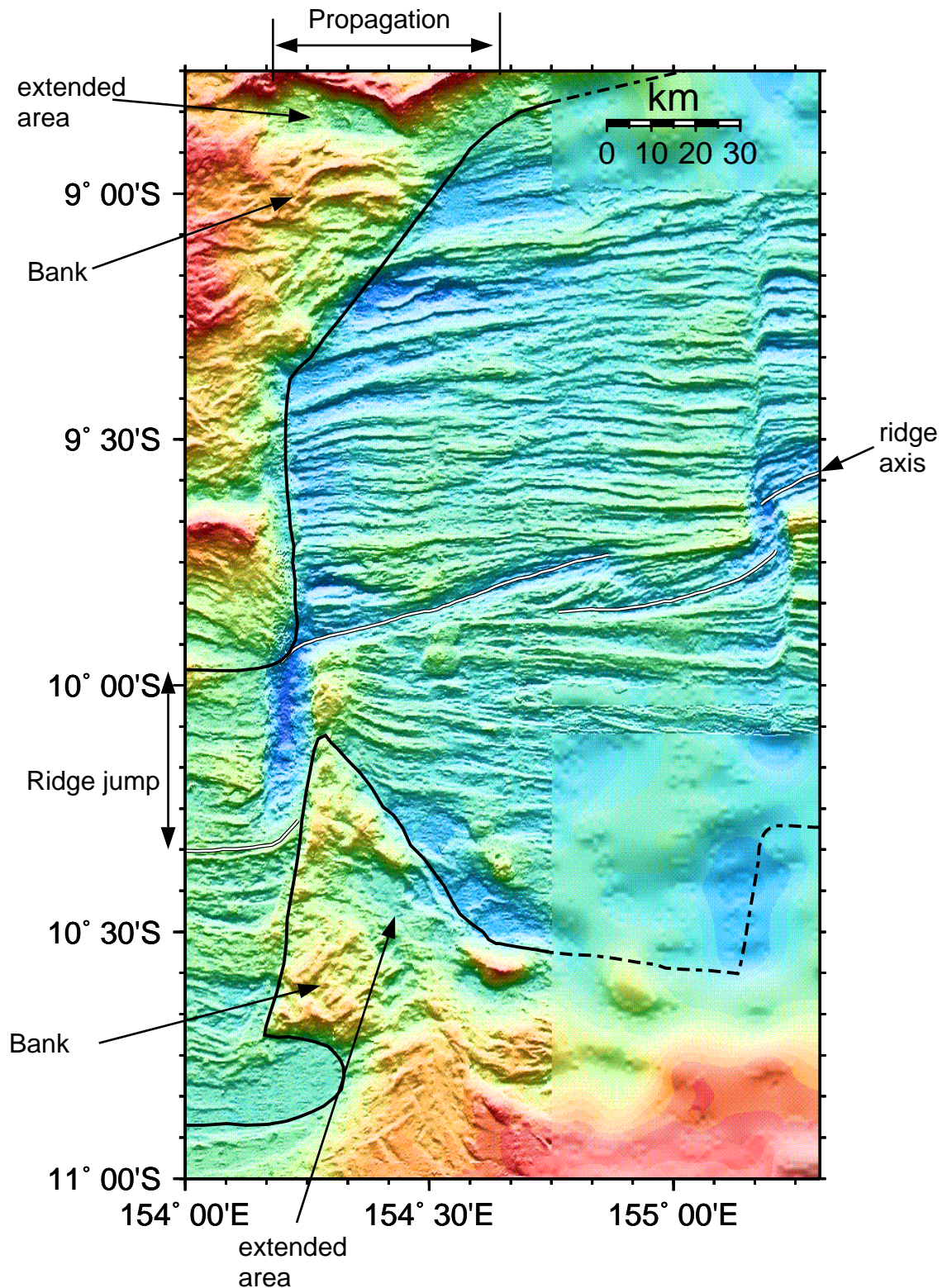


Figure 6.2. Detailed bathymetry of a segment of the Woodlark Basin (Figure 2.7 of Andrew Goodlife, PhD. thesis). Here propagation and ridge jump of seafloor spreading are observed. During propagation the seafloor fabric is at an oblique angle to the margin, juxtaposing progressively younger magnetic anomalies against the margin (Figure 6.1). As seafloor spreading propagates the oceanic fabric dies out against an area of elevated bathymetry (Bank), leaving abandoned areas which might be highly extended. Although the Galicia Interior Basin is much bigger than the extended areas observed here, we suggest that this situation might be analogous to what happened at the West Iberia margin. This might imply that propagation of seafloor spreading against the Galicia Bank left the Galicia Interior Basin abandoned.

difficult to test this hypothesis because we don't know if the origin of the continent ocean transition is continental or oceanic. For instance, the transects along the Iberia Abyssal Plain and the Galicia Interior Basin-Deep Galicia Margin (Figure 3.5, chapter 3) show that the width of the extended crust offshore varies significantly. This suggests that the amounts of crustal extension were very different along these two transects and thus that the hypothesis of Martin (1984) may not be valid here. But, if the continent ocean transition zone is assumed to be of continental origin, then the width of the extended continental lithosphere is very similar along the two transects, validating the hypothesis of Martin (1984). This would imply that deformation in the crust has been decoupled from deformation in the mantle during extension.

2. Oceanic point of view. When a seafloor spreading ridge propagates into rifted continental lithosphere progressively younger magnetic anomalies onlap against the continental margin. (Figure 6.1, Vink, 1982). We speculate that seafloor spreading might have propagated from the Iberia Abyssal Plain to the west of the Galicia Bank. However this is difficult to prove because rifting in the Deep Galicia Margin began during the Cretaceous magnetic quiet period and hence the relationship between the magnetic anomalies and the continental margin cannot be determined. Nevertheless, we can try to compare the observations at the west Iberia margin with those made at young basins where continental rifting and seafloor spreading is occurring nowadays, e.g. the Woodlark basin (Figure 5.1, chapter 5). Here three distinct stages during the transition from rifting to spreading have been identified: nucleation, propagation and stalling (Taylor et al., 1999, Goodlife, 1988). In each of these the relationship between the magnetic oceanic anomalies and the extensional fabric at the continent ocean boundary is different (Figure 6.1). In the Woodlark basin it appears that several small basins developed at the same time over a broad area (Taylor et al., 1999). When seafloor spreading propagates through one of them (e.g. the Deep Galicia margin), it leaves other highly extended basins abandoned by the side (e.g. the Galicia Interior Basin, Figure 6.2). This suggests that seafloor spreading propagation is a self driven process and does not depend directly on the degree of extension of the continental lithosphere. Following this interpretation, it may be possible that the last stages of continental rifting may be driven by the incipient propagation of a seafloor spreading ridge.

This discussion underscores the necessity to jointly investigate the mechanics of continental break-up and the transition to oceanic spreading at active margins. At these margins, precise tectonic reconstructions can be performed which are of fundamental importance when trying to understand the relationship between continental extension and seafloor spreading.

## REFERENCES

- Agrinier P., Cornen, G., and M. O. Beslier, Mineralogical and oxygen isotopic features of serpentinites recovered from the ocean/continent transition in the Iberia Abyssal Plain, *Proc. Ocean Drill. Program Sci. Results*, 149, 541-549, 1996.
- Asimov, P.D., Hirschmann, M.M., E.M. Stolper, An analysis of variation in isentropic melt productivity, *Phil. Trans. R. Soc. Lond. A*, 1997.
- Axen, G., Pore pressure, stress increase and fault weakening in low-angle normal faults. *J. Geophys. Res.*, 97, 8979-8991, 1992.
- Banda, E., Torne, M., and Talwani, M.. Rifted Ocean-Continent Boundaries, Kluwer NATO ASI Series C, vol. 463, 387 pp., 1995.
- Bassi G., C.E. Keen and P. Potter, Contrasting styles of rifting: models and examples from the eastern canadian margin, *Tectonics*, 12, 639-655, 1993.
- Bassi, G., Relative importance of strain rate and rheology for the mode of continental extension, *Geophys. J. Int.*, 122, 195-210, 1995.
- Beslier, M-O, M. Ask, and G. Boillot, Ocean-continent boundary in the Iberia Abyssal Plain from multichannel seismic data, *Tectonophysics*, 218, 383-393, 1993.
- Berryhill, J., Wave equation datuming, *Geophys.*, 44, 1329-1333, 1979.
- Berryhill, J., Wave equation datuming before stack, *Geophys.*, 49, 2064-2066, 1984.
- Berryhill, J. and Y. C: Kim, Deep water peg leg and multiples: emulation and suppression, *Geophys.*, 51, 2177-2184, 1986.
- Boillot, G., J.L. Auxietre, J.P. Dunand, P.A. Dupeuble, A. Mauffret, The northwestern Iberian margin: a Cretaceous passive margin deformed during Eocene, in Talwani, M., Hay, W., and Ryan W.B.F. (Eds.), *Deep Drilling Results in the Atlantic Ocean: Continental Margin and Paleoenvironment*. Am. Geophys. Union, Maurice Ewing Ser., 3, 138-153, 1979.
- Boillot, G., G. Feraud, M. Recq, J. Girardeau, "Undercutting" by serpentinite beneath rifted margins: The examples of the west Galicia margin (Spain), *Nature*, 341, 523-525, 1989.
- Boillot, G., and E. Winterer, Drilling on the Galicia margin: Retrospect and prospect, *Proc. Ocean Drill. Program Sci. Results*, 103, 809-828, 1988.
- Bown, J. W., and R. S. White, Effect of finite extension rate on melt generation at rifted continental margins, *J. Geophys. Res.*, 100, 18,011-18,029, 1995.
- Brace, W. F. and D. L. Kohlstedt, Limits on lithospheric stress imposed by laboratory experiments, *J. Geophys. Res.*, 85, 6248-6252, 1980.
- Brun, J. P., M. O. Beslier, Mantle exhumation at passive margins, *Earth Planet. Sci. Lett.*, 142, 161-173, 1996.
- Buck, W. R., Modes of continental extension, *J. Geophys. Res.*, 96, 20,161-20,178, 1991.



- Buck, W. R., Flexural rotation of normal faults, *Tectonics*, **5**, 959-973, 1988.
- Bunch, A.W.H., A detailed seismic structure of Rockall Bank (55°N, 15°W): A synthetic seismogram analysis, *Eart. Planet. Sci. Lett.*, **35**, 453-463, 1979.
- Capdevila R. and D. Mougnot, Pre-Mesozoic basement of the western Iberian continental margin and its place in the Variscan belt, *Proc. Ocean Drill. Program Sci. Results*, **103**, 3-12, 1988.
- Chalmers, J. A., Laursen, K.H., 1995, The Labrador Sea: the extent of continental crust and the timing of the start of sea-floor spreading, *Marine and Petroleum Geology*, **12**, 205-217, 1995.
- Chalmers, J.A., The continental margin off southern Greenland: along-strike transition from an amagmatic to a volcanic margin. *J. Geol. Soc. London*, **154**, 571-576, 1997.
- Chian, C., C. Keen, I. Reid and K. Loudon, Evolution of nonvolcanic rifted margins of the Labrador Sea, *Geology*, **23**, 589-592, 1995.
- Chian, C., K. E. Loudon, T. A. Minshull and R. B. Whitmarsh, Deep structure of the ocean-continent transition in the southern Iberia Abyssal Plain from seismic refraction profiles: Ocean Drilling Program (Legs 149 and 173) transect, *J. Geophys. Res.*, **107**, 7443-7462, 1999.
- Christensen, N., W. Mooney, Seismic velocity structure and composition of the continental crust: A global view, *J. Geophys. Res.*, **100**, 9761-9788, 1995.
- Coffin M.F., and O. Eldholm, Large Igneous Provinces: Crustal structure, dimensions, and external consequences, *Rev. Geophys.*, **32**, 1-36, 1994.
- Cole, J.E., and Peachey, J., 1999. Evidence for pre-Cretaceous rifting in the Rockall Trough: an analysis using quantitative plate tectonic modelling. In: Fleet, A.J., and Boldy, S.A.R. (eds) *Petroleum Geology of NW Europe: Proceedings of the 5th conference*, 359-370.
- Comas, M., L. F. Jansa, and M. Sarti, The late Jurassic carbonate platform of the Atlantic Western Iberian Margin. *Congr. geol. Granada, II*, Libro de Simposios, pp. 333-342.
- Córdoba, D., E. Banda and J. Ansorge, P-wave velocity-depth distribution in the Hercynian crust of northwest Spain, *Phys. Earth Planet. Inter.*, **51**, 235-248, 1988.
- Dean, S. M., T. A. Minshull, R. B. Whitmarsh, K. E. Loudon, Deep structure of the ocean-continent transition in the southern Iberia Abyssal Plain from seismic refraction profiles: II. The IAM-9 transect at 40°20' N, *J. Geophys. Res.*, **105**, 5859-5885, 2000.
- Denelle, E., Y. Dezard, and J. Raoult, 2-D prestack depth migration in the (S-G-W) domain, paper presented at the 56th meeting, Soc. of Explor. Geophys., Houston, Tex., 1986.
- Discovery 215 Working Group, deep structure in the vicinity of the ocean-continent transition zone under the southern Iberia Abyssal Plain, *Geology*, **26**, 743-746, 1998.
- Dunbar, J.A. and D. Sawyer, How preexisting weaknesses control the style of continental break-up, *J. Geophys. Res.*, **94**, 7287-7292, 1989.

- Dupeuble, P.A., G. Boillot and D. Mougénot, Late Jurassic-earliest Cretaceous limestone dredged from the Galicia margin. In: G. Boillot, E.L. Winterer, A.W. Meyer et al., Proc. Init. Rep. ODP, 103(A), 99-105, 1987.
- England, P., Comment on "Brittle failure in the upper mantle during extension of continental lithosphere" by Dale S. Sawyer, *Geophys. Res.*, 91, 10,487-10,490, 1986.
- England, P., Constraints on extension of continental lithosphere, *J. Geophys. Res.*, 88, 1145-1152, 1983.
- England, R.W., and Hobbs, R.W. The structure of the Rockall Trough imaged by deep seismic reflection profiling. *J. Geol. Soc. London*, 154, 497-502, 1997.
- England, P. and J. Jackson, Migration of the seismic-aseismic transition during uniform and nonuniform extension of the continental lithosphere, *Geology*, 15, 291-294, 1987.
- Escartín, J., G. Hirth and B. Evans, Nondilatant brittle deformation of serpentinites: Implications for Mohr-Coulomb theory and the strength of faults, *J. Geophys. Res.*, 102, 2897-2913, 1997a.
- Escartín, J., G. Hirth and B. Evans, Effects of serpentinitization on the lithospheric strength and the style of normal faulting at slow-spreading ridges, *Earth Planet. Sci. Lett.*, 151, 181-189, 1997b.
- Fernández, M., I. Marzán, A. Correia and E. Ramalho, Heat flow, heat production, and lithospheric thermal regime in the Iberian Peninsula, *Tectonophysics*, 291, 29-553, 1998.
- Finlayson, D. M., C. D. N. Collins, I. Lukaszuk and E. C. Chudyk, A transect across Australia's southern margin in the Otway basin region: crustal architecture and the nature of rifting from wide-angle seismic profiling, *Tectonophysics*, 288, 177-189, 1998.
- Finkebeiner, T., C. A. Barton and M. D. Zoback, Relationships among in-situ stress, fractures and faults, and fluid flow: Monterey formation, Santa Maria Basin, California, *AAPG Bulletin*, 81, 1975-1999, 1997.
- Fitch, A.A., (editor), *Developments in Geophysical Exploration. methods -1*. Elsevier Applied Science publishers, 1979,
- Flueh, E. R. and J. Bialas. A digital, high data capacity ocean bottom recorder for seismic investigations. *Int. Underwater Systems Design*, 18, 3: 18-20, 1996.
- Gradstein, F.M, F. P. Agterberg, J. G. Ogg, J. Hardenbol, P. van Veen, J. Thierry, and Z. Huang. A mesozoic time scale, *J. Geophys. Res.*, 99, 24,051-24,074, 1994.
- Graham, R., The role of shear belts in the South Harris igneous complex, *J. Struct. Geol.*, 2, 29-37, 1980.
- Griffin, W., and S. O'Reilly, The lower crust in eastern Australia: xenolith evidence, *Spec. Publ. geol. Soc. London*, 24, 363-374, 1986.
- Goetze, C., and B. Evans, Stress and temperature in the bending lithosphere as constrained by experimental rock mechanics, *Geophys. J. R. Astron. Soc.*, 59, 463-478, 1979.

- Gonzalez, A., D. Cordoba and D. Valdes, Seismic crustal structure of the Galicia continental margin, NW Iberian Peninsula, *Geophys. Res. Lett.*, 26, 1061-1064, 1999.
- Goodlife, A. M., The rifting of continental and oceanic lithosphere: observations from the Wooflark Basin, PhD. Thesis, 1998, Univeristy of Hawaii.
- Groupe Galice, The continental margin off Galicia and Portugal: acoustical stratigraphy, dredge stratigraphy and structural evolution, in J.C. Sibuet, et al., eds: Initial Reports of Deep Sea Drilling Project, 47: Washington D.C. U.S. Government printing Office, 633-662, 1979.
- Handy M. R., The exhumation of cross sections of the continental crust: structure, kinematics and rheology, in *Exposed cross sections of the contiental crust*, edited by M. H. Salisbury, and D. M. Fountain, *Kluwer Academic Publishers*, 317, 485-507, 1990.
- Hauser, F., B.M. O'Reilly, A.W.B. Jacob, P.M. Shannon, J. Makris and U. Vogt, The crustal structure of the Rockall Trough: differential stretching without underplating, *J. Geophys. Res.*, 100, 4097-4116, 1995.
- Hess, P. C., *Origins of Igneous Rocks*, 336 pp., Harvard University press, Cambridge, 1989.
- Hill, E.J., Baldwin, S.L., and Lister, G.S.. Unroofing of active metamorphic core complexes in the D'Entrecasteaux Islands, Papua New Guinea, *Geology*, 20, 907-910, 1992.
- Hinz , K., A hypothesis on terrestrial catastrophes. Wedges of very thick oceanward dipping layers beneath passive continetal margins - their origin and paleoenviromental significance. *Geologisches Jahrbuch E22*, 3-28,1981.
- Hitchen, K., and Ritchie, J.D. New K-Ar ages and a provisional chronology for the offshore part of the British Tertiary Igneous Province. *Scott. J. Geol.*, 29, 73-85, 1993.
- Hoffmann H. J. and T. J. Reston, The nature of the S reflector beneath the Galicia Bank rifted margin: Preliminary results from pre-stack depth migration, *Geology*, 20, 1091-1094, 1992.
- Hooper, J. R. and W. R. Buck, The effect of lower crustal flow on continental extension and passive margin formation, *J. Geophys. Res.*, 101, 20,175-20,194, 1996.
- Hooper, J. R. and W. R. Buck, Styles of extensional decoupling, *Geology*, 26, 699-720, 1988.
- Hubral, P, Time migration: some ray theoretical aspects, *Geophys. Prospect.*, 25, 738-745, 1977.
- Jackson, Active normal faulting and crustal extension, in *Continental Extensional Tectonics*, Geological Society Special Publication No. 28, pp. 3-17, 1987.
- Jarvis, G.T. and McKenzie, D.P., Sedimentary basin formation with finite extension rates, *Earth and Planet. Sci. Letts.*, 48b, 42-52, 1980.
- Joppen, M., and White, R.S., The structure and subsidence of Rockall Trough from two ship seismic experiments, *J. Geophys. Res.*, 95, 19821-19837, 1990.
- Kirby, S. H., Rheology of the lithosphere, *Rev. Geophy.*, 21, 1458-1487, 1983.

- Klitgord, K.D., and H. Schouten, Plate kinematics of the central Atlantic. In: P.R. de Vogt and B.D. Tulchocke (Editors), *The Geology of North America. Vol. M, The Western Atlantic region*. geol. Soc. Am. Bulder, Colo., 351-378, 1986.
- Kopp, C. Struktur und tektonische Mechanismen der Nord-Sulawesi Subduktionszone (Indonesien), 1997, P.h.d. Thesis, University of Kiel.
- Klemperer, S.L., and Hobbs, R.H.. *The BIRPS Atlas*. Cambridge University Press, 124 pp., 1991.
- Kohlstedt, D. L., B. Evans, S. J., Mackwell, Strength of the lithosphere: constraints imposed by laboratory experiments, *J. Geophys. Res.*, 100, 17587-17602, 1995.
- Krawczyk, C. M., T. J. Reston, M. O. Beslier, and G. boillot, Evidence for detachment tectonics on the Iberia Abyssal Plain rifted margin, *Proc. Ocean Drill. Program Sci. Pesults*, 149, 603-615, 1996.
- Koch, P. S., *Rheology and microstructures of experimnetally deformed quartz aggregates* , Ph. D. thesis, Univ. Calif. Los Angeles, 464 pp., 1983
- Kronenberg, A. K., and J. Tullis, Flow strength of quartz aggregates: grain size and pressure effects due to hydrolitic weakening, *J. Geophys. Res.*, 89, , 4281-4297, 1984.
- Kusznir, N., and R. G. Park, The extensional strength of continental lithosphere: Its dependence on geothermal gradient, and crustal composition and thickness, in *Continental Extensional tectonics*, edited by M. P. Coward, J. F. dewey, and P.L. Hancock, *Spec. Publ. geol. Soc. London*, 28, 35-52, 1987.
- Lachenbruch, A., Crustal temperature and heat production: implications of the linear heat-flow relation, *J. Geophys. Res.*, 75, 3291-3300, 1970.
- Larner, K., and C. Beasley, Cascaded migrations: improving the accuracy of finite-difference migration, *Geophys.*, 52, 618-643, 1987.
- Latin, D. and N. White, Generating melt during lithospheric extension: Pure shear vs. simple shear, *Geology*, 18, 327-331, 1990.
- Lefort, J.P., The main basement features recognized in the northern part of the North Atlantic area, in *Initial Repots of te Deep Sea Drilling Project*, 80: Washington D.C., U.S., Governemnt Printing Office, 1103-1114, 1984.
- Lister, G.S., G. A. Davis, The origin of metamorphic core complexes and detachment faults formed during Tertiary continental extension in the northern Colorado River region, U.S.A., *J. Struct. Geol.*, 11, 65-94, 1989.
- Lowe, C. and A.W.B. Jacob, A nort-south seismic refraction profile across the Caledonian Suture zone in Ireland, *Tectonophysics*, 186, 297-318.
- Luetgert, J. H. MacRay - Interactive two-Dimensional Seismic Raytracing for the Macintosh. U.S. Geological Survey open file Report 92-356, 1992.

- Malod J.A., and A. Mauffret, Iberian plate motions during the Mesozoic, *Tectonophysics*, 184, 261-278, 1990.
- Martin, A. K. Propagating rifts: crustal extension during continental rifting. *Tectonics*, 3, 611-617, 1984.
- Mamet, B, M.C. Comas and G. Boillot, Late Paleozoic basin on the West Galicia Atlantic margin, *Geology*, 19, 738-741, 1991.
- Mauffret, A., and L. Montardet, Seismic stratigraphy off Galicia (Spain). *Proc. Ocean Drill. Program Sci. Results*, 103,, 13-20, 1988.
- McKenzie, D., Some remarks on the development of sedimentary basins, *Earth Planet. Sci. Lett.*, 40, 25-32, 1978.
- McKenzie, D.P. and Bickle, M.J.. The volume and composition of melt generated by extension of the lithosphere. *J. Petrology*, 29, 625-679, 1988.
- Marret, R., Allemndiger, R., Amount of extension on "small" faults: An example from the Viking graben, *Geology*, 20, 47-50, 1992.
- Mauffret, A., D. Mougénot, P.R. Miles and J.A. Malod, Results from Multichannel reflection profiling of the tagus Abyssal Plain (Portugal) - Comparison with the Canadian margin, in *Extensional tectonics and stratigraphy of the North Atlantic*, *Am. Soc. Pet. Geol. mem.*, 46, 379-393, 1990.
- Mougénot, D., *Geologie de la Marge Portugaise*, *These de Doctorat D'Etat es Sciences Naturelles*, University Pierre et Marie Curie, Paris VI, 1988.
- Moullade, M., M.P. Brunet, and G. Boillot, Subsidence and deepening of the Galicia margin: the paleoenvironmental control., *Proc. Ocean Drill. Program Sci. Results*, 103, 733-740, 1988.
- Montenat C., F. Guery, and P.Y. Berthou, Mesozoic evolution of the Lusitanian basin: comparison with the adjacent margin, *Proc. Ocean Drill. Program Sci. Results*, 103, 757-775, 1988.
- Murillas, J., D. Mougénot, G. Boillot, M. C. Comas, E. Banda and A. Mauffret., Structure and Evolution of the Galicia Interior Basin (Atlantic western Iberian continental margin), *Tectonophysics*, 184, 297-319, 1990.
- Musgrove, F.W., and Michener, B.. Analysis of pre-Tertiary rifting history of the Rockall Trough, *Petroleum Geoscience*, 2, 353-360, 1996.
- Mutter, J.C., Mutter, C.Z., and Fang, J.. Analogies to oceanic behaviour in the continental breakup of the western Woodlark Basin. *Nature*, 380, 333-337, 1996.
- Mutter, J.C., Margins declassified, *Nature*, 364, 393-394, 1993.
- Nadin, P.A., Houchen, M.A., and Kusznir, N.J.. Evidence for pre-Cretaceous rifting in the Rockall Trough: an analysis using quantitative 2D structural/stratigraphic modelling. In: Fleet, A.J., and Boldy, S.A.R. (eds) *Petroleum Geology of NW Europe: Proceedings of the 5th conference*, 371-378, 1999.

- Newman, W., N. White, Rheology of the continental lithosphere inferred from sedimentary basins, *Nature*, 385, 621-624, 1997.
- Nicholls, I.A., J., Ferguson, H., Jones, G.P., Marks, and J.C. Mutter, Ultramafic blocks from the ocean floor southwest of Australia, *Earth and Planet. Sci. Lett.*, 56, 362-374, 1981.
- ODP Leg 173 Shipboard Scientific Party, Drilling reveals Transition from continental breakup to early magmatic crust, *EOS Trans, AGU, vol. 79*, 180-181, 1998.
- Ogg, J. G., Early Cretaceous and Tithonian magnetostratigraphy of the Galicia margin, *Proc. Ocean Drill. program, Sci. results*, 103, 659-682, 1988.
- O'Hanley, D. S., *Serpentinites: records of Tectonic and Petrological History, Oxford Monogr. Geol. Geophys.*, no 34, 277 pp., Oxford Univ., New York, 1996.
- O'Reilly, B.M., Hauser, F., Jacob, A.W.B., and Shannon, P.M., The lithosphere below the Rockall Trough: wide-angle seismic evidence for extensive serpentinisation., *Tectonophysics*, 255, 1-23, 1996.
- Parsons, T., and Thompson, G.. Does magmatism influence low-angle normal faulting? *Geology*, 21, 247-250, 1993.
- Percival, J., A possible exposed Conrad Discontinuity in the Kapuskasing uplift, Ontario, *AGU Geodynamics Series*, 14, 135-141, 1986.
- Phipps Morgan, J., E. M. Parmentier, and J. Lin, Mechanisms for the origin of mid-ocean ridge axial topography: Implications for thermal and mechanical structure at accreting plate boundaries, *J. Geophys. Res.*, 92, 12,823-12,836, 1987.
- Phipps Morgan, J., The thermodynamics of pressure-release melting of a veined plum-pudding mantle, submitted 2000.
- Phipps Morgan, J. and Chen, Y. The genesis of oceanic crust: magma injection, hydrothermal circulation, and crustal flow. *J. Geophys. Res*, 98, 6283-6298, 1993.
- Pérez-Gussinyé, M., T. J. Reston, D. Sawyer, C. R. Ranero and E. Flueh, The structure of the Galicia Interior Basin: west of Iberia (abstract), *EOS Trans, AGU*, 79, 1998.
- Pickup, S. L. B., R. B. Whitmarsh, C. M. R. Fowler and T. J. Reston, Insight into the nature of the ocean-continent transition from a deep multichannel seismic reflection profile, *Geology*, 24, 1079-1082, 1996.
- Pinheiro, L.M., R.B. Whitmarsh, and P.R. Miles, The ocean-continent boundary off the western continental margin of Iberia, II. crustal structure in the Tagus Abyssal Plain, *Geophys. J. Int.*, 109, 106-124, 1992.
- Quesada, C., P.E. Fonseca, J. Munha, J.T. Oliveira, and A. Ribeiro, The Beja-Acebuches ophiolite (Southern Iberia Variscan fold belt): geological characterization and geodynamic significance. *Bol. Geol. Miner.* , 105, 3-49, 1994.
- Rabinowitz, P.D., S.C: Cande, and D.E. Hayes, Grand Banks and J-anomaly Ridge, *Science*, 202, 71-73, 1978.

- Rasmussen, E.S., Lomholt, S., Andersen C., Vejbaek, O.V., Aspects of the structural evolution of the Lusitanian Basin in Portugal and the shelf and slope area offshore Portugal, *Tectonophysics*, 300, 199-225, 1999.
- Read, H. H., The Coast around Portsoy, in *Nort-east Scotland: the Daldrian*. Geologists Association Guide No 31, edited by *Benham & Co*, 1960
- Reid, I., Crustal structure of a nonvolcanic rifted margin east of Newfoundland, *J. Geophys. Res.*, 99, 15,161-15,180, 1994.
- Reston T. J., The structure of the crust and the uppermost mantle offshore Britain: deep seismic reflection profiling and crustal cross-sections, in *Exposed cross sections of the continental crust*, edited by M. H. Salisbury, and D. M. Fountain, *Kluwer Academic Publishers*, 317, 603-621, 1990.
- Reston, T. J., C. M. Krawczyck, D. Klaeschen, The S reflector west of Galicia (Spain): Evidence from prestack depth migration for detachment faulting during continental breakup, , *J. Geophys. Res.*, 101, 8075-8091, 1996.
- Reston, T.J., The S refelector west of Galicia: the seismic signature of a detachment fault. *Geophys. J. Int.*, 127, 230-244, 1996.
- Reston, T. J., Perez-Gussinye, M., pennell, J., Stuberauch, A., Structure of the Porcupine Basin, talk presented at Geosciences U.K. Meeting, 2000.
- Ryan, W.B.F., et al., Gorringe Bank. Site 120: Initial reports of the Deep Sea Drilling project, 13: Washington D.C., U.S. Government Printing Office, 19-41, 1973.
- Ryan, M.P., Neutral buoyancy and the mechanical evolution of magmatic systems, in *Magmatic processes: Physiochemical Principles*, *Geochem. Spec. Pub. 1*, 259-287, 1987.
- Salisbury M. H. and D. M. Fountain, *Exposed cross-sections of the continental crust*, 662 pp., Kluwer Academic Publishers, 1990.
- Sawyer, D. S., et al., *Proceedings of the Ocean Drilling Program, Initial Reports*, 149, 719 pp., Ocean Drill. program Sci. Results, 149, 471-488, 1996.
- Sawyer D. S., C. Zelt, T. J. Reston, Imaging above and below the S reflector, Galicia Bank Basin, MCS and OBS results(abstract), *EOS Trans, AGU*, 79, 1998.
- Sclater, J.G. and M. Shorey, Mid-Jurassic through mid-Cretaceous extension in the Central Graben of the North Sea - part 2: estimates from faulting observed on a seismic reflection line, *Basin Research*, 1, 000-000, 1989.
- Sherwood, J., Depth sections and interval velocities from surface seismic data, *Leading Edge*, 8-9, 44-49, 1989.
- Sibson, R. H., 1985. A note on fault reactivation. *J. Struct Geol.*, 7, 751-754.
- Sibuet, J.C., W.B.F. Ryan, et al., Init. Rep. DSDP, 47 (2). 787 pp, 1979.

- Smith, G. D., *Numerical Solution of Partial Differential Equations: Finite Difference Methods*, Oxford Applied Mathematics and Computing Science Series, Oxford University Press, 1985.
- Smith, W.H.F, and D.T. Sandwell, Marine gravity field from declassified Geosat and ERS-1 altimetry (abstract), *EOS Trans. AGU*, 76(46), Fall Meet. Suppl. F156, 1995.
- Smythe, D.K.. Rockall Trough - Cretaceous or Late Paleozoic? *Scott. J. Geol.* , **25**, 5-43, 1989.
- Srivastava, S.P., Results from a detailed aeromagnetic survey across the northeast Newfoundland margin, Part II, Early opening of the North Atlantic between the British isles and Newfoundland, *Mar. Pet. geol.*, 5, 324-327, 1988.
- Srivastava, S.P., and J. Verhoef., Evolution of Mesozoic sedimentary basins around the North Central Atlantic: a preliminary plate kinematic solution. In Parnell, J. (Ed.), *Basins of the Atlantic Seaboard: Petroleum Geology, Sedimentology and Basin Evolution*, *Geol. Soc. Spec. Publ. London*, 62:397-420, 1992.
- Srivastava, S.P., and Roest, W.R., Nature of thin crust across the SW Greenland margin and its bearing on the location of the Continent-Ocean boundary. *Kluwer NATO ASI Series C*, 463, 95-119, 1995.
- Scholz, C. H., The brittle plastic transition and the depth of faulting, *Geolog. Rundschau*, 77/1, 319-328, 1988.
- Shelton, G., and J. A. Tullis, Experimental flow laws for crustal rocks (abstract), *EOS Trans. AGU*, 62, 396, 1981.
- Sheriff, R.E. and L.P Geldart, *Exploratin Seismology*, Cambridge University Press, 2nd edition, 1995.
- Sibson R. H., J. Mcmoore and R. H. Rankin, Seismic pumping - a hydrothermal fluid transport mechanism, *J. Geol. Soc. London*, 131, 653-659, 1975.
- Sonder L.J. and P. England, Effects of a temperature-dependent rheology on large-scale continental extension, *J. Geophys. Res*, 94, 7603-7619, 1989.
- Taylor, B., Goodliffe, A., Martinez, F., and Hey, R., Continental rifting and initial seafloor spreading in the Woodlark Basin. *Nature*, 374, 534-537, 1995
- Taylor, B., Goodliffe, A., and Martinez, F., How continents break up: Insights from Paspua New Guinea. *J. Geophys. Res.*, 7497-7512, 104, 1999.
- Tulcholge, B.E., and W.J. Ludwig, Structure and origin of the J anomaly Ridge, western North Atlantic Ocean, *J. Geophys. Res.*, 87, 9389-9407, 1982.
- Tullis, T. E., Horowitz, F. G., Tullis, J., Flow law of polyphase aggregates from end-member flow laws, *J. Geophys. Res.*, 96, 8081-8096, 1991.
- Ulmer, P., and V. Trommsdorf, Serpentinite stability to mantle depths and subduction-related magmatism, *Science*, 268, 858-861, 1995.



- Vigneresse, J.L., Intrusion level of granitic massifs along the Hercynian belt: balancing the eroded crust, *Tectonophysics*, 307, 277-295, 1999.
- Vink, G., Continental rifting and the implications for plate tectonic reconstructions, *J. Geophys. Res.*, 87, 10,677-10,688, 1982.
- Wernicke, B., Uniform-sense normal simple shear of the continental lithosphere, *Can. J. Earth Sci.*, 22, 108-125, 1985.
- White, N., Nature of lithospheric extension in the North Sea. *Geology*, 17, 101-196, 1989.
- Whitmarsh, R. B. and P. Miles, Models of the development of the West Iberia rifted continental margin at 40°30' N deduced from surface and deep tow magnetic anomalies, *J. Geophys. Res.*, 100, 3789-3806, 1995.
- Whitmarsh, R. B., and D. S. Sawyer, The ocean/continent transition beneath the Iberia Abyssal Plain and continental-rifting to seafloor-spreading processes, *Proc. Ocean Drill. Program Sci. Results*, 149, 713-733, 1996.
- Whitmarsh, R. B., R. S. White, S. J. Horsefield, J. Sibuet, M. Recq and V. Louvel, The ocean-continent boundary off the western continental margin of Iberia: Crustal structure west of Galicia Bank, *J. Geophys. Res.*, 101, 28, 291-28314, 1996.
- Wilson, R.C.L., R. N. Hiscott, M. G. Willis and F.M. Gradstein, The Lusitanian Basin of West-Central Portugal: Mesozoic and Tertiary Tectonic, Stratigraphic, and Subsidence history, in *Extensional tectonics and stratigraphy of the North Atlantic*, *Am. Soc. Pet. Geol. mem.*, 46, 341-361, 1990.
- Wilson, R. C. L., D. S. Sawyer, R. B. Whitmarsh, J. Zerong, and J. Carbonell, Seismic stratigraphy and tectonic history of the Iberia Abyssal Plain, *Proc. Ocean Drill. Program Sci. Results*, 149, 617-633, 1996.
- Wood, L.C., R.C. Heiser and S.T. Riley, The debubbling of marine source signatures, *Geophys.*, 43, 715-729, 1978.
- Yilmaz, O, Seismic data processing, Investigations in geophysics, Vol. 2. - SEG, Tulsa (OK), 526 pp., 1987.
- Zandt, G., and C. J. Ammon, Continental crust composition constrained by measurements of crustal Poisson's ratio, *Nature*, 374, 152-154, 1995.
- Zelt, C.A., Sawyer D.S. and E.T. Knoll, Seismic velocity structure of the Iberia margin from simultaneous wide-angle and zero-offset traveltimes inversion, *EOS Trans, AGU*, 80, 1999.

## ACKNOWLEDGEMENTS

When you write a thesis it seems you're never going to finish, but at last, you do it!. Here I want to thank everybody that made it possible.

First of all I want to thank Cesar Ranero and Tim Reston. They have permanently supervised my work, given me very good ideas about what to do next and discussed very long and at any time about the topics that are presented in this work. Working with them has made a lot of fun and gave me the feeling I was really doing something new and interesting. Without their help this thesis wouldn't be as it is.

I also want to thank Jason Phipps Morgan who has helped me a lot during the work. He stayed with me during long hours helping me to introduce his melt calculations in my codes, chapter 5 wouldn't exist without his help. He also had the patience of answering my endless list of questions about the mechanics of extension. I'm very happy to have met him and have had the opportunity to work with him.

I want to thank Ernst Flueh and Roland von Huene for giving me the opportunity to do a PhD. at Geomar. Ernst Flueh also helped me with the modelling of the wide angle data and gave me freedom to go to as many meetings as I wanted.

Stephan Rouzo was a very good friend and always helped me generously with the programming of my codes. I have missed the coffee breaks at his office since he is not here. The dinners at Geraldine and Stephan's home are amongst the most memorable things I will take away from Kiel.

Dirk Klaeschen helped with some of the processing of the data and always was there to give good ideas how to improve it. Thanks also to Ruediger, Willi Weinrebe, Martin and Gerd they have always helped with computer and printing problems.

My roommate Urte Domaschk and Holger Busche have always been very nice to me, and very good friends. They helped me in anything I needed and gave me moral support in the last stages of my thesis. Also, Arnim Berhorst, Joerg Petersen, Thomas Leythausen, Irgard, Heidrun, Christian Kopp (who also helped me with the wide angle modelling), have been good friends and was nice to go out with them to experience the night life in Kiel. I also want to thank my homemates, Ingo and Stephan for being really nice with me and also for keeping the dinner warm when I came very late from work.

I also want to thank all my friends "abroad", Magda, Marta, Olga, Itziar, Tiago, my sister Laura and my brother Joaquim for keeping regular e-mail contact with me and giving constant moral support.

At last, but not least, I want to thank my parents for given me a good education and a very easy view of life.

This work was supported by a "la Caixa"/D.A.A.D. grant and a Marie Curie grant of the European Union. I am thankful to the oil company REPSOL which provided part of the MCS data used for this PhD.

**CURRICULUM VITAE**

Name	Marta Pérez Gussinyé
Date and Place of Birth	04.04.1972 in Barcelona
Citizenship	Spanish
1978-1986	Primary School: Escola Aster, Hospitalet de l'Infant, Tarragona, Spain
1986-1990	High School: Institut Pons d'Icart, Tarragona, Spain.
1990-1996	M.S.c. in Physics (speciality Physics of the Earth and Cosmos), Univeristat de Barcelona, Spain.
since July 1996	Research Assistant at Geomar.

# APPENDIX 1

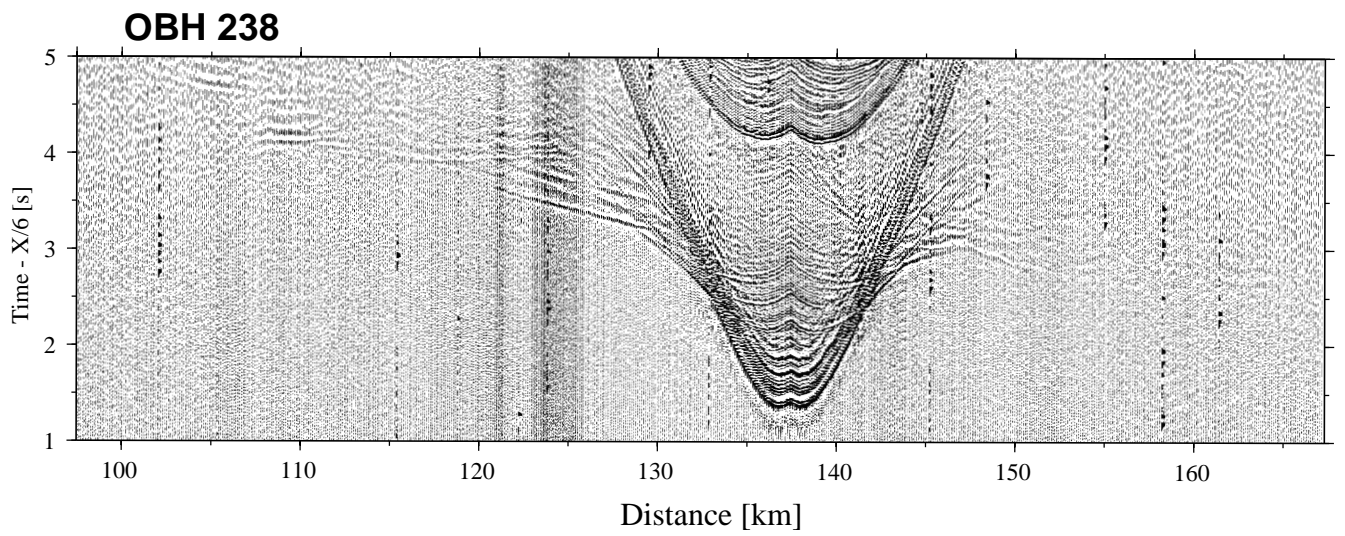
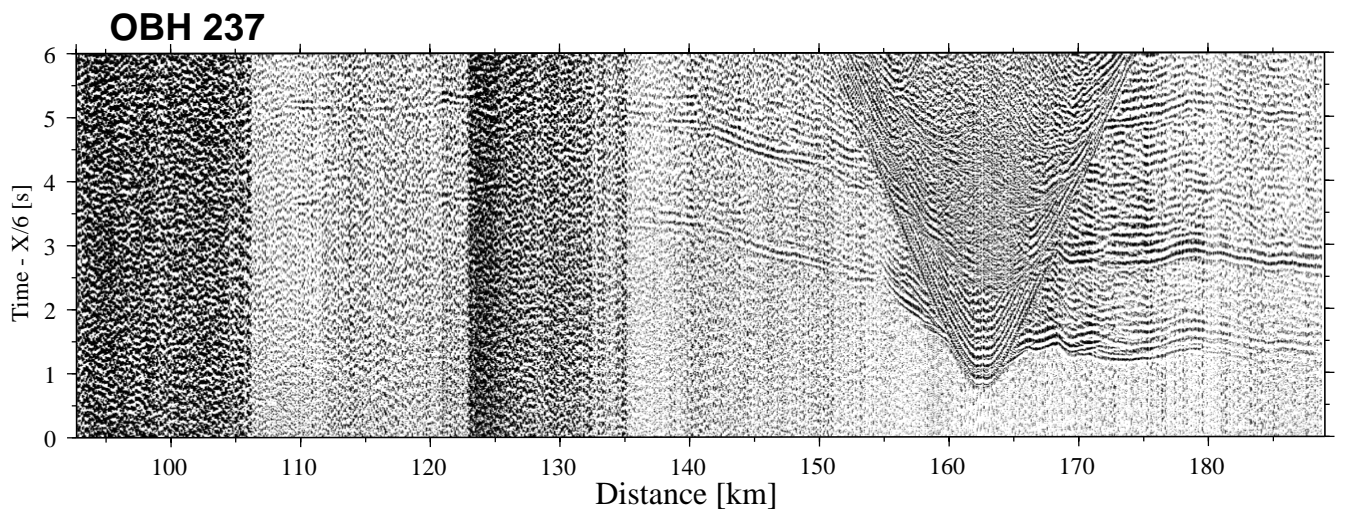
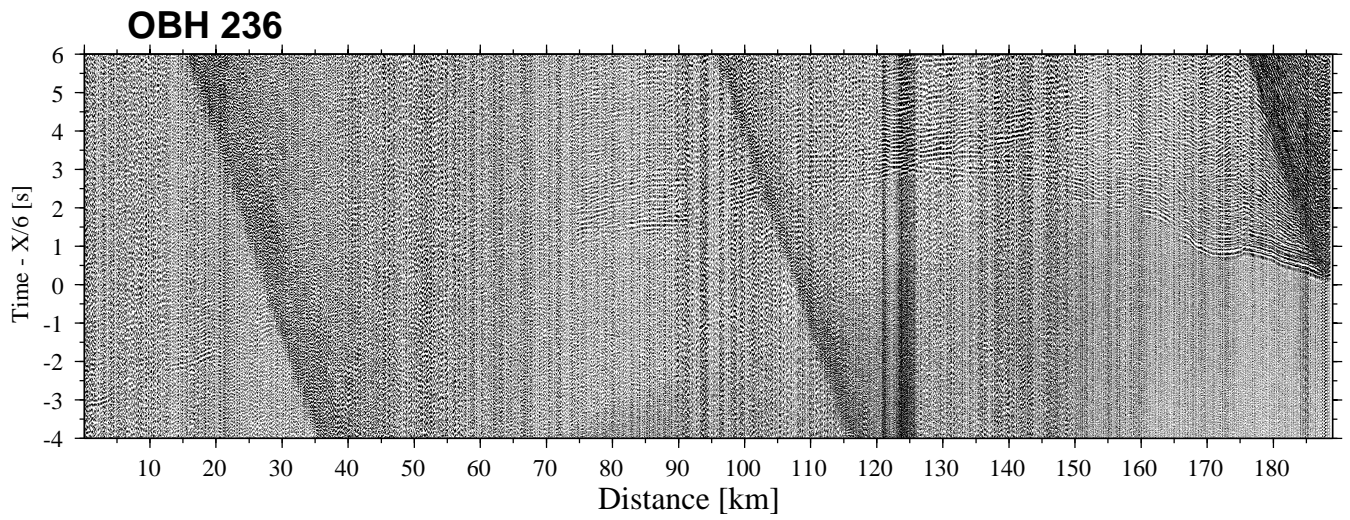
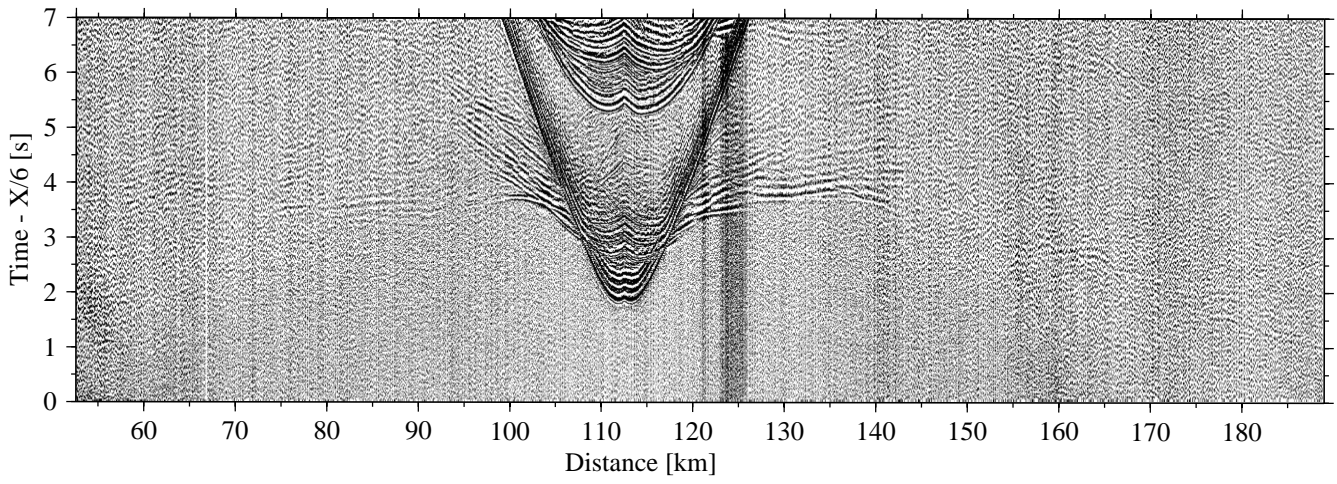
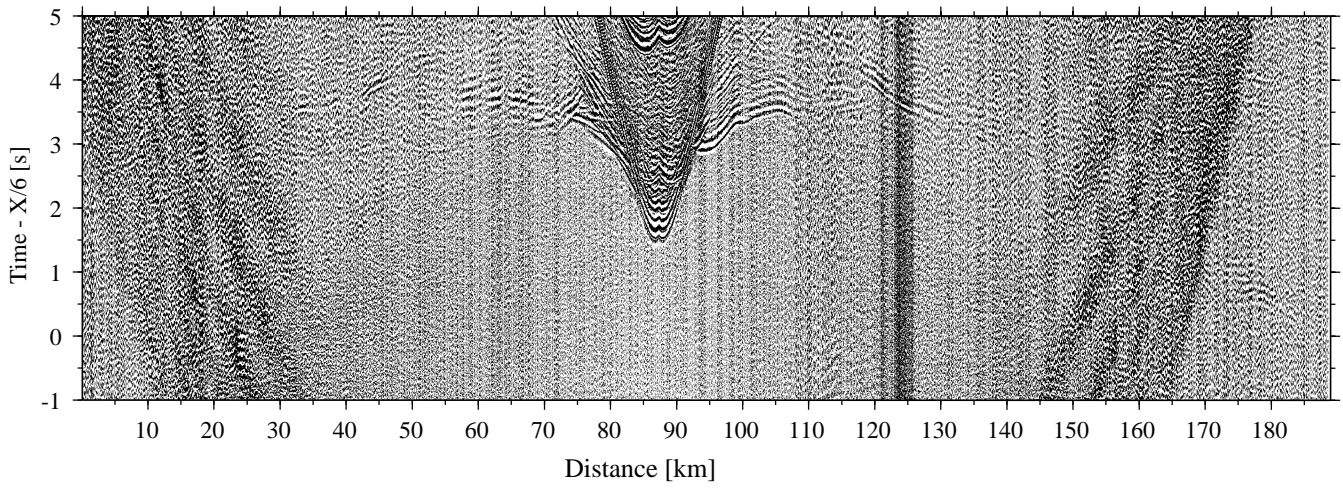


Figure App.1. Processed seismic records of OBHs 236, 237 and 238.

### OBH 239



### OBH 240



### OBH 242

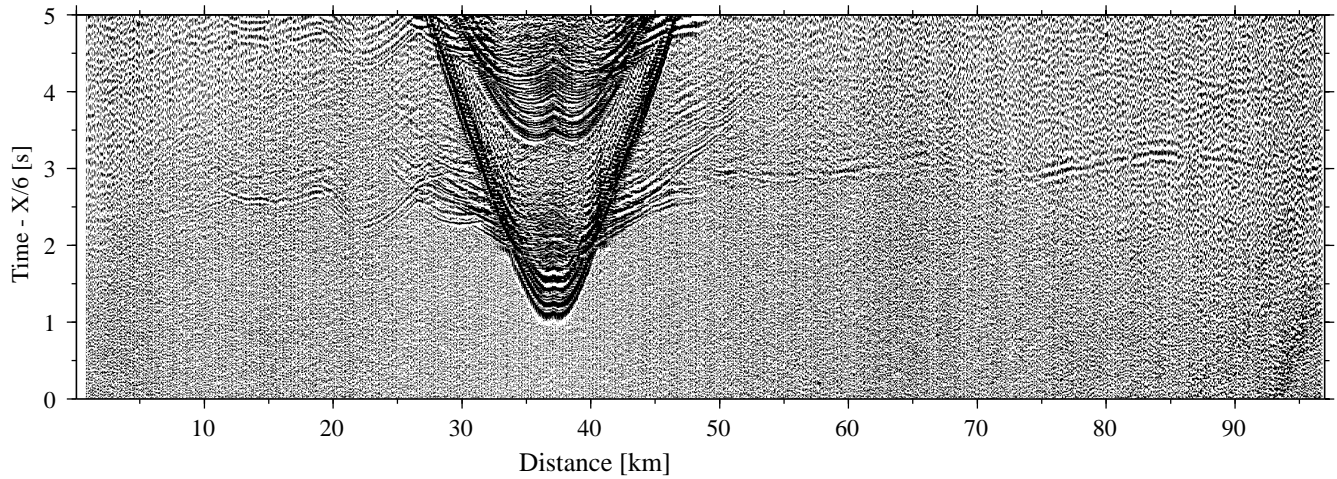


Figure App.2. Processed seismic records of OHBs 239, 240 and 242.